

Photochromic molecular switches: Thienyl-based polyphenylenes and the π -delocalisation effect on photochemical properties

Bryan Irwin



Trinity College Dublin
Coláiste na Tríonóide, Baile Átha Cliath
The University of Dublin

A thesis submitted to the University of Dublin for the degree of
Doctor of Philosophy

School of Chemistry

January 2018

Trinity College Dublin

This thesis has been submitted as an exercise for a degree at this university. Due acknowledgements and references are given to the work of others where appropriate. All work given is original and was carried out by the author alone

.....

Bryan Irwin

Acknowledgements

Firstly, I would like to thank my supervisor, Professor Sylvia Draper, for her constant support, guidance and advice that she offered throughout the course of my research so far, helping me to keep both my perspective and footing. A HUGE, most sincere thank you to the Draper Group. The girls, Claire, Martha, Nidhi and Lu, who have been so helpful and understanding. Thank you to the boys, Eugene, Colin and Justo. A special shout out to my partner in crime, Junsì, who kept me sane as a desk buddy for all these years. Thank you to past group members Niamh, who continues to be an inspiration and proof reader, Colm, Lankani, Nitheen but a special thank you goes out to Dr Gearóid O'Maille, without whom this project would never have seen fruition. Your support, advice and knowledge have been life-changing. But of course, to Robb, my work wife, thank you for all the coffee and the chats we had these past four years, I apologise that never liked you at first, you've been invaluable.

A thank you to all the technical staff, Dr Martin Feeney and Dr Gary Hessman in mass spectrometry, and Dr Manuel Ruether and Dr John O'Brien in NMR spectroscopy who not only processed my never-ending stream of NMR's but also took the time to sit down and help me understand what was going on within them. Thanks to Dr. Brendan Twamley. I'd also like to thank all of the administrative staff, Tess, Helen, Jennifer and Anne-Marie, and to the technical staff of the undergraduate labs, Patsy, Peggy, Dorothy and Peter.

Finally, a thank you to all my family who helped me get this far. To my Mum and Dad and their never-ending stream of support, from the all-night writing to the crazy mood swings. To my sisters, Carly and Heather, ever the understanding pains of my life. My grandparents, your constant support was so needed. To my extended family, thank you.

Thank you to everyone who has made this possible, all my friends who have shown nothing but support. To Brian and Vicky, thank you for the crazy trip to LA and the nights I will never forget. To Amy, who came back into my life when I needed her the most. To John, for being the big brother I never knew I needed.

And Jonathan and Gary, two of the most important people in my life, without you none of this would have been possible, you truly are the most understanding people I have ever been fortunate to meet, you have no idea how lucky I am to know you. Thank you for everything.

“The inside of our own minds are the scariest things there are.”

- Robin McKinley

Summary

Chapter 1: This chapter begins with a general introduction into the vast field of molecular machinery, prominently focusing on molecular switches and those that experience an internal cyclisation upon exposure to specific wavelengths of light. Photoresponsive molecules such as those based on dithienylethenes have become targets in the drive to miniaturise optoelectronic devices. On irradiation, they are able to respond and record the event *via* a range of processes (including bond breaking and reforming) so as to offer new opportunities at a molecular level for high density data storage and fast data retrieval systems. This chapter then introduces the unique but predominantly vast chemistry involved in polycyclic aromatic hydrocarbons (PAHs) and their heteroatom analogues. This is then expanded upon with a discussion of current 1,10-phenanthroline based metal complexes and their enhanced photochemical properties. This is finally rounded off with a short discussion in the overlap that may potentially exist within these three areas of research, how to potentially manipulate the unusual photochemical effects displayed by each and how to tune these effects in terms of synthetic adaptability.

Chapter 2: This chapter describes the synthetic routes towards novel photochromic molecular switches generated from dithienylethene, and the optimisation of these molecular systems. Five novel molecular switches were prepared, showcasing the synthesis, characterisation and photophysical properties exhibited by the compounds. The synthesis evolved via a sequence of Sonogashira cross-coupling reactions and Diel-Alder cycloadditions. ^1H NMR showcases the chemical shifts inherently applicable to the two synthesised photoisomers due to the change in their structural geometry and electronic distribution. UV-Vis absorption spectroscopy and the emissive photophysical properties of the synthesised materials allowed for the quantum yield of photocyclisation to be evaluated in most cases.

The first part of the chapter deals with the synthesis of these ethynyl-based polycyclic aromatic materials, and diverges into the understanding of the chemical activity of their brominated precursors.

The second part of the chapter explores the photophysical properties and the spectroscopic assignment of these family of compounds, including their mirroring emissive profiles and

how a bridging ethynyl-group between the dithienyl core and these delocalised platforms can affect intermolecular communication or inhibit photocyclisation.

Chapter 3: This chapter begins with a discussion of the attempts to incorporate thiophene rings into polyphenylene type structures and explore their potential as both delocalised 2D graphene-like platforms and as switching structures. Synthetic routes in this area revolved around the substitution of phenyl rings with thienyl-analogues in previously reported dynamic pathways, specifically focusing on the Diels-Alder cycloaddition of 2,3,4,5-terraphenylcyclopentadienone and 2-methyl-3-bromo-5-ethynylthiophene groups. The photophysical and photochromic possibilities of these systems are discussed, with particular emphasis, however, on the NMR spectroscopic characterisation of these isomers. Hexaphenylbenzene platforms, and their mono-, di- and poly- substituted thiophene counterparts are analysed in depth, and a comparative synopsis is drawn for each unique system. The second half of the chapter specifically deals with the photochromic activity of some of these synthesised switches and how incorporation of the dithienylethene backbone *into* the rotating ring system effects overall switch performance.

Chapter 4: The work in this chapter is notable divided into three distinct parts. The first part describes the synthesis of a novel series of 3- and 3,8-aryl-1,10-phenanthroline ligands and their corresponding Ir(III) complexes. The NMR shifts between species are discussed, and the photophysical properties of the complexes are explored for potential future applications.

The second part of the chapter is a theoretical investigation of compound, and precursor, 1,2-bis(5-phenylacetylene)-2-methylthiophen-3-yl)perfluorocyclopentene, and a review of the crystallographic viewpoint of the molecular switch in the solid state. The compound shows a high degree of thermal stability, and a substantial hyperchromic intensity shift when compared to much more complex systems.

The third part of the chapter is an amalgamation of the three areas briefly explored in the previous work in this thesis. Complex **Ir-5** was synthesised with a dithienylethene core, an extensive heteroatom π -platform ligand and an Ir(III) metal centre. The photophysical properties of the complex is explored, with an analysis of its overlapping triplet energy levels and their affect on the photophysical properties.

Chapter 5: Provides a full account of the experimental work carried out in this research.

Table of Contents

	Page
1. The theory, synthesis and photophysical properties of photochromic molecular switches generated from dithienylethene.....	1
1.1 Introduction.....	2
1.2 Molecular Switches.....	3
1.2.1 Types of Molecular Switches.....	5
1.2.1.1 Host-guest Molecular switches.....	5
1.2.1.2 Mechanically interlocked molecular switches.....	5
1.2.1.3 Photochromic Molecular switches.....	6
1.3 Diarylethenes.....	12
1.3.1 Thermal Conversion.....	14
1.3.2 Fatigue Resistance.....	17
1.3.3 Absorption Spectra.....	17
1.3.4 Quantum Yield.....	19
1.3.5 Emission and non-destructive readout capabilities.....	20
1.3.6 Electrochemical properties.....	21
1.4 Chemical Actinometry.....	21
1.5 Tuning of Photochemical Properties.....	23
1.6 Polycyclic Aromatic Hydrocarbons (PAHs).....	23
1.6.1 The use of Hexaphenylbenzenes and Hexabenzocoronenes in Molecular Switches.....	25
1.6.2 Synthesis of Hexabenzocoronenes.....	27
1.6.3 Thienyl-substituted hexaphenylbenzene derivatives and hetero-atom containing superbenzenes.....	28
1.7 Other Applications of Molecular Switches.....	30
1.8 Molecular Switch Decay.....	32
1.9 1,10-Phenanthroline.....	33
1.9.1 Derivatives of 1,10-Phenanthroline.....	34
1.10 Ruthenium and Iridium Complexes.....	35
1.10.1 Ruthenium and Iridium 1,10-Phenanthroline Complexes.....	37

1.10.2 Polyphenylenes as ligands in encapsulated metal complexes.....	38
1.10.3 Photochemical properties of Iridium in molecular switches.....	39
1.11 Project Aims.....	40
2. Thienyl and Alkynyl-based polycyclic aromatic hydrocarbon appendages and comparing the photophysical properties of their photochromic analogues.....	42
2.1 3-bromo-2-methyl-5-(1-ethynylPAH)thiophene appendages.....	43
2.2 Synthesis of 3-bromo-2-methyl-5-(1-ethynylPAH)thiophene appendages.....	44
2.2.1 Microwave Chemistry.....	44
2.2.2 Solvent choice for microwave reactions.....	44
2.2.3 Microwave assisted organic synthesis.....	45
2.2.4 Synthesis of 3,5-dibromo-2-methylthiophene, 1	46
2.2.5 Synthesis of 3-bromo-2-methyl-5-(4- <i>tert</i> -butylphenylacetylene)thiophene, 2	47
2.2.6 Synthesis of 3-bromo-5-(4-((4- <i>tert</i> -butyl)phenyl)ethynyl)phenyl)-2-methylthiophene, 3	48
2.2.7 Synthesis of 3-bromo-2-methyl-5-(1-ethynlnaphthalene)thiophene, 4	49
2.2.8 Synthesis of 3-bromo-2-methyl-5-(1-ethynlpyrene)thiophene, 5	50
2.2.9 Synthesis of precursor iodo-hexaphenylbenzene, 6	50
2.2.10 Synthesis of 3-bromo-2-methyl-5-(1-ethynlHPB)thiophene, 7	51
2.3 Characterisation of bromo-thienyl compounds, 2, 3, 4, and 5.....	52
2.3.1 NMR Characterisation of 2	52
2.3.2 NMR Characterisation of 3	52
2.3.3 NMR Characterisation of 4	54
2.3.4 NMR Characterisation of 5	65
2.4 UV-Vis absorption of compounds 2-5.....	57
2.5 Dithienylethene-based molecular switches with 1-ethynylaryl appendages.....	58
2.5.1 General lithiation procedure for generating 1-ethynylaryl dithienylethene-based switches.....	59

2.5.2	Synthesis of 1,2-Bis(5-(4- <i>tert</i> -butylphenylacetylene)-2-methylthiophen-3-yl)perfluorocyclopentene), 8	60
2.5.3	Synthesis of 3,3'-(perfluorocyclopent-1-ene-1,2-diyl)bis(5-(4-((4-(<i>tert</i> -butyl)phenyl)ethynyl)phenyl)-2-methylthiophene), 9	60
2.5.4	Synthesis of 1,2-Bis(5-(4- <i>tert</i> -butylphenylacetylene)-2-methylthiophen-3-yl)perfluorocyclopentene), 10	61
2.5.5	Synthesis of 1,2-Bis(5-(4- <i>tert</i> -butylphenylacetylene)-2-methylthiophen-3-yl)perfluorocyclopentene), 11	62
2.5.6	Synthesis of 1,2-Bis(5-(4- <i>tert</i> -butylphenylacetylene)-2-methylthiophen-3-yl)perfluorocyclopentene), 12	63
2.6	Characterisation of compounds 8-12...64	
2.6.1	NMR Characterisation of 8	64
2.6.2	NMR Characterisation of 9	65
2.6.3	NMR Characterisation of 10	67
2.6.4	NMR Characterisation of 11	68
2.6.5	NMR Characterisation of 12	69
2.7	Spectroscopic analysis of compounds 2, 3, 4, 5 and 7, and switches 8-12.....69	
2.7.1	Photochemical analysis of compounds 2, 3, 4 and 5	70
2.7.1.2	<i>Photochemical properties of 8</i>	70
2.7.1.3	<i>Emission of compound 8</i>	74
2.7.1.4	<i>Photophysical Analysis of 9</i>	76
2.7.1.5	<i>Emission and Excitation Spectra of switching complex 5</i>	80
2.7.1.6	<i>Photophysical Analysis of 10</i>	82
2.7.1.7	<i>Photochemical properties of Compound 11</i>	84
2.7.1.8	<i>Photochemical properties of Compound 12</i>	85
2.8	Comparative photophysical properties.....86	
2.9	Fatigue resistance in compounds 8 and 9.....87	
2.10	Thermal conversion.....89	
2.11	Quantum Yield.....89	
2.11.1	Quantum Yield of switch 9	91
2.12	Electrochemical analysis of 8.....92	
2.13	Conclusions & Future Work.....93	

2.13.1 Computational Analysis.....	94
3. Hexaphenylbenzene and polyphenylene π-platforms with thienyl substituents, synthesis and photochemical properties.....	99
3.1 Tetraarylcyclopentadienone systems , synthesis and characterisation	
3.1.1 Synthesis and ¹ H NMR of 2,3,4,5-tetra-(4- <i>tert</i> -butylphenyl)cyclopenta-2,4-dienone, 13	100
3.1.2 Synthesis of tetraarylcyclopentadienones 14-16	102
3.1.3 ¹ H NMR spectra of tetraarylcyclopentadienones 14, 15 and 16	103
3.2 Synthesis and characterisation of polyphenylene appendages.....	107
3.2.1 Characterisation of polyphenylene compounds 17 and 18	108
3.2.1.1 ¹ H NMR of polyphenylene compounds 17 and 18	109
3.2.2 Synthesis of symmetric dithienyl compound 18	111
3.2.2.1 ¹ H NMR spectra of compound 18	113
3.2.3 Synthesis of 3-bromo-5-(4''-(<i>tert</i> -butyl)-3',4',5',6'-tetrakis(4-(<i>tert</i> -butyl)phenyl)-[1,1':2',1''-terphenyl]-4-yl)-2-methylthiophene, 19	114
3.2.3.1 NMR Characterisation of 19	115
3.3 Synthesis of polyphenylene based switches.....	117
3.3.1 Characterisation of polyphenylene switches.....	118
3.4 Trimerisation of asymmetric thienyl-phenyl acetylenes.....	122
3.5 Photochemical measurements of switches X and X.....	126
3.6 Conclusion and Future Work.....	129
3.6.1 Retrosynthetic Analysis of the DTE-based Switches.....	129
3.6.1.1 Synthesis of 3,3'-(perfluorocyclopent-1-ene-1,2-diyl)bis(5-(4''-(<i>tert</i> -butyl)-3',4',5',6'-tetrakis(4-(<i>tert</i> -butyl)phenyl)-[1,1':2',1''-terphenyl]-4-yl)-2-methylthiophene).....	130
3.6.1.2 Characterisation of Compound X.....	131
3.6.1.3 Preliminary Photophysical Analysis X.....	132
3.6.2 Cyclodehydrogenation of aromatic π -platforms.....	132
3.6.3 Cyclotrimerisation of more extended linear-thienyl acetylenes.....	136

4. Investigating 1,10-phenanthroline based Ir(III) complexes and their potential use as photochromic molecular switches.....	140
4.1 Substituted 1,10-Phenanthroline With Acetylenic Tethers as Linkages.....	141
4.2 Synthesis of Ir(III) 1,10-phenanthrolines complexes.....	142
4.2.1 Synthesis of 1,10-phenanthroline ligand.....	142
4.2.2 Coordination of Iridium centres.....	143
4.3 Structural Characterisation of Ir-1 - Ir-4.....	144
4.3.1 NMR Spectra Analysis of Ir-1 - Ir-4.....	144
4.3.2 Crystallographic analysis of Ir-1.....	148
4.3.3 Spectroscopic analysis of compounds Ir-1 and Ir-2.....	149
4.3.4 Spectroscopic analysis of compounds Ir-3 and Ir-4.....	150
4.3.5 Comparative analysis of UV-Vis absorption patterns of Ir-1 – Ir-4.....	152
4.4 Ir(III) 1,10-phenanthroline platform molecular switch.....	153
4.4.1 Synthetic Route.....	153
4.4.1.1 <i>Synthesis and NMR analysis of (3) 3,3-(perfluorocyclopent-1-ene-1,2-diyl)bis(2-methyl-5-(phenylethynyl)thiophene), model compound 1 (MC1).....</i>	<i>154</i>
4.4.1.2 <i>Photochemical Analysis of Compound MC1.....</i>	<i>155</i>
4.4.1.3 <i>DFT Analysis of Compound MC1.....</i>	<i>157</i>
4.4.1.4 <i>Quantum Yield of MC1.....</i>	<i>159</i>
4.4.1.5 <i>X-Ray Crystallography Analysis of Compound MC1.....</i>	<i>160</i>
4.4.2 Retrosynthetic Route 2.....	161
4.4.2.1 <i>Synthesis of of 5,7-diphenyl-6H-cyclopenta[ff][1,10]phenanthrolin-6-one.....</i>	<i>161</i>
4.4.2.2 <i>Synthesis and NMR characterisation of IrTTPBP.....</i>	<i>163</i>
4.4.2.3 <i>Photochemical Analysis of IrTTPB.....</i>	<i>165</i>
4.3 Ir (III) based molecular switch.....	167

4.3.1 Synthesis and NMR analysis of 6-(4-(3,3,4,4,5,5-hexafluoro-2-(2-methyl-5-(phenylethynyl)thiophen-3-yl)cyclopent-1-en-1-yl)-5-methylthiophen-2-yl)-5,7,8-tri-phenylbenzo[f][1,10]phenanthroline (8).....	167
4.3.1.1 NMR Analysis of Compound 8.....	168
4.3.1.2 Photochemical Analysis of Compound 8.....	169
4.3.1.3 Synthesis and analysis of Ir (III) complex 9.....	171
4.3.1.4 Photochemical analysis of 9.....	173
4.4 Conclusion and Future Work.....	176
5. Experimental.....	183

List of Figures

Figure 1.1 Molecular switches and their use throughout nature and scientific technology, from human vision and discotic liquid crystals on surfaces, to using conformational changes to inhibit changes on a macroscale, such as pushing a ball of silica across a medium or tuning the upconverting ability of a photosensitiser.....	2
Figure 1.2 Generic structure of a Rotaxane and Catenane.....	6
Figure 1.3 Simplified state model for azobenzene. ϵ are the excitation coefficients and Φ labels the quantum yields.....	9
Figure 1.4 Switches MSF-1 and MSF-2 , designed by Heller et al.....	12
Figure 1.5 Diarylethene bond rotation can be thought of like a lock and key, only in the correct conformation and with the correct force will the lock open and close.....	14
Figure 1.8. Molecular Switch UV-Vis Spectra showing both closed form (---) and open form (—).....	18
Figure 1.9. Examples of polycyclic aromatic hydrocarbons (PAHs).....	23
Figure 1.10 Structure of hexa-peri-hexabenzocoronene and its relationship with 2D graphene-sheets.....	25
Figure 1.11. Hexa-functionalised hexaphenylbenzene displaying photoinduced molecular switching (DTE = dithienylethene, BPEA = bis (phenylethynyl)anthracene).....	27
Figure 1.12 Hexaphenylbenzene condensation through the acid catalysed School reaction.	28
Figure 1.13 Hexa(2-thienyl)benzene compounds studied by Yoshida and Geng.....	29
Figure 1.14 Activation of fluorophore via photoswitching.....	30
Figure 1.15 1,10-Phenanthroline and the numbering system adopted.....	32
Figure 1.16 Types of electronic transitions observed upon photoexcitation of Ir (III) and Ru (II) complexes.....	36
Figure 1.17 Molecular structures of Ir(III) complexes bearing i) substituted 1,10-phenanthroline ligands, Ir-A and Ir-B. ii) unsubstituted 1,10-phenanthroline Ir-C.....	37
Figure 1.18 Molecular structures of Ru(II) bearing substituted phen ligands, Ru-1 and Ru-2.....	38
Figure 1.19 Jablonski Diagram for Ir(III) based switches.....	30
Figure 2.1 The target 3-bromo-2-methyl-5-(1-ethynylPAH)thiophene appendages.....	43
Figure 2.2 ¹ H NMR spectrum of compound 2 (CDCl ₃ , 400 MHz, RT).....	52
Figure 2.3 ¹ H and ¹³ C NMR of compound 3, methyl groups removed for clarity (CDCl ₃ , 400 MHz, RT).....	54

Figure 2.4 The ¹ H NMR spectrum of 4 (CDCl ₃ , 400 Hz, RT).....	55
Figure 2.5 The ¹ H and ¹³ C NMR of 5 , with assignment of the proton signals and corresponding carbon signals (CDCl ₃ , 600 MHz, RT).....	55
Figure 2.6 The HMBC NMR spectra of 5 , highlighting the aromatic region for the assignment of the carbon signals.....	56
Figure 2.7 Normalised UV-Vis absorption spectrum of 5 in CH ₂ Cl ₂ (1 x 10 ⁻⁴ M).....	57
Figure 2.8 UV-Vis absorption spectrum of compounds 2 , 3 , 4 and 5 (CH ₂ Cl ₂ , 1 x 10 ⁻⁵ M, RT).....	58
Figure 2.9 Dithienylethene-based molecular switches with 1-ethynylaryl appendages..	58
Figure 2.10 Photochromic behaviour of 10 in both solid and solution states.....	61
Figure 2.11 ¹ H NMR spectrum of photochromic compound 4o (open form), showing selectively highlighted areas of interest, and assignment of the proton signals, in CDCl ₃ (400 MHz, RT).....	65
Figure 2.12 The aromatic regions of the ¹ H NMR spectra of (a) the open isomer and (b) the closed isomer of 9 (only the structure of the open isomer is shown for simplicity)....	66
Figure 2.13 ¹ H NMR of open isomer (10o).....	68
Figure 2.14 ¹ H NMR of compound 11 (CDCl ₃ , 400 MHz, RT).....	68
Figure 2.15 ¹ H NMR and HSQC NMR experiments of compound 12	69
Figure 2.16 UV-Vis absorption spectra of the two photoisomers of 8o and 8c , in CHCl ₃ at room temperature. Inset shows bond rearrangement and colour of compound when subjected to λ ₁ and λ ₂	70
Figure 2.17 UV-Vis absorption spectrum of 8 in CHCl ₃ , transitioning from open to “closed”, recorded over 5 minutes after 30 second intervals of irradiation with short range UV light (λ = 254 nm). Inset shows absorbance increase at 608 nm as function of time.	71
Figure 2.18 Comparison of absorption spectra for 4 : open (---), PSS (···), and calculated closed form (—), in CHCl ₃ . Isobestic point of 334 nm is retained, even in the calculated closed form spectrum.....	73
Figure 2.19 Emission and Excitation spectra of photochromic compound, 4 in CHCl ₃ . Excitation at 330 nm produced emission spectrum (—), and emission at 395 nm produced excitation spectrum (—).....	74
Figure 2.20 a) Absorption spectra of 4 , open form (···) and PSS (—), and emission spectra of 4 (---), λ _{ex} = 330 nm, showing spectral overlap and b) Fluorescence spectral	

changes of compound 4o in benzene upon irradiation with $\lambda = 364$ nm light, with excitation wavelength of 330 nm, concentration of 1×10^{-4} M.....	75
Figure 2.21 (a) Absorption spectra of 9 while irradiated with UV light ($\lambda = 365$ nm), recorded at 30 second intervals, inset, graph showing the increase of absorbance at 613 nm as a function of time (1×10^{-5} M) and (b) absorption spectra of 9o (.....) and 9c (——) showing the difference in absorption at 328 nm and 613 nm between the two isomers.	77
Figure 2.22 Figure 2.22 DFT calculations for molecular switch, both isomers 9o and 9c . Initial primary HOMO-LUMO energy gap correlates well with experimental values....	80
Figure 2.23 Absorption spectra of 3 (——) and 9o (----).....	79
Figure 2.24	79
Figure 2.25 (a) comparison of the emission (——), excitation (——) and absorption (.....) spectra of 9o ; (b) emission spectra of 9 before, during and after irradiation with UV light.....	80
Figure 2.26.....	81
Figure 2.27. Comparison of the UV-Vis absorption spectra of 10o and 10c , inset shows sample under short range UV light (364 nm).....	82
Figure 2.28. Absorbance spectrum of 10 from open to closed, recorded after 30 second intervals under short range UV radiation. Inset shows absorbance at 620 nm as a function of time.....	83
Figure 2.29 The excitation and emission spectra of 10 . Excitation at 405 nm (—) and 380 nm (—), while emission was irradiated at 320 nm (—). Results congruent with a single species.....	84
Figure 2.30. UV-Vis absorption of compound 11	84
Figure 2.31	85
Figure 2.32 Normalised UV-Vis absorption spectrum (1×10^{-5} M) and emission spectrum (1×10^{-6} M), run in CH_2Cl_2 , RT.....	86
Figure 2.33. Normalised UV-Vis of open and closed form isomers (CH_2Cl_2 , 1×10^{-5} M).....	86
Figure 2.34 Fatigue resistance of 8 in hexane solution. Percentage absorbance of first PSS cycle at $\lambda = 608$ nm plotted against cycle number, showing the cycle number dependence of absorbance of irradiated samples.....	88
Figure 2.35 (a) absorption spectra of 5 recorded after 0 cycles (——), 10 cycles (——), 20 cycles (——), 30 cycles (——) and 40 cycles (——); (b) plot of absorbance at 613	

nm vs number of cycles to find the number of cycles needed to decrease the absorbance to 80 % of its initial value.....	88
Figure 2.3690	
Figure 2.37 Photocyclisation quantum yield measurements for compound 4 , in CHCl ₃ at RT. a) irradiating with $\lambda = 330$ nm for 5 minutes and b) plot of closed form concentration vs photon dose with respect to time.....	90
Figure 2.38 (a) absorption spectra of 9 recorded at 30 second intervals when irradiated with 365 nm light from a Xe lamp; (b) plot of concentration of cuvette versus photon dose with respect to time.....	91
Figure 2.39 Linear graph of $y = mx$, where the slope is the quantum yield, Φ	92
Figure 2.40 Cyclic voltammogram carried out in dry, degassed CH ₃ CN on compound 4 , at a scan rate of 0.1 V/s.....	93
Figure 2.41 Cyclic voltammogram carried out in dry, degassed CH ₃ CN on compound 8 , at a scan rate of 0.1 V/s.....	95
Figure 2.42 HBC and N-HSB based molecular switches.....	97
Figure 3.1 ¹ H NMR of 2,3,4,5-tetra-(4-tert-butylphenyl)cyclopenta-2,4-dienone in CDCl ₃ (400 MHz, RT).....	102
Figure 3.2 ¹ H NMR spectra of tetraarylcyclopentadienone compounds X, X and X in CDCl ₃ (400 MHz, R.T.).....	106
Figure 3.3 Comparison of ¹ H NMR spectra of compounds 14, 15 and 16.....	107
Figure 3.4 (a) ¹ H NMR spectra of compound 17 in CDCl ₃ (400 MHz, RT) showing magnification of the aromatic region. Atom labelling as per figure inset.....	109
Figure 3.5 HH-COSY experiment for compound 17	110
Figure 3.6 ¹ H NMR of 18 in CDCl ₃ (400 MHz, RT), with inset showing symmetry of compound and also splitting pattern observed in the aromatic and aliphatic regions.....	111
Figure 3.7 Overall synthetic pathway from starting material to final product.....	112
Figure 3.8. The two intermediates in the reaction pathway to compound DTR	113
Figure 3.9. ¹ H NMR of L18 . The intermediate precursor displays an almost identical proton spectrum to the final compound DTR , though slight more upfield (CDCl ₃ , 400 MHz, RT).....	113
Figure 3.10 ¹ H and ¹³ C NMR of 18	114
Figure 3.11 ¹ H NMR of compound 19 (CDCl ₃ , 400 MHz, RT).....	115
Figure 3.12 ¹³ C NMR spectrum of compound 19 (101 MHz, CDCl ₃ , RT).....	117

Figure 3.13 Absorption and emission spectrum from compound 19 , run in CH ₂ Cl ₂ (1 x 10 ⁻⁵ M). Spectra are normalised to show the difference in emission between high- and low-energy excitation wavelengths.....	117
Figure 3.14 Photochromic ability of proposed compound 21	118
Figure 3.15 ¹ H NMR of 21 , with a focus on the aromatic region (CDCl ₃ , 400 MHz, RT).....	119
Figure 3.16 HMBC NMR experiments run on compound 21	119
Figure 3.17 HSQC and ¹ H- ¹ H COSY experiments of compound 21	120
Figure 3.18 ¹ H NMR of compound X.....	120
Figure 3.19 HMBC assignment of compound.....	120
Figure 3.20 Comparison of the relative shifts seen in the X and X.....	121
Figure 3.21 Comparison of the relative shifts seen in the X and X.....	122
Figure 3.22 ¹ H NMR of the sym and anti-isomers of X.....	123
Figure 3.23 Examination of the aliphatic region of the ¹ H spectrum of 22	124
Figure 3.24 The aromatic region of the ¹³ C spectrum of trimer 22	125
Figure 3.25 A hexasubstituted metallacycloheptatriene and the resulting hexasubstituted phenyl product.....	126
Figure 3.26 HMBC and HSQC experiments performed on trimer 22 (CDCl ₃ , 600 MHz, RT).....	126
Figure 3.27 UV-Vis absorption spectrum for the photocyclisation of switch 20 . Irradiation wavelength λ = 320 nm. (CH ₂ Cl ₂ , 1 x 10 ⁻⁵ M).....	127
Figure 3.28 UV-Vis absorption spectrum for the photocyclisation of switch 21 . Irradiation wavelength λ = 330 nm. (CH ₂ Cl ₂ , 1 x 10 ⁻⁵ M).....	127
Figure 3.29 Normalised absorption spectra of compounds 20 and 21	128
Figure 3.30. Photophysical absorption of compound DAE.....	129
Figure 3.31 Preliminary ¹ H NMR of compound X.....	131
Figure 3.32 Absorption spectra of 10o (.....) and 10c (——).....	132
Figure 3.33 (a) cyclodehydrogenation attempts using molecular switch X would allow a carbon-carbon bond formation between the 4-position carbon and the adjacent phenyl ring. This coupling was hoped to hinder the formation of stable side products (b) and also allow a more conjugated absorption pattern in the closed form isomer.....	133
Figure 3.34 Initial cyclodehydrogenation attempts using DDQ in acidic conditions resulted in a plethora of luminescent compounds from precursor X.....	134
Figure 3.35 DFT calculations for future HBC-based dithienylethene switches. HOMO of compound lies across the sterically hindered and overlapping tert-butyl groups of the	

inner phenyls, whilst the LUMO sits slightly more spread across the dithienylethene-octafluorocyclopentene core.....	135
Figure 3.36	136
Figure 3.37 Variable temperature NMR studies of compound X (20 °C, 40 °C, 60 °C, 80 °C, CDCl ₃ , 400 MHz, RT).....	137
Figure 4.1 Conjugated 1,10-phenanthroline derivatives.....	141
Figure 4.2 ¹ H NMR spectrum of Ir-1 and Ir-2 showing complete assignment of the proton signals (400 MHz, CD ₂ Cl ₂ , RT).....	145
Figure 4.3 ¹ H NMR spectrum of Ir-3 and Ir-4 showing complete assignment of the proton signals, with inset showing methyl signals present further upfield (400 MHz, CD ₂ Cl ₂ , RT).....	146
Figure 4.4 (a) Overlaying ¹ H NMR spectra of (a) Ir-1 and Ir-3 , (b) Ir-2 and Ir-4	149
Figure 4.4(b) ¹ H NMR of Ir-1 – Ir-4 stacked showing downfield phen-singlet in bromine substituted complexes (blue), the thienylacetylene substituted complexes (red), and the growth of the thienyl proton signal in Ir-3 and Ir-4	150
Figure 4.5 Asymmetric unit of Ir-1 with atomic displacement parameters shown at 50% probability and (b) Packing structure diagram of Ir-1 viewed along the b-axis.....	151
Figure 4.6(a) Absorption spectra of complexes Ir-1 and Ir-2 in varying solvents (1 x 10 ⁻⁵ M), showing both normalised and unaltered transitions.....	152
Figure 4.6 (b) Emission studies of Ir-1 and Ir-2 , carried out in air and under argon (1 x 10 ⁻⁶ M). Both solutions showed significant emission quenching when exposed to air...	153
Figure 4.7 Absorption spectra of complexes Ir-1 and Ir-2 in varying solvents (1 x 10 ⁻⁵ M), showing both normalised and unaltered transitions.....	154
Figure 4.8 Emission of Ir-3 and Ir-4 carried out in air and under an argon atmosphere.....	154
Figure 4.9 Normalised UV-Vis absorption of Ir-1 , Ir-2 , Ir-3 and Ir-4	155
Figure 4.10 ¹ H NMR (400 MHz) of Compound 3 in CDCl ₃ with aromatic region magnified.....	155
Figure 4.11 ¹⁹ F NMR, showing the splitting pattern of the fluorinated backbone.....	155
Figure 4.12 UV-Vis Spectra of Compound 3 in DCM with conc. 1 x 10 ⁻⁵ M when irradiated with UV light with time intervals of 30 seconds and plot showing the increase in absorption at 603 nm with respect to exposure time.....	156

Figure 4.13 DFT (B3LYP, 6-31g basis set) visualisation of compound 3 's MOs, displaying the HOMO and LUMO orbitals of both photoisomers.....	157
Figure 4.14 TD-DFT calculations for compound X. ^a Only selected excited states were considered. The numbers in parentheses are the excitation energy in wavelength. ^b Oscillator strength. ^c H stands for HOMO and L stands for LUMO. Only the main configurations are presented. ^d coefficient of the wavefunction for each excitations. The CI coefficients are in absolute values.....	158
Figure 4.15 (a) UV-Vis Spectra of 3 displaying the large differences in the absorption between the PSS and open states at 603 and 310 nm (b) displays the plot used in the evaluation of the quantum yield of 5 through establishing a ratio between reacted molecules and photon flux.....	159
Figure 4.16 X-ray crystallographic analysis of 3 . A clear, pale-blue rod-like crystal of 3 , approximate dimensions 0.060 mm x 0.080 mm x 0.320 mm, was used analysis and yielded the shown unit cell and packing structure. Compound showed photochromic switching capability in both solid and whilst in solution.....	160
Figure 4.17 ¹ H NMR of 7 in CDCl ₃ displaying large amounts of non-first order coupling in the aromatic region. Upfield methyl signals not shown for clarity.....	164
Figure 4.18 Photochemical analysis of compound 7 showing (a) increased luminescent intensity upon degassing with Ar, suggesting strong phosphorescent character, (b) solvation studies of 7 , and (c) excitation and emission spectra under Ar ($\lambda_{\text{exc}} = 440 \text{ nm}$, $\lambda_{\text{em}} = 610 \text{ nm}$, $1 \times 10^{-6} \text{ M}$).....	165
Figure 4.19 Initial computational experiments show (a) the selected orientation of the organic π -platform, (b) the HOMO character of the ligand which exists mainly on the thienyl moieties and (c) the LUMO which is delocalised across the phen moiety and through the spinning triphenyl groups.....	166
Figure 4.20 ¹ H NMR of Compound 14 in CDCl ₃ with overlapping phenyl signals highlighted.....	168
Figure 4.21 HSQC of compound X.....	169
Figure 4.22 (a) UV-Vis Spectrum of 8 (b) UV-Vis Irradiation Spectrum of 8	169
Figure 4.23 (a) Luminescence quenching of 8o and (b) emission, excitation & absorption Spectra of 8o	170
Figure 4.24 ¹ H NMR of 9 displaying a very similar spectral pattern to that of 8 , however with the additional signals corresponding to ppy ligands and subsequent shielding of the phenanthroline protons upon complexation.....	171
Figure 4.25 ¹³ C spectrum of Ir-7	178

Figure 4.26 HMBC of Ir(III) switching complex Ir-8	178
Figure 4.27 (a) Absorption spectrum of open and PSS states of 9 (2.5×10^{-5} M) and (b) isomer interconversion and phosphorescence of 9 in air.....	173
Figure 4.28 (a) comparison of the luminescence intensity under Argon and in air, (b) the excitation, emission & absorption in CH ₃ CN at 1.2×10^{-5} M concentration and (c) UV-Vis irradiation spectrum of 9	174
Figure 4.29 Comparison of absorbance spectras of (a) 6 , 7 , 8o and 9o and (b) 3c , 8c and 9c	175
Figure 4.30 Symmetrical side product from the Diels-Alder reaction may be used to investigate unsymmetrical metallic system, or possibly in the use of cation capture.....	176
Figure 4.31 Low Temperature, 77 K, study of complex 9 , with a notable blue-shift occurring between the emission profiles.....	178
Figure 4.32 Cyclic voltammetry of complex 9 upon a continuous oxidation cycle and the corresponding change in absorption spectra indicating photocyclisation has occurred..	180

List of Schemes

Scheme 1.1 Switching between two reversible photoisomers with an azobenzene moiety.	7
Scheme 1.2 Representation of the photoisomerisation that occurs with spiropyrans.....	10
Scheme 1.3 Photoisomerisation reactions that occur in photoswitchable fulgides.....	11
Scheme 1.4. Typical conformations of diarylethenes.....	13
Scheme 1.5 Structure of (a) hexaphenylbenzene and (b) hexa-peri-hexanbenzocoronene.	26
Scheme 1.6 Synthesis of hexaphenylbenzene derivatives (i) benzophenone, 300 C, (ii) Co ₂ (CO) ₈ , dioxane reflux (iii) CuCl ₂ /AlCl ₃ or Cu(OTf) ₂ /AlCl ₃ or FeCl ₃ /CH ₃ NO ₂ (R, R' and R'' refer to alkyl substituents.....	27
Scheme 1.7 Decay of Diarylethene based molecular switch.....	32
Scheme 1.8 Synthesis of Brominated 1,10-Phenanthrolines (Phen-2-7). Three synthetic routes include the use of i) 1,10-phenanthroline monohydrochloride monohydrate, Br ₂ , PhNO ₂ . ii) Fuming Sulfuric acid (30%), Br ₂ . iii) Br ₂ , pyridine, 1-chlorobutane, S ₂ Cl ₂ . iv) SCl ₂ , Br ₂ , pyridine, 1-chlorobutane. v) SOCl ₂ , Br ₂	33
Scheme 1.9 Ru(II) dendritic polypuridine complex (i) o-xylene (solvent), 140 C, 97 % (ii) RuCl ₂ (DMSO) ₄ , DMF, 140 C, 55 %	39

Scheme 2.1 Catalytic bromination reaction of 2-methylthiophene using NBS and perchloric acid, at room temperature, to yield compound 1	47
Scheme 2.2 Synthetic route to compound 2 , (i) TMSA, CuI, P(Ph) ₃ , Pd(PPh ₃) ₂ Cl ₂ , NHEt ₃ , DMF, 120 °C, 25 minutes, (ii) KF, TBAF, MeOH, THF, overnight, RT and (iii) 1 , CuI, P(Ph) ₃ , Pd(PPh ₃) ₂ Cl ₂ , NHEt ₃ , DMF, 130 °C, 30 minutes.....	47
Scheme 2.3 Synthesis of 3 , (i) THF, ethylene glycol, 2 M NaCO ₃ , PdCl ₂ (PPh ₃) ₂ (1 mol %), 80 °C, 17 h, 58 %.....	48
Scheme 2.4 Sonogashira coupling of 1-ethynlthiophene and 3,5-dibromo-2-methylthiophene using standard and microwave chemistry (Pd(Ph ₃) ₂ Cl ₂ , CuI, PPh ₃ , 110 °C, 20 mins, 71 %.....	49
Scheme 2.5 Sonogashira coupling of 1-ethynlthiophene and 3,5-dibromo-2-methylthiophene using a microwave. (i) TMSA, Pd(Ph ₃) ₂ Cl ₂ , CuI, PPh ₃ , 110 °C, 2 x 10 mins, (ii) KOH, MeOH, overnight, 51 % (iii) Pd(Ph ₃) ₂ Cl ₂ , CuI, PPh ₃ , 130 °C, 30 minutes, 70 %.....	50
Scheme 2.6 Synthesis of iodohexaphenylbenzene, 6 (i) Benzophenone, 280 °C, 2 hours, 280-300 °C 16 hours, Ar (65 %).....	51
Scheme 2.7 Synthesis of 3-bromo-2-methyl-5-(1-ethynlHPB)thiophene, 7	51
Scheme 2.8 Reaction of n-BuLi, brominated thienylethynylaryl appendages and perflurocyclopentene to yield target switching compounds.....	59
Scheme 2.9 Lithiation of compound 8 , generating photochromic molecular switch 4 , (i) carried out at -78 °C in THF with octaflurocyclopentene and n-BuLi, 2 hours, Ar, 61 % yield. Inset shows real time photochromic ability of 8 on silica column.....	60
Scheme 2.10 Synthesis of 9 , (i) THF, Et ₂ O, BuLi, -78 °C, 1.5 h; (ii) THF, -78 °C, 4 h, 63 %	61
Scheme 2.11 Reaction of 4 , n-BuLi and perflourcyclopentene that generates photochromic molecular switch 10 , (i) carried out at -78 °C in THF with octaflurocyclopentene and n-BuLi, 2 hours, Ar (49 % yield).....	61
Scheme 2.12 Reaction of 5 , n-BuLi and perflourcyclopentene that generates photochromic molecular switch 11 , reaction under Ar in THF, 1 hour, (45 %).....	63
Scheme 2.13 Synthetic procedure towards molecular switch 12 (i) n-BuLi, octaflurocyclopentene, -78 °C, 2hrs, 65 % (ii) KF, TBAF, MeOH/THF, overnight, 81 % (i) Pd(PPh ₃) ₂ Cl ₂ , CuI, PPh ₃ , iodohexaphenylbenzene, NHEt ₂ , overnight, 90 °C.....	64

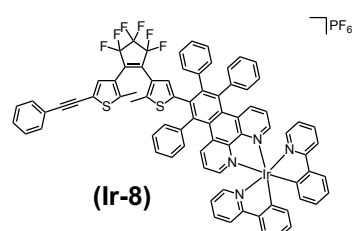
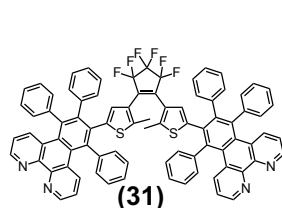
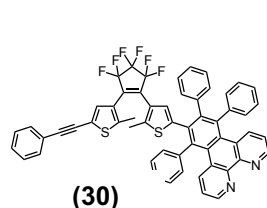
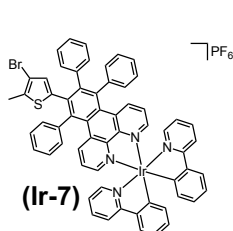
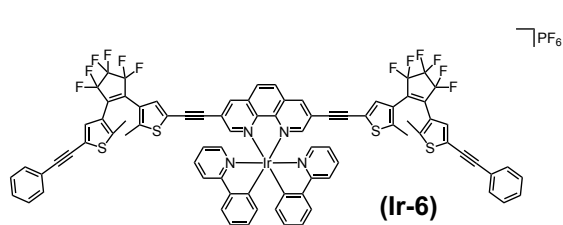
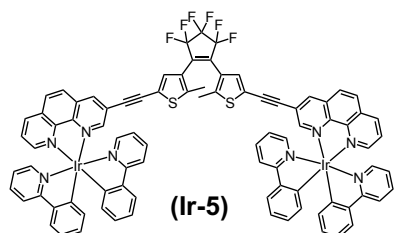
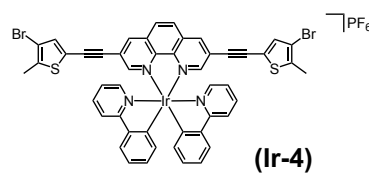
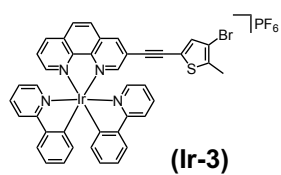
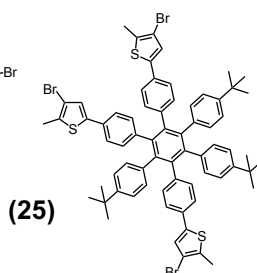
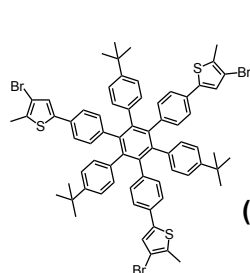
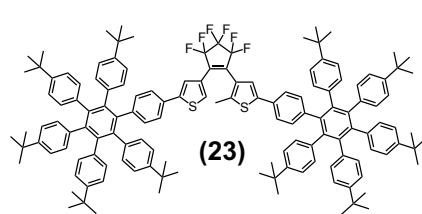
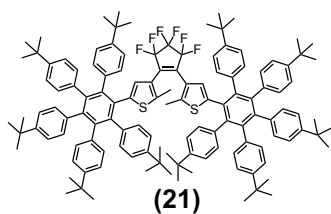
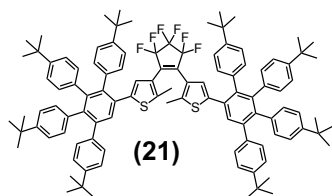
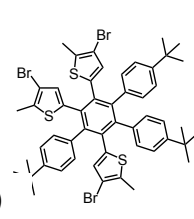
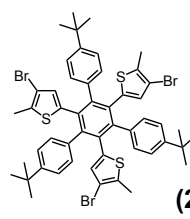
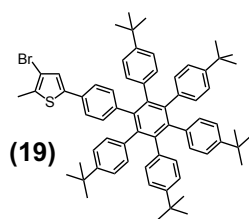
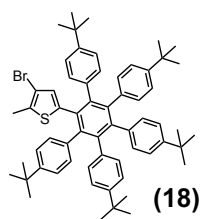
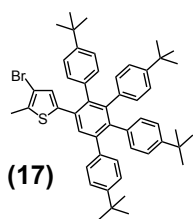
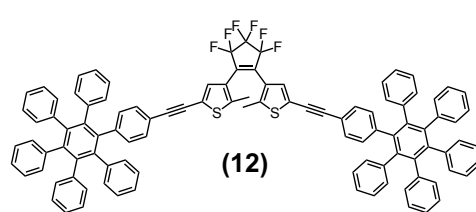
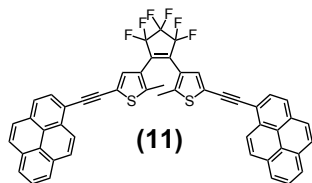
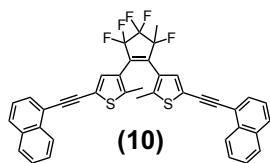
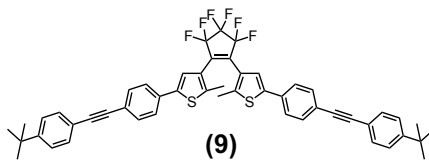
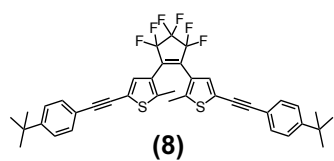
Scheme 3.1 Synthetic route for the formation of substituted hexaphenylbenzenes, divided into constituent parts: (i) procedure of des Abbayes to synthesise 1,3-diarylpropanones (red); (ii) procedure of Mueller-Westerhoff for the synthesis of 1,2-diketones (blue); (iii) two-fold Knoevenagel reaction for the synthesis of tetraphenylcyclopentadienones...	102
Scheme 3.2. Synthetic route and reactions of 13 , with L13 and L14 , (i) in the presence of KOH in ethanol at 95 C for an hour(81 %).	103
Scheme 3.3 The syntheses of tetraarylcyclopentadienones, 14-16 , (i) KOH, CH ₃ CH ₂ OH, 90 °C.	104
Scheme 3.4 Syntheses of thienyl-HPB compounds 17 and 18 , (i) Benzophenone, 250 °C, 6 hours, Ar (ii) Benzophenone, 300 C, overnight, Ar.	108
Scheme 3.5 Mechanism proposed by Hart et al, using excess phenylmagnesium bromide and showing key intermediates.	112
Scheme 3.6 Synthesis of 19 , benzophenone, 300 °C, 5.5 h, 19 %	115
Scheme 3.7 Synthesis of 10 , (i) benzophenone, 9 , 300 °C, 5.5 h, 0.32 %	132
Scheme 3.8 (i) n-BuLi (x 5 equiv), octafluorocyclopentene (in xs)in THF at -78 C, 4 hrs, under Ar (ii) n-BuLi, 2 , overnight, under Ar.	140
Scheme 3.9 An alternate pathway to product XA, XB and XC, with n-BuLi, octafluorocyclopentene and compound 2 in THF: diethyl ether at -78 C, under Ar.	141
Scheme 4.1. Synthesis of 3-bromo-1,10-phenanthroline (i) Br ₂ , S ₂ Cl ₂ , pyridine, 1-chlorobutane, 80°C, 12 h, yield: 50%	142
Scheme 4.2 The coordination reactions of brominated ligands using the same reagents to form complexes Ir-1 and Ir-2 (i) [Ir(ppy) ₂ (μ-Cl)] ₂ , CH ₂ Cl ₂ , 40 °C, 16 h. Yields: 96 % Ir-1 and 94 % Ir-2 .	143
Scheme 4.3 The Sonogashira cross-coupling reactions towards final Ir(III) cyclometallated complexes Ir-3 and Ir-4 , (i) 3-bromo-2-methyl-5-ethynlthiophene, Pd(PPh ₃) ₂ Cl ₂ , PPh ₃ , CuI, Et ₃ N/DMF(2:5), 60°C, 24 h and (ii) 3-bromo-2-methyl-5-ethynlthiophene, Pd(PPh ₃) ₂ Cl ₂ , PPh ₃ , CuI, Et ₃ N/CH ₃ CN(2:5), 60°C, 17 h.	144
Scheme 4.4 Retrosynthetic analysis towards (a) precursor compound MC1 and (b) Ir-TTPBP .	153
Scheme 4.5 Optimised synthetic routes to 4 . i) MeOH, KOH, rt, 12 h, 56 %. ii) Al ₂ O ₃ , chlorobenzene, 130 °C, 24 h. iii) Microwave assisted synthesis; Al ₂ O ₃ , 1:9/CH ₂ Cl ₂ :THF, 125 °C, 150 W, 0.5 h.	161

Scheme 4.6 Synthesis of **7** through complexation of **6** to Ir(ppy)₂ following heating for 12 hours at 45 °C and consequent exposure to a source of the counterion PF₆⁻163
Scheme 4.7 Restrosynthetic analysis of molecular switches **8** & **9**.....167

List of Compounds.....xxii

Abbreviations.....xxiii

List of Compounds



Abbreviations

μL	micro-litre
μs	micro-second
1D	one-dimensional
2D	two-dimensional
A	area
Å	Angstrom
a.u.	arbitrary units
Abs.	Absorption
AcOH	acetic acid
Anal.	elemental analysis
Ar	aryl
bby	2,2-bipyridine
br	broad
C	Celsius
Calcd.	calculated
cat.	catalytic
cm⁻¹	wavenumber
COSY	Correlation Spectroscopy
CT	charge transfer
CV	Cyclic voltammograms
d	doublet
dd	doublet of doublets
DFT	Density Functional Theory
DEPT	Distortionless Enhancement by Polarisation Transfer
DMPD	1,4-dimethylpiperazine-2,3-dione

DMSO	Dimethyl Sulfoxide
e⁻	electron
E	Redox Potential
e.s.	excited state
em.	emission
eq.	equivalents
ESI-MS	Electrospray mass spectrometry
EtOH	ethanol
exc.	excitation
fl.	Fluorescence
g	gram
g.s.	ground state
HBC	hexa-peri-hexabenzocorone
HMBC	Heteronuclear Multi-Bond Connectivity
HOMO	Highest Occupied Molecular Orbital
HPB	Hexaphenylbenzene
h	hour
HSQC	Heteronuclear Single Quantum Coherence
Hz	Hertz
IC	Internal conversion
IL	Intra-ligand
IR	Infrared
ISC	Inter-system crossing
<i>J</i>	Coupling constant
K	Kelvin
<i>kJ</i>	kilojoule

LMCT	Ligand-to-metal charge transfer
LUMO	Lowest Unoccupied Molecular Orbital
m	multiplet
M	metal
M	molarity
min.	minimum
mol	mole
m.p.	melting point
<i>m/z</i>	mass to charge ratio
MALDI-TOF	matrix assisted laser desorption/ionisation – time of flight mass spectrometry
max	maximum
Me	methyl
mg	milligram
MHz	megahertz
ml	millilitre
MLCT	Metal-to-ligand charge transfer
MS	Mass spectrometry
nm	nanometre
NMR	Nuclear Magnetic Resonance
ns	nanosecond
Nu-	nucleophile
OLED	organic light emitting diode
ox.	Oxidation
PAH	polycyclic aromatic hydrocarbons
Ph	phenyl
phen	1,10-phenanthroline

ppm	parts per million
PSS	Photostationary State
R_f	Retention factor
RT	room temperature
s	singlet
sec	second
sh	shoulder
solv.	solvent
t	triplet
TDDFT	time dependent density functional theory
tert	tertiary
THF	tetrahydrofuran
TLC	thin layer chromatography
TMS	trimethylsilylacetylene
UV-Vis	ultraviolet-visible
V	volt
vs.	versus
°	degrees
δ	chemical shift
Δ	heat
ε	molar absorption coefficient
φ	quantum yield
λ	wavelength
%	percentage

- 1. The theory, synthesis and photophysical properties of photochromic molecular switches generated from dithienylethene**

1.1 Introduction

Information storage is at the forefront of materials science due to an exponential increase in the demand for faster, more efficient and higher density data storage units, and for miniaturised devices. Light-driven photochromic switching compounds form one of the most active areas of research, operating at both the molecular and supramolecular scales. This work describes a series of dithienylethene-based switches synthesised with appended polyaromatic “ligands” of increasing conjugation, designed to explore the effects of increased aromaticity of both the appendages, and of the coordination environment of the thienyl-core, on the molecules’ photophysical properties. Studies of these systems allow insight into the use of these switches in memory devices, as well as into the effect substituents play on the bulk properties of the system. In this case, aromatic moieties and how they influence colour change, photochemical quantum yield, fatigue resistance, thermal conversion, as well as photostationary state conversion. Further tuning of the synthetic design, redox and photophysical properties are ongoing to establish the potential of these new systems in a range of device applications.

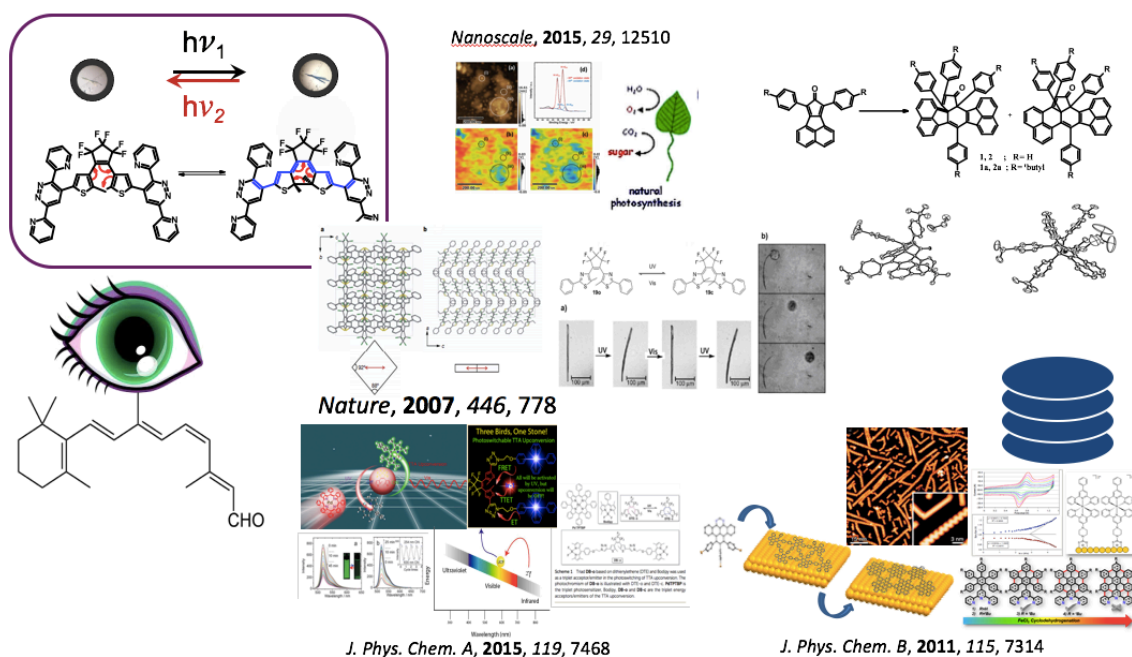


Figure 1.1 Molecular switches and their use throughout nature and scientific technology, from human vision and discotic liquid crystals on surfaces, to using conformational changes to inhibit changes on a macroscale, such as pushing a ball of silica across a medium or tuning the upconverting ability of a photosensitiser.

Molecular switches, and molecular nanomachinery technology has gained significant interest in the last number of years, due this exponential rise in the fields of computer science and technology for increased efficiency. Molecular electronics can help to extend Moore's Law – the prediction that the number of transistors on integrated circuits will double approximately every two years – beyond the physical limits of silicon devices. It involves incorporating functions and properties of traditional semiconductors (such as transistors and diodes) into single molecules, providing advantages such as small size, low cost and being able to tailor device properties. As such, much of the research being conducted internationally is to address these types of problems and produce viable options. However, the power of the molecular switch allows a great deal of control over normally infallible photophysical pathways. This can range from the signal induction in synthetic photosynthesis, to the more interesting but equally mostly irrelevant paper published in Nature in 2007¹, of a group who used the size and conformation changes inherent in photochromic crystals to push a ball of silica across a solvated media. With the ability to elicit change from a microscale in a minute bond rotation, and act consequentially up to the macroscale, in molecular shuttles and nano-machinery, our understanding of the molecular switch technology could have a profound effect on the evolution of our technological limits.

1.2 Molecular Switches

Molecular switches are compounds that can convert between one distinguishable form and another on exposure to an external stimulus, be it light²⁻⁴, electricity⁵, pH⁶, temperature⁷, electrochemical reduction⁸ or any combination thereof.⁹ One of the oldest and most common types of these switches in chemistry is the pH indicator, which changes colour as a function of the acidity of a solution.⁸ Although generally very simple molecules, molecular switches can act as the basis for much bigger and more complex molecular machinery and supramolecular frameworks. Switching molecules play key roles in information technology and in the field of advanced materials, in applications of optical memory devices, photo-switches and future use in molecular electronics and nanomachinery.¹⁰ Originally inspired by nature, researchers are now examining a multitude of aspects of molecular switches, and how their environment and ligand associations affect their various opto-electronic properties. Molecular switches have generated a large degree of interest in material science due to their potential application in the field of computing, with the 2016 Nobel Prize in Chemistry awarded “for the design and synthesis of molecular machines”¹¹, a component of the nano-machinery research of this report. Their potential for high-density storage,

Chapter 1: Introduction

increased data interpretation efficiency and high speed at the nano- and even picosecond scale, all present as enormous advantages over current semi-conductor technologies. Secondary applications have also been investigated; such as molecular shuttles¹², photochemical manipulation of nanoscale structures¹³, photocatalysis¹⁴ and sensors¹⁵. A variety of structures have been identified capable of operating as photochromic molecular switches; these include azobenzenes¹⁶, stilbenes¹⁷, spiropyrans¹⁸, viologens¹⁹, salicylaldehydes²⁰, furylfulgides²¹ and diarylethenes (DTEs).²² The latter are the focus of this project, with aims to optimise current molecular designs and address any prevalent and ongoing limitations to improve the operation of the switching phenomenon. These include fatigue resistance, non-destructive fluorescence readout and quantum yield efficiency.

Light-driven photochromic molecular switches form one of the most active areas of inquiry due to their use in devices that operate at both a molecular and supramolecular scale, and the often-reversible generation of two distinct chemical isomers upon irradiation of each isomer with different wavelengths of light. However, various other stimuli may be used instead, and more recently in tandem with one another, and switches may be designed and synthesised based on these external and conformational requirements. Nature itself probably affords some of the best-known examples of how these systems affect and impact our daily lives. In an oversimplification of our internal mechanics, at a basis level, human beings are, despite the deliberate contradiction, merely extremely complex computers. Our own visual perception, our ability to see the world through the “extraction and processing of data” from visible light, is itself a photochromic switching process. At a fundamental level, our sense of sight comes from the change in the isomerisation of a molecule, a chromophore 11-*cis*-retinal, and the protein conformational conversions that occur to accommodate this light-induced structural change.²³ Molecular switches offer a very advantageous avenue for a wide-range of interconnecting fields. Faster data processing and high-density data storage technologies are in development, with photochemical processes currently being exploited for use in these potential applications. It has been calculated that an estimated 2×10^9 data bits cm^{-2} can be achieved for the world of data-handling²⁴ as the need for faster, smaller and more powerful data-storage units becomes exponentially greater. A green and much more energy efficient by-product of this is that the use of fast, high quantum yield processes could potentially reduce the heat load of computing devices, and thus produce far more efficient and sustainable systems.

1.2.1 Types of Molecular Switches

The following section gives an outline into the types of molecular switches that have been synthesised. Molecular switches that react under the influence of light are said to be photochromic i.e. they undergo reversible transformations when irradiated with light of a suitable wavelength.²⁵ Such photochromic compounds may be divided into two distinct groups, the T-types²⁶ (thermally reversible) and P-types²⁶ (photochemically reversible), and usually exist in two distinct forms classified as “open” and “closed”. The distinction stems from the potential pathways of cycloreversion that results in the formation of the open isomer. P-type switches exclusively react due to light exposure while T-types will decompose thermally to the isomer of the lowest ground state energy. The large difference in stability observed between the isomers of the T-types has served to focus attention on the P-types (furylfulgides and diarylethenes) which have come to the fore in molecular switch research.²⁷ Of these two molecular P-types, however diarylethenes are generally favoured due to their higher fatigue resistance and more manageable synthesis.²⁸

1.2.1.1 Host-guest Molecular switches

In host-guest chemistry the bistable states of molecular switches differ in their affinity for guests. Many early examples of such systems are based on crown ether chemistry. The first switchable host is described in 1978 by Desvergne & Bouas-Laurent^{29,30} who create a crown ether via photochemical anthracene dimerisation. Although not strictly speaking switchable the compound is able to take up cations after a photochemical trigger and exposure to acetonitrile gives back the open form. In 1980, Yamashita et al.³¹ constructed a crown ether already incorporating the anthracene units (an anthracenophane) and also studied ion uptake vs photochemistry. Also in 1980 Shinkai threw out the anthracene unit as photoantenna in favor of an azobenzene moiety³² and for the first time envisioned the existence of molecules with an on-off switch. In this molecule light triggers a trans-cis isomerisation of the azo group which results in ring expansion. Thus in the trans form the crown binds preferentially to ammonium, lithium and sodium ions while in the cis form the preference is for potassium and rubidium (both larger ions in same alkali metal group). In the dark the reverse isomerisation takes place. Shinkai employs this device in actual ion transport mimicking the biochemical action of monensin and nigericin.^{33,34} In a biphasic system, ions are taken up triggered by light in one phase and deposited in the other phase in absence of light.

1.2.1.2 Mechanically interlocked molecular switches

These types of switches differ from most others in that the connections between the various molecules is based on structural topology, interlocked, kinetically trapped macrocycles and not through traditional covalent or ionic bonding.³⁵ Catenanes and rotaxanes, composed of two or more interlocking components, are the main types (Figure 1.2) and these spawned the term topological isomers.³⁶ Frisch and Wasserman in 1961 described this class of molecule, showing that the newly configured topological isomer of two macrocyclic compounds was chemically distinct from the reactivity of the individual macrocycles. Studies of these mechanically interlocking species have shown them to possess a unique bistability due to differing recognition sites and has given rise to the “molecular shuttle” described by Stoddart in 1991.³⁷ This shuttle was the basis for more intricate and advanced molecular systems that could be used for data storage, which was later described by the same author in 1994.³⁸ In 2004 Heath *et al*³⁹ used molecular shuttles in an experimental DRAM circuit, in which bistable, [2]rotaxane molecules served as the data storage elements.

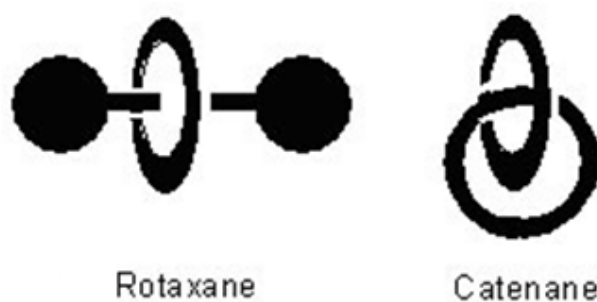


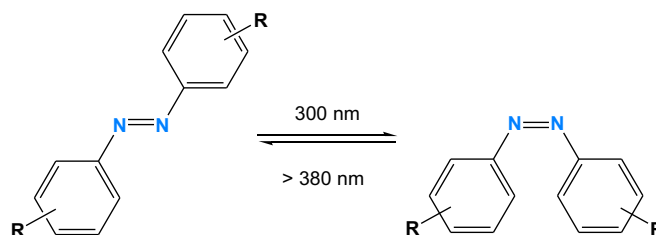
Figure 1.2 Generic structure of a Rotaxane and Catenane

1.2.1.3 Photochromic Molecular switches

Photochromic switches are systems that use light to generate differentiated isomers, due to their fast response times and the compatibility of light with a wide range of condensed phases.⁴⁰ Light is also particularly effective in its ability to spatially and temporally induce structural and functional changes in molecules and materials while at the same time having the potential to be non-destructive.⁴¹ Switching molecules absorb photons of light and in turn use the energy generated to close/open bonds. These types of molecules encompass the main focus of this research, with particular emphasis on diarylethene derivatives with thienyl rings. The “ligand” substituents affect the fatigue resistance of the compound, that is the number of repeatable cycles a switch can undergo before performance is notably decreased, much in the way of turnover numbers (TON's) of biological catalysts and photocatalytic devices. The difference in the ability of the transmission of electronic interactions over the structure of the molecule is also affected by substituent type, as well as the isomerisation of

the compound and its molecular symmetry. π -conjugation is interrupted whilst the switch is in its open form, causing a degree of electronic localisation, but not while the switch is closed. Modulation of absorption and emission response is due to this increase in the degree of π -conjugation, and the increase in the planarity of the molecule, upon closure. A change in the absorption spectra between open and closed, most notably the new absorption peak found in the visible region of the closed isomer, is responsible for the colour change from clear to coloured.⁴²

Organic photochromic molecular switches can switch between two thermally addressable states (as shown in Scheme 1.1) with stimulated conversion taking place by the irradiation of a particular wavelength of light. These two isomers not only differ in their absorption spectra profiles, but in many various secondary properties such as geometrical structures, oxidation potentials, quantum yields⁴³, refractive indices, dipoles, electro-conductivities etc.⁴⁴ Both states of the switch should be able to be addressed separately and these differences can help in the identification of the isomer type generated and in the comparison of the properties of the two forms.



Scheme 1.1 Switching between two reversible photoisomers with an azobenzene moiety.

Photochromic compounds have really only gained significant interest over the past few decades or so, due to the notable work of Masahiro Irie and Kingo Uchinda, though work in the field has extended back as far as the 1960's. These compounds have come under much scientific inquiry due to their potential applications in not only various industrial settings, but in commercial environments as well, such as recordable compact discs⁴⁵ and light sensitive sunglasses.⁴⁶ Photochromism, as mentioned before, denotes the light activated reversible transformation between two chemical isomers, which display absorption spectra that are not only different but also readily distinguishable.^{47,48} Thus the molecular structure and function of these molecules changes upon irradiation and, if incorporated into functional molecules such as polymers, can cause drastic changes in the bulk properties of the compound by responding almost instantaneously to external stimuli at a molecular level.⁴⁰

Thus we have a way of not only manipulating the conductive and opto-electronic properties of the system, but potentially their geometric structures in space as well. Construction of the basal photochromic units is based on numerous classes of organic molecules and ligands. These include spiropyrans^{49,50}, azobenzenes⁵¹, fulgides⁸, spirooxazines⁵⁰ and switches based on C=C double bond *cis-trans* isomerisation.⁴⁰ During bond rearrangement, unwanted side products are generated at low quantum yields due to the facile nature of the photoexcited states, which limits a switch's durability, and build up as the cycle continues. This will directly affect the fatigue resistance and bulk nature of the system demonstrated by individual classes of molecule. Overcoming this is a current primary research goal for potential applications.

Azobenzenes are a subclass of photochromic molecules that have been investigated for decades and still continues to generate new and unique optic results, which are put to numerous uses in switchable catalysts⁵², biomolecules⁵³ and liquid crystals⁵⁴. It is characterised as by two phenyl rings bridged together with an azo linkage (-N=N-). As seen with many photo-switching molecules it is the aromatic components that gives rise to the intense optical absorption spectra, as well as the substituent moieties added on the backbone of the switch. A major advantage of azobenzene type switches is their ease of synthesis, however the disadvantage lies in the fact that thermal isomerisation can occur at room temperature. The two states that exist are the thermally stable E configuration (*trans*) and the meta-stable Z isomer (*cis*). Irradiating light within the band of the *trans* state will cause a photochemical isomerisation. However, this now generated *cis* isomer can thermally relax back to its previous E state, though the lifetime of the species can typically depend on the substitution patterns and local environment. This can also mean that other conditions, such as pH, temperature and solvent type may all have a role to play. Irradiation however with light corresponding to the Z isomer absorption band can also cause the reverse isomerisation to occur. The process works by a photon of light being absorbed by the molecule, which leads to movement of the phenyl rings about the azo bond. Even with the possible thermal relaxation possibilities, this is one of the cleanest photoreactions that exists, as it does not generate a significant amount side products. Figure 1.3 shows the state model for azobenzene.

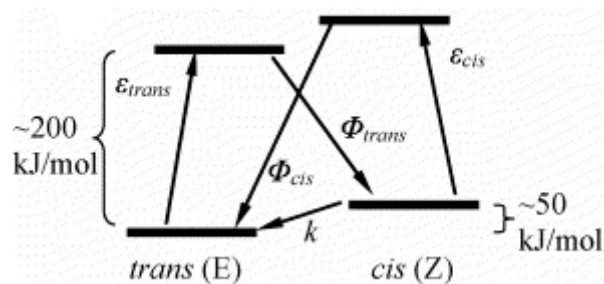


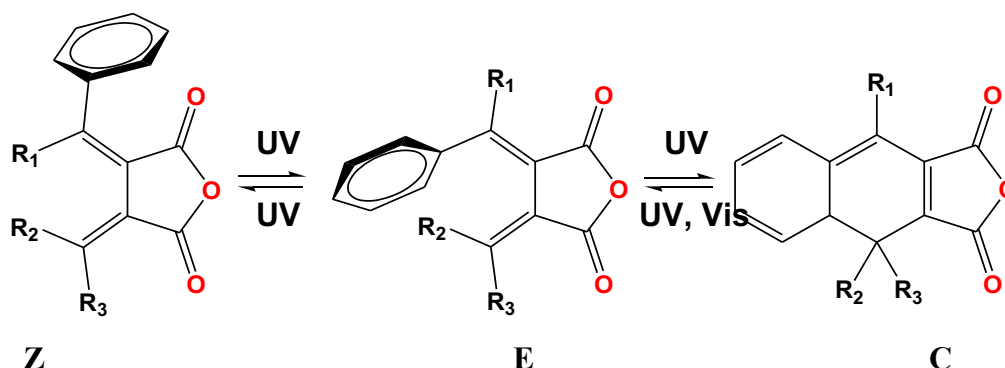
Figure 1.3 Simplified state model for azobenzene. ϵ are the excitation coefficients and Φ labels the quantum yields.

The photochromism of spiropyrans was first described by Fischer and Hirshberg in 1952.⁵⁵ At that time, spiropyrans in solution were known to exist in a thermal equilibrium with a colored modification. Fischer and Hirshberg showed that the same colored species formed upon UV excitation.⁵⁵ The colored form reverts thermally to the parent spiropyran at room temperature. This process can be accelerated by excitation with visible light. Researchers postulated that in the colored species the bond between the oxygen atom and the spiro-carbon was broken^{56,57}, but initially there was no general agreement on the exact structure of this molecule. In the 1960s, the colored modification was proven to be a merocyanine-type molecule, with a delocalised structure in between the quinoid and zwitterionic forms.^{58,59} Fischer et al. found that, depending on the temperature, different species were formed upon excitation of a spiropyran.⁶⁰⁻⁶⁴ They attributed this phenomenon to the formation of different geometric isomers. In the merocyanine, all three bonds between the two ring structures have a bond order >1 and are therefore rigid. This situation yields a total of eight possible isomers. All the experimentally observed isomers were assumed to have a trans-arrangement at the central bond. The corresponding cis-isomers were ruled out for steric reasons. Theoretical calculations predict the TTC isomer to be the most stable one.⁶⁵⁻⁶⁷ Time-resolved absorption techniques have shown that the different isomers can be interconverted by irradiation.⁶⁸⁻⁷⁰ Although in most cases the closed-ring spiropyran is the more stable structure at room temperature, several systems have been identified in which the open merocyanine form is the thermally stable one.⁷¹⁻⁷³

Scheme 1.2 represents the light-activated isomerisation of spiropyran moieties, switching between a stable and meta stable state using UV/Vis radiation. The spirocyclic “closed” isomer is typically hydrophobic while the zwitterionic merocyanine isomer to highly polar

photocoloration process.⁸⁷ They proved that the color change was in fact the result of the 6π -electrocyclisation of a fulgide to a dihydronaphthalene succinic anhydride-type structure that could be reverted thermally or photochemically to the original fulgide, or could be oxidised to a naphthalene succinic anhydride. Hart and Heller⁸⁸ showed that the photoinduced process obeys the Woodward-Hoffmann rules. In 1984, Kaftory obtained a crystal of the colored form of a fulgide and studied it by X-ray diffraction, thereby determining the structure of the cyclised molecule unequivocally. When neither of the two substituents at the methyldiene opposite to the aryl group is a hydrogen, and hydrogen abstraction is therefore not possible, [1,5]-H⁸⁸ or [1,3]-H^{90,91} shifts can occur instead, creating more stable aromatic structures.

Aside from diarylethenes themselves, fulgides are probably the best candidates for use in optical memory devices due to their high thermal stabilities and fatigue resistance.⁹² When irradiated with the appropriate UV light, the colorless isomer of a fulgide (**E**), changes through a cyclic reaction into a coloured isomer (**C**). This process obeys the Woodward-Hoffmann rules (i.e. the photochemical rearrangement occurs in conrotatory fashion). The **E** form can also convert into another form while the photocyclisation is occurring due to a simple photochemical **E-Z** double bond isomerisation. **C** and **Z** both absorb UV light, so converting between **E** and **Z** forms, and between **E** and **C** forms, continue until a photostationary state (PSS) is reached. But only **C** absorbs visible light, so by irradiating the **C** form by visible light causes only the transformation from the **C** to **E**, until the **C** form disappears completely. Since change in absorption is the requirement for photochromism, the transformation between **E** and **C** forms is usually termed fulgide photochromism as shown in Scheme 1.3 below.⁸



Scheme 1.3 Photoisomerisation reactions that occur in photoswitchable fulgides

In attempts to overcome the undesirable side-reactions, Heller et al. designed mesitylfulgide **MSF-1**.⁹³ As there are no hydrogens on either of the carbons involved in the formation of the new bond, the abovementioned side reactions cannot occur. An additional advantage of this design turned out to be that in the closed form the steric repulsion between the methyl groups on both sides of the new bond prevents the disrotatory thermal ring-opening process, making it the first example of a fulgide for which the cyclised form is thermally stable at room temperature. The main disadvantage of this system was the slow photocyclisation. This problem was overcome by replacing the mesityl by a dimethylfuryl group and by the introduction of an additional methyl group, forming fulgide **MSF-2**.⁹⁴ This molecule has all the advantages of previous fulgides, but also undergoes significantly faster cyclisation.

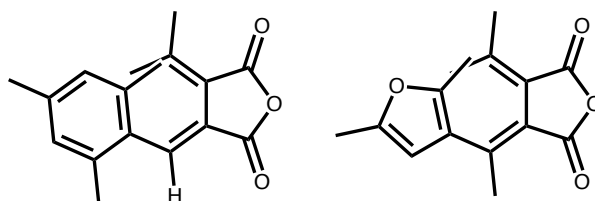


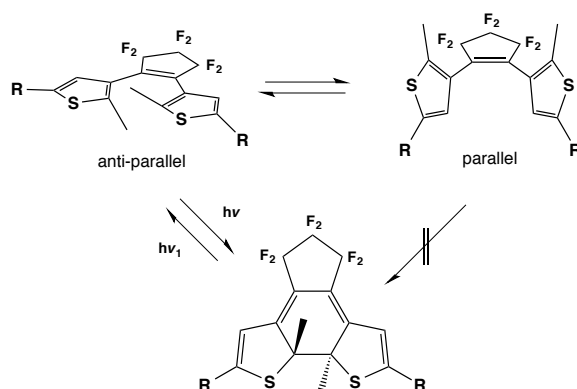
Figure 1.4 Switches **MSF-1** and **MSF-2**, designed by Heller et al.

1.3 Diarylethenes

Diarylethenes, a subclass of photochromic materials, are one of the main focal points of current photochromism research. As molecular switches, they exist as thermally stable isomers, typically a colourless open-ring form and a coloured closed-ring form generated upon specific irradiation wavelengths (Scheme 1.4).⁹⁵ Their thermal stability and high fatigue resistance are one of the main reasons that they are chosen for use in various applications.⁹⁶

Absorption spectroscopy⁹⁷ studies and NMR analysis applied to photochromic investigations⁹⁸ show that diarylethenes have two open-ring conformers; C_s (mirror) symmetry is found in the *parallel* form and C_2 symmetry in the *antiparallel*. The closed form exists as an enantiomeric pair (*R,R* and *S,S*) due to asymmetric carbon atoms.¹ Open forms of the diarylethene moiety contain a hexatriene structure, but only one shows photoactivity through its photoexcited state and undergoes induced cyclisation in a conrotatory fashion to the closed form.^{1,98} The thermal back-reaction would have to occur in a disrotatory mode, in accordance with the Woodward-Hoffman rules. This means that as the *trans*-methyl constituents sterically hinder the back-reaction, there is a resulting high thermal stability in

the closed-ring isomer. Specifics in the type of aryl groups chosen do also affect this property. Only through the irradiation of the molecule with, in a majority of cases, visible light does the closed form undergo the transition to the open form. The conrotatory photocyclisation reaction is only achieved when the open-ring form is in C_2 symmetry, in the *antiparallel* conformation. According to Irie *et al.*, “since the interconversion between the conformers occurs in a time scale larger than the excited-state lifetime, only the light absorbed by the *antiparallel* form can induce photocyclisation”.⁹⁹



Scheme 1.4. Typical conformations of diarylethenes.

The open isomer is generally colourless and the closed isomer often deeply coloured e.g. yellow, red or blue (depending on its structure) due to electronic and geometrical differences between their molecular arrangements. The open-ring form is non-planar due to the free rotation available around the ethene moiety and aryl groups. This means that there is a localisation of the π -electrons around this aromatic region and thus a lack of localised π -electron density around the double bond. The absorption maximum is usually found in the UV range³ and occurs when the molecule is open, both in the *parallel* and *antiparallel* conformations. Ring closure of the excited state of the *antiparallel* form leads to a planar central diarylethene moiety through photocyclisation and the formation of a central carbon-carbon bond. This delocalises the π -electron density across the whole molecule and leads to an absorption maximum that extends into the visible region, and a higher polarisability overall.¹⁰¹

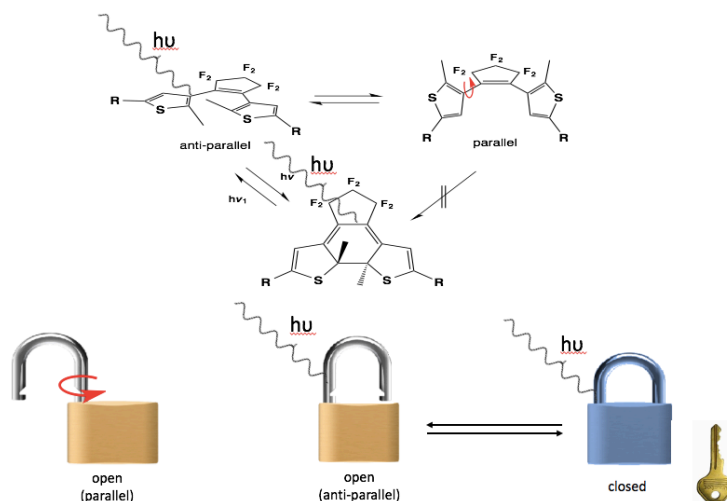


Figure 1.5 Diarylethene bond rotation can be thought of like a lock and key, only in the correct conformation and with the correct force will the lock open and close.

By using these specific wavelengths of light what is effectively generated is an “ON/OFF” style device. Studies carried out on photochromic diarylethenes have indicated that the 5- and 5'- positions of the five-membered ring aryl moieties, most notably in thiophene derivatives, are the most influential when it comes to the colouration efficiency of the switch, allowing for further tunability of the device.¹⁰² The alkane backbones usually chosen for photochromic work are perfluorocyclopentene ring systems, though four- or six-membered rings sometimes appear in literature, due to the prevention of *cis* to *trans* photoisomerisation. Recent work has also suggested that cyanide moieties, or even large polycyclic aromatics, may be used instead with variant results. Decreasing the ring size of the perfluorocyclopentene shifts the closed ring absorption maximum to longer wavelengths. Ring size also controls the planarity of the molecule, and thus controls the extent of the π -conjugation in the closed form. The cyclisation quantum yield as a result of this is also dependent on ring size, with higher values being observed for six-membered rings. Five membered rings take both of these attributing factors into account and are the most appropriate cycloalkane structure. In the following few sections, some of the key photophysical and chemical features of this photochromic family of compounds are discussed.

1.3.1 Thermal Conversion

Photochromic chromophores are divided into two distinct subclasses. If the isomers are thermally unstable and revert to their previous states even when subjected to dark conditions

they are known as thermally reversible types (T-types). Most photochromic molecules belong to this class. Molecules that are thermally stable, which includes most synthesised diarylethene compounds, are photochemically reversible types (P-types). Some P-type molecules have shown thermal irreversibility at significantly raised temperatures ($\sim 150\text{ }^{\circ}\text{C}$) for extended periods of time, which makes them very useful in molecular switching devices.¹⁰³ Open ring isomers are generally thermally stable. This can be seen from state correlation diagrams of the electrocyclic reactions of much more basic substructure units, which serve as a synthetic basis for a photochromic switches diarylethene core, as shown in Figure 1.6

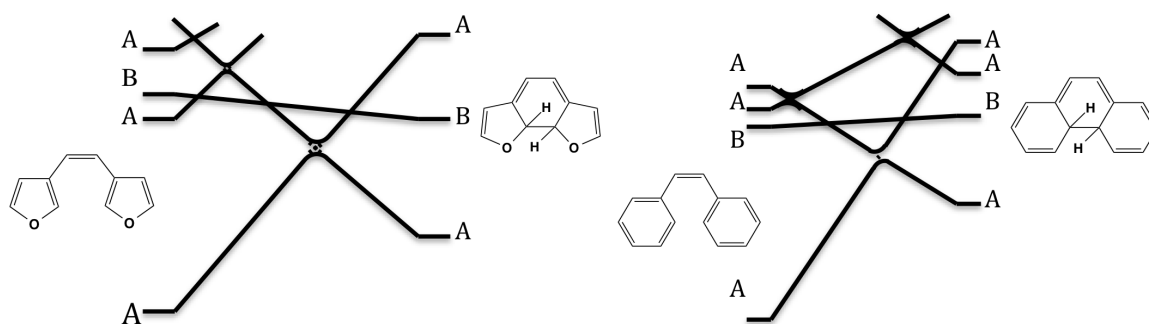


Figure 1.6 State Correlation diagrams for electrocyclic reactions of 1,2-di(3-furyl)ethene and 1,2-phenylethene. The right hand side of each diagram represents the closed ring conformations of each molecule, with the central hydrogens in a trans configuration. Relative energy differences between open- and closed-ring isomers are 9.2 and 27.3 kcal/mol, respectively.

The ground state of the open-ring reactant molecule is lower in energy than the generated closed-ring isomer. The thermal stability of this closed ring form is largely dependent on the aryl groups assigned to be a part of the molecular backbone of the compound. Furyl, thienyl and thiazole based rings, which have low aromatic stabilisation energies, show the strongest degree of thermal stability. Photo-generated states containing phenyl, pyrrole or indole rings are generally thermally unstable, due to having much higher aromatic stabilisation energies. Irie and co. have shown varying levels of thermal stability and conversion for numerous synthesised switches, with lifetimes ($t_{1/2}$) ranging from 37 seconds at room temperature to > 90 days at $80\text{ }^{\circ}\text{C}$. Electron withdrawing groups at the 5- and 5'-position and bulky substituents at the 2- and 2'-position, can cause deviations for the aromatic stabilisation energy rule as the photo-generated central carbon-carbon bond becomes significantly weakened due to the presence of these groups. Thermal stability is an extremely important

factor in the development of switches with real-world applications, and novel switches are designed to avoid the problem of a thermochromic response.

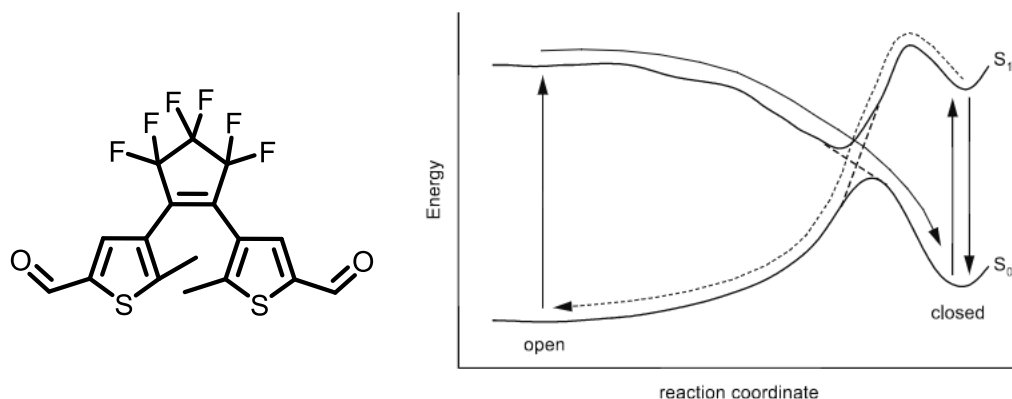


Figure 1.7. Schematic illustration of the S_0 and S_1 potential energy surfaces of DTE-1o/DTE-1c as sections along the reaction coordinate.

Early studies on diarylethenes employing transient absorption techniques with picosecond time resolution showed that both the cyclisation and cycloreversion processes are very fast, with time constants $\tau < 10$ ps. Ern et al. conducted a thorough study of the excited-state properties of dithienylcyclopentene, DTE-1, shown in Figure 1.7 combining femtosecond transient absorption techniques and excited-state potential energy surface calculations. They found that upon excitation of the open-ring species, structural relaxation occurs along a barrierless pathway on the S_1 potential energy surface, followed by a decay to the ground state via a conical intersection. From this point, either the closed form is formed, or the molecule returns to the open form. The high quantum yield for the cyclisation of this molecule shows that the former process is preferred. The entire cyclisation process occurs with a time constant $\tau = 2.0$ ps. Upon excitation of the closed form, an excited state species is formed with a lifetime $\tau = 13$ ps. The relatively long lifetime reveals that for the closed form, barrierless relaxation along the excited state surface toward the conical intersection is not possible. Instead, the species relaxes to a local minimum on the excited state energy surface, and from there the decay to the ground state is dominated by internal conversion. Only a small fraction of the excited-state species crosses the barrier to the conical intersection and proceeds in the direction of the open-ring structure. Further studies by the same research group on several other diarylethenes showed that this excited-state model is generally applicable to diarylethene-type molecules. Quantum chemical calculations carried out by another group support the findings of Ern et al. Uchida et al. reported that, in rare

cases, relaxation to an unreactive local minimum on the excited-state energy surface can occur upon excitation of an open-form diarylethene, but for most systems this pathway is unimportant.

1.3.2 Fatigue Resistance

All molecules within a diarylethene switching system may convert from their open forms to their closed form (or *vice versa*) upon the irradiation of the right wavelength source. However, this is not often the case. A 100 % conversion between both isomers after irradiation of λ_1 and λ_2 is the ideal of a perfect molecular switching network. However, not all molecules will revert perfectly between the two states. A reason for non unity yield in diarylethene derivatives is due to steric considerations, in which a mixture of the *parallel* and *antiparallel* conformers exist together.³ As discussed, only the *antiparallel* configuration is photoactive so at any one time only those in this confirmation will “close” when irradiated with light of the correct wavelength.

Photochromic compounds are, by their very nature, accompanied by a rearrangement of chemical bonds. Due to the promotion of an electron into a higher energy orbital, the rearrangement reaction may compete with other photochemical reaction pathways and it is this process that can allow unwanted photochemical side reactions to occur. This will hinder the number of cycles a photochromic compound may endure before there is a noticeable difference in overall performance of the system. As an example, in a system that contains a sample switch, there is a clean conversion between the open and closed states. However, if a competing side reaction generated from the photoexcited state of the open form, that has a quantum yield of 0.001, is also occurring, then after just a 1,000 cycles, the initial concentration of the open isomer will have decreased by over 63 % due to degradation.³²

1.3.3 Absorption Spectra

Even though a substantially wide-range of diarylethene-derived systems exist today, and more are currently in development, it is possible to describe some of their spectroscopic behaviour in general terms. Absorption spectra of the two isomers are perhaps the most fundamentally different and the most identifiable characteristics, due to their very definition as photochromic compounds. The absorption spectrum of the ring-open form consists of n- π^* and π - π^* bands of the thiophene-moieties, at the wavelengths between 200 and 300 nm. The absorption spectrum of the open-ring isomer can also depend on the upper alkene

Chapter 1: Introduction

structures, and ring structures such as maleic anhydride and maleimide can have a moderate bathochromic shift on the absorption bands. Irradiation into the UV bands using ultraviolet light results in photocyclisation, and continued exposure of the sample will eventually lead to a photostationary state (PSS). This system is made up of switches in their closed isomer form, but usually contains some of the open form due to the incomplete photocyclisation often seen during these processes. This is also partly due to the fact that the closed form absorbs in the UV region of the spectrum.

The most prominent change observed is the growth of the characteristic highly red-shifted ground state to the first excited state transition absorption band, $S_0 \longrightarrow S_1$, now found in the visible region, giving the molecule its distinctive colouration. Irradiating into the visible region of the PSS absorption spectrum results in the decolouration or bleaching of the system due to photocycloreversion. Though photocycloreversion often has a lower quantum yield than the photocyclisation process, the solution is generally bleached within a few minutes of continuous irradiation. A significant challenge with these systems is that the readout must be non-destructive – i.e. the probing light must not induce a photochromic response while the data is being read. In development of device applications such as in optical memory media, it is desired to develop photochromic compounds that have sensitivity in the wavelength region of *ca.* 650 – 850 nm. Manipulation of the substituents is a prominent goal due to their effect on the absorption maxima observed, in an attempt to develop near-infrared light sensitive photochromic compounds.

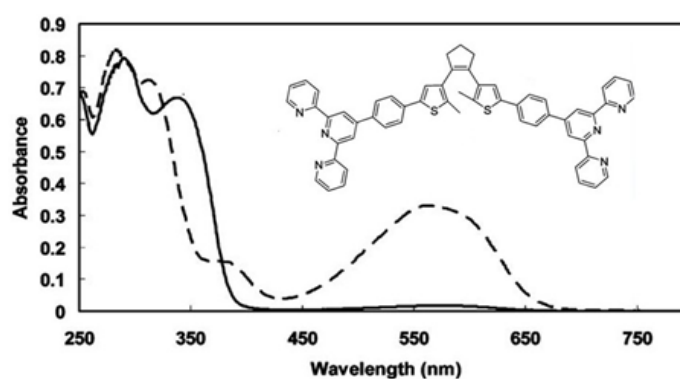


Figure 1.8. Molecular Switch UV-Vis Spectra showing both closed form (- - -) and open form (—)

Switches thus present with two main absorbance maxima, correlating to the $n \rightarrow \pi^*$ and $\pi \rightarrow \pi^*$ transitions of the thiophene moieties in both the closed and open isomers. The

increased level of delocalisation observed in the closed isomer results in a bathochromic shift in the absorption, maxima in the case of the compound seen in Figure 1.8, from 255 nm to 552 nm.¹⁰⁴ In the open form the electron density is localised to the thiophene rings while in the closed form conjugation is extended outwards into the π systems of the phenyl spacer and terminal tripyridine. The lowering of the HOMO-LUMO gap observed in the closed form shifts the $\pi \rightarrow \pi^*$ transition of the thiophene system into the visible region leading to the yellow colour observed in the compound. Diarylethene derivatives with second and third row metal centres display at least one extra peak corresponding to the MLCT transition, though this peak may be obscured beneath much more intense spin-allowed transitions. The energy of this absorption may be tuned via alteration of the metals, ligands and the level of delocalisation within the system. In this manner the metal centre may be used as a photosensitiser. It has been shown that irradiation at the MLCT absorption can lead to photocyclisation.¹⁰⁵ Hect *et al.* has discerned that this may increase the fatigue resistance as it prevents the 1,2-dyotropic rearrangement that results in the major side product of isomer interconversion. As these MLCT transition bands usually occur at lower energies than the $\pi \rightarrow \pi^*$ of the central thiophenes they may be exploited in the interconversion of isomers, provided their quantum yield is sufficiently high

1.3.4 Quantum Yield

As discussed previously, the photocyclisation reaction for diarylethenes may only proceed when the two rings are in an *antiparallel* conformation. As it is only this C_2 symmetry conformer that is photoactive, its proportion in the system directly affects the overall photocyclisation quantum yield. Quantum yield can be described here as the number of photons absorbed by the system to cause a photocyclisation reaction per photons emitted by the irradiating light. As the open form conformers are generally thought to exist in a 1:1 ratio, this makes the presence of each atropisomer roughly 50 % (rapid interconversion between the two isomers is often difficult). Some quantum values in the literature are thus corrected to account for this “equal” balance of *parallel* and *antiparallel*, making them artificially high and therefore unreliable, as a system in actuality may preferentially take on one conformation over another. This also means that the quantum yield of photocyclisation for a system may in reality be half of the reported value. Numerous methods have been employed, however, to increase the amount of the *antiparallel* form a system adopts, strategies such as increasing the steric bulk at the 5- and 5'-thienyl positions (e.g. with large polycyclic aromatic hydrocarbons), or by confining the switch in space. This is done in a

molecular framework by only allowing confirmations of the desired photoactive state to occur, taking advantage of the differences in molecular structure between the two isomeric forms.

The low photocycloreversion quantum yields seen in diarylethene based molecular switches is often attributed to the large extension of the π -conjugation throughout the closed form. The antibonding nature in the excited singlet state of the central photo-generated carbon-carbon bond decreases with the extension of π -conjugation, and the weak antibonding character is considered to decrease the light induced cycloreversion quantum yields. Uchinda *et al* showed this for numerous compounds, with various quantum yields reported, and in other cases this value has been shown to be quite high, with values of 0.76 reported by van Esch *et al.* for some perfluorodithienylcyclopentene switches.¹⁰⁶

The efficiency of the cycloreversion process depends on other factors than that of the cyclisation reaction. Some types of diarylethenes show intrinsically high cycloreversion quantum yields, but for simple representatives of the popular class of dithienylperfluorocyclopentenes the yields only occasionally exceed 0.1 and often are much lower.¹⁰⁷ Cycloreversion quantum yields depend on the extent of conjugation in the closed-form molecule. Upon substitution of the diarylethene with groups extending the π -conjugation, the cycloreversion efficiency decreases.^{108,109} Irie *et al.*¹⁰⁸ ascribed this feature entirely to a decrease in anti-bonding nature of the reactive C-C bond in the singlet excited state, while Bens *et al.*¹⁰⁹ assume that a decrease of the excited state lifetime upon increase of the conjugation also plays a role. Significantly higher cycloreversion quantum yields can be achieved by substituting the methyls in the 2-positions of the thienyl rings with electron-withdrawing cyano groups. The inverse effect is observed when the methyls are replaced by electron-donating methoxy groups. These substitutions do not significantly affect the cyclisation efficiency.

1.3.5 Emission and non-destructive readout capabilities

Radiative emission from the first excited singlet state, S_1 , to the lower energy ground state, S_0 , is deemed fluorescence. It is a competing pathway in the photophysical and photochemical processes an absorbing compound may undergo after absorbing a photon of light. Open-forms of the diarylethenes can be quite strongly fluorescent, depending on the attachment of a fluorophore, a fluorescent chemical compound. However, the closed-form

isomer can usually quench this fluorescence through energy transfer upon system photocyclisation using UV light. The difference in the fluorescent intensities of the isomers are invaluable in fluorescent photoswitching and fluorescent imaging, and tuning of their characteristic emission and absorption profiles in solid state and in solution help to generate non-destructive readout capabilities in optical devices.

1.3.6 Electrochemical properties.

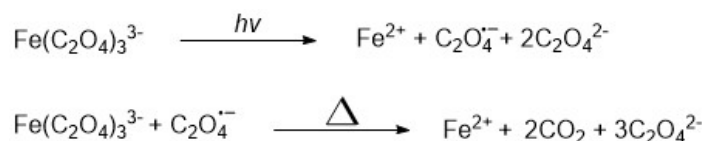
In their closed form, diarylethenes are oxidised and reduced more easily than in their open forms. In 1995, Koshido et al. described a diarylethene that underwent cycloreversion upon oxidation of the closed-form molecule.¹¹⁰ Since then, it has been shown that both the cyclisation and the ring-opening reactions can be triggered by oxidation in certain cases. In 2005 three research groups independently published studies on the mechanism behind the oxidative cyclisation/cycloreversion process.¹¹¹ Their results are largely in agreement. It has been found that most diarylethenes can either undergo the oxidative cyclisation or the oxidative cycloreversion reaction. The direction of the reaction depends on the relative stability of the cationic species. If the open-form cation is lower in energy than the cation of the cyclised molecule, electrochemical ring-opening will occur. If the cation of the cyclised species is lower in energy, however, oxidative cyclisation will be observed. By introducing proper substituents, the stability of the cations can be influenced and the direction of the reaction can be reversed.

1.4 Chemical Actinometry

As the quantum yield is calculated in solution, both the photoreactive antiparallel and photoinactive parallel configurations of the open isomer are present in near equal amounts, this theoretically halves the calculated value. Irie *et al.* displayed that this may be circumvented through the analysis of the switch in the crystalline phase¹¹² in which the molecules are arranged in the anti-parallel configuration of the crystal lattice. This method has yielded values close to unity. In the case of this project the steric bulk introduced by the iridium metal centre, its ligands and the system of phenyls used in its coupling to the dithienylethene moiety were expected to reduce the preponderance for the parallel configuration. The evaluation of quantum yield is determined through chemical actinometry. The number of photons emitted per second by a fluorescence spectrometer may be calculated through monitoring the photochemical reaction of ferrioxalate. Proposed by Hatchard and

Chapter 1: Introduction

Parker in 1956, upon light excitation potassium ferrioxalate decomposes as per the following equation



Equation 1.1 Photochemically Driven Decomposition of Ferrioxalate

Chelation of phenanthroline ligands to the ferrous ions being formed may be monitored by the change in absorption at 510 nm. The non-complexed ferrous ions will not absorb at the given wavelength and as a result the moles of chelated ferrous ions formed is given by

$$\text{Moles of } \text{Fe}^{2+} = \frac{V_1 \times V_3 \times \Delta A(510 \text{ nm})}{10^3 \times V_2 \times l \times \epsilon(510 \text{ nm})}$$

Equation 1.2 Determination of $[\text{Fe}^{2+}]$

where all volumes are given in millilitres and V_1 corresponds to the irradiated volume, V_2 to the sample used in UV-Vis analysis and V_3 to the volume after chelation of phenanthroline. l is the length of the cell used, $\Delta A(510 \text{ nm})$ is the difference in absorbance between the irradiated sample and the previous absorbance taken in the dark and $\epsilon(510 \text{ nm})$ is that of the $\text{Fe}(\text{phen})_3$ complex. With the number of moles of Fe^{2+} calculated the number of photons absorbed per unit time ($\frac{N h \nu}{t}$) given in moles/second may be determined thus

$$\frac{N h \nu}{t} = \frac{\text{moles of } \text{Fe}^{2+}}{t \times F \times \phi}$$

Equation 1.3: Determination of Photon Flux

Where t is irradiation time and F is the mean fraction of light absorbed by the ferrioxalate solution. The value for $\frac{N h \nu}{t}$ may then be considered then as a constant in consequent quantum yield evaluations in which the number of reacted molecules per unit time is monitored via changes in absorbance maxima²⁶.

$$\phi = \frac{\text{number of reacted molecules per unit time}}{\text{number of photons absorbed per unit time}}$$

1.5 Tuning of Photochemical Properties

The photochemical properties of the switch may be tuned via the sidechains on the dithienylethene backbone and the resultant effect observed may be quantitatively measured in respect to quantum yield and fatigue resistance analysis. Quantum yield is defined as the number of reacted molecules or switches turned “on” per unit time relative to the number of photons irradiated per unit time. Fatigue resistance refers to the systems resistance to decay upon successive isomer interconversions. Molecular switches based on dithienylethene derivatives have three main domains that may be varied to tune the properties of the switch. The backbone which connects the dithienyl domains may be altered to induce a red shift in absorbance maxima of the compound, reduce the compounds sensitivity to hydrolysis or to increase solvency¹¹³.

Common adaptations to the backbones are octafluorocyclopentene, diarylmaleimides and maleic anhydrides. The groups situated at the 2 and 2' positions of the thiophene rings are required to have π -bonds in order to facilitate the lowering of the HOMO-LUMO gap. The extent of this delocalisation determines the difference in absorbance maxima of the switch isomers and as such the absorbance maximum of the closed form may be influenced through chemical modification. These systems have been shown to facilitate a wide variety of moieties with varying effects. In recent years, incorporation of phenanthroline derivatives has garnered interest in materials and inorganic chemistry due to its sp^2 configuration, its notable effect on the HOMO-LUMO energies in complexes, and the presence of nitrogens within the ring structure which may be used in chelation of a metal centre and afford a degree of aromaticity to the system. However, little research has been undertaken regarding 1,10-phenanthroline substituents incorporated into photochromic structures.

1.6 Polycyclic Aromatic Hydrocarbons (PAHs)

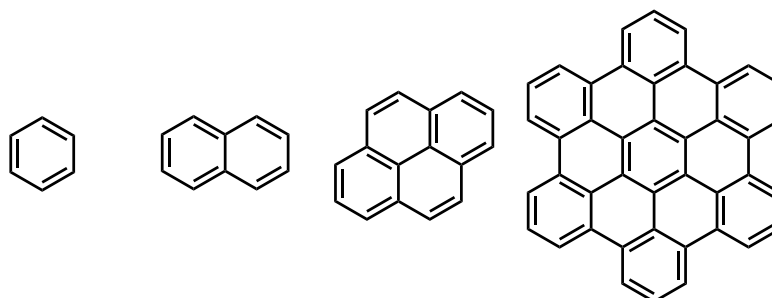


Figure 1.9. Examples of polycyclic aromatic hydrocarbons (PAHs)

Chapter 1: Introduction

Polycyclic aromatic hydrocarbons (PAHs) are large, two-dimensional graphite sections, usually thought of as homologues between the properties of molecular benzene and those of graphene, an indefinitely large aromatic molecule. Graphene based materials, and their heteroatom analogues, have in recent times gained significant scientific interest due to their numerous beneficial chemical and physical properties, and applications, such as low weight and high strength, and their extremely efficient heat and electrical conductivity. The rigidity and shape of hexaphenylbenzene molecules have been exploited in the generation of large surface polyphenylene support frameworks for multi-chromophoric arrays. Mullen et al. have prepared a series of these light harvesting arrays, in which three different types of chromophore are incorporated into a rigid polyphenylene scaffold.¹¹⁴ By attaching a donor moiety on the periphery and an acceptor in the centre, efficient transfer of excitation is achieved by production of an energy gradient between the periphery and the core.¹¹⁵ Importantly, application of a rigid polyphenylene framework ensures that self quenching of the chromophores is not observed as backfolding of dendrimeric branches is not possible.

As a further example, Moore and co-workers prepared artificial functional analogues of natural photosynthetic antenna-reaction centre complexes, in which the hexaphenylbenzene serves as a scaffold to organise five bis(phenylethynyl)anthracene antenna moieties and one porphyrin fullerene dyad as an electron donor-acceptor unit.¹¹⁶ The molecular architecture facilitates rapid and efficient singlet energy transfer from all antenna moieties to the porphyrin, with a quantum yield near unity, upon which photoinduced electron transfer occurs. The efficient coupling of light harvesting antennae with an electron donor-acceptor system is facilitated by the hexaphenylbenzene core, in which photoactive subunits are tethered via acetylene linkages.

Work presented here serves as an initial stepping stone to these multi-functional processes, and to future work in metal-complexation using nitrogen-doped hexasuperbenzenes (N-HSB). More work on functionalising PAH backbones, previously developed by past group members, is also currently underway.

1.6.1 The use of Hexaphenylbenzenes and Hexabenzocoronenes in Molecular Switches

HBC (hexa-*peri*-hexabenzocoronene) is a discotic polycyclic aromatic hydrocarbon (PAH), which consists of 42 carbon atoms.¹¹⁸ PAHs are defined as fused ring materials which consist of sp^2 carbons.³⁵ HBCs are analogous with graphene and have extensive electron delocalisation and are chemically stable.¹¹⁹ These graphene based materials, and their heteroatom analogues, have in recent times gained significant scientific interest due to their numerous beneficial chemical and physical properties, and applications, such as low weight and high strength, and their extremely efficient heat and electrical conductivity.

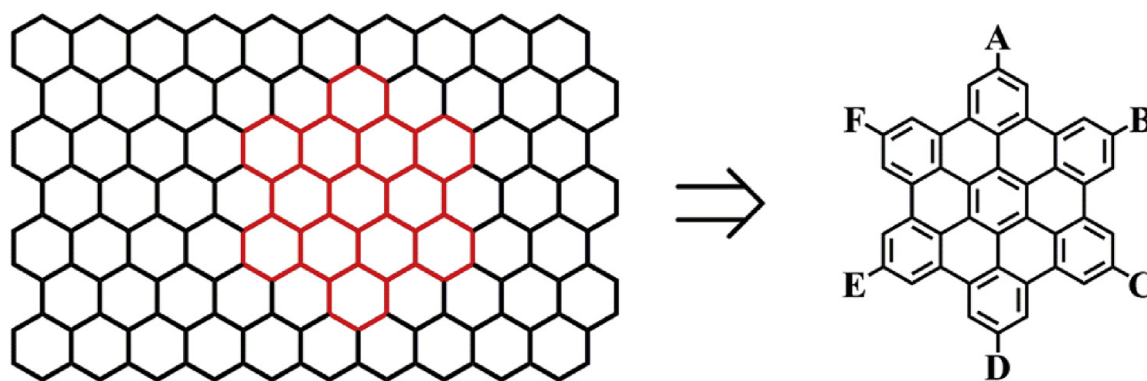
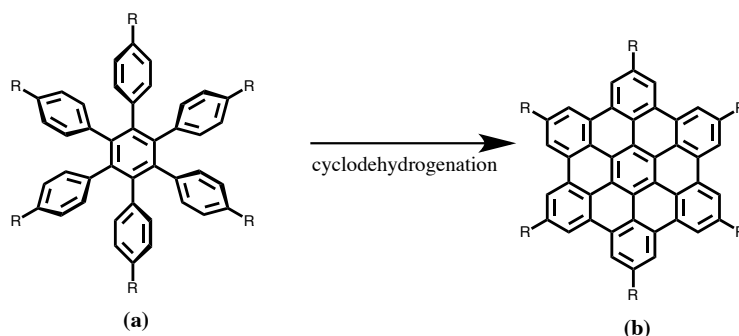


*Figure 1.10 Structure of hexa-*peri*-hexabenzocoronene and its relationship with 2D graphene-sheets*

Polycyclic aromatic hydrocarbons, such as the hexa-*peri*-hexabenzocoronene (HBC) shown in Figure 1.10, allow easy, lab-scale synthetic routes to assessing PAH functionality in various systems. These include a route to finding more effective diarylethene based switches, a primary goal of this research. Increased photocyclisation and photocycloreversion quantum yield efficiency, more highly red-shifted closed-isomer absorption spectra, increased fatigue resistance of the compound caused by the theoretically plausible cyclodehydrogenation reaction with the dithienyl-moiety are but a few of the proposed optoelectronic properties hoped to be realised. These structures may also be potentially realised as viable contestants in the field of single-molecule fluorescence photoswitching, an essential pathway in ultrahigh-density optical memories and super-high-resolution fluorescence imaging. Research in this area has been hampered so far by the destructive readout pathways, which exist for current photochromic models. Design of such novel systems would allow non-destructive fluorescence readout capability and storage of

processed data within a system, with photo-induced electron transfer serving as the photoswitching mechanism.



Scheme 1.5 Structure of (a) hexaphenylbenzene and (b) hexa-peri-hexanbenzocoronene.

The prerequisite in the synthesis of HBCs is hexaphenylbenzene (HPB). HPBs have the same number of phenyl rings as HBCs, however, the rings are not fused and hence the molecule is less aromatic than HBC. The HPB molecule contains six peripheral phenyl rings which have free rotation around the central ring, which resemble a propeller¹²⁰ (Scheme 1.5). HBPs can then be converted to the planar HBCs by carrying out a cyclodehydrogenation.

Recently, Moore et al have applied hexaphenylbenzene as a scaffold for the preparation of a molecular switch which also functions as a molecular analogue to a transistor (Figure 1.11).¹¹⁷ Five light harvesting chromophores, bis(phenylethynyl)anthracene (BPEA) and a dithienylethene photochrome are organised by a central hexa-ethynyl-polyphenylene scaffold. When the DTE is in its open form, fluorescence derived from the BPEA moieties is observed, with a quantum yield near unity. When the DTE is closed, induced by a steady state illumination of the hexad with an excitation wavelength $\lambda = 365$ nm, BPEA fluorescence is strongly quenched by energy transfer to the closed DTE. This emission may be modulated by illumination with red light of wavelength $>\lambda 610$ nm, which induces the photoisomerisation to the open form and consequently increases BPEA emission. Essentially, the molecule acts as a nanoscale transistor, in which $\lambda_{em} = 520$ nm fluorescence is the device output and the modulating $\lambda = 610$ nm illumination acts as a gate voltage of the transistor. The ability to control intense shorter wave fluorescence with longer wave light is relatively unusual and may have applications in biomedical imaging, facilitating the detection of emission from a probe molecule without interference from other materials.

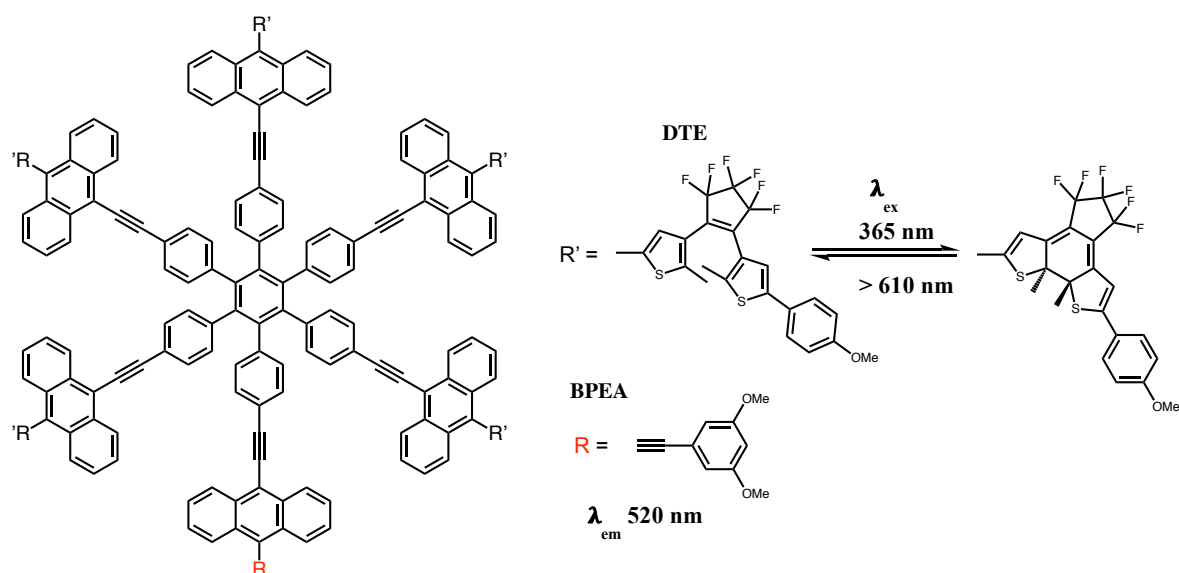
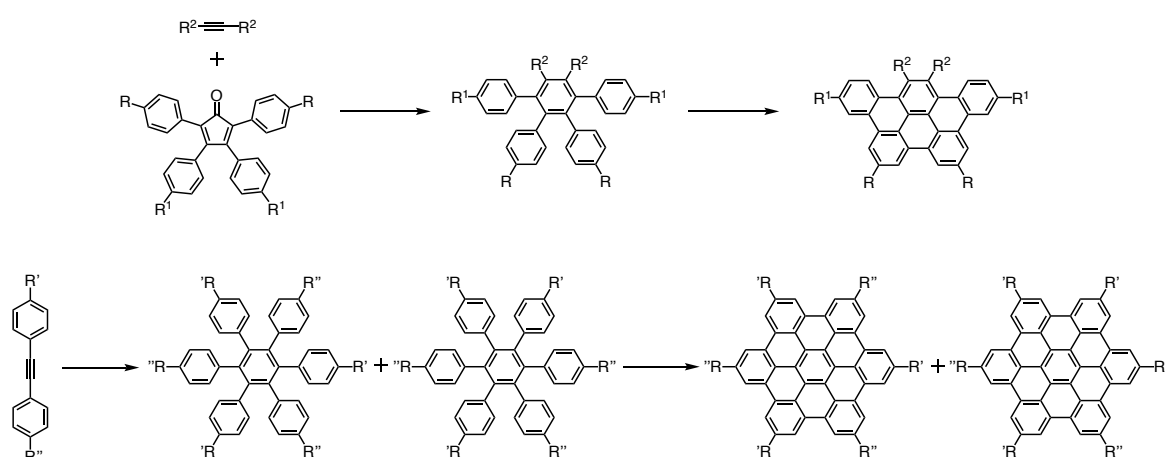


Figure 1.11. Hexa-functionalised hexaphenylbenzene displaying photoinduced molecular switching (DTE = dithienylethene, BPEA = bis (phenylethynyl)anthracene)

1.6.2 Synthesis of Hexabenzocoronenes

The Diels Alder [4+2] cycloaddition is a principal step in the formation of HBC and HPB-type compounds, during which a tetraarylcyclopentadienone (previously generated from a two-fold Knoevenagel condensation between a prop-2-one and a diketone) is reacted with a suitable acetylene. Unlike previously reported cyclotrimerisation reactions, the Diels-Alder route allows the incorporation of homo and hetero substituents into both the core and the periphery of the π -framework, and thus can generate products that would otherwise be synthetically unattainable.



Scheme 1.6 Synthesis of hexaphenylbenzene derivatives (i) benzophenone, 300 °C, (ii) $\text{Co}_2(\text{CO})_8$, dioxane reflux (iii) $\text{CuCl}_2/\text{AlCl}_3$ or $\text{Cu}(\text{OTf})_2/\text{AlCl}_3$ or $\text{FeCl}_3/\text{CH}_3\text{NO}_2$ (R , R' and R'' refer to alkyl substituents).

Further intramolecular oxidative cyclodehydrogenation of HPB subunits through the Scholl reaction produces the corresponding planarised polycyclic structure. The elimination of two aryl-bound hydrogen atoms initiates the formation of an aryl-aryl C-C bond between two adjacent phenyl ring pairs. The C-C bonds are formed in a step-wise manner, with the formation of the first usually being the slowest. This is known as the “slippery slope” affect.¹²¹ The reaction becomes increasingly exergonic as each successive bond is formed. Apposite oxidant conditions, such as $\text{CuCl}_2/\text{AlCl}_3$, have been reported in the literature, and $\text{Cu}(\text{OTf})_2/\text{AlCl}_3$ or FeCl_3 are suitable reagents for alykly substituted HPB platforms. Wong *et al.* have recently reported the successful cyclodehydrogenation of electron-poor arenes containing bromine, fluorine and CF_3 containing substituents, using $\text{DDQ}/\text{CF}_3\text{SO}_3\text{H}$. It is this route and mechanism that is employed in the work presented here, in the hopes of enhancing their potential in molecular switch applications.

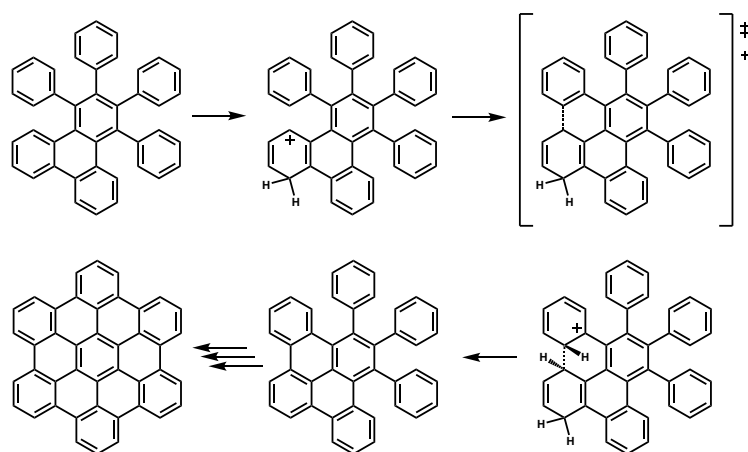


Figure 1.12 Hexaphenylbenzene condensation through the acid catalysed Scholl reaction.

1.6.3 Thienyl-substituted hexaphenylbenzene derivatives and hetero-atom containing superbenzenes

In 2002, Draper *et al.* reported the development of a new family of ligands. The nitrogen hetero-superbenzenes (N-HSB) are graphitic nanostructures containing electroactive imines on the periphery.¹²² The inclusion of the electronegative nitrogen atom confers electron accepting ability on the ligand, and allows for increased electron carrier transport, making the family suitable for optoelectronic applications such as LED based devices. These molecules also have the added advantage of increased solubility over their all carbon analogues, and are designed to accommodate bidentate coordination to a range of transition metals such as ruthenium and iridium. The group have reported the fully cyclised N-HSB,

as well as the daughter compounds in the series N- $\frac{1}{2}$ HSB, N- $\frac{2}{3}$ HSB and N- $\frac{5}{6}$ HSB. Incorporation of sulphur atoms into these frameworks may offer similar or greater synthetic and electrochemical advantages over their nitrogen and carbon-based analogues. A number of systems involving multiple thiophenes around a benzene core have been reported in the literature. In the work of Brusso, tetra-substituted thienyl benzenes have been prepared via Stilles coupling.¹²³ The reactivity of these systems towards oxidative carbon-carbon bond formation, along with the electrochemical and photochemical properties of the species formed has been examined.

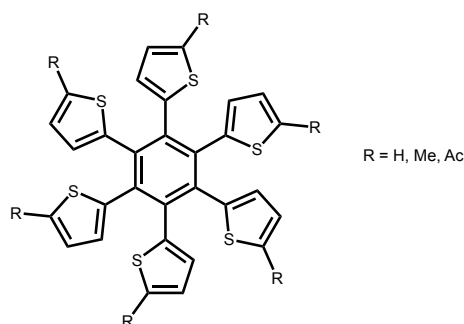


Figure 1.13 Hexa(2-thienyl)benzene compounds studied by Yoshida and Geng.

In the work of Yoshida^{124,125}, rhodium catalysts were used to successfully trimerise bis(2-thienyl)acetylene, to produce hexa(2-thienyl)benzene in a 49 % yield (Figure 1.13). This “starburst” type hexa-thienyl compound in which six thiophene substituents are substituted on a central benzene ring has been found to form an electroactive film on the surface of the electrode upon repeated cyclic voltammetry scans between 0.2 and 0.8 V. When the 5-position of each thiophene was substituted with a methyl or acetyl group, electrochemical analysis showed no film formation on the surface due to the lack of available sites on the thiophene for polymerisation. Building on this work, Geng *et al*¹²⁶ prepared a series of substituted hexa(2-thienyl)benzenes in which the 5-positions on the thiophene are substituted with long chain hydrocarbons. These compounds were found to form liquid crystal mesophases, which are stable over larger rangers than their all carbon analogues. Using the basis of these studies, these molecular frameworks may prove insightful in the venture for faster and more efficient photochromic switches, as well as allowing the possibility of further expansion of these hexaarylcores into areas of overlapping materials science and tuneable control on these unique properties through open and closed interconversion.

1.7 Other Applications of Molecular Switches

Applications of molecular switches are not limited to optical memory devices; they can also be used in catalysis and reactivity^{127,128}, fluorescence^{129,130} and highly selective sensors for the detection of various ions and biomolecules.^{131,132} By incorporating photochromic chromophores into reactants or products of a thermal reaction, when and where the chemical process occurs can be controlled. Molecular changes in the photochromic molecule can be translated into reactivity differences via geometrical changes (e.g. in azobenzenes) or electronic changes (e.g. in diarylethenes).¹²⁷ In general, excited open-form diarylethenes and their corresponding closed forms do not emit light. However, in rare cases, weak fluorescence is detected. Most notably, bis(2-thienyl)perfluorocyclopentene-type molecules have been shown to emit light in their open forms. Fluorescence has also been observed for the open form of a diarylethene incorporating one thiophene and one benzothiophene group, a diarylethene dimer with one photochromic unit in the open and the other in the closed form, and for both the open and closed forms of a diarylethene substituted with long conjugated side-chains. As shown previously in this application, light can be used as a gating stimulus and so it can switch a reaction component from being inactive to active or vice versa. Research has also been carried out on the temporal and spatial control of catalysis by incorporating photochromic moieties into the structure of some catalysts.¹²⁸ Photoactivatable fluorophores are chromophores which can be switched from a non-fluorescent reactant to a fluorescent product upon irradiation with light at a suitable wavelength of activation (Figure 1.14).¹²⁹ They had initial uses in following the progress of photochemical reactions but applications have now expanded into high resolution fluorescent imaging.¹³⁰

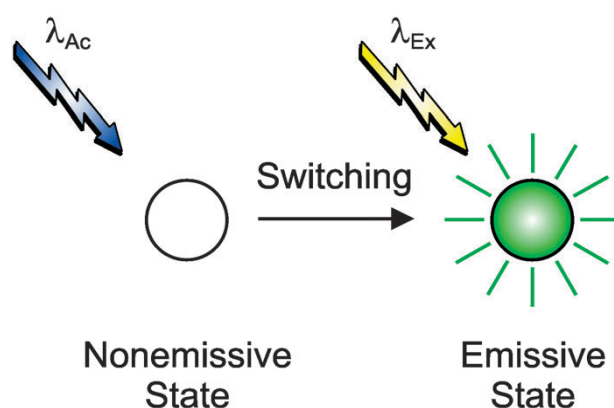


Figure 1.14 Activation of fluorophore via photoswitching.

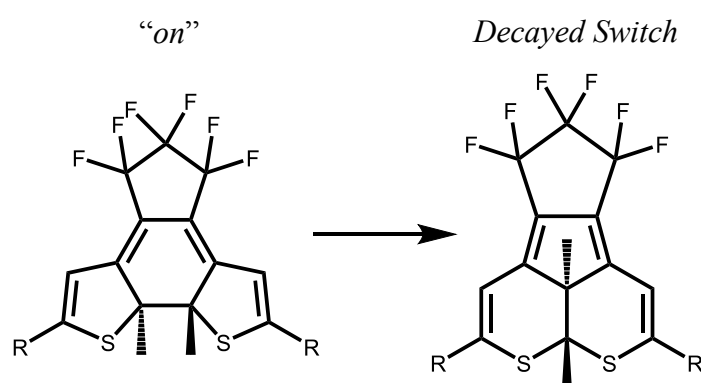
Asymmetrical diarylethene-based molecular switches have been recently synthesised and studied which have one R-group that acts as a highly selective ligand for metal ion coordination. The advantage of using diarylethene based ion sensors is that ion complexation/dissociation can be controlled by irradiating the switch with UV or visible light of different wavelengths in contrast with traditional ion sensors that can only be used once. These ion-sensors have also been shown to be active in living cells, therefore these fluorescent chemosensors can find applications in both environmental monitoring and biological studies in the future.¹³²

Molecular switches are analogous to the bits of information which are currently used for data storage, the isomers ground states “on” and “off” are often interpreted in terms of 1’s and 0’s. Current semiconductor technology stores bits of information in transistors as 1’s or 0’s in a similar manner, as dictated by a controller. By measuring the voltage across these transistors, the “value” of the data stored may be resolved. Molecular switches use UV-Visible light as a readout method in the place of voltage. It is necessary for this process to be facile and non-destructive to ensure that the data is not erased. The processing of “reading” the data occurs via evaluation of spectral changes near the absorption bands corresponding to the two isomer states. The speed of the read-out process coupled with the molecular size of the switches results in a realisable data density of 2×10^9 bits cm^{-3} . However, in their practical application, photofatigue associated with the processes of oxidation, elimination and rearrangements results in loss of data and therefore the prevention of their use.

Incorporation of molecular switches into OLEDs enables isolation of specific areas of the device for emission¹³³ which presents with many advantages for signing applications. This can be achieved by doping the electroluminescent layer with polymers of dithienylethenes (DTEs) and placing a layer of DTE polymer between the emissive layer and the anode. Crosslinking of DTE into a polymeric form shows favourable optical properties, namely prevention of inactivation of switch molecules associated with habitation of the parallel conformation, thereby increasing the quantum yield. Certain considerations must be taken in the use of molecular switches in this fashion, the emissive material must not have considerable overlap with the absorbance maxima of the photoswitch being used to prevent unwanted photocyclisation or photocycloreversion.

1.8 Molecular Switch Decay

The decay of switching performance results from various side reactions involving the “on” ground state isomer and the process of isomerisation. These reactions include oxidation, elimination and rearrangements. Identified by Irie *et al.* the main by-product forms from a 1,2-dyotropic rearrangement¹³⁴ (Scheme 1.7), the mechanism for which has not been determined though is thought to proceed through a concerted mechanism via radical or ionic intermediates. It is the compounds susceptibility to these parasitic side reactions which determines the overall fatigue resistance of the organic frameworks involved.



Scheme 1.7 Decay of Diarylethene based molecular switch

There are two components of fatigue resistance evaluation; cycling mode and continuous mode. In the cycling mode the compound is exposed to cycles of short ($\lambda < 310$ nm) and long wavelength irradiation to full colouration and consequently to full bleaching, the number of cycles required to reduce the products concentration to 80% of its original is the quoted value for the compounds fatigue resistance. In the continuous mode the sample is exposed to UV light only for an equivalent time to the total cycles, the reduction in product concentration is then evaluated. The concentration values however, may be misleading as often side products may absorb in the same regions as the original switch, either that of the closed or open form. This issue is circumvented by evaluating the number of active molecules as a ratio of initial isomer absorbances to that of irradiated isomer absorbances as shown

$$\text{number of active molecules} = \frac{\text{Final Absorbance of Open} - \text{Final Absorbance of Closed}}{\text{Initial Absorbance of Open} - \text{Initial Absorbance of Closed}}$$

The fatigue resistance values yielded from the continuous and cycling modes may be compared to determine if the compound in question degrades as a result of side reactions

involving isomer interconversion or the concentration of a specific isomer. A lower fatigue resistance value for cycling indicates side products are formed during isomer interconversion, while a lower value for continuous indicates the closed form isomer is susceptible to side reactions¹³⁵. In this project the installation of the ppy chelated iridium metal centre via a delocalised π -platform is hoped to retard this process due to the metal's donation of electrons into the delocalised ligand system.

1.9 1,10-Phenanthroline

1,10-Phenanthroline (phen) is a rigid, planar, and aromatic bidentate ligand, which possesses many desirable properties for coordination chemistry (Figure 1.15).¹³⁶ The presence of the two N atoms in the phen framework confers it π -electron withdrawing character. Moreover its rigidity and the fixed position of the N-donor atoms, makes it an entropically better chelating molecule than the more common 2,2'-bipyridine (bpy).¹³⁷

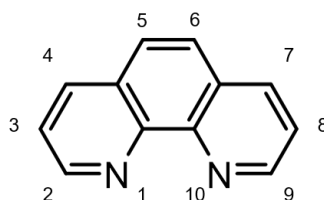


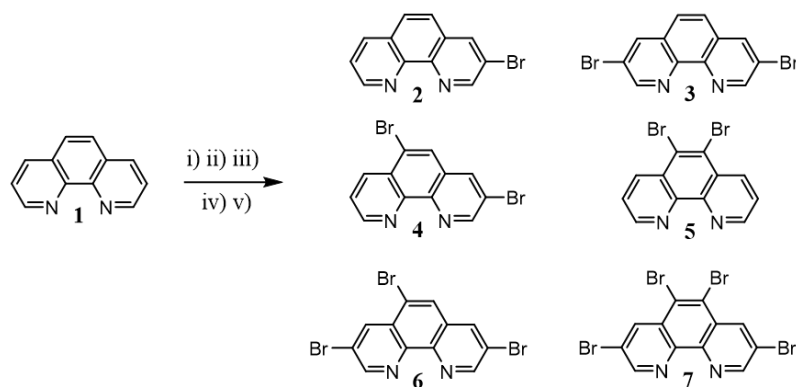
Figure 1.15 1,10-Phenanthroline and the numbering system adopted.

The rigid framework of 1,10-phenanthroline and its high affinity toward various cations are attractive features for the construction of tunable chromophores.¹³⁸ Unfortunately, the phen itself is weakly emissive, showing a low quantum yield (from $\Phi_{\text{em}} = 0.01$ in water to $\Phi_{\text{em}} = 0.001$ in cyclohexane),¹³⁹ and a short life time ($\tau < 1$ ns in CH_2Cl_2).¹⁴⁰ The weak fluorescence can be attributed to the similar energies of the singlet excited states $\pi - \pi^*$ and $n - \pi^*$ (emission mainly from $\pi - \pi^*$ and non-radiative decay from $n - \pi^*$). However, the modification of phen side chains has a direct influence on the electronic transitions, so derivatives of phen with conjugated systems that extend the π conjugation, tend to possess more desirable electrochemical and photophysical properties.¹⁴¹⁻¹⁴³

Because of its structure and chemical properties, phen has found applications in a range of fields including catalysis,¹⁴⁴ DNA intercalation¹⁴⁵ and material science.¹⁴⁰

1.9.1 Derivatives of 1,10-Phenanthroline

It is possible to make derivatives of phen by substitution at different positions.¹⁴⁶ A common pathway to functionalise phen is by nucleophilic and electrophilic substitutions. The 2,9 and 4,7-positions are the most active positions towards nucleophilic substitutions, while electrophilic reagents preferentially attack positions 5,6 or 3,8, where electron densities are higher.¹⁴⁷ The conditions to prepare unsymmetrical halogenated phen have also been reported,¹⁴⁸ which are even less common systems.¹³⁷ Bromination of phen has become a popular way of halogenation, and different strategies have been proposed to achieve this goal. The degree of bromination will vary depending on the conditions used, however different brominated derivatives are usually obtained regardless the chosen method (Scheme 1.8).¹⁴⁹



Scheme 1.8 Synthesis of Brominated 1,10-Phenanthrolines (Phen-2-7). Three synthetic routes include the use of i) 1,10-phenanthroline monohydrochloride monohydrate, Br₂, PhNO₂. ii) Fuming Sulfuric acid (30%), Br₂. iii) Br₂, pyridine, 1-chlorobutane, S₂Cl₂. iv) SCl₂, Br₂, pyridine, 1-chlorobutane. v) SOCl₂, Br₂.

Tzalis *et al.* reported the synthesis of brominated **Phen-1** when reacting 1,10-phenanthroline monohydrochloride monohydrate with bromine, using nitrobenzene as a solvent.¹⁵⁰ This yielded mainly **Phen-2** and **Phen-3**, with the presence of other further substituted side products. Nakano *et al.* described a method for the bromination of **Phen-1** that involves the use of fuming sulfuric acid and yields mainly the 5,6-dibrominated product (**Phen-5**).¹⁵¹

Saitoh *et. al* found that the bromination of phen, mainly in the 3, and 3,8 positions could be carried out using a sulfur monochloride (S₂Cl₂) catalyst, leading to **Phen-2** and **Phen-3** without the use of carcinogenic reagents or harsh reaction conditions.¹⁵² Other methods have also been described to get mainly the brominated derivatives **Phen-4** and **Phen-6** involving

sulfur dichloride (SCl_2) as catalyst,¹⁴⁹ while the tetrabrominated Phen-7 can be prepared using thionyl chloride (SOCl_2).¹⁵³

The interest towards the halogenation of phen is due to its versatility as a starting material, as it can be used to prepare a broad range of derivatives *via* C-C coupling reactions. This can generate, for example, more conjugated systems with interesting photochemical properties that can be tuned depending on the position and the nature of the substituted moiety.^{143,151,152,156}

1.10 Ruthenium and Iridium Complexes

Iridium and ruthenium complexes have been extensively studied for applications in electroluminescence, photosensitisers, hydrogen fuel generation photocatalysts, OLEDs, and in photovoltaics.^{13,22,23} Ruthenium usually display an oxidation state of +2, coordinated to N^N ligands, such as bipyridine (bpy), in octahedral polypyridine complexes.¹⁵⁹ Iridium commonly appears with an oxidation state of +3, and can be coordinated to lone pairs of electrons from the N or C atoms.¹⁶⁰ One popular method to synthesise Ru(II) complexes involves the reaction of a bpy ligand with $\text{RuCl}_3 \cdot x\text{H}_2\text{O}$ to generate $[\text{Ru}(\text{bpy})_2]\text{Cl}_2$. The complex can then be coordinated to various N^N ligands, resulting in the formation of octahedral Ru(II) complexes. The $(\text{PF}_6)^-$ anion is typically required as a counter ion in order to generate the final product.¹⁶¹

For Ir(III), the most common method is to react a C^N ligand, such as 2-phenylpyridine (ppy), with $\text{IrCl}_3 \cdot 3\text{H}_2\text{O}$ to obtain the dichloride bridge Ir(III) dimer, $[\text{Ir}_2(\text{ppy})_4\text{Cl}_2]$. The chlorine atoms can then be replaced by C^N, N^N or O^O ligands, to yield the final octahedral Ir (III) complex. Ru(II) and Ir(III) complexes possess desirable photophysical properties, and can be excited to a singlet state. Triplet excited states are then generated *via* intersystem crossing (ISC). Emission from this state yields phosphorescence. Three types of electronic transitions can be observed upon photoexcitation of Ir (III) and Ru (II) complexes: these include Ligand Centred (LC), Metal Centred (MC) and Metal-to-Ligand Charge Transfer (MLCT) (Figure 1.2). A singlet LC excited state (^1LC) is formed when an electron is promoted from π_{L} to $^1\pi_{\text{L}}$. Promotion from π_{M} to $^1\sigma_{\text{M}}$ generates a singlet MC excited state (^1MC), and from π_{M} to $^1\pi_{\text{L}}$ forming the $^1\text{MLCT}$ excited state. Due to the heavy atom (H-A) effect, the triplet excited states, ^3LC and $^3\text{MLCT}$, can be readily populated *via* ISC. These states can decay to the ground state, and emit *via* phosphorescence.

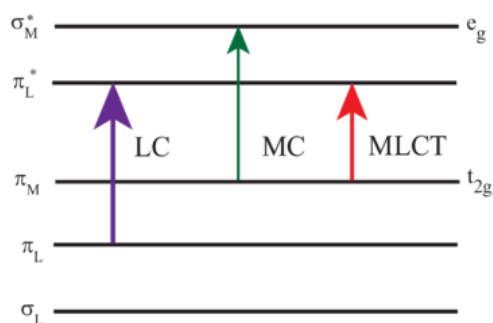


Figure 1.16 Types of electronic transitions observed upon photoexcitation of Ir (III) and Ru (II) complexes.

The π -acceptor/ σ -donor properties of the coordinated ligands help to stabilise the metals in their low oxidation states.¹³⁹ The σ -donating capabilities of the ligands also increases electron density around the metal centre, and promotes $d-\pi^*$ back-bonding and MLCT transitions. The HOMO-LUMO gap of the complexes can be tuned with the modification of the coordinated ligands, increasing their potential applications.¹⁶²

Iridium in particular has experienced a similar trajectory to dithienylethene in terms of a recent resurgence in interest and the number of research papers published.¹⁵⁶ This interest arose due to its potential in photosensitisation and upconversion, and its photochemical properties e.g. the nature of the absorption and emission of its complexes and their high quantum yields. The metal exhibits electronic properties comparable to those of other d^5/d^6 metal complexes, iron(II), ruthenium(II), osmium(II) and rhenium(III), but is often used in their place because of efficient intersystem crossing properties observed at room temperature. In the complex synthesised, chelation is completed with phenylpyridine ancillary ligands as the photochemistry of these is well understood. The metal may be incorporated into the target compound in various ways such as through a direct σ -bond to one of the thienylethene moieties. However, due to the recent research of metal complexes coordinated to twisted delocalised π -platforms and their use in solar cells and water splitting, a similar approach was undertaken here, with the metal and thienyl switching moieties connected via a bidentate ancillary ligand such as 1,10-phenanthroline. While multimodal switches based on iridium metals σ -bond directly to the thienyl moieties have been explored¹⁵⁷, the use of iridium in the optimisation of a switch's photochromic and photochemical reactivity in terms of fatigue resistance has not yet garnered much interest. The exploration of this property is one of the main aims of this research.

1.10.1 Ruthenium and Iridium 1,10-Phenanthroline Complexes

The use of phen as an auxiliary ligand in Ir(III) and Ru(II) complexes can further enhance their photophysical properties. One way in which this is achieved is by improving absorption in the visible region that is traditionally low in these complexes. The attachment of light-harvesting chromophores to phen derivatives has shown to be an efficient way to broaden absorption wavelengths and improve absorption intensities.¹⁶³ Ma et al. reported the synthesis of Ir(III) complexes bearing phen derivatives, which directly influenced the extent of absorption in the visible region.¹⁴⁸ The compound **Ir-A** (Figure 1.17) bears an unsubstituted phen ligand and displays a relatively weak absorption in the visible region ($\lambda = 400$ nm; $\epsilon = 5.07 \cdot 10^3 \text{ M}^{-1} \text{ cm}^{-1}$). However, the complexes **Ir-B** and **Ir-C** possess substituted auxiliary phen ligands, which display improved absorption efficiencies, with **Ir-A** showing an intense peak at $\lambda = 486$ nm ($\epsilon = 1.09 \cdot 10^5 \text{ M}^{-1} \text{ cm}^{-1}$), and **Ir-B** possessing a similar intense peak at $\lambda = 484$ nm ($\epsilon = 1.12 \cdot 10^5 \text{ M}^{-1} \text{ cm}^{-1}$).¹³

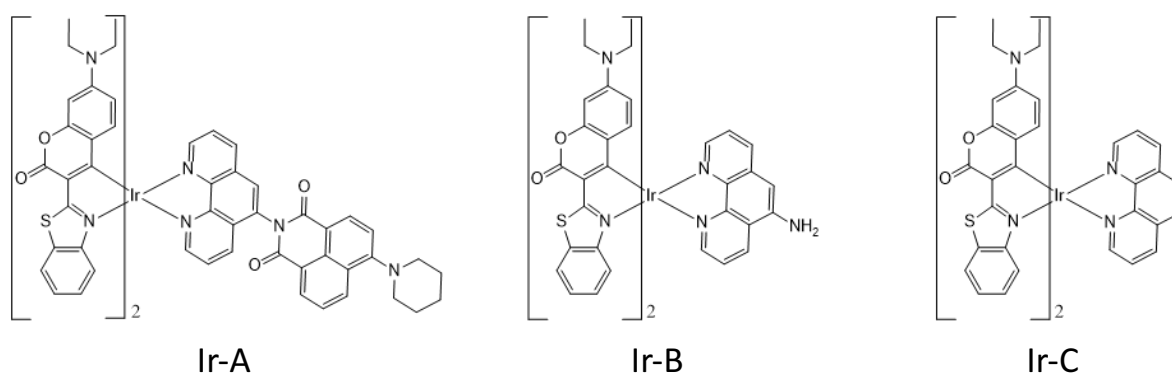


Figure 1.17 Molecular structures of Ir(III) complexes bearing i) substituted 1,10-phenanthroline ligands, **Ir-A** and **Ir-B**. ii) unsubstituted 1,10-phenanthroline **Ir-C**.

Auxiliary ligand modification has also demonstrated the ability to improve the triplet excited state lifetimes (τ_T) of Ir(III) and Ru(II) complexes. Lu et al. reported the synthesis of a number of Ru(II) complexes bearing phen ligands derivatised with pyrene chromophores (Figure 1.17), which demonstrated improved τ_T values and potential applications in triplet-triplet annihilation (TTA) photosensitisers and in singlet-oxygen generation (SOG).²¹

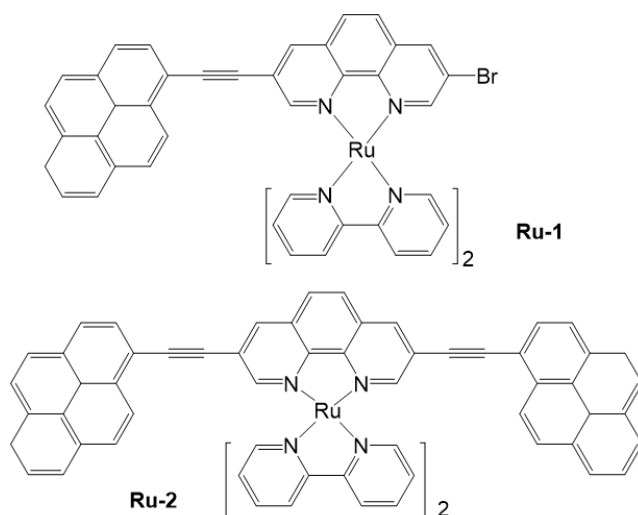
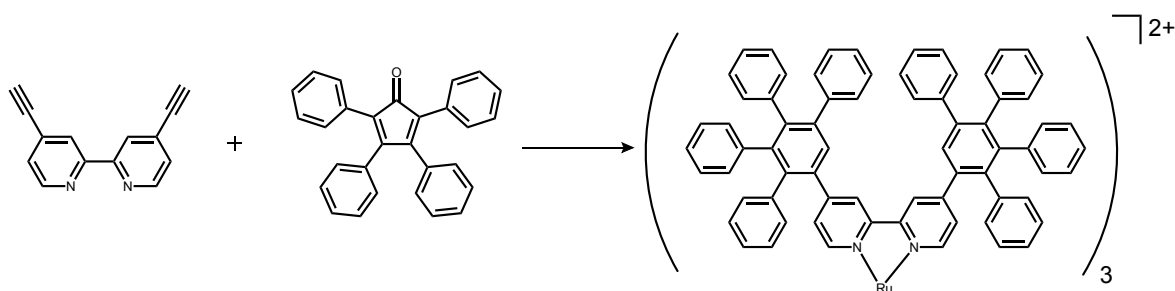


Figure 1.18 Molecular structures of Ru(II) bearing substituted phen ligands, Ru-1 and Ru-2.

Ru-1 contains a substituted phen ligand bearing an ethynyl-pyrene side chain at the 3-position, and another brominated chain that can undergo further derivatisation at the 8-position. This reported a triplet excited state lifetime of $\tau_T = 148 \mu\text{s}$. However, the phen ligand in **Ru-2** possesses two ethynyl-pyrene side chains, each at the 3 and 8-positions, and reported a lower triplet excited state lifetime of $\tau_T = 59.1 \mu\text{s}$. This demonstrates the complexity of the tuning process, and leaves plenty of scope for further studies to gain insight into the relationship between the molecular structure and the photophysical properties of these complexes.¹⁵⁶

1.10.2 Polyphenylenes as ligands in encapsulated metal complexes

Several examples of polyphenylenes derivatives as dendrimeric polypyridal ligands have been published within the last decade.^{164,165} In these cases the polyphenylene scaffolds are used as a rigid matrix in which radial arms of the dendrons do not allow backfolding so that the coordination complexes are highly shape persistent. The first shape persistent dendrimers based on octahedral geometry employ $[\text{Ru}(\text{bpy})_3]^{2+}$ as the photoactive transition metal centred core, where G1 is the first generation dendrimer.¹⁶⁴ The polyarylbiopyridine ligands are prepared by divergent methods via a series of Diels-Alder cycloadditions between bis-ethynyl-bipyridine and a suitably substituted tetracyclopentadienone. A series of dendritic complexes with a phosphorescent Ir(III) core, based on the cyclometallating ligand phenyl pyridine ($\text{N}^{\wedge}\text{C}$ coordination mode) have also been described, as has their relative performances in phosphorescent organic light emitting devices (PhOLEDs).¹⁶⁵



Scheme 1.9 Ru(II) dendritic polypuridine complex (i) *o*-xylene (solvent), 140 °C, 97 % (ii) $\text{RuCl}_2(\text{DMSO})_4$, DMF, 140 °C, 55 %

In these complexes, the rigid polyphenylene dendrons essentially encapsulate the metal centre to prevent Ir(III) cores from triplet-triplet annihilation. As a consequence, photoluminescent quantum yields of the complexes are significantly improved relative to the parent $[\text{Ir}(\text{phenylpyridine})_3]$ complex. With increasing generation, an increase in quantum yield of emission is observed due to the greater shielding of the phosphorescent core by the structurally rigid dendrons. The effect of the polyphenylene framework about the phosphorescent metal centre also provides an effective charge carrier mobility from the periphery of the dendrimer to the Ir(III) core, a property which can be carefully modulated on the basis of molecular architecture and dendrimer generation.

1.10.3 Photochemical properties of Iridium in molecular switches

Iridium, as a heavy atom exhibits strong spin – orbit coupling¹⁶⁶, increasing the accessibility of the triplet excited state. This in turn allows for a higher degree of intersystem crossing between singlet and triplet excitation states resulting in radiative relaxation in the form of phosphorescence. The long relaxation times associated with these excitations increases the intensity of spectral bands associated with photocyclisation and photocycloreversion, making the read-out process more efficient. This can be observed clearly through stacking of the absorbance and emission spectra, where a high degree of overlap indicates the increased “allowedness” of the triplet state excitation. However as shown in Figure 1.19, the introduction of the metal centre may result in a reduction in quantum yield through loss of energy via charge transfer from the ligand to the metal and consequent emission. If the platform introduced between the metal centre and the DTE moiety is of the correct level of conjugation and the $^3\text{MLCT}$ has a higher quantised energy than that of the ^3IL , this could potentially be avoided.

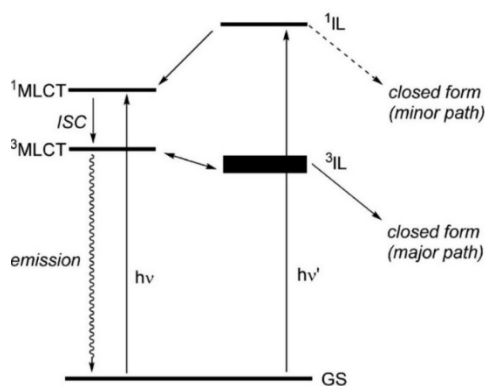


Figure 1.19 Jablonski Diagram for Ir(III) based switches

1.11 Project Aims

The aim of this project is to synthesise DTE-based molecular switches and to study their quantum yield and fatigue resistant properties by carrying out photophysical analysis on the product. The intention is to synthesise products whose closed isomer absorbs light at long wavelengths such as between 600 and 800 nm. This is achieved through the delocalisation of π -electrons throughout the entire molecule. Each chapter explores a potential new route of design and is explored through a unifying theme that is amalgamated toward the end of this research. Thienyl-appendages were designed in order of increasing aromaticity. Substitution at the 5-position of the thiophene is the most well-chemically understood and incorporation of an acetylene linker was hoped to facilitate sufficient communication between the dithienylethene core and the photoactive aromatic moieties. To our knowledge, no definitive photochemical study has been undertaken for these brominated thiophene appendages or their corresponding photochromic analogues, to which they act as precursors. The pyrene and naphthalene units provided a chromophore with an intermediate platform size to the smaller units and the larger HPB compound. The inclusion of the uncyclised polyphenylene system allows for additional comparison between this study work already undertaken within the Draper group. Further studies of these polyphenylene systems and their relationship with the dithienylethenes ability to undergo photochromic cyclisation was also studied, and π -platforms synthesised that would allow further synthetic pathways to be realised. This culminates in the study of 1,10-phenanthroline based systems and their corresponding Ir(III) complexes. Substitution at the 3,8-position was specifically chosen to allow for stabilisation of the excited states, and the 1,10-phenanthroline based π platform was synthesised as a viable chelation site and as a sufficiently delocalised platform.

2. Thienyl and Alkynyl-based polycyclic aromatic hydrocarbon appendages and comparing the photophysical properties of their photochromic analogues

This chapter and its initial work describes the synthetic routes towards novel photochromic molecular switches generated from dithienylethene, and the optimisation of these molecular systems. Five novel molecular switches were prepared, showcasing the synthesis, characterisation and photophysical properties exhibited by the compounds. The synthesis evolved via a sequence of Sonogashira cross-coupling reactions and Diel-Alder cycloadditions. Polycyclic aromatic hydrocarbons describe a vast, and potentially viable, though unexplored, area of research in regards to labile switch ability. The aromatic rings provide an extensive electron cloud, and due to the dual symmetrical nature of these compounds, this cloud could initiate a push-pull analogue within the compounds. This, coupled with the extensive conjugation inherent in polycyclic aromatics, would allow for a much smaller HOMO-LUMO gap, and such, a greater red-shift absorption into the visible spectrum for the switches closed form. Sonogashira cross-coupling reactions were investigated in all cases as it is a facile carbon-carbon coupling reaction, and allows for an added extension of the products red-shift absorption. The highly fluorescent nature of these appendages also afforded a viable pathway to explore non-destructive fluorescent readout, a newer, less explored use for these dithienyl-based compounds, which prospers on the idea of using much lower energy emission to control the switches on/off effect.

NMR showcased the chemical shifts inherently applicable to the two synthesised photoisomers (open and closed) due to the change in their structural geometry and electronic distribution. UV-Vis absorption spectroscopy and the emissive photophysical properties of the synthesised materials allowed for the quantum yield of photocyclisation to be evaluated. The first part of this work dealt with the synthesis of these ethynyl-based polycyclic aromatic materials, and diverged into the understanding of the chemical activity of their brominated precursors. The second part of this work explored the photophysical properties and the spectroscopic assignment of these family of compounds, including their mirroring emissive profiles and how a bridging ethynyl-group between the dithienyl core and these delocalised platforms can affect intermolecular communication or inhibit photocyclisation.

All results were interpreted in terms of absorption wavelengths, emission profile, quantum yield of photocyclisation and fatigue resistance. It was hoped that increasing the molecular weight of the polycyclic appendage would afford more desirable photophysical properties that could be explored to the point of device implementation. These large planar platforms provide a robust starting point for future photoswitching analysis. Synthesis of the brominated analogues is shown first, before discussing their parent switch compounds.

2.1 3-bromo-2-methyl-5-(1-ethynylPAH)thiophene appendages

2-methylthiophene, 1-bromonaphthalene and pyrene are all commercially available materials. All starting material purity was tested before undertaking any large scale reactions. Although some of the target compounds involved had previously been prepared via a traditional Sonogashira coupling¹⁶⁷, numerous target compounds were instead successfully synthesised via a modified version of Gourdon's microwave assisted Sonogashira coupling, a chemical strategy that has recently grown in interest over the last number of years.^{168,169} It offers strategic advantages over traditional conductive heating methods, however, as shall be seen, not all substrates were viable to be reaction in this way. Five target brominated-thiophene appendage compounds were to be synthesised, each bearing an ethynyl moiety, and substituted by varying polycyclic aromatic hydrocarbons. Though these type of compounds show great potential in the fields of material science, as of yet, very little work has been recorded in the area of molecular switching compounds. Here, direct comparison of their physical, photophysical and chemical properties will be explored. The synthetic route towards all compounds will be discussed in detail in the following sections, followed by the characterisation and the analysis of the photophysical features that represent key components of photochromic technology. The optimisation of the synthetic routes and the spectroscopic analysis of the compound are the core basis of this work, leading into new, novel molecular switches designed to incorporate a broad spectrum of uses.

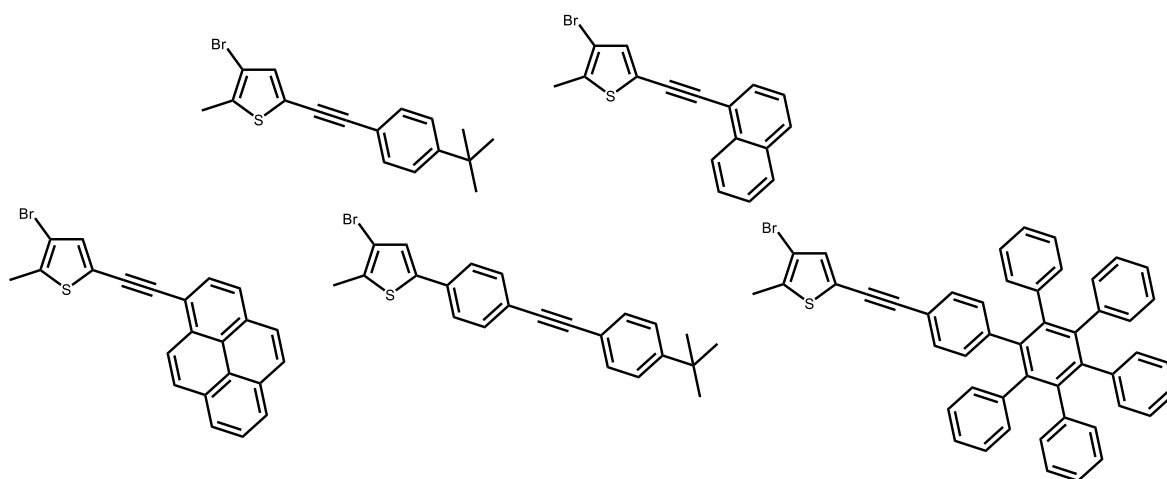


Figure 2.1 The target 3-bromo-2-methyl-5-(1-ethynylPAH)thiophene appendages

2.2 Synthesis of 3-bromo-2-methyl-5-(1-ethynylPAH)thiophene appendages

2.2.1 Microwave Chemistry

Microwave technology was developed in the 1940s as an essential part of RADAR transmitters. The next thirty years saw its widespread use as a domestic appliance for heating water laden food stuffs and for industrial processes such as the drying of nylon fibres. It was not until 1986, that Gedye¹⁷⁰ and Majetich¹⁷¹ proved that a variety of organic reactions could be accelerated under microwave conditions. Since then the use of microwave dielectric heating in organic, inorganic and organometallic chemistry has flourished, with over 2000 papers describing the application and benefits of this relatively new technique for the synthesis of new compounds.¹⁷² Microwaves are a type of electromagnetic energy found at the lower frequency end (300 to 300,000 MHz) of the electromagnetic spectrum. They comprise both an electric and magnetic field, however, only the former transfers heat to a substance. Only molecular rotations are affected as the energy in microwave photons is insufficient to break molecular bonds (0.20 kJ/mole compared to 330 - 510 kJ/mole) i.e. the effect of microwave absorption can be described as purely kinetic. Before the advent of microwave reactors, chemical syntheses were exclusively accomplished by conductive heating using an external heat. This process can mean that the temperature of the reaction vessel is higher than that of the reaction mixture (until thermal equilibrium is reached). In comparison, microwave heating is a more efficient process. It is dependent on a number of different factors, one of which is the dielectric constant (ϵ') of the solvent or substrates. Typically, microwave energy is transferred to the reaction mixture by two mechanisms - dipole rotation or ionic conduction. Unlike conductive heating, the microwaves couple directly to the molecules present in the reaction mixture (*vide infra*) meaning that the process is not dependent on the thermal conductivity of the reaction vessel, resulting in an instantaneous rise in temperature due to localised superheating of any molecules that react with either of the two fundamental mechanisms for energy transfer mentioned previously.

2.2.2 Solvent choice for microwave reactions

Dipole rotation is a process by which polar molecules try to orient themselves with the rapidly changing electric field of the microwave. It is the rotational motion of the molecule as it tries to align itself with the electric field that results in the transfer of energy in the form of heat. Any polar species i.e. solvent, substrate or reactant will undergo this process of energy transfer but to varying degrees. The efficacy of heating by dipole rotation is

dependent upon the reaction mixture's characteristic dielectric relaxation time, which is itself dependent on both the temperature and the viscosity of the reaction mixture. Ionic conduction only occurs if there are free ions or ionic species present in the substance being heated. Similar to dipole rotation, ionic motion is generated as the molecules align themselves with the rapidly changing electric field causing instantaneous superheating as outlined above. As the temperature increases the transfer of energy becomes more efficient.¹⁷³⁻¹⁷⁵

Solvents play a very important role in microwave chemistry.^{173,176,177} One of the most important characteristics of a suitable solvent for microwave synthesis is its polarity as the greater the polarity of the reaction mixture, the greater its ability to couple with the microwave energy. There are many factors that influence the efficacy of microwave heating, but the main three factors are dissipation factor, dielectric constant and dielectric loss. Molecules with large dipole moments also have large dielectric constants as polarisation largely depends on dipole rotation. The dielectric relaxation time (which is the time it takes a molecule to achieve 63% of its return to randomised disorder once the electric field has been removed) has a large effect on the three main parameters.^{174,175} The dielectric relaxation time can be influenced by the volume of the reaction mixture, the frequency of the microwave energy, the temperature of the reaction and the functional groups present. As most commercial microwave reactors are set to a frequency of 2450 MHz only temperature can externally change the three main parameters i.e. as the temperature increases, the relaxation time and dielectric parameters will decrease resulting in less efficient coupling to the electric field.¹⁷³⁻¹⁷⁶ Hence, when choosing a solvent for microwave syntheses the most important consideration is not the boiling point (as microwave energy will reach and bypass the boiling point of most solvents in seconds) but a high dielectric loss value.

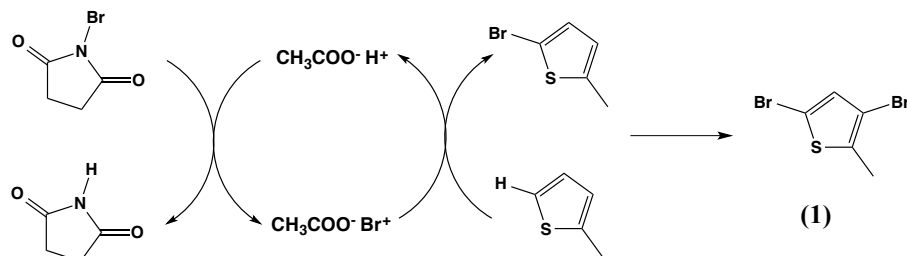
2.2.3 Microwave assisted organic synthesis

In the literature examples of microwave assisted organic synthesis for almost every type of organic reaction can be found. Some inorganic reactions have also been improved using microwaves including a range of metal catalysed coupling reactions such as Stille couplings¹⁷⁸, Suzuki couplings¹⁷⁹, Negishi couplings¹⁸⁰, Heck couplings¹⁸¹, cyanation reactions¹⁸² and Sonogashira cross couplings^{183,184}. There are also many examples of time consuming Diels-Alder reactions being improved under microwave conditions with reaction times being decreased dramatically.¹⁸⁴⁻¹⁸⁶ Gourdon *et al* have reported the synthesis of N-

HSB-like compounds from the cyclodehydrogenation of hetero-oligophenylenes which were synthesised using microwave heating. They found that by using microwave heating that the Sonogashira cross-coupling reactions were completed in less than thirty minutes in good yields, the acetylene 5-(phenylethynyl)pyrimidine was produced in 93% yield which is significantly higher than the same reaction carried out under conventional heating methods.¹⁸⁷⁻¹⁸⁹ The Diels-Alder reactions were performed in diphenylether at 260 °C for 45 min, again a shorter reaction time than similar cycloaddition reactions reported in the literature.¹⁹⁰

2.2.4 Synthesis of 3,5-dibromo-2-methylthiophene, **1**

Literature procedures describing the synthesis of 3,5-dibromo-2-methylthiophene, **1**, treat 2-methylthiophene with a slight excess of bromine in acetic acid at 0 °C overnight.¹⁹⁰ Initial attempts at this reaction proved the product was somewhat difficult to purify. To overcome this, *N*-bromosuccinimide (NBS) was chosen as an alternative reagent, thereby allowing reaction to be carried out at room temperature. The protonation of NBS with strong, highly lipophilic acid, such as perchloric acid, can generate positive halonium species capable of halogenating aromatics in a catalytic manner in low polarity media, such as hexane, as shown in Scheme 2.1

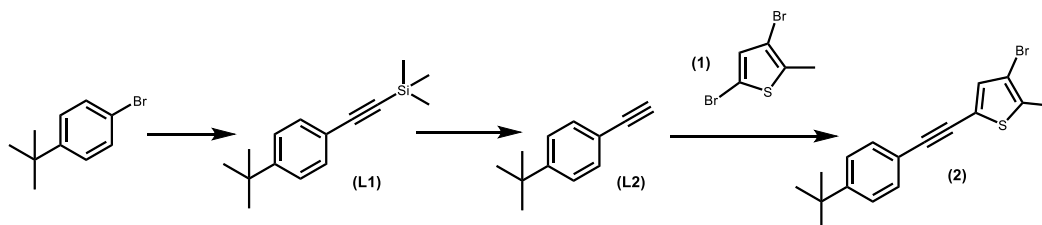


Scheme 2.1 Catalytic bromination reaction of 2-methylthiophene using NBS and perchloric acid, at room temperature, to yield compound 1.

The site blocking of the methyl group and addition of a slight excess of NBS (2.3 equiv) allowed desired double bromination of the thiophene. Bromine provides the most useful scope in terms of analytic reaction methods. The starting material can be easily reproducible in fast reaction times, and allow large quantities of product to be generated. Arylbromides also react quite readily in both Sonogashira cross-coupling reactions in lithium-halogen exchange reactions. As aryl-iodides react quite easily in cross-coupling reactions, it was

hoped to avoid the di-substituted ethynyl-product by using bromine, acting as an energy barrier when coupled with the sterics of the methyl group. NMR (nuclear magnetic resonance) was run and the spectra corresponded well with those in the literature.

2.2.5 Synthesis of 3-bromo-2-methyl-5-(4-*tert*-butylphenylacetylene)thiophene, 2

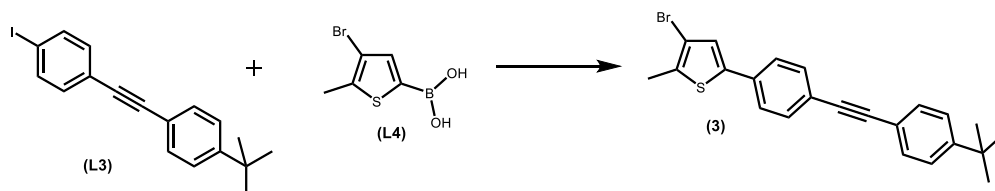


Scheme 2.2 Synthetic route to compound 2, (i) TMSA, CuI, P(Ph)₃, Pd(PPh₃)₂Cl₂, NHEt₃, DMF, 120 °C, 25 minutes, (ii) KF, TBAF, MeOH, THF, overnight, RT and (iii) 1, CuI, P(Ph)₃, Pd(PPh₃)₂Cl₂, NHEt₃, DMF, 130 °C, 30 minutes.

The Sonogashira cross-coupling reaction of 1-bromo-4-*tert*-butylphenyl is shown in Scheme 2.2. The reaction involves the generation a carbon-carbon bond between an aryl halide and a terminal alkyne through the use of a zerovalent palladium catalyst, and a copper (I) halide salt as co-catalyst, creating arylalkynes through sp^2 - sp couplings.^{191,192} As described, microwave related couplings are emerging as an efficient route in the synthesis of these reactions, delivering high yields in short periods of time. Microwaves can pass through a reaction vessel and cause dielectric heating within the solution, such that the reaction is independent of the thermal conductivity of the vessel itself. Due to the lower reactivity generally seen in aryl bromide species, triphenylphosphine improves the stability of the palladium catalyst, and longer reaction times are viable, thus promoting full conversion.¹⁹³ The relative reactivities of organic halides follows the reactivity of oxidative addition of the organic halides, with aryl iodides being more reactive than their chlorinated counterparts. Scheme 2.2 (a) shows the reaction conditions between the bromine of the thiophene moiety and the terminal hydrogen of trimethylsilylacetylene (TMSA). Pd(PPh₃)₂Cl₂ was synthesised, due to its lower reactivity to air to other high yielding palladium Sonogashira catalysts e.g. Pd(PPh₃)₄.¹⁹² 1-trimethylsilyl(4-*tert*-butylphenylacetylene) is initially generated, but this can be deprotected through the use of TBAF and potassium fluoride, Scheme 2.2 (b). A subsequent Sonogashira reaction, of 4-*tert*-butylphenylacetylene, L2, with compound 1 (Scheme 2.2 (c)), synthesised 3-bromo-2-methyl-5-(4-*tert*-butylphenylacetylene)thiophene, 2. Assignment of the product signals was achieved by ¹H NMR, ¹³C NMR, ¹H-¹H and ¹³C-¹H COSYs (correlation spectroscopy), and

confirmed by mass spectrometry, an analytical technique that helps identify the amount and type of chemicals present in a sample by measuring the mass-to-charge ratio and the abundance of gas ions.

2.2.6 Synthesis of 3-bromo-5-(4-((4-*tert*-butyl)phenyl)ethynyl)phenyl)-2-methylthiophene, **3**



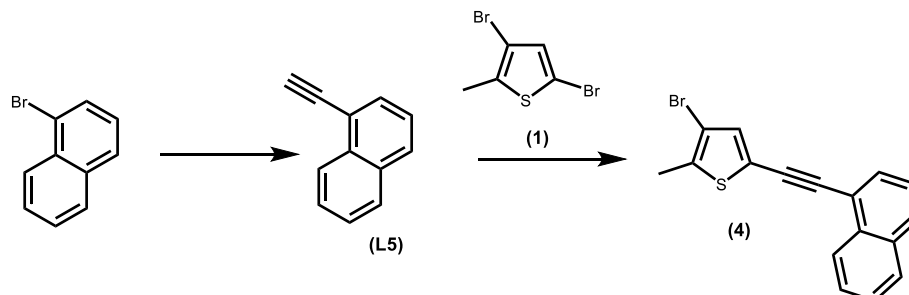
Scheme 2.3 Synthesis of 3, (i) THF, ethylene glycol, 2 M NaCO₃, PdCl₂(PPh₃)₂ (1 mol %), 80 °C, 17 h, 58 %.

The precursor diphenylacetylene molecule (**L3**) was synthesised via a Sonogashira cross-coupling reaction carried out under N₂. The reaction was catalysed by PdCl₂(PPh₃)₂, with CuI as a co-catalyst, according to standard literature procedures.¹⁹¹ The reaction mixture was refluxed at 80 °C for 1 hour and yielded a creamy yellow solid (Scheme 2.3), which was suspected as a mixture of the desired cross-coupled product and a homo-coupled side product, due to previously reported work-up analysis. Column chromatography was carried on silica with hexane as eluent in an attempt to purify the mixture. However, this speculated side product ran very close to **L3** on the column and hence the two products could not be separated fully, even after multiple separations. It was hoped that **L4** would have little to no interaction with the homo-coupled product, which is lacking the iodide substituent, and thus allow further purification in the next stage. **L3** was fully characterised fully by ¹H and ¹³C NMR, and APCI⁺ mass spectrometry, in accordance with literature values.

The synthesis of **3** was carried out via a Suzuki coupling reaction between **L3** and (4-bromo-5-methylthiophen-2-yl)boronic acid, **L4**, under Ar using PdCl₂(PPh₃)₂ as a catalyst. **L4** was first synthesised by reacting 3,5-dibromo-2-methylthiophene, **1**, with *n*-BuLi at -78 °C and a subsequent reaction with triisopropyl borate to give **L4** (Scheme 2.3). **L3** and **L4** (in excess) were refluxed overnight under the aforementioned reaction conditions at 80 °C and produced a brown solid. This was recrystallised using cold methanol to give an orange/brown solid. The purpose of including Na₂CO₃ in the reaction mixture was to increase the nucleophilicity of the organic group in the organoboronic acid. The

nucleophilicity of the R-group in the organoboronic acid was poor, however, when a base, such as Na_2CO_3 , was coordinated to the boron atom of the boronic acid, it increased the nucleophilicity of the R-group and this facilitated the transmetallation step of the Suzuki reaction.¹⁹⁴

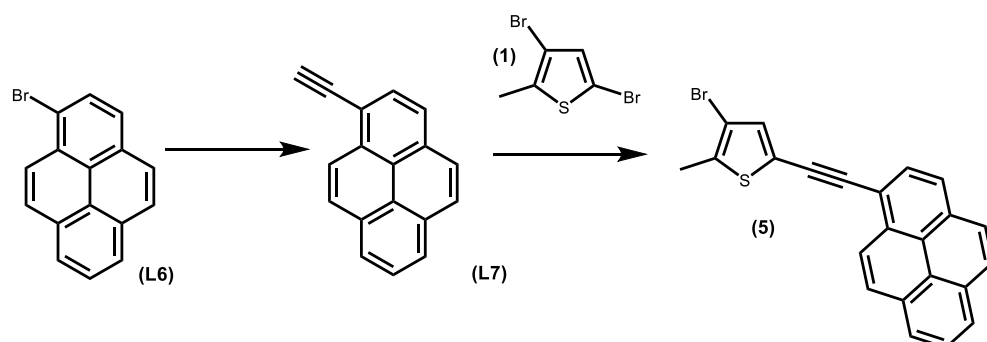
2.2.7 Synthesis of 3-bromo-2-methyl-5-(1-ethynlnaphthalene)thiophene, 4



Scheme 2.4 Sonogashira coupling of 1-ethynlthiophene and 3,5-dibromo-2-methylthiophene using standard and microwave chemistry ($\text{Pd}(\text{Ph}_3)_2\text{Cl}_2$, CuI , PPh_3 , 110°C , 20 mins, 71 %

Compound 4 was synthesised by combining molar equivalents of 1-ethynynaphthalene and 3,5-dibromo-2-methylthiophene. The two reactants underwent microwave mediated Sonogashira coupling. Irradiation of 1-bromonaphthalene and TMSA in a solution of NHET_2 : DMF (5: 2) for 20 minutes produced the desired protected product. This yellow oil was purified by silica column chromatography eluting with hexane, and deprotected overnight using KF and TBAF . Following work-up, the product **L5** was obtained as a yellow oil in a higher yield (65 %) than literature reports using traditional methods.¹⁶⁷ Coupling of the dibromothiophene **1** and **L5** was attempted using traditional Sonogashira coupling methods. Even though microwave heating has previously recorded higher yields, reliability of standard cross coupling methods was chosen instead to proceed. **1** and **L5** were heated to 110°C in a NEt_3 :DIPA mixture for 8 hours, with $\text{Pd}(\text{PPh}_3)_3\text{Cl}_2$ as catalyst, and CuI as co-catalyst. Further PPh_3 was added for increased catalyst stability. Due to the highly selective nature of this reaction, the reaction proceeded quite rapidly, and product noticeably began to crash out after 4 hours. The vessel was left for a further 4 hours to ensure completion. Upon neutralisation and extraction with CH_2Cl_2 , solvent was removed in vacuo and the product was obtained as a dark white-powder. Further purification of this compound was achieved by precipitation using methanol in high yields (71 %). The product was precipitated as a pale grey powder using methanol. ^1H NMR and ^{13}C NMR spectra were easily assigned due to the similarities to the starting materials.

2.2.8 Synthesis of 3-bromo-2-methyl-5-(1-ethynlpyrene)thiophene, 5



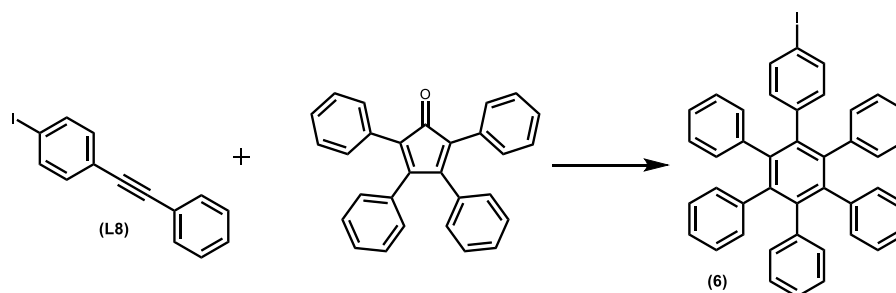
Scheme 2.5 Sonogashira coupling of 1-ethynlthiophene and 3,5-dibromo-2-methylthiophene using a microwave. (i) TMSA, Pd(Ph₃)₂Cl₂, CuI, PPh₃, 110 °C, 2 x 10 mins, (ii) KOH, MeOH, overnight, 51 % (iii) Pd(Ph₃)₂Cl₂, CuI, PPh₃, 130 °C, 30 minutes, 70 %.

Synthesis of 3-bromo-2-methyl-5-(1-ethynlpyrene)thiophene, 5, was achieved using similar methodology as previously described. Pyrene was brominated according to literature procedures to produce 1-bromopyrene, **L6**.¹⁹⁵ This was then further reacted in a Sonogashira cross-coupling microwave reaction, and the crude was subsequently deprotected in a one-pot overnight synthesis. Upon extraction of the product using diethylether, the solvent was removed and the product appeared as a dark brown oil. Purification via column chromatography (eluent: hexane) afforded the desired product as a luminescent yellow solid in moderate yields (51 %). This was further reacted with compound **1** in a microwave vessel at 130 °C for 30 minutes in DMF: NHET₂ (2: 5). The reaction was quenched with acid and the product extracted using ethyl acetate. Column for purification run using hexane as initial eluent, followed by CH₂Cl₂: hexane (1: 10) to yield final product as a dark yellow solid. (70 %)

2.2.9 Synthesis of precursor iodo-hexaphenylbenzene, 6

Towards the preparation of switch **12**, an two iodated synthon was prepared, with the hopes of further reactivity potential. The first of these, 1-iodo-4-(phenylethynyl)benzene, was synthesised via a Sonogashira, palladium-catalysed, cross-coupling reaction between 4-iodobenzene and 1-phenylacetylene using an analogous procedure that was described for the arylacetylene precursors discussed previously. Iodo-hexaphenylbenzene was prepared via a Diels-Alder cycloaddition between iodo-diphenylacetylene, **L8**, and tetraphenylcyclopentadienone (commercially available), in a benzophenone melt at elevated

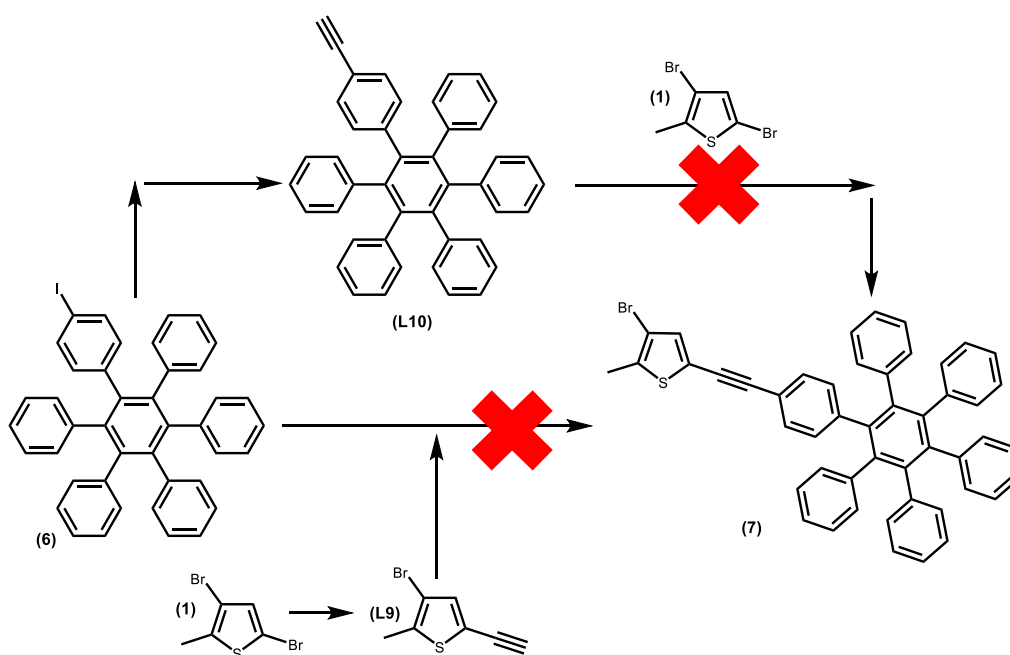
temperatures. The target compound was obtained as a precipitate from excess methanol as dark brown powder. However, further purification via silica column chromatography using CH_2Cl_2 : hexane (3: 7) as eleuent was utilised to remove unreacted benzophenone and starting materials. Product was recrystallised from methanol as a yellow powder in 65 % yield. Synthesis of iodo-diphenylacetylene and iodo-hexaphenylbenzene have been previously reported within the research group in the preparation of similar platforms.¹⁸



Scheme 2.6 Synthesis of iodo-hexaphenylbenzene, 6 (i) Benzophenone, 280 °C, 2 hours, 280-300 °C 16 hours, Ar (65 %)

2.2.10 Synthesis of 3-bromo-2-methyl-5-(1-ethynylHPB)thiophene, 7

Iodo-hexaphenylbenzene, 6, shown in Scheme 2.7, is employed in the preparation of the novel compound 3-bromo-2-methyl-5-(1-ethynylHPB)thiophene, 7. Two routes were initially employed, and Sonogashira cross-coupling reactions were undertaken both in a microwave reaction vessel and through standard convection heating. Scheme 2.7 shows both synthetic routes.



Scheme 2.7 Synthesis of 3-bromo-2-methyl-5-(1-ethynylHPB)thiophene, 7

Unfortunately, neither of these reaction methods proved viable and as such a new method for the synthesis of a HPB containing switch were undertaken. As such, the photophysics of the brominated-thienyl precursor could not be studied.

2.3 Characterisation of bromo-thienyl compounds, 2, 3, 4, and 5

2.3.1 NMR Characterisation of 2

The ^1H NMR of **2** is shown in Figure 2.2. The simplicity of the molecule allowed for facile assignment of the spectrum. Though both aromatic, thienyl and phenyl protons appear at different chemical shifts in ^1H NMR spectra, and so are readily distinguishable in the spectrum. The two doublets at $\delta = 7.36$ and 7.42 ppm, showing a slight roofing effect due to their environment, are assigned to those of the phenyl ring, and the singlet at $\delta = 7.12$ ppm is assigned to that of the proton at the 4-position of the thiophene, integrating for 1 H. This suggests the proton on the thienyl ring is slightly more shielded than those of the phenyl rings, due in part to its aromaticity and subsequent resonance forms, and also due to being adjacent to the bromine atom. The aliphatic region displays two signals, both singlets, at $\delta = 2.38$ ppm and 1.32 ppm, integrating for 3 H and 9 H, assigned to the methyl and tert-butyl functional groups respectively.

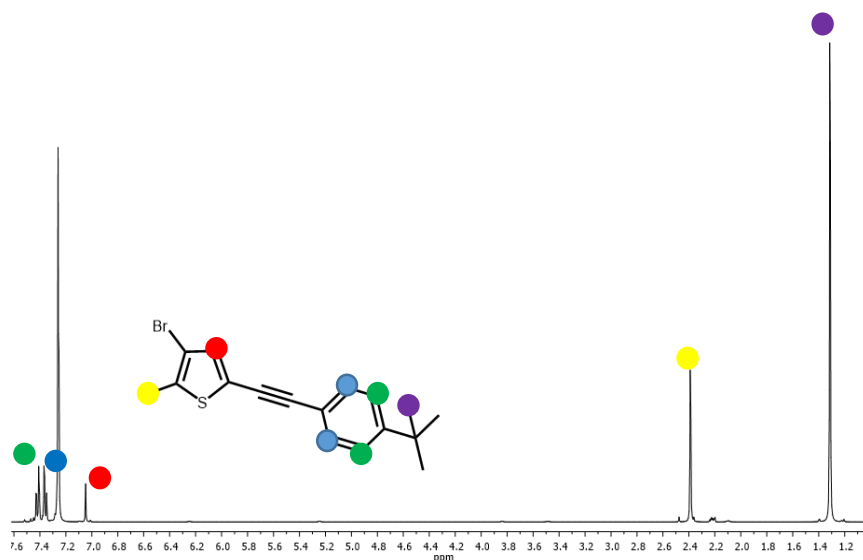


Figure 2.2 ^1H NMR spectrum of compound **2** (CDCl_3 , 400 MHz, RT)

2.3.2 NMR Characterisation of 3

Compound **3** was fully characterised using NMR spectroscopy (Figure 2.3) and mass spectrometry. On the ^1H NMR spectrum, the doublet at $\delta = 7.50$ ppm and the multiplet signal at $\delta = 7.49$ - 7.48 ppm along with the pair of doublets at $\delta = 7.47$ and 7.37 ppm were assigned

to the protons on the two phenyl rings. The doublet at $\delta = 7.50$ ppm integrated to two protons and had a coupling constant of 2.28 Hz. The multiplet at $\delta = 7.49$ -7.48 ppm integrated to two protons and the doublets at $\delta = 7.47$ and 7.37 ppm, which both had a coupling constant of 8.60 Hz, integrated to two protons each. A roofing effect was seen between the proton signal at $\delta = 7.47$ and 7.37 ppm and this confirmed, along with the identical coupling constants, that these signals represented protons on the same phenyl ring. The singlet at $\delta = 7.14$ ppm integrated to one and represented the single proton on the thiophene ring. The singlet present at $\delta = 2.43$ ppm integrated to three protons and this represented the protons of the methyl group on the thiophene ring. The protons on the *tert*-butyl groups were represented by the singlet peak at $\delta = 1.33$ ppm which integrated to nine protons. The ^{13}C NMR was resolved and the proton signals for the aromatic protons were differentiated with the aid of HSQC and HMBC 2D NMR spectra. The carbon signals at $\delta = 132.23$, 131.46, 125.14 and 125.52 ppm each coupled to an aromatic proton signal on the HSQC and hence were assigned to the carbons on the phenyl rings which were attached to protons. There was also an obvious coupling between the proton signal for the *tert*-butyl protons and the carbon signal at $\delta = 31.31$ ppm; therefore, this carbon signal was assigned to the methyl carbons on the *tert*-butyl group.

In the HMBC spectrum, the *tert*-butyl protons also coupled to carbon signals at $\delta = 34.95$ and 151.84 ppm. These quaternary carbons were assigned to the quaternary carbon on the *tert*-butyl group and the quaternary aromatic carbon adjacent to the *tert*-butyl group, respectively. The signal at $\delta = 151.84$ ppm also coupled to the proton signal at $\delta = 7.47$ ppm on the HMBC spectrum; therefore, this confirmed that this aromatic proton signal corresponded to the proton in the ortho-position, with respect to the *tert*-butyl group, of the phenyl ring adjacent to the *tert*-butyl. The proton signal at $\delta = 7.14$ ppm coupled to the carbon signal at $\delta = 126.09$ ppm on the HSQC spectrum; hence, this signal was assigned to the only carbon which was directly attached to a proton on the thienyl ring. This proton coupled to a carbon signal at $\delta = 134.34$ ppm which also coupled to a proton signal at $\delta = 2.43$ ppm on the HMBC spectrum. This carbon signal could therefore be assigned to the carbon attached to the methyl group on the thiophene ring. The signal for the methyl protons on the thiophene ring also coupled to the carbon signals at $\delta = 110.23$ and $\delta = 15.05$ ppm on the HMBC and HSQC spectra, respectively. The former peak represented the quaternary

carbon attached to the bromine atom and the latter signal corresponded to the methyl carbon on the thienyl ring.

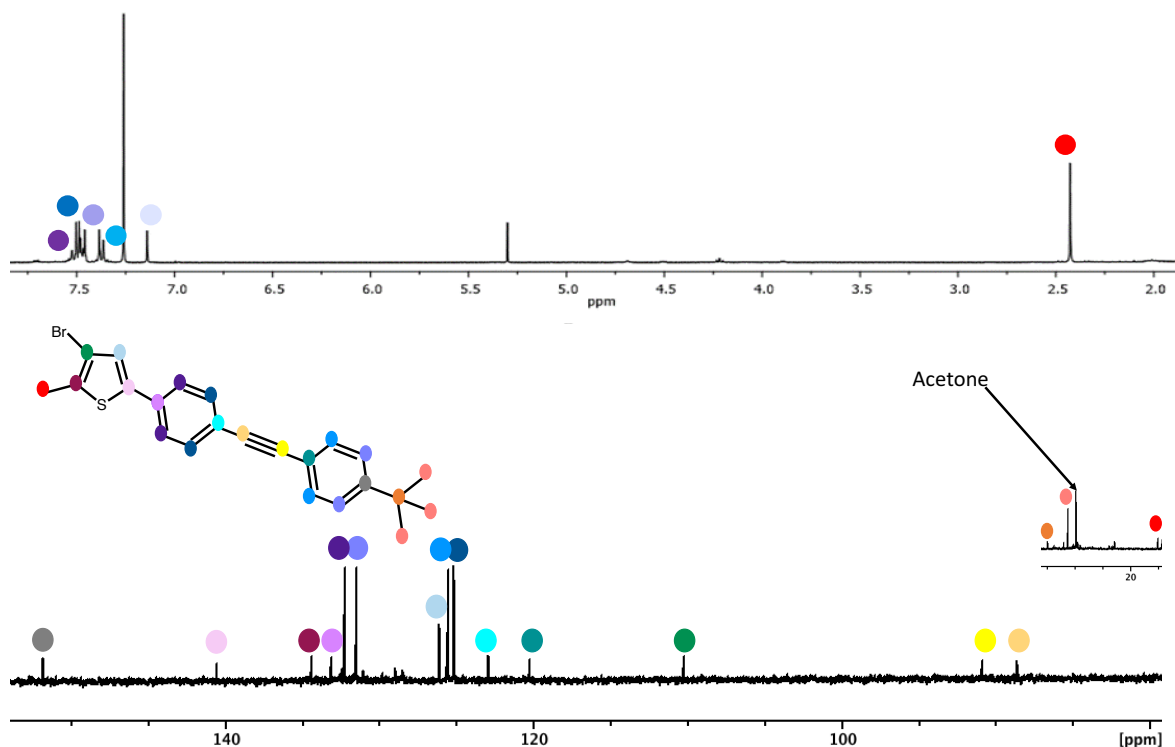


Figure 2.3 ^1H and ^{13}C NMR of compound **3**, methyl groups removed for clarity (CDCl_3 , 400 MHz, RT)

2.3.3 NMR Characterisation of **4**

The ^1H NMR spectrum of **4** is presented in Figure 2.4, and is comprised of three methyl protons and a single thienyl proton, with an additional three doublets and four triplets allocated to the naphthyl group. A ^1H - ^1H COSY experiment for **4** identified one three spin system and one four spin system as expected. The sole triplet of the three-spin system was distinguished at $\delta = 7.45$ ppm. It couples to two of four doublets at $\delta = 7.82$ ppm and 7.75 ppm. The doublet adjacent to the acetylene appears slightly more upfield and is assigned the doublet at $\delta = 7.75$ ppm. The proton residing next to the acetylene is the more deshielded of the remaining doublets and has been labelled accordingly at $\delta = 8.34$ ppm. The two triplets situated on the four-spin system appear at $\delta = 7.62$ and 7.58 ppm. 1D selective ROESY experiment identified the doublet at $\delta = 7.62$ ppm as the proton adjacent to the doublet at $\delta = 8.34$ ppm. The thienyl proton appears as a singlet at $\delta = 7.17$ ppm and integrates for one proton.

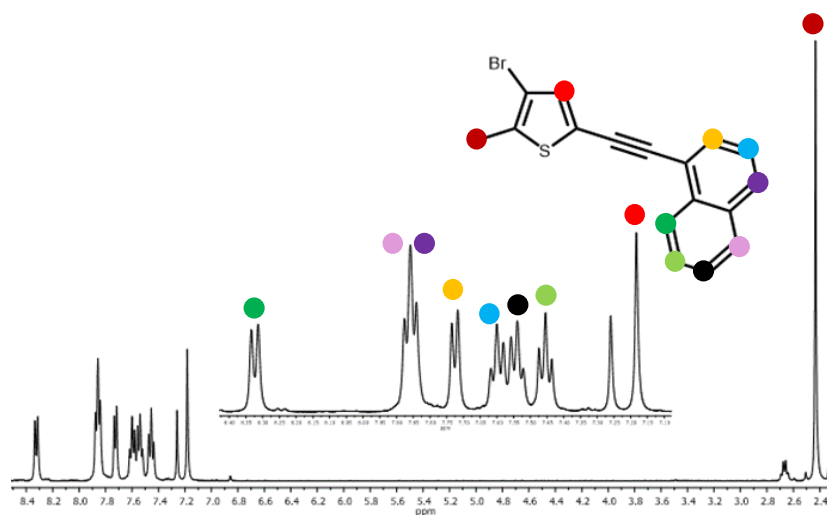


Figure 2.4 The ^1H NMR spectrum of **4** (CDCl_3 , 400 Hz, RT)

2.3.4 NMR Characterisation of **5**

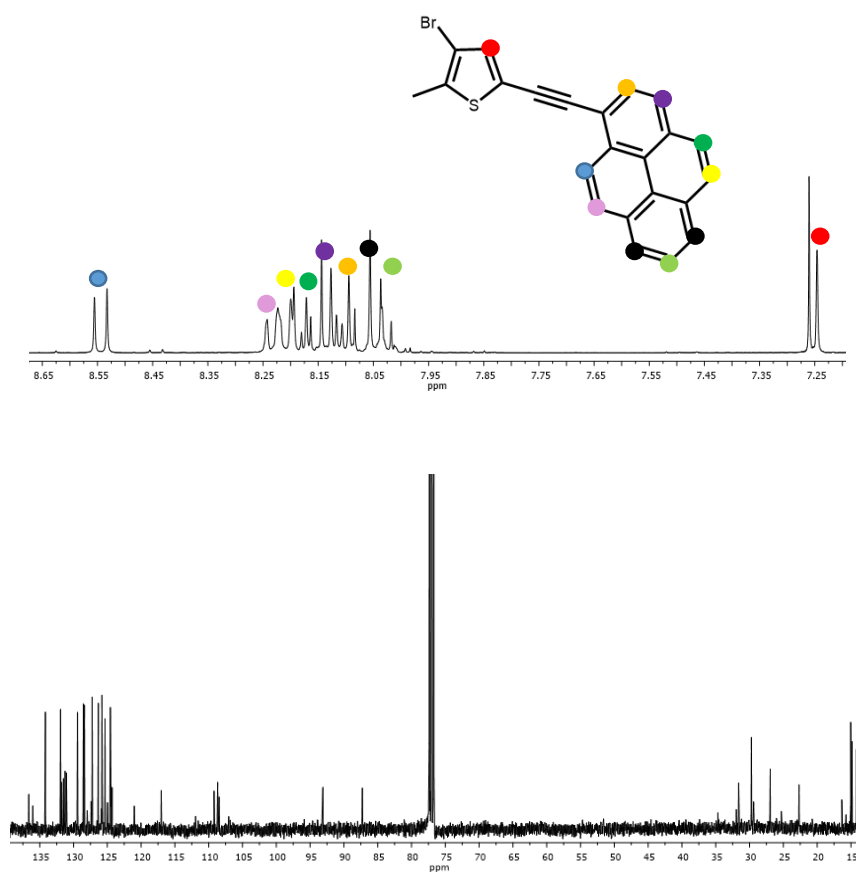


Figure 2.5 The ^1H and ^{13}C NMR of **5**, with assignment of the proton signals and corresponding carbon signals (CDCl_3 , 600 MHz, RT).

Figure 2.5 shows ^1H and ^{13}C NMR spectrum obtained for **5**. The large overlapping multiplet between $\delta = 8.00$ and 8.25 ppm contains the majority of the signals attributed to the pyrene moiety. Examination of the HH-COSY experiment proved to be very futile in the assignment of many spin systems, therefore alternative 1D experiments were employed. Selective ROESY experiments through irradiation at various resonances enabled the assignment of neighbouring spins, such as the one below the acetylene linker. Selective TOCSY also proved quite useful in assignment of the chromophore signals, and was used to establish the relative order of the three doublets between $\delta = 8.05$ and 8.15 ppm, each of which integrate for one proton. Irradiation of the central doublet reveals connectivity to the other two. This experiment was repeated by irradiating for a short period of time at $\delta = 8.05$ ppm, which revealed a correlation to the doublet at $\delta = 8.10$ ppm only, thus verifying the order in which the doublets have been assigned. The thienyl proton again appears a singlet at $\delta = 7.25$ ppm, more downfield with respect to the corresponding signals seen in compounds **2**, **3** and **4**. The ^{13}C carbon is also shown and assignment of the carbon signals were done through HSQC and HMBC experiments after the initial proton signals had been established.

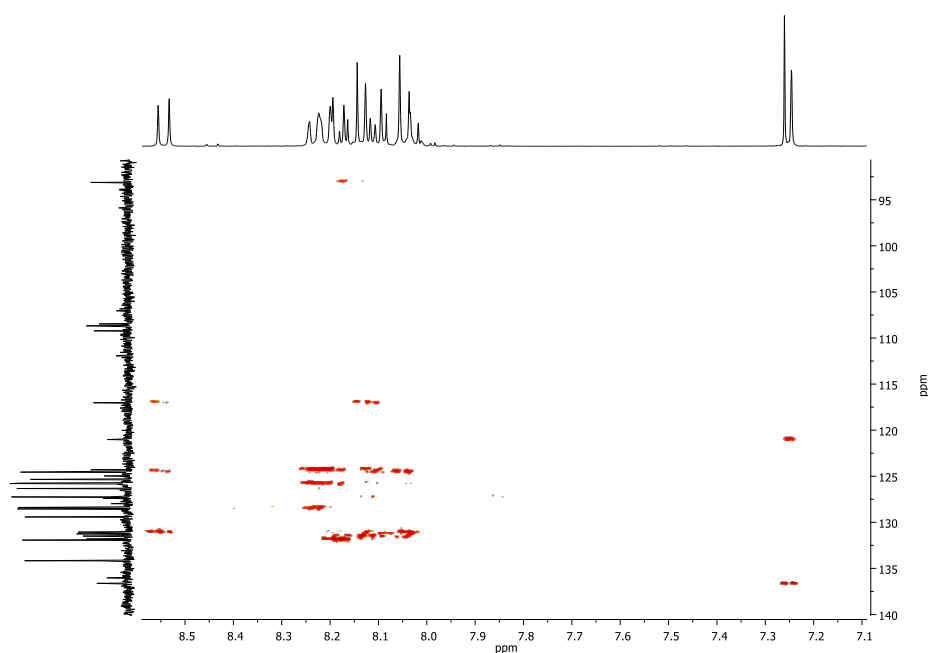


Figure 2.6 The HMBC NMR spectra of **5**, highlighting the aromatic region for the assignment of the carbon signals.

Figure 2.6 shows the absorption and emission spectra of **5** in CH_2Cl_2 . The compound shows very intense, structured absorption bands, which are analogous with pyrene and pyrene-

based conjugated systems. The intensity of the peak at $\lambda = 350$ nm is attributed to the additive pattern of the thienyl ring, which also absorbs strongly in this region. The excitation however is very broad and featureless, which is not usually indicative of emissive pyrene monomers, which have an equally structured emission pattern as to their absorption pattern, with more obvious fine structure in their results. The broad featureless absorption seen here is more commonly seen in pyrene excimer formation, which occurs at higher concentrations.¹⁹⁶ This would be congruent with the molarity of compound made up for these analytical tests (1×10^{-4} M). This was purposely undertaken, as a direct comparative can be made about the stacking of the pyrene moieties in compound **5** and in compound **11**, as will be seen. The propensity to form this stacking structure is diminished upon lithiation and subsequent reaction with octafluorocyclopentene to make switch **11**. Excimer formation is seemingly unhindered in compound **5** with the sterics of the brominated ethynylthiophene having little influence on the excimer formation or on its distinctive photophysical emission. Extension of this conjugated system via a perfluorinated backbone and mirrored pyrene-appendage has interesting photochemical properties but does not inhibit excimer formation exactly as seen here.

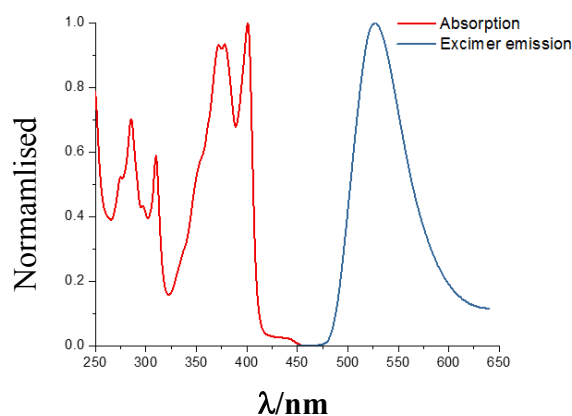


Figure 2.7 Normalised UV-Vis absorption spectrum of **5** in CH_2Cl_2 (1×10^{-4} M)

2.4 UV-Vis absorption of compounds 2-5

The UV-Vis absorption spectra of compounds **2**, **3**, **4** and **5** are shown in Figure X. Compounds **2**, **3** and **4** are generally featureless, with only a few notable absorption maxima in the UV region of the spectrum, normally attributed to high energy transitions occurring within the molecule, π - π^* . The fine structure of the absorption pattern may indicate a more intricate level of communication within the compounds, with the phenylene spacer group of compound **3** hindering sufficient electronic pathways, whilst in **2** and **4**, due to the smaller

side and only a single acetylene spacer group, more definitive transitions can occur. This is also reflected in the higher level of fine structure in the compounds. In phenylacetylene, absorption in the UV region ($\lambda > 250$ nm) is usually quite low and generally only occurs at much lower wavelengths. As such, the λ_{max} of compound **3**

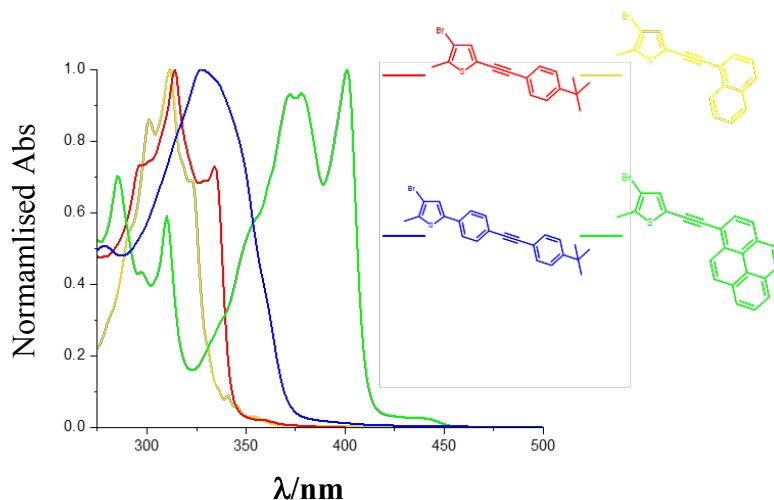


Figure 2.8 UV-Vis absorption spectrum of compounds **2**, **3**, **4** and **5** (CH_2Cl_2 , 1×10^{-5} M, RT)

As such, the λ_{max} of compound **3**, $\lambda_{\text{max}} = 330$ nm, may be an internal transition within the thienylphenyl moiety only, as thienyl transitions are shown to occur in this wavelength range, though the broadness of the peak may also be attributed to a slight degree of conjugation within the system. Electronic transitions in pyrene are well understood, and each individual peak in its absorption spectrum indicates the level of conjugate absorption in the system, as evidenced by the overall red-shift in the visible region, as well as the red-shift of the thiophene absorption to $\lambda = 370$ nm.

2.5 Dithienylethene-based molecular switches with 1-ethynylaryl appendages

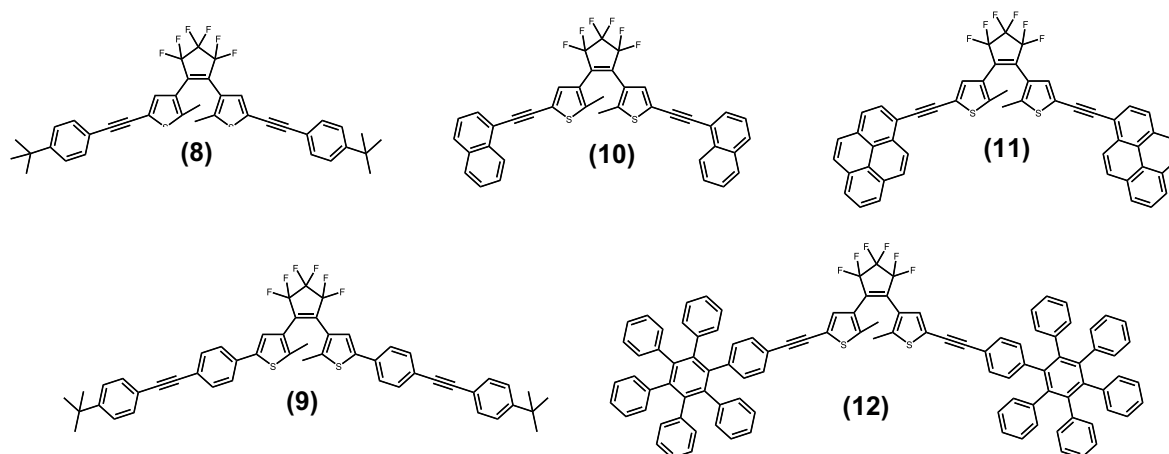
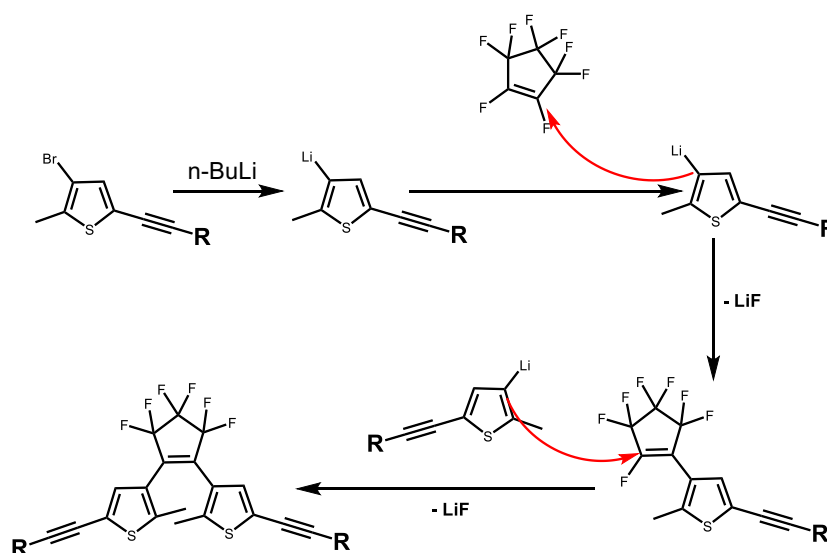


Figure 2.9 Dithienylethene-based molecular switches with 1-ethynylaryl appendages

Figure 2.9 shows the five ethynylPAH-based dithienylethene switch products that were synthesised for the study of their photochromic properties via precursor compounds **2**, **3**, **4**, **5**, **6** and **7**. Increasing of conjugation within the system had unique and unexpected effects, with switch **10** showing the most potential in terms of quantum yield, fatigue resistance, absorption maximum and intensity of photocyclisation. A further study of the cyclodehydrogenated product of **12** had hoped to be undertaken also, but thus far current reaction methods have failed to produce the desired product. The ethynyl-bridge switch, **L12**, alone has showcased itself impressive photochromic ability, and thiophene-PAH directly substituted switches showed a 30 nm blue shift compared to their acetylene-based counterparts.¹⁹⁷ For switches **8-11**, the brominated precursors already discussed allowed for direct routes to the final products. Switch **12** however proved more difficult to work with, due to its size in comparison to the octafluoro-backbone, as well as its degree of insolubility, and so an alternate method was devised for this compound.

2.5.1 General lithaithion procedure for generating 1-ethynylaryl dithienylethene-based switches.

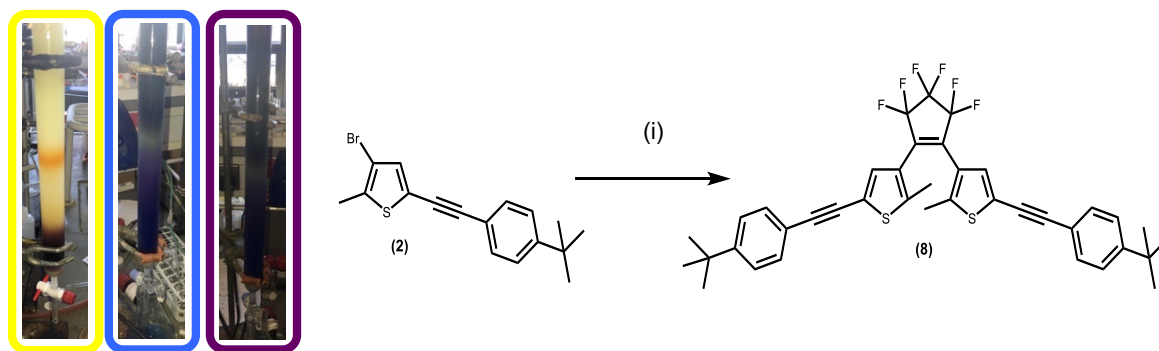


Scheme 2.8 Reaction of $n\text{-BuLi}$, brominated thienylethynylaryl appendages and perfluorocyclopentene to yield target switching compounds.

Addition of octafluorocyclopentene moiety varied between polycyclic aromatic hydrocarbon structures. Both direct addition of the backbone and addition in still-dried THF/diethyl ether was undertaken.

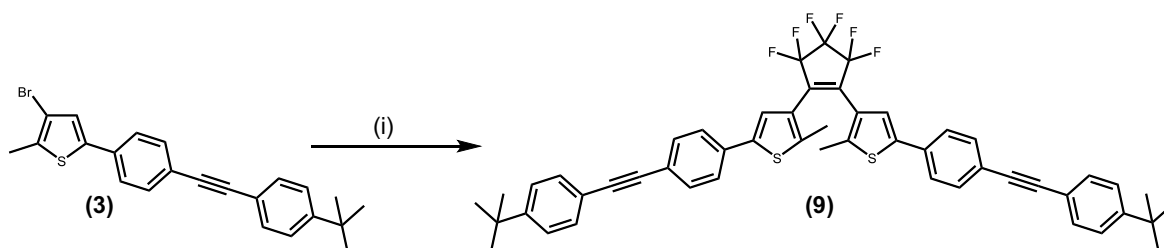
2.5.2 Synthesis of 1,2-Bis(5-(4-*tert*-butylphenylacetylene)-2-methylthiophen-3-yl)perfluoro cyclopentene), **8**

Compound was lithiated upon reaction with *n*-BuLi in THF at -78 °C, and was accompanied by an immediate colour change from yellow to dark red. Octafluorocyclopentene was added upon cooling, *via* cannula, into a degassed system. Initial reactions proved unsuccessful and use of a gas-tight syringe and injection of the octafluorocyclopentene directly into the system proved much more successful, and reduced reaction time significantly. Upon neutralisation of the reaction, the molecular switch was purified by column chromatography on SiO₂ using hexane as eluent, to produce a dark blue photoswitching powder in 65 % yield. The solid product showed photochromic capability under visible and UV light as well as photochromic switching in solution (Scheme 2.9).



Scheme 2.9 Lithiation of compound **8**, generating photochromic molecular switch **4**, (i) carried out at -78 °C in THF with octafluorocyclopentene and *n*-BuLi, 2 hours, Ar, 61 % yield. Inset shows real time photochromic ability of **8** on silica column.

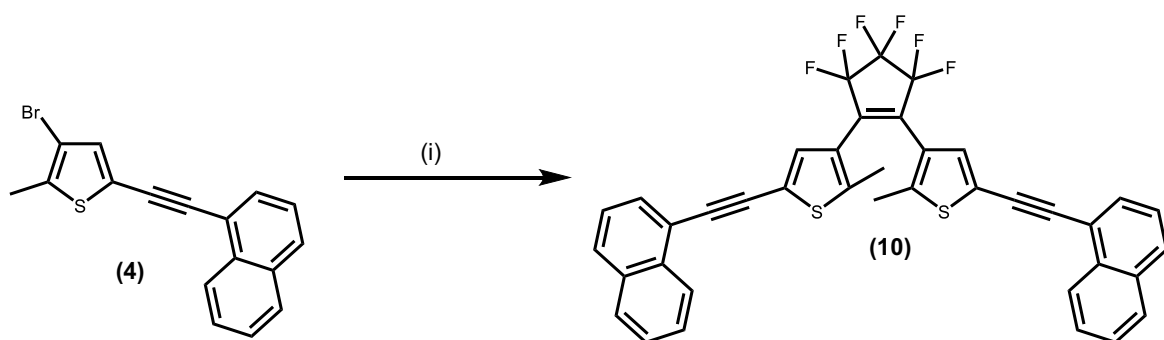
2.5.3 Synthesis of 3,3'-(perfluorocyclopent-1-ene-1,2-diyl)bis(5-(4-((tert-butyl)phenyl)ethynyl)phenyl)-2-methylthiophene), **9**



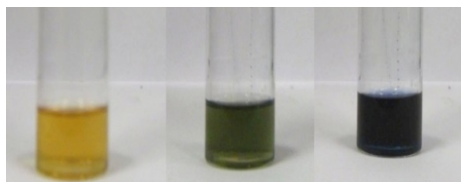
Scheme 2.10 Synthesis of **9**, (i) THF, Et₂O, BuLi, -78 °C, 1.5 h; (ii) THF, -78 °C, 4 h, 63 %.

The synthesis of molecular switch **9** was performed by the lithiation of **3** followed by the addition of octafluorocyclopentene to the reaction mixture. Both steps were carried out at very low temperatures, between -78 and -90 °C. This synthesis required strict anhydrous conditions and hence, although dry solvents were used in the reaction, addition of molecular sieves were required to both the reaction flask and the flask containing the octafluorocyclopentene solution. Solution was then neutralised with HCl (10 %) and extracted with diethyl ether. The organic layer were removed using vacuum to produce a dark brown product. This crude sample showed no initial photochromic activity, however, upon purification using silica chromatography with hexane as eluent, the product was obtained as a light blue powder (63 %)

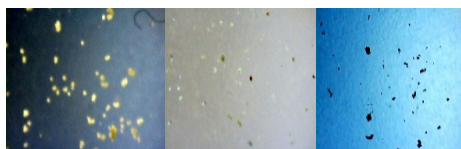
2.5.4 Synthesis of 1,2-Bis(5-(4-tert-butylphenylacetylene)-2-methylthiophen-3-yl)perfluoro cyclopentene), **10**



Scheme 2.11 Reaction of **4**, *n*-BuLi and perfluorocyclopentene that generates photochromic molecular switch **10**, (i) carried out at -78 °C in THF with octafluorocyclopentene and *n*-BuLi, 2 hours, Ar (49 % yield)



The first step of the procedure was to be carried out at $-78\text{ }^{\circ}\text{C}$. *n*-BuLi was used to elicit the halogen-lithium exchange and thus allow addition to the perfluorocyclopentene moiety. Reaction was allowed to stir at low temperature for 6 hours until a slight colour change was observed, followed by the slow acclimation of the reaction vessel to room temperature

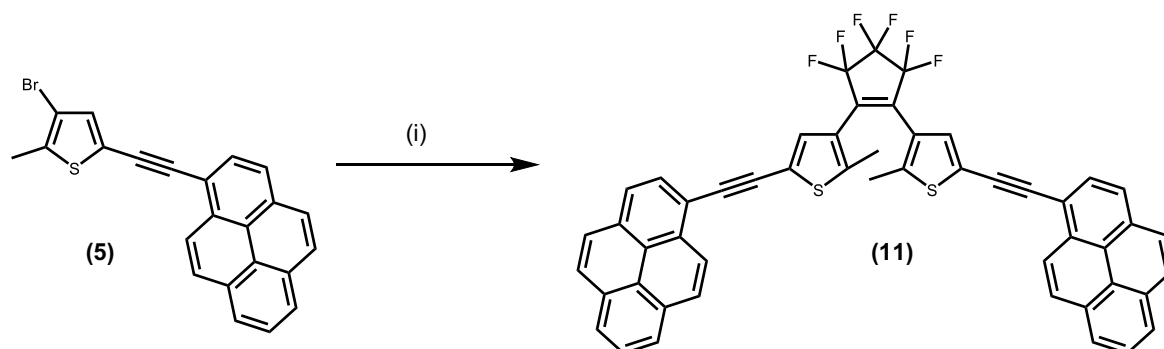


overnight Electron spray mass spectrometry of the product proved insufficient and so MALDI-TOF mass spectrometry was required for proper assignment of the mass. Photochromic ability of switch **10** in solution and as a solid are shown in inset picture. Irradiating **10o** (open form isomer) with short range UV light (360 nm) generates the closed form, **10c**, while illumination of the closed isomer with visible light switches it back to the open form. The crystals were grown by dissolving sample of **10** in dichloromethane and layering with methanol and hexane. However, though crystals were obtained, they were unable to be analysed for single crystal X-ray diffraction and therefore only images using recording imagery on an optical microscope were obtained instead. The microscope was able to capture in real time the changing isomerisation of the molecular switches at a macro level by inducing the photocycloreversion with its own visible light. These images were taken at varying stages of the reversion. It is interesting to note that these photochromic changes and its viability at solid state suggest a real-time change in the structure of the crystal lattice of the compound, with this being reflected in alterations to the overall size and shape at the macro scales. Attempts to obtain definitive crystal structures of the open and closed forms of this compound are still ongoing

2.5.5 Synthesis of 1,2-Bis(5-(4-*tert*-butylphenylacetylene)-2-methylthiophen-3-yl)perfluoro cyclopentene), **11**

Molecular switch **11** was synthesised in a similar manner to that previously discussed for switches 8-10. Starting material **5** was lithiated with *n*-BuLi in THF for an hour, and the resulting species was allowed to react with perfluorocyclopentene overnight, with the temperature left at $-78\text{ }^{\circ}\text{C}$ for at least four hours. This carbon-carbon bond formation is the rate determining step in these reactions, and a slow colour change from dark brown/purple to yellow is observed. As with all previous reactions, this reaction is extremely sensitive, to moisture especially, which may react faster with the lithiated “transition state” to quench

the starting material. Use of slight excess of titrated *n*-BuLi and molecular sieves helped to impede this side reaction, a side reaction which prevents the recovery of any starting materials due to removal of the reactive bromine upon initial lithiation.

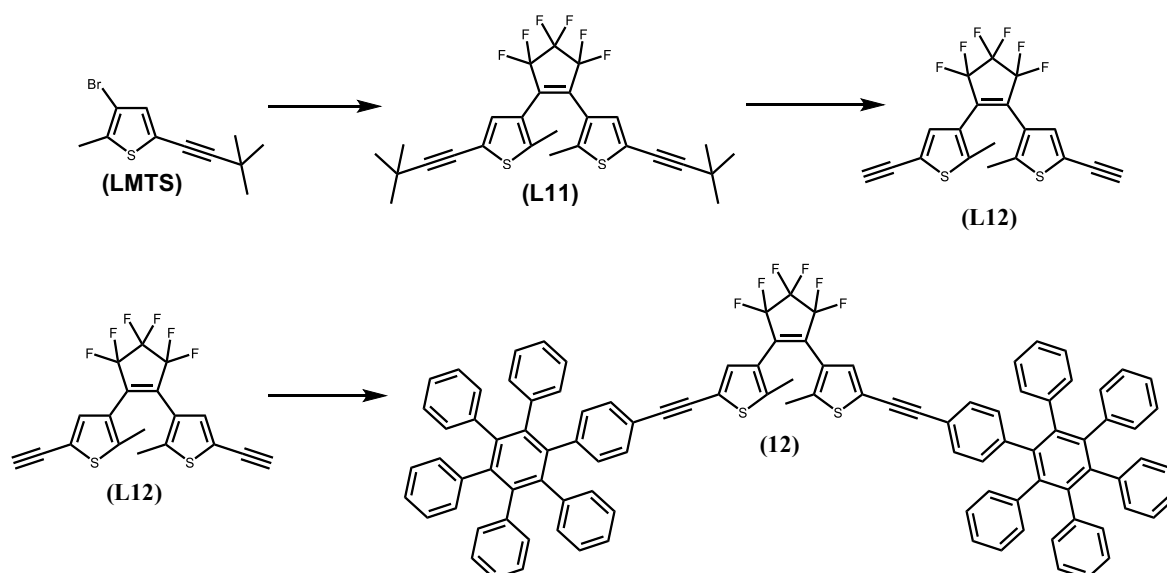


*Scheme 2.12 Reaction of 5, *n*-BuLi and perfluorocyclopentene that generates photochromic molecular switch 11, reaction under Ar in THF, 1 hour, (45 %)*

These final steps represent the most frustrating of the synthetic processes of molecular switch generation, as due to the octafluorocyclopentene's low boiling point (b.p. 25 °C), and subsequent storage (0 – 10 °C), moisture is inherently present in the reaction upon the addition of the fluorinated backbone. An immediate colour change from dark brown to orange is noted when this quenching occurs. As such, each lithiating switch reaction required repeating numerous times to extrapolate ideal reaction conditions. Switch 11 was purified via column chromatography using hexane: CH₂Cl₂ (1:1) as eluent, with the product running much slower across the stationary phase than expected. The product was obtained as a yellow powder which displayed photochromic activity only at higher concentrations (yield 45 %).

2.5.6 Synthesis of 1,2-Bis(5-(4-*tert*-butylphenylacetylene)-2-methylthiophen-3-yl)perfluoro cyclopentene), 12

Due to the failing reaction to produce the thienyl-HPB precursor 7, an alternative method of reactivity was approached. Compound **LTMS** was synthesised and then lithiated by stirring with *n*-BuLi at -78 °C in dry, degassed THF: diethyl ether (1: 1, v/v, 100 mL) for two hours.¹⁹⁸ The resulting species was reacted with perfluorocyclopentene overnight, furnishing the trimethylsilyl-DTE protected core, **L11**. The trimethylsilyl protecting groups were then removed, following purification using silica chromatography (using hexane as eluent), by stirring the solution in a NaOH/TBAF mixture in THF/MeOH to give 1,2-bis(2-methyl-5-ethynyl-3-thien-yl)perfluorocyclopentene, **L12**.



Scheme 2.13 Synthetic procedure towards molecular switch **12** (i) *n*-BuLi, octafluorocyclopentene, $-78\text{ }^{\circ}\text{C}$, 2hrs, 65 % (ii) KF, TBAF, MeOH/THF, overnight, 81 % (i) $\text{Pd}(\text{PPh}_3)_2\text{Cl}_2$, CuI, PPh_3 , iodohexaphenylbenzene, NHEt_2 , overnight, $90\text{ }^{\circ}\text{C}$

This was then reacted overnight, at $90\text{ }^{\circ}\text{C}$, with iodohexaphenylbenzene, **6**, using $\text{Pd}(\text{PPh}_3)_2\text{Cl}_2$ as a catalyst in a Sonogashira cross-coupling reaction. The final product was purified using silica chromatography due to the extremely low yield of the reaction (16 %). The low yield may be due to the instability of switching precursor, **L12**, which was seen to decompose after a short period of time. The reasons for this possible instability are thus far unknown, even when sample is stored in the dark. The silylated starting material **LTMS** was shown to undergo a similar decomposition. Product **12** was obtained as a yellow powder, which showed small photochromic activity upon exposure to UV light.

2.6 Characterisation of compounds 8-12

2.6.1 NMR analysis of **8**

Assignment of the geometric structure of compound **4** was achieved using ^1H NMR, ^{13}C NMR, ^1H - ^1H COSY, HSQC and a long range HMBC. Initial assignment through the use of the ^1H NMR spectrum of the open form confirmed the presence of expected number of proton signals (Figure 2.11). The phenyl ring protons appear in the region between $\delta = 7.36 - 7.45$ ppm, a typical region for aromatic signals, as two double bonds integrating for 4 protons each, and a singular thienyl proton appears at $\delta = 7.24$ ppm, overlapping with solvent CDCl_3 signal. The methyl groups appear at $\delta = 1.93$ ppm and the *tert*-butyl hydrogen signals appear at $\delta = 1.35$ ppm, integrating to 3 and 9 protons respectively. No distinction could be

made between *antiparallel* and *parallel* forms of the open isomer ^1H NMR spectrum, suggesting rapid interconversion is occurring. The ^{13}C spectrum, coupled with the acquired HSQC (*Heteronuclear Single Quantum Coherence*) spectrum allowed identification of the carbon atoms. The photostationary state (PSS) “closed” form NMR was also analysed to assess prominent chemical shifts between the two distinguishable forms. The most noticeable of these is the shift of the thienyl, H_4 , proton, on going from $\delta = 7.24$ ppm in the open to $\delta = 6.46$ ppm in the PSS form. The delocalisation of the π -electrons upon closed-ring conjugation shows a shielding affect on the chemical shift. Consequently, the thienyl proton of the starting material of the final step, **2**, has an intermediate chemical shift between that of the open and closed forms at $\delta = 7.04$ ppm, due to the electron cloud within the aryl thiophene substituent itself. The reverse is seen of the thienyl methyl signals, as their new more defined stereochemistry is deshielded from the magnetic field. The “closed” form NMR suggests an unequal mixing of the photoisomers, with mixing of signals expected due to the incomplete photocyclisation reaction occurring throughout the system and so conversion ratio could not be established through the basis of NMR alone do to the overlap of signals in the PSS spectrum. A “roofing” affect is also observed for the signals in the aromatic region, a high-order splitting pattern that takes place when chemical shift difference in hertz is much less or the same that order of magnitude as the J coupling.

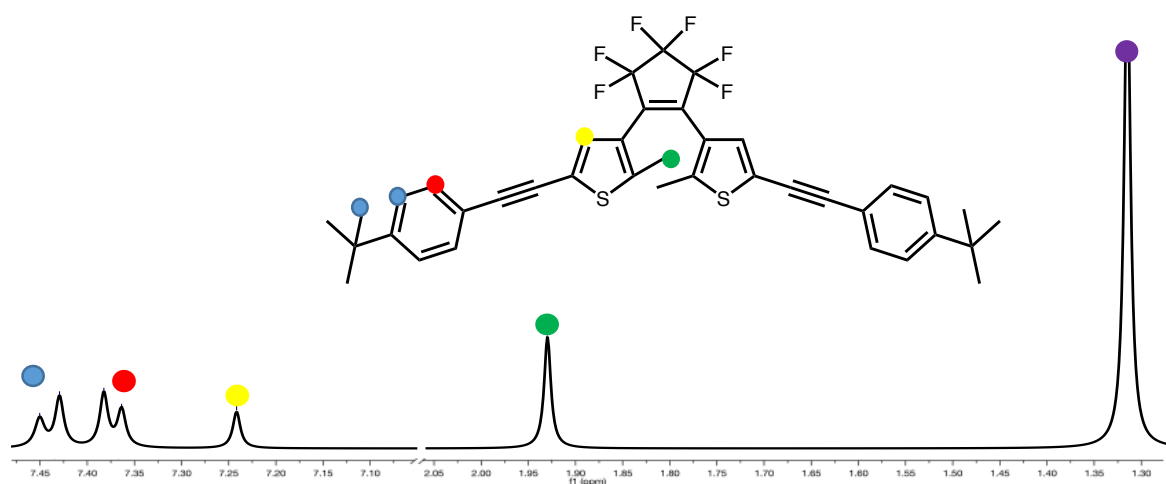


Figure 2.11 ^1H NMR spectrum of photochromic compound **80** (open form), showing selectively highlighted areas of interest, and assignment of the proton signals, in CDCl_3 (400 MHz, RT).

2.6.2 NMR Characterisation of 9

Compound 9 was fully characterised using NMR spectroscopy and mass spectrometry. NMR spectra were recorded for both the open and closed isomers of **5**. A C_2 axis of symmetry results in somewhat simpler NMR spectra. In the open isomer (**5o**), the aromatic signals that appear as doublets at $\delta = 7.56$ (●), 7.52 (●) and 7.41 ppm (●), along with the multiplet at $\delta = 7.54$ - 7.53 ppm (●), on the ^1H NMR spectrum, were assigned to the protons on the phenyl rings (Figure 2.1). The integration of each of these signals represented four protons. The doublet at $\delta = 7.56$ ppm had a coupling constant equal to 5.48 Hz. The coupling constants for the resonances at $\delta = 7.52$ and 7.41 ppm were equivalent and had a value of 8.72 Hz. The singlet at $\delta = 7.31$ ppm (●) was assigned to the aromatic proton on the thienyl ring. In the aliphatic region of the spectrum, there were two singlets present: one at $\delta = 2.50$ ppm with an integration value of six protons and the other at $\delta = 1.36$ ppm, which integrated to represent eighteen protons. From these integration values, the resonance at $\delta = 1.36$ ppm was assigned to the protons on the *tert*-butyl groups and the peak at $\delta = 2.50$ ppm corresponded to the methyl protons attached to the thiophene ring. HSQC and HMBC 2D spectra were used to differentiate between the different proton signals on the phenyl rings and to assign the resonances on the ^{13}C NMR spectrum. On the HSQC spectrum, the aromatic protons at $\delta = 7.56$, 7.52 and 7.31 ppm coupled to carbon signals at $\delta = 132.29$, 131.49 and 122.66 ppm respectively. The proton resonances at $\delta = 7.54$ - 7.53 ppm and $\delta = 7.41$ ppm coupled to the same carbon signal at $\delta = 125.52$ ppm. The proton peaks at $\delta = 2.50$ and 1.36 ppm were coupled to the carbon signals at $\delta = 14.81$ and 31.25 ppm, respectively. On the HMBC spectrum, the proton signal at $\delta = 1.36$ ppm coupled to the quaternary carbon signals at $\delta = 34.91$ ppm and 151.86 ppm. The resonance at $\delta = 34.91$ ppm was assigned to the quaternary carbon on the *tert*-butyl group. The peak at $\delta = 151.86$ ppm was determined to represent the quaternary aromatic carbon adjacent to the *tert*-butyl. The proton signal at $\delta = 2.50$ ppm showed coupling to the carbon signals at $\delta = 120.73$ ppm and 143.62 ppm and these carbon resonances also coupled to the thienyl proton at $\delta = 7.31$ ppm. The signal at $\delta = 143.62$ ppm was assigned to the carbon nucleus on the thienyl ring adjacent to the methyl substituent. The resonance at $\delta = 120.73$ ppm corresponded to the quaternary carbon adjacent to the cyclopentene ring. The proton resonance at $\delta = 7.31$ ppm was also coupled to the carbons at 142.00 ppm and 132.68 ppm. The carbon signal at $\delta = 132.68$ ppm coupled strongly to the proton signal at 7.56 ppm. Hence, this carbon resonance was assigned to the quaternary phenyl carbon adjacent to the thiophene ring.

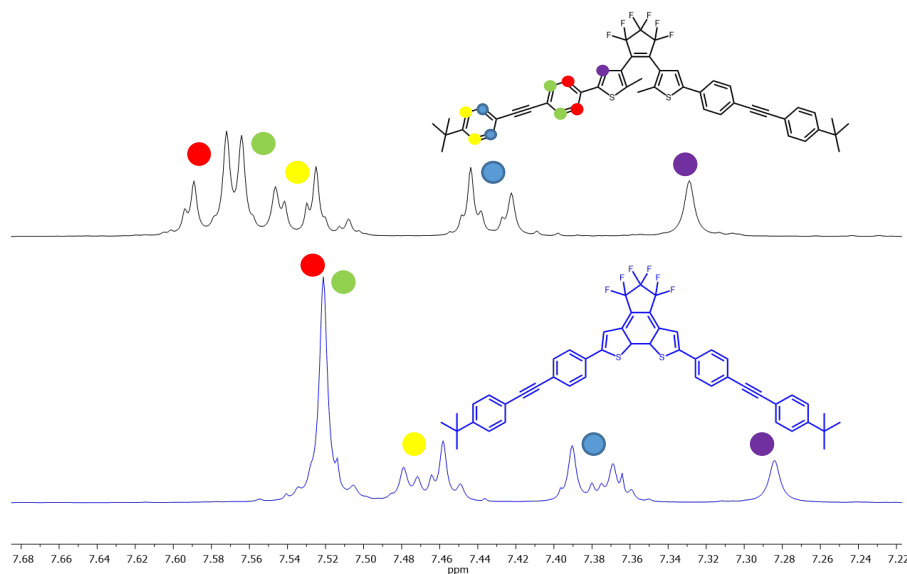


Figure 2.12 The aromatic regions of the ^1H NMR spectra of (a) the open isomer and (b) the closed isomer of **9**

The carbon peak at 142.00 ppm was therefore assigned to represent the carbon nucleus on the thiophene adjacent to the phenyl ring. The proton peak at $\delta = 7.54\text{--}7.53$ ppm coupled to the quaternary carbon signal at $\delta = 123.30$ ppm and this carbon peak was assigned to the quaternary aromatic carbon adjacent to the acetylene moiety. There was long-range coupling observed between the proton resonance at $\delta = 7.52$ ppm and the quaternary signal at 91.11 ppm and this carbon peak was assigned to acetylene carbon on the *tert*-butyl end of the acetylene bridge. The other carbon on acetylene moiety corresponded to the signal at 88.51 ppm. The quaternary carbon resonance at 120.17 ppm coupled to the proton signal at 7.41 ppm and this carbon signal represented the quaternary nucleus on this phenyl ring adjacent to the acetylene bridge.

One of the main differences between the NMR spectra of **9o** and the closed isomer (**9c**) was that in the spectra for **9c** the signals were shifted upfield relative to **9o** (Figure 2.1). There were signal shifts of approximately 0.04 ppm between the ^1H NMR spectra of **9o** and **9c**. This can be attributed to greater electron delocalisation in the closed isomer and hence the nuclei are more effectively shielded. Another major difference between the two ^1H NMR spectra is that in the spectrum for **9c** the signals for the protons on the phenyl rings adjacent to the thiophenes appear as a singlet, rather than a doublet, at $\delta = 7.52$ ppm.

2.6.3 NMR Characterisation of 10

An NMR was run on this open form, **10o**, and compared to a sample that had been irradiated under a UV irradiation for the same length of time. The second sample was the photostationary state of the switch. Most prominent on the proton NMR was the shift in the thienyl hydrogen, H₄, going from $\delta = 7.20$ ppm in the open form to $\delta = 6.62$ ppm in the closed form. The delocalisation of the π -electrons upon closed-ring conjugation has a shielding affect on the chemical shift. Consequently, thienyl protons of the starting material 3,5-dibromo-2-methylthiophene, **1**, has an intermediate chemical shift between that of the open and closed forms at $\delta = 6.88$ ppm, due to the electron cloud within the aryl thiophene substituent. Using this proton, or the methyl signal, assignment of the percentage conversion between open and closed in the PSS may be postulated. However, the methyl signals were initially hidden within side-product impurity signals and could not be clearly identified. An ¹⁹F NMR was run on both (**10o**) and (**10c**) instead, and a comparison between the F₆ shifts signals established the amount of open form in each. Integrating beneath the open and closed signals in the PSS enabled a conversion of 90 % to be estimated. A ¹H NMR spectrum of (**10o**) is shown below to show the lone H₆ signal. ¹H and ¹³C NMR, as well as HSQC, HH COSY and ¹⁹F NMR were all required to fully assign the proper signals to the structure completely.

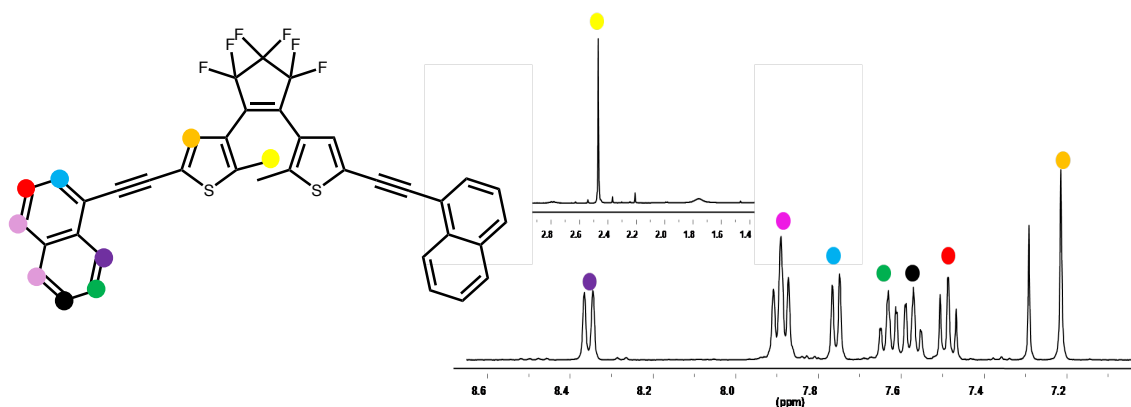


Figure 2.13 ¹H NMR of open isomer (**10o**) in CDCl₃ (400 MHz, RT).

Compound **11** showed a similar NMR pattern to its brominated precursor, however two of the doublets on the unsubstituted side, shown in pink, presented as single proton signal, a pair of overlapping doublets and could be distinguished as readily as in compound **4**. All other proton peaks were very well defined as part of the geometric structure assignment and characterisation of **10**.

2.6.4 NMR Characterisation of **11**

The proton spectrum of compound **11** was readily assigned due to the previous assignment of the brominated precursor discussed already. There was shift in the proton signals of the pyrene appendage, with all signals appearing between $\delta = 8.0$ and 8.54 ppm. The thienyl proton shows the most significant shift, with a much more upfield signal at 6.83 ppm. This is an extremely interesting shift for this proton in particular, due to the more shielded nature it now experiences. Conjugation upon generation of the dithienylethene molecular switches has been shown to have a complimentary deshielding effect on the thienyl protons in particular when in the open form. However, here the opposite is seen. This suggests that there is a considerable electronic extension of the pyrene moieties in this configuration, that allows for a much more chemically inert environment around the central aromatic rings. The only other feature of the proton spectrum are the methyl proton signals, appearing as a singlet at 2.31 ppm and integrating for 3 H. The pyrene signal adjacent to the acetylene group is shown in blue, a doublet integrating for 1 H. This proton experiences the most deshielded signal due to the triple bond character of the ethynyl moiety that it lies parallel to ($\delta = 8.54$ ppm). This is due to the acetylenes magnetic anisotropic effects, and the shielding cone the electrons produce within the bond.

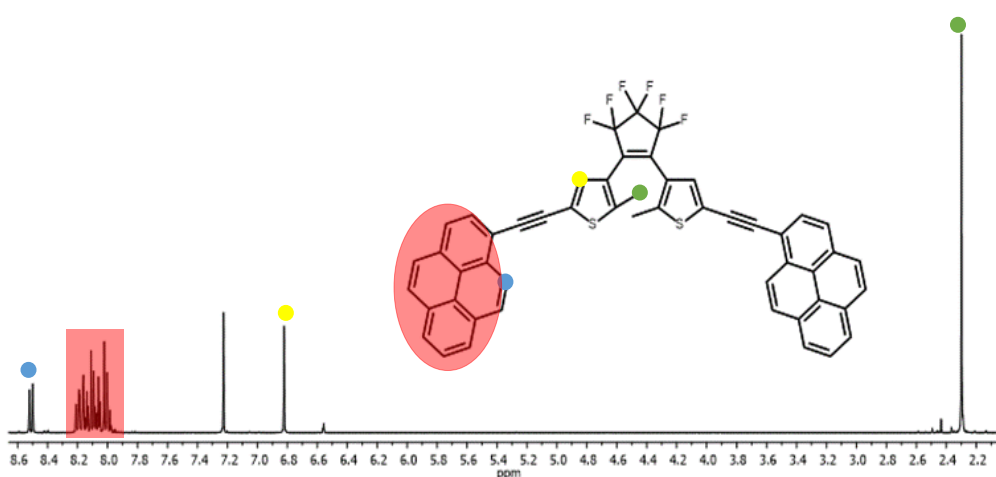


Figure 2.14 ^1H NMR of compound **11** (CDCl_3 , 400 MHz, RT)

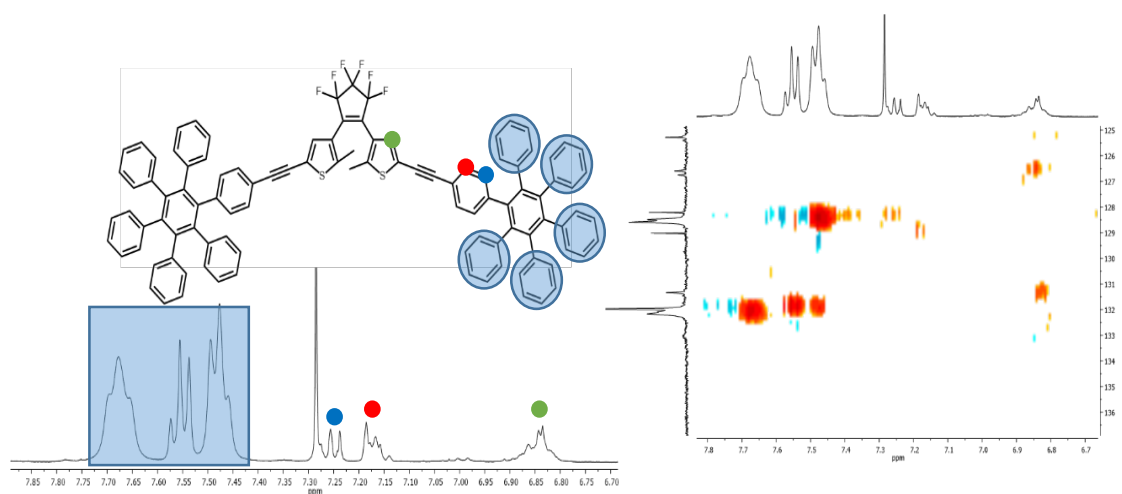
2.6.5 NMR Characterisation of **12**

Figure 2.15 ^1H NMR and HSQC NMR experiments of compound **12**.

The proton NMR for compound **12** is presented in Figure 2.15. The hexaphenylbenzene appendage was readily distinguishable as five sets of signals, appearing from $\delta = 7.15 - 7.75$ ppm. This extensive range for a quite symmetrical system can be understood in terms of the acetylene linker. The phenylacetylene moiety has a unique chemical environment due to the nature of the triple bonds electron cloud. The doublets at $\delta = 7.17$ and 7.25 ppm were assigned to the protons of the phenylacetylene ring, due to this more shielded nature compared to their more freely rotating counterparts. The thienyl proton appears at $\delta = 6.48$ ppm, and appears to be a distorted singlet; this may be due to preliminary switching occurring around the thiophene rings. The phenyl protons seem to be exhibiting a stacking nature due to the broadening and the lack of fine structure in the system, and appear as a series of multiplets in the more downfield range of the spectrum. What is interesting to note is the downfield shift exhibited by compound **12**, when compared to its iodohexaphenylbenzene precursor. The addition of an extended thienylacetylene moiety to this PAH may have a withdrawing effect on the rotating phenyl rings through the central benzene, and as such the electron cloud exists in a linear fashion from this benzene ring across the fluorinated backbone. The six protons in free benzene have a characteristic shift at $\delta = 7.33$ ppm, and so loss of this shielding electron cloud correlates with the results seen here. HSQC and HMBC long range analysis allowed for the assignment of carbon signals within the structure.

2.7 Spectroscopic analysis of compounds 2, 3, 4, 5 and 7, and switches 8-12

Irradiating a solution of compounds **8-12** with visible light causes a photocycloreversion-derived colour change from dark blue to clear, and subsequent irradiation with UV light causes reverse photocyclisation back to blue. This initial colour change due to irradiation of light of different wavelengths is indicative of a photochromic switch. UV-Vis absorption spectra were recorded for both the open and the PSS forms of the product, with variance of solvent, irradiating wavelength, and analysis of open to closed conversion as a function of irradiating time. Fatigue resistance and thermal conversion were both examined, and quantum yield of the photocyclisation reaction, $\phi_{o \rightarrow c}$, was undertaken using chemical actinometry. Preliminary fluorescence spectra were recorded due to the potential interest of these switches in fluorescence imaging experiments, and some compounds were tested to observe any electrocyclisation electrochemically mediated switching that may be occurring. All recordings were carried out in the dark, under constant temperature and in a sealed cuvette. **Xo** denotes the photoswitching compound in the open form, whilst **Xc** denotes the photostationary state (PSS) of the molecule, unless where otherwise stated (**X= 8-12**).

2.7.1 Photochemical analysis of compounds 2, 3, 4 and 5

2.7.1.2 Photochemical properties of 8

Absorption spectra, for both the open form and photostationary state, were recorded for compound **8**. A solution of **8**, in CHCl_3 , was irradiated with visible light to ensure a pure open isomer concentration had formed, before the UV-Vis measurements were taken. Irradiating with short wave UV light ($\lambda = 335 \text{ nm}$), allows photocyclisation to the closed form to occur (Figure 2.16).

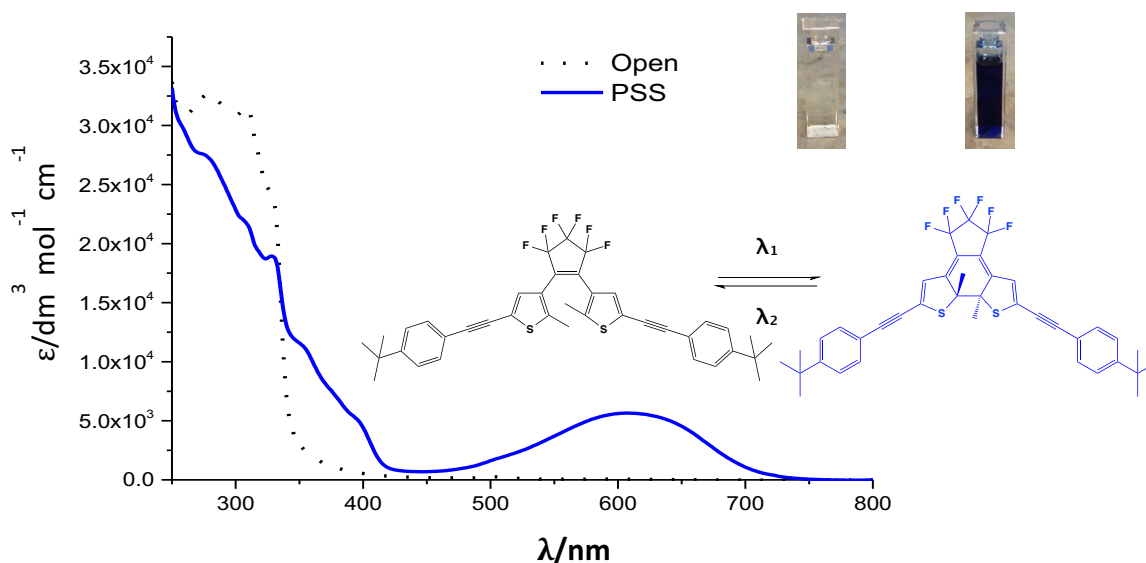


Figure 2.16 UV-Vis absorption spectra of the two photoisomers of **8o** and **8c**, in CHCl_3 at room temperature. Inset shows bond rearrangement and colour of compound when subjected to λ_1 and λ_2 .

The open form mostly absorbs in the UV region of the spectrum, with a λ_{max} of around 276 nm ($\epsilon = 33,000 \text{ dm}^3 \text{ mol}^{-1} \text{ cm}^{-1}$) and 311 nm ($\epsilon = 32,000 \text{ dm}^3 \text{ mol}^{-1} \text{ cm}^{-1}$). The PSS also absorbs in the UV region, though not as strongly as the open form. There is a discernible difference in the visible portion of the spectrum between the open and PSS forms of the switch with an additional $\lambda_{\text{max}} = 608 \text{ nm}$ ($\epsilon = 5,700 \text{ dm}^3 \text{ mol}^{-1} \text{ cm}^{-1}$) recorded for the predominantly closed form (Figure 2.16). The increased absorption in the red region accounts for the intense blue colour of the molecule after it has been subjected to UV light. These absorbances are attributed to the $n\text{-}\pi^*$ and $\pi\text{-}\pi^*$ electronic transitions that occur within its geometric structure. The bands become more structured with the increased rigidity of the system upon closure, and a red shift to low energy bands due to the increased conjugation arising from the cyclisation, with the π -electrons delocalizing further into the substituents, is observed. This high degree of conjugation compared to the open isomer, as well as the increased planarity of the closed form, stabilises the Lowest Unoccupied Molecular Orbital (LUMO) and destabilises the Highest Occupied Molecular Orbital (HOMO), resulting in a highly bathochromic absorbance shift into the red region.

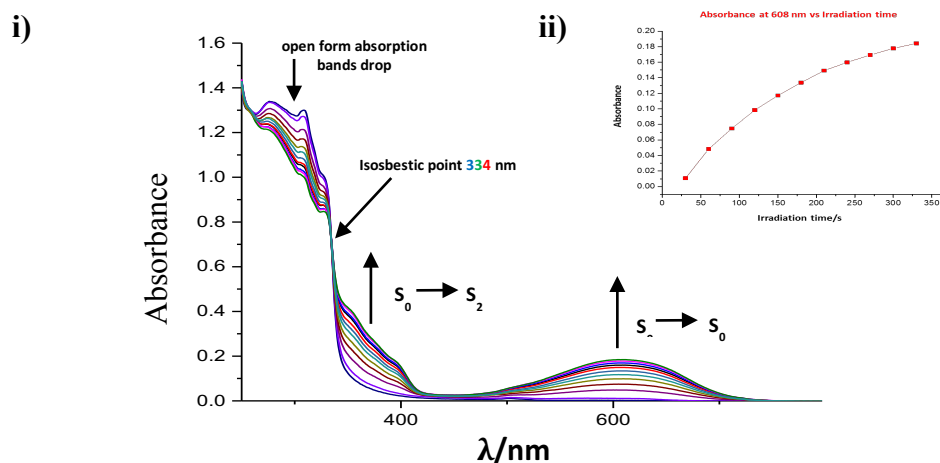


Figure 2.17 UV-Vis absorption spectrum of **8** in CHCl_3 , transitioning from open to “closed”, recorded over 5 minutes after 30 second intervals of irradiation with short range UV light ($\lambda = 254 \text{ nm}$). Inset shows absorbance increase at 608 nm as function of time.

A sample of **8** was irradiated with $\lambda = 254 \text{ nm}$ at 30 second intervals, recording from the pure open form, over a period of 5 minutes to yield the spectrum presented in Figure 7 a). As the intensity of the open form bands decrease, there is a corresponding increase in the $S_0 \longrightarrow S_2$ and $S_0 \longrightarrow S_1$ transitions at 340 nm and 608 nm respectively. The increase, however, is non-linear and inset b) shows the “levelling off” of the absorbance as it increases towards the PSS as a function of time. This deviance from increasing linearity is due to the build up of other absorbing species within the system, yielding a mixture of closed- and open-form atropisomers.

A calculated fully closed spectrum can be postulated mathematically in order to compare isomer concentration in solution and the extent of conversion, similar to the calculation method of Gearóid O Máille and Maria Indelli.¹⁶⁹ A sample was irradiated with monochromatic light of 300 nm for 120 s and absorbance at the bands undergoing most significant change (i.e. $\lambda = 311 \text{ nm}$ and $\lambda = 608 \text{ nm}$) noted at t_0 and at 30-second intervals. In order to maximise absorbance of the incident photons, the concentration of the sample was adjusted to ensure an absorbance of over 1 at 300 nm ($4 \times 10^{-5} \text{ M}$). Using the equations below, it is possible to calculate the drop in concentration of the open form ($\Delta C_{30 \text{ s}}$) from the change in absorbance at $\lambda = 311 \text{ nm}$ from t_0 to 30 s ($\Delta A_{30 \text{ s}}^{311 \text{ nm}}$), utilising $\epsilon_{311 \text{ nm}} = 32,110 \text{ dm}^3 \text{ mol}^{-1} \text{ cm}^{-1}$. As the drop in the open form concentration must be equal to the amount of closed form generated, this can be used to calculate a molar absorption coefficient for **8c**.

$$\Delta C_{30\text{ s}} = \frac{\Delta A_{30\text{ s}}^{311\text{ nm}}}{\epsilon_{311\text{ nm}}}$$

$$\epsilon_{608\text{ nm}} = \frac{\Delta A_{30\text{ s}}^{608\text{ nm}}}{\Delta C_{30\text{ s}}}$$

This procedure was repeated for $\Delta C_{60\text{ s}}$ and $\Delta C_{90\text{ s}}$ using the absorbance changes from t_0 to 60 s and t_0 to 90 s respectively. The data is tabulated in Table 1.

t	$\Delta A_{t/s}^{311\text{ nm}}$	$\Delta C_{t/s}/M$	$\epsilon_{608\text{ nm}}/\text{dm}^3\text{ mol}^{-1}\text{ cm}^{-1}$
30 s	0.0902	3.82×10^{-6}	12,107
60 s	0.1323	5.60×10^{-6}	12,969
90 s	0.1690	7.16×10^{-6}	13,479

Table 2.1 Calculated $\epsilon_{608\text{ nm}}$ values for fully closed compound **8c**

The values obtained showed an average molar absorption coefficient of $\epsilon_{608\text{ nm}} = 12,852\text{ dm}^3\text{ mol}^{-1}\text{ cm}^{-1}$ for the fully closed system **4c**. The photostationary state was achieved through the irradiation of the sample with $\lambda = 254\text{ nm}$ of monochromatic light until no further changes in absorbance occurred. As this PSS contains a mixture of concentrations of the open and closed form of the isomer, an approximated UV-Vis absorption spectrum of the pure closed form was then obtained through calculations by taking the advantage of the additive nature of absorbances. This gives rise to an appropriately scaled absorbance spectrum of the open form, which can then be subtracted from the observed PSS spectrum to yield a UV-Vis spectrum for the fully closed form (Figure 2.18). The calculated spectrum (blue) contains expected features of the complete closed form spectrum, notably the retention of the isosbestic point at 334 nm, the drop in intensity at 311 nm, coupled with an increase in the ground state to the first and second excited state absorption transitions, $S_0 \longrightarrow S_2$ and $S_0 \longrightarrow S_1$ at 340 nm and 608 nm respectively.

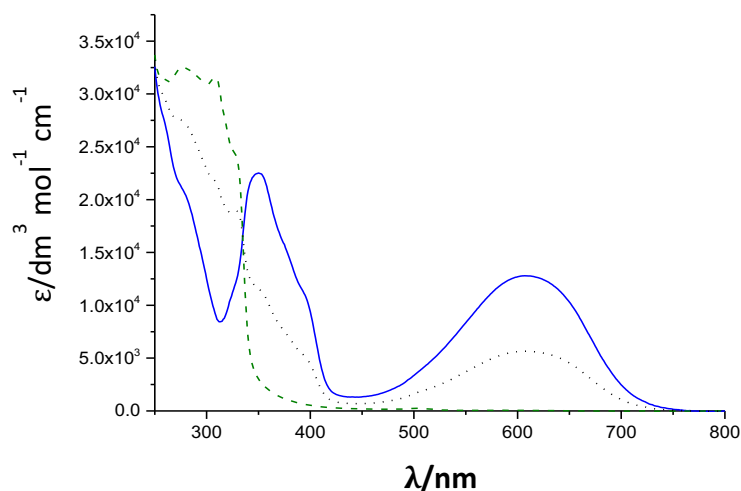


Figure 2.18(a) Comparison of absorption spectra for **4**: open (---), PSS (···), and calculated closed form (—), in CHCl_3 . Isobestic point of 334 nm is retained, even in the calculated closed form spectrum.

It is evident in the spectrum (Figure 2.18(a)) that even with short UV wavelengths of light, in regions the compound absorbs, full conversion of **8** does not occur, and approximately half the concentration of the photostationary state remains as the open-isomer. The conversion proportion α_{PSS} , for **8** was calculated, using the concentration of the closed form of the PSS (using initial concentration) and calculated closed form spectra. $\alpha_{\text{PSS}} = 0.44$, and hence 56 % of the concentration remains in the open form at the PSS. In materials, full conversion to the closed form is rare, and as such photophysical properties at the PSS must be regarded. However, a PSS to the complete closed form is ideal, especially in fluorescence imaging applications.¹⁹⁹

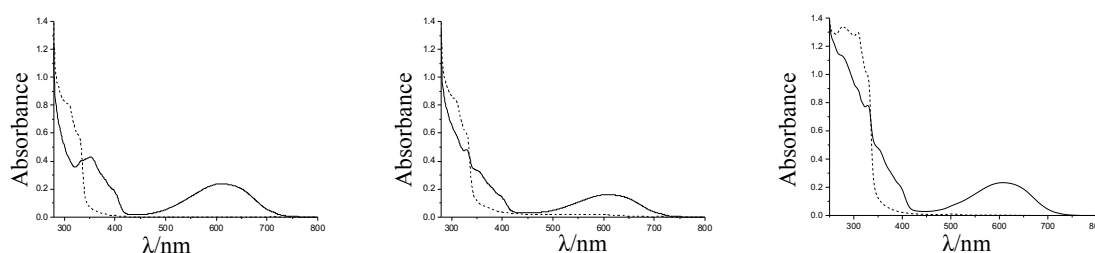


Figure 2.18(b) Absorption spectra of **8** in a) benzene, irradiating at 254 nm, open (---) and closed (—), b) benzene, irradiating at 311 nm, open (---) and closed (—) and c) chloroform, irradiating at 311 nm, open (---) and closed (—).

The absorption spectra of **8** in various solvents and at different excitation wavelengths was also recorded. Irradiating at higher wavenumbers correlates to a stronger absorbance thus more efficient conversion to the closed/PSS form. This correlates with optical memory applications, where longer wavelengths of lower energy are more beneficial and ideally required. The noticeable difference in absorbance intensity was attributed to concentration effects of the samples. Solvent has no observable influence of the position of λ_{max} (608 nm), even with increasing solvent polarity. The isosbestic point of $\lambda = 334$ nm was maintained in all cases.

2.7.1.3 Emission of compound **8**

Photoswitching molecules have attracted increasing interest because of their potential applications in optical memories and as molecular switches and fluorescent biological markers. In current systems, the fluorescence spectrum overlaps well with the absorption spectrum of the closed-ring isomer of the diarylethene unit, while the absorption spectrum of the open-ring isomer locates shorter than the fluorescence spectrum. Therefore, fluorescence being quenched does not take place in the open-ring isomer system, whilst it is quenched by intramolecular energy transfer when the switch unit converts from the open- to the closed-ring isomers. However, fluorescent induction may also cause the photocycloreversion reaction to occur, if emission and absorption overlap is substantial and $\phi_{e \rightarrow o}$ is large, which would lead to the destruction of “memory” within devices.

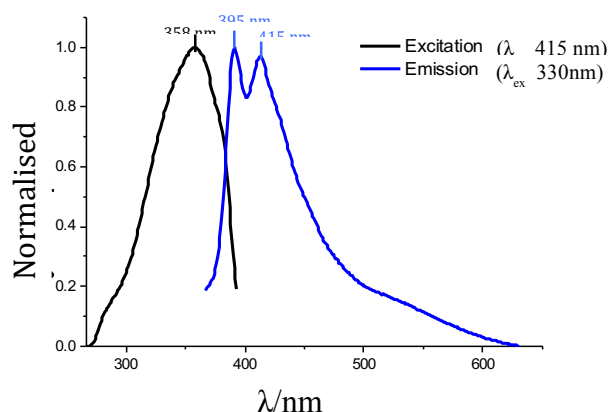


Figure 2.19 Emission and Excitation spectra of photochromic compound, **8** in CHCl₃. Excitation at 330 nm produced emission spectrum (—), and emission at 395 nm produced excitation spectrum (—).

Figure 2.19 shows the excitation and emission spectra of the dithienylethene switch **4o**. Emission ($\lambda_{\text{ex}} = 330$ nm) is shown and excitation spectra obtained through the irradiation at both 395 nm and 415 nm were identical. By using dilute solutions, it is ensured that the relationship between the fluorescence intensity of the sample and the concentration is proportional. Emission spectrum of the appendage moiety **L2**, 4-*tert*-butylphenylacetylene, was recorded, and a single emission peak at 364 nm was observed, $\lambda_{\text{ex}} = 300$ nm.

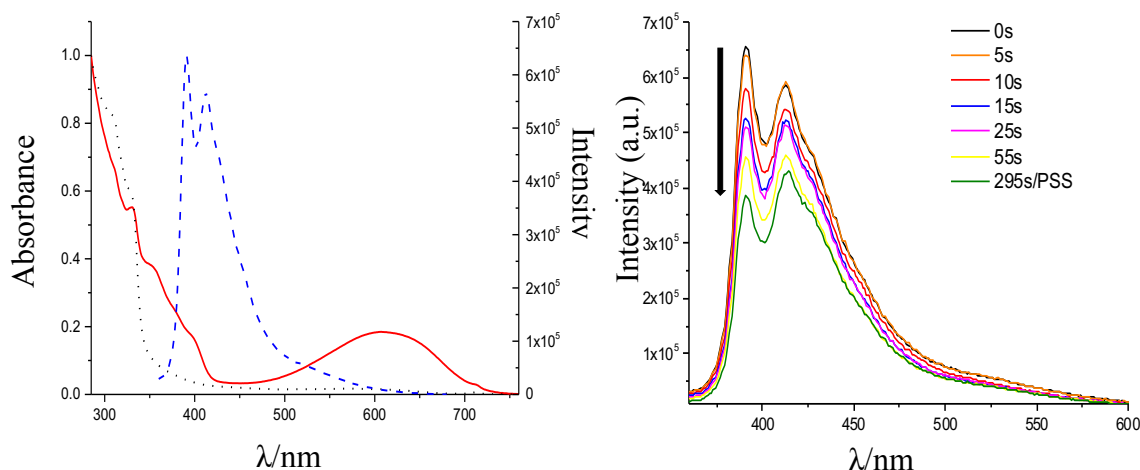


Figure 2.20 a) Absorption spectra of **8**, open form (· · ·) and PSS (—), and emission spectra of **8** (- - -), $\lambda_{\text{ex}} = 330$ nm, showing spectral overlap and b) Fluorescence spectral changes of compound **8o** in benzene upon irradiation with $\lambda = 364$ nm light, with excitation wavelength of 330 nm, concentration of 1×10^{-4} M.

Figure 2.20 a) for compound **8**, shows the overlap between the emission and absorption spectrum of compound **8** in solution. Overlap of the spectrum can cause quenching of the open form emission through energy transfer.¹⁰⁷ Figure 2.20 b) shows the fluorescence spectral changes of the switch **8** along with the photocyclisation experiment. The strongest and most prominent emission peaks for the open isomer occurs at $\lambda = 415$ and 395 nm, respectively ($\lambda_{\text{ex}} = 330$ nm). Irradiating the sample with short wave UV light causes the fluorescence to be quenched by the photogenerated closed form isomers. This is achieved through fluorescence resonance energy transfer (FRET) between the closed and open-forms of the switch. However, the fluorescence of the system is only partly quenched due to the incomplete conversion of open- to closed-forms at PSS, with the remaining open-isomers contributing to the remnant fluorescence. Numerous methods to combat this problem have been proposed, first by Irie²⁰⁰ and then Tian *et al*,²⁰¹ reported using multiple dithienylethene moieties linked onto one fluorophore to minimise this remnant fluorescence. For fluorescent

imaging functionality, emission at longer wavelengths and an excitation outside of the absorption bands is required.¹⁹⁹

Table 2 summarises the optical properties of photochromic compound **8**. λ_{\max} and ϵ_{\max} are the maximum absorption wavelength and the molar absorption coefficient at maximum absorption wavelength respectively. $\phi_{o \rightarrow c}$ is the photocyclisation quantum yield upon irradiation with light $\lambda = 330$ nm. α_{PSS} is the fractional percentage of the closed form in the PSS upon irradiation with $\lambda = 330$ nm calculated from the fully closed form spectrum. P_{open} ($= 1 - \alpha_{\text{PSS}}$) is the proportion of the open form isomer present in the PSS. R_{calc} ($= 1/P_{\text{open}}$) is the calculated fluorescence “on/off” quenching ratio, with the hypothesis that the closed form of the DTE does not fluoresce. R_{meas} is measured by comparing the fluorescence intensity peaks of the open form before irradiation and of the PSS form after irradiation at λ_{\max} . λ_{em} is $\lambda = 395$ and 415 nm.¹⁹⁹ The R_{calc} and R_{meas} correlate well, with a deviance from the values due to the closed form quenching the fluorescence of the open forms in solution. These values also indicate a good correlation between the open and closed forms at PSS

Compound	λ_{\max} (nm)/ ϵ_{\max} (dm ³ cm ⁻¹ mol ⁻¹)		$\phi_{o \rightarrow c}$	α_{PSS} (%)	P_{open} (%)
	Open	Closed(PSS)			
8	276/33,000	608/5,700	0.22	44	56
	311/32,000				

Table 2.1 Summary of the optical properties of compound **8** in CHCl₃.

2.7.1.4 Photophysical Analysis of **9**

When a 1×10^{-5} M solution of **9** was prepared in CH₂Cl₂, the solution had a blue colour which had an absorption maximum on the UV-vis spectra at 613 nm. Upon irradiation with UV light ($\lambda_{\text{ex}} = 365$ nm), the colour of the solution intensified. When irradiated with visible light, the solution changed to colourless. The blue colour returned to the solution upon immediate UV irradiation. The colourless sample corresponded to the open isomer of **9** (**9o**) and the blue colour represented **9** in the photostationary state (PSS) (**9c**). Due to the wavelength of UV light used, the molecular switch was shown to be continually switching between the open and closed forms, and thus a fully closed form could not be isolated. For

simplicity, the PSS of **9** was labelled as **9c**. These observed colour changes confirmed that the molecular switch **9** was indeed photochromic.

The UV-Vis absorption spectrum was recorded for **9o**, followed by irradiation with UV light ($\lambda = 365$ nm) for a total of five minutes, at 30 second intervals (Figure 2.21) The absorption maximum at 613 nm steadily increased as the sample was irradiated with UV light for approximately the first 90 seconds; at which point the increase in absorbance began to level off (Figure X). This levelling off was due to the formation of other photo-generated side products and the ongoing equilibria between the open and closed states.

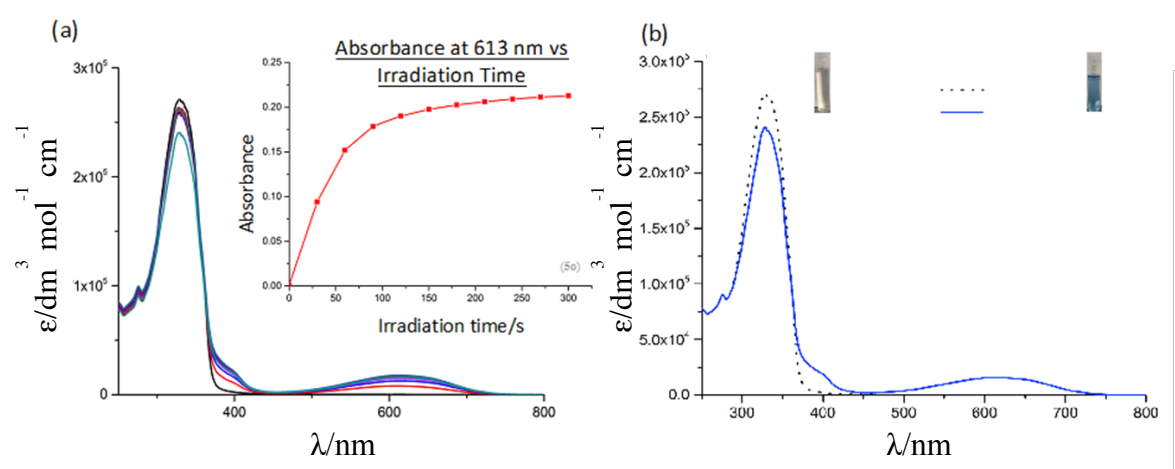


Figure 2.21 (a) Absorption spectra of **9** while irradiated with UV light ($\lambda = 365$ nm), recorded at 30 second intervals, inset, graph showing the increase of absorbance at 613 nm as a function of time (1×10^{-5} M) and (b) absorption spectra of **9o** (.....) and **9c** (—) showing the difference in absorption at 328 nm and 613 nm between the two isomers.

The λ_{max} at 328 nm ($\epsilon = 270,789 \text{ dm}^3 \text{ mol}^{-1} \text{ cm}^{-1}$) decreased as the sample was irradiated with UV light ($\lambda = 365$ nm). These observations could be explained by the switching between the open and closed forms of **9**. In the open form, electron density is concentrated around the two thiophene rings and therefore the compound absorbed light at relatively short wavelengths, and as such the absorptions are attributed to the $\pi\text{-}\pi^*$ electronic transitions that occur within its geometric structure. In contrast, in **9c**, there was greater π -conjugation due to the bond formed between the thienyl rings. As a result, the electron density is delocalised more throughout the molecule and the absorption is shifted to longer wavelengths. As the compound was irradiated with more and more UV light, the absorption band at 613 nm ($\epsilon =$

$17,724 \text{ dm}^3 \text{ mol}^{-1} \text{ cm}^{-1}$) increases, along with the decrease of the absorption band at 328 nm ($\epsilon = 262,067 \text{ dm}^3 \text{ mol}^{-1} \text{ cm}^{-1}$).

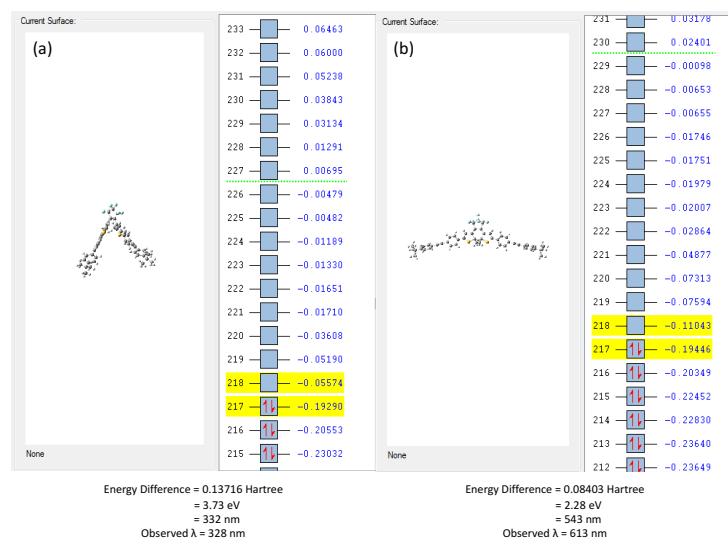


Figure 2.22 DFT calculations for molecular switch, both isomers **9o** and **9c**. Initial primary HOMO-LUMO energy gap correlates well with experimental values.

Preliminary DFT calculations were also carried out on **9o** and **9c** to determine the HOMO-LUMO energy gap and the extent of π -conjugation in each of the isomers. In **9o**, the HOMO-LUMO gap was found theoretically to be 0.13716 Hartree which equated to 3.37 eV ($\lambda_{\text{HOMO-LUMO}} = 332 \text{ nm}$). The HOMO-LUMO gap in **9c** was calculated to be 0.08403 Hartree which was equivalent to 2.28 eV ($\lambda_{\text{HOMO-LUMO}} = 543 \text{ nm}$). Both DFT results correlated well with the values for λ_{max} on the **9o** and **9c** absorption spectra. The HOMO and the LUMO was seen to extend over the diphenylacetylene moiety in both the open and closed forms of **9**. Another interesting observation that was made with regard to the DFT calculations was that the HOMO energies of the open and closed isomers were almost identical. It was the LUMO energy value that changed upon switching from **9o** to **9c** which resulted in the reduction of the HOMO-LUMO gap on going from the open to closed isomer.

Figure 2.23 (a) shows the absorption precursor **3**, and molecular switch **9**. The absorption maxima of both are almost identical, though there is an almost double increase in intensity of this peak in switch **9** and the difference in the value of extinction coefficients between the open isomer and **9** in the open form is quite apparent. Due to the fact **9o** contains twice the number of thienyl-units, which were attributed to the absorption in this region, this spectral analysis seems to again confirm that the strong aromatic absorption of the rings and accounts

for twice number of transitions occurring in the molecular switch compared to the unsubstituted moiety.²⁰²

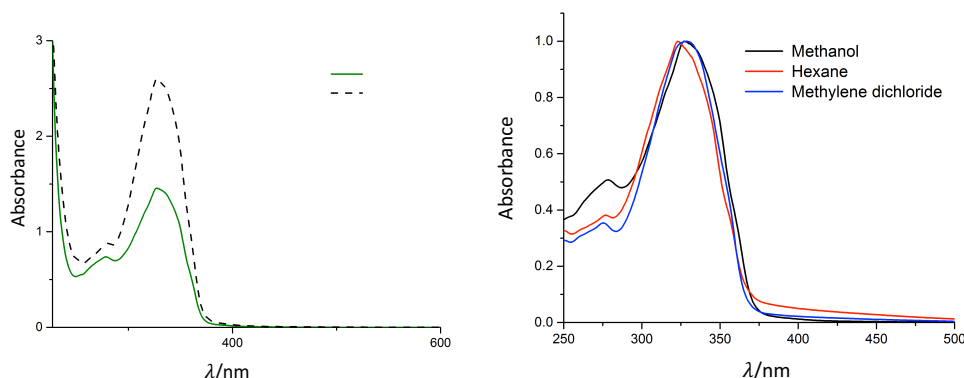


Figure 2.23 Absorption spectra of **3** (—) and **9a** (---) (CH_2Cl_2 , $1 \times 10^{-4} \text{ M}$) and (b) solvatochromism studies of compound **9**. (RT, $1 \times 10^{-4} \text{ M}$)

Figure 2.23 (b) shows the absorption spectra of switch **9a** in solvents of varying polarity to ascertain the nature of the absorption band at 328 nm. In polar solvents, such as methanol, the absorption band is shifted to longer wavelengths and in non-polar solvents, e.g. hexane, the opposite effect is seen. These observations confirm the transition that this absorption band represented, in this case a $\pi\text{-}\pi^*$ interaction within the thiophene rings. A slight red-shift upon increasing solvent polarity is observed, usually indicative of these $\pi\text{-}\pi^*$ transitions, occurs, but the shift is almost of negligible effect so it is not possible to speculate definitively, though this would be congruent with the results thus far.

2.7.1.5 Emission and Excitation Spectra switching complex **5**

Excitation and emission spectra were recorded for **9a** using a $1 \times 10^{-6} \text{ M}$ solution in CH_2Cl_2 (Figure 2.25a). The compound was excited with UV light at a wavelength of $\lambda_{\text{ex}} = 330 \text{ nm}$ to produce the emission spectrum, with an $\lambda_{\text{em}} = 458 \text{ nm}$. This wavelength was then used as the detection wavelength to obtain the excitation spectrum. The excitation spectrum matched well with the original absorption spectrum. This was to be expected as the absorption spectrum represents all transitions from the ground state to excited states ($S_0 \rightarrow S_1$, $S_0 \rightarrow S_2, \dots$, $S_0 \rightarrow S_n$), while the excitation spectrum represents the transition from S_0 to S_1 . Both spectra include the transition $S_0 \rightarrow S_1$. Tests were then carried out to determine if the intensity of fluorescence diminished upon switching from **9a** to **9c**. There was no change observed in the fluorescence intensity between **9a** and **9c** i.e., no fluorescence quenching was seen to occur (Figure 2.25b).

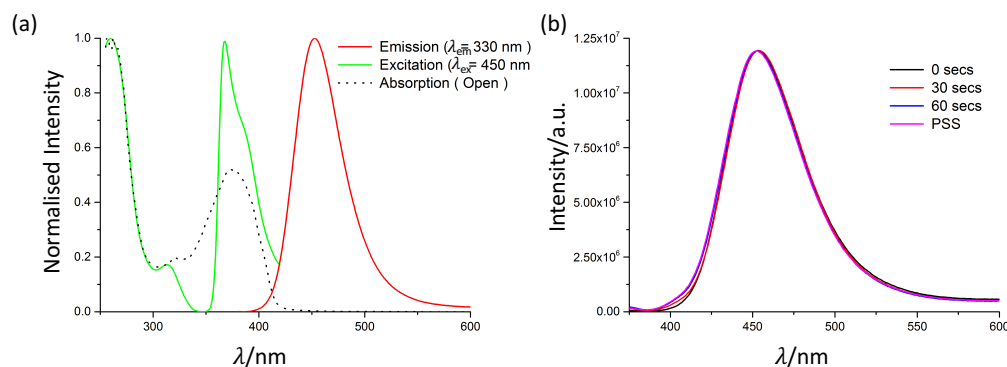


Figure 2.25 (a) comparison of the emission (—), excitation (—) and absorption (.....) spectra of **9o**; (b) emission spectra of **9** before, during and after irradiation with UV light.

Due to this, the efficiency of the switch was hindered, which explained the presence of the thiophene-centred $\pi\text{-}\pi^*$ absorption band in the **9c** absorption spectrum (Figure 2.25(a)). A noticeable difference in the absorption and excitation spectra occurs in the 350 nm range. Though at first this seems promising, due to the introduction of light wavelengths that may not induce fluorescence and thus allow for a pathway that predominantly results in photocyclisation, it also accounts for the complete independence of the thiophenes to the ethynylbenzene moiety, through the use of a phenyl spacer. As such, switch **9** has congruent photophysical properties to that of a dithienylethene switch with a singular phenyl appendage, though notably more red-shifted, most likely due to the slight increase in conjugation.

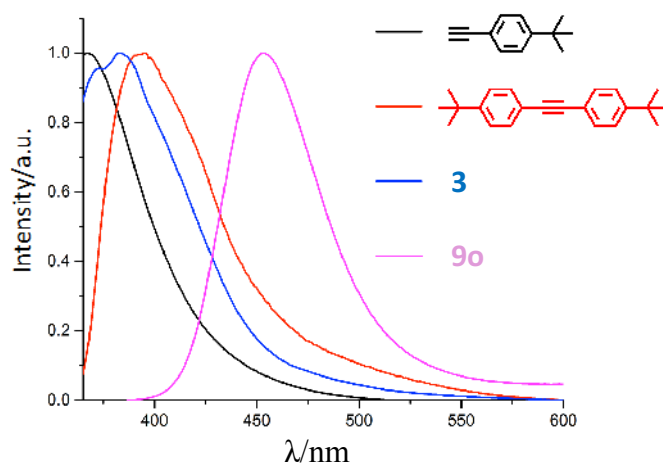


Figure 2.26 Emission spectra of selected polyaromatic groups (CH_2Cl_2 , $1.5 \times 10^{-6} \text{ M}$)

Figure 2.26 shows the luminescent profile and emission studies model compounds- 1-ethynylphenyl, a tert-butyl substituted diphenylacetylene and compounds **3** and **9o**. All samples were excited at $\lambda_{\text{ex}} = 330 \text{ nm}$. The red-shift of the emission was surprising, as the emission of the ethynylphenyl appendage was thought to be independent of the remaining system. However, this may not wholly be the case, as the smaller HOMO-LUMO gap in the final compound suggests at least some degree of stabilisation upon the addition of the fluorinated backbone, but that the affinity of this emission is far enough from the centre thienyl units that even upon closing, the electron is falling from a LUMO on the thiophenes into the HOMO of the phenyl appendages, acting as a photochemical funnel in switching processes. The conjugation allows for a delocalised spread of electron density and stabilising the HOMO-LUMO energy levels. The lack of a double maxima emission, a notable feature thus far described for switch **8**, and seen in other PAH based switches, ascribed to anti-parallel and parallel conformers having slightly unique emission profiles, further suggest the high level of independence of the switching appendages of **9**, and sole emission from the ethynylphenyl group itself. The indication that the fluorescence of the molecule originates from the diphenylacetylene moiety is consistent with the initial DFT calculations and may explain the lack of fluorescence quenching upon photocyclisation from **9o** to **9c**.

2.7.1.6 Photophysical Analysis of **10**

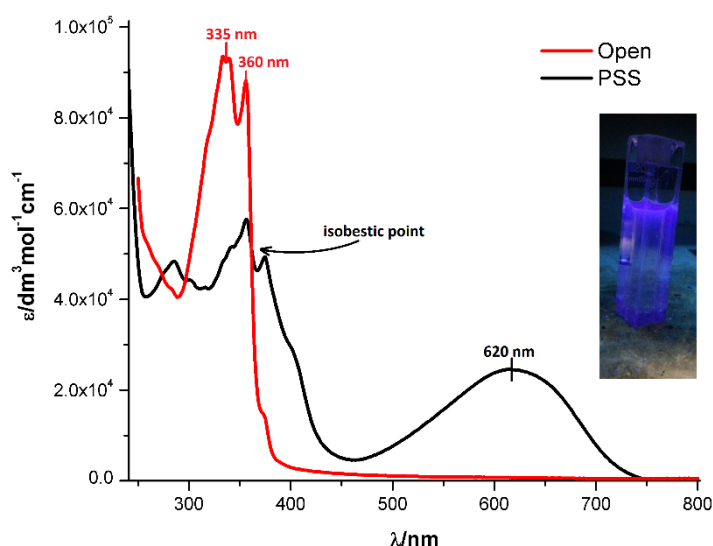


Figure 2.27. Comparison of the UV-Vis absorption spectra of **10o** and **10c**, inset shows sample under short range UV light (364 nm)

Figure 2.27 above is the absorption spectra of both the open and the photostationary state of the molecule. The open form most clearly absorbs in the UV region of the spectrum, with a λ_{max} of around 335 nm ($\epsilon = 92\,000\text{ dm}^3\text{ mol}^{-1}\text{ cm}^{-1}$) and 360 nm ($\epsilon = 88\,000\text{ dm}^3\text{ mol}^{-1}\text{ cm}^{-1}$). The PSS also absorbs in the UV, but absorbs more strongly in the visible region, with the highest visible ϵ value ($24\,525\text{ dm}^3\text{ mol}^{-1}\text{ cm}^{-1}$) occurring at around 620 nm. Absorbance here in the red region accounts for the blue colour of the molecule when hit with UV light. The closed isomer of the naphthalene switch is highly conjugated, more so than compounds **8** or **9**. This conjugation further stabilises the LUMO and destabilises the HOMO, resulting in a highly bathochromic absorbance shift into the red region. An isobestic point appears at 361 nm. The presence of an isobestic point in figure 2.28 indicates that there is only two species in equilibrium (i.e. open and closed) as it would be very unlikely to have three or more species with the same absorbance at the same wavelength. The inset picture indicates to the fact that although at first a linear plot is observed, it will eventually begin to level off as the increasing concentration of the closed form absorbs some of the incident radiation. Increasing conjugation so far suggests an increasing bathochromic shift.

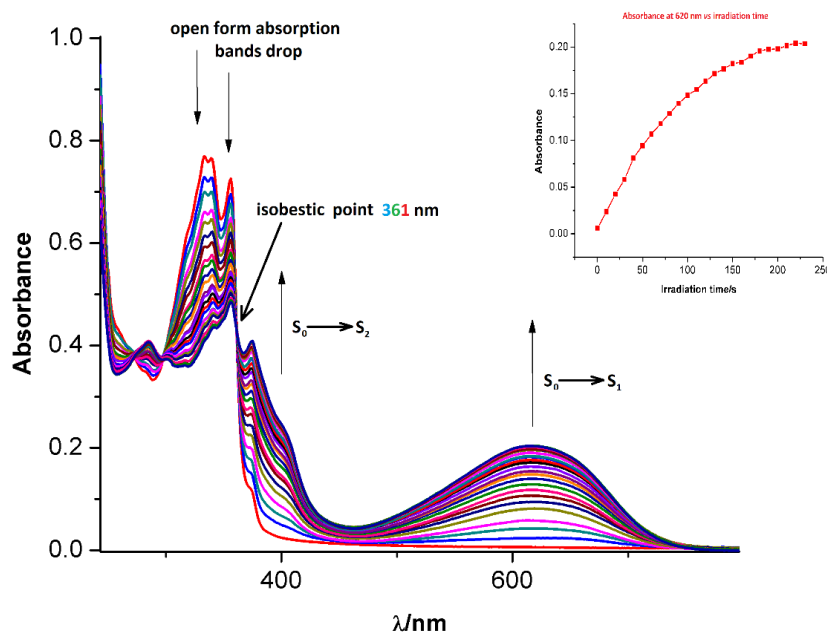


Figure 2.28. Absorbance spectrum of **10** from open to closed, recorded after 30 second intervals under short range UV radiation. Inset shows absorbance at 620 nm as a function of time

Figure 2.29 shows the excitation and emission spectra of the open form species. In order to prove that the emission arises from a single species, excitation spectra were obtained through

irradiation at 380 nm and 405 nm. Both excitation spectra were the same and appeared as a slightly distorted mirror images of the emission spectrum. Excitation spectra were practically identical to the absorption spectrum of the open form, verifying this species as the emitting compound. Despite the large propensity of the naphthalene moiety to emit light and thus compete with the switching process, a large photocyclisation result is seen. 1-ethynylaphthalene may represent the ideal middle ground of π -electron extension and molecular switch performance. As a quite simple compound, it represents an ideal model compound for study. At $\lambda = 380$ nm, there appears to be no Stokes Shift between the emission and absorption spectra. It describes the loss of energy of an emitted photon from a molecules excited state relative to the energy of the photon absorbed by the ground state of the same electronic transition. This would indicate that at this wavelength, the energy of photons absorbed and emitted are exactly the same as to be expected. There is however a notable overlap in both the emission and excitation spectra, occurring at 380 nm.

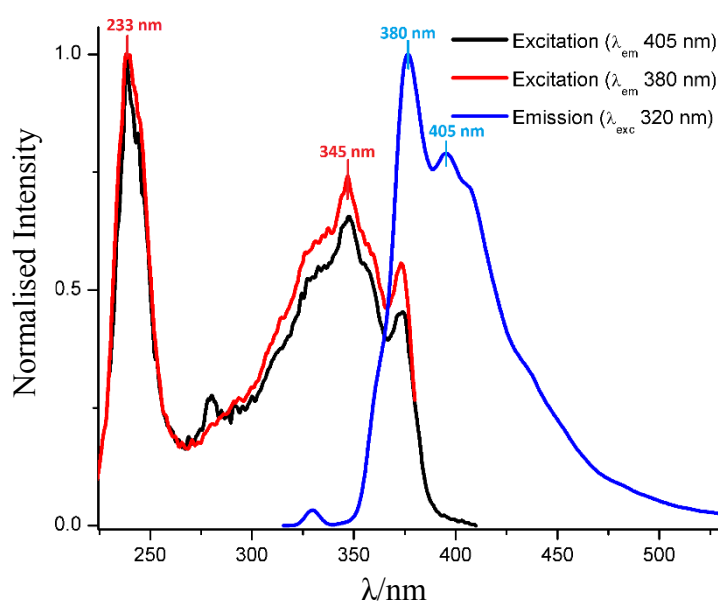


Figure 2.29 The excitation and emission spectra of **10**. Excitation at 405 nm (—) and 380 nm (—), while emission was irradiated at 320 nm (—). Results congruent with a single species.

2.7.1.7 Photochemical properties of Compound 11

Irradiation with monochromatic light ($\lambda = 365$ nm) had little effect on the absorption spectrum of **11**. This is most likely due to the high degree of photoactive luminescence that is usually seen in pyrene and pyrene based compounds. Pyrene has been shown to display at least five distinct types of luminescence. It was this broad and efficient photochemical

processes that would attract the use of pyrene in photochemically dominated processes such as switch synthesis. It was hoped that two possible outcomes could be achieved in attaching a photoactive pyrene moiety to an organic molecular switch centre – either an enhanced/modified switching process due to tapping into previously inaccessible absorption wavelengths, or the on/off switching of the emission response of the pyrene, depending on the state of the switch. Increasing the size of the aromatic counterparts had thus far yielded valuable results, and pyrene was reasonably a next step extension of this synthetic analysis. However, the absorption and emission of the pyrene moieties here supersede the switching pathway of compound **11**.

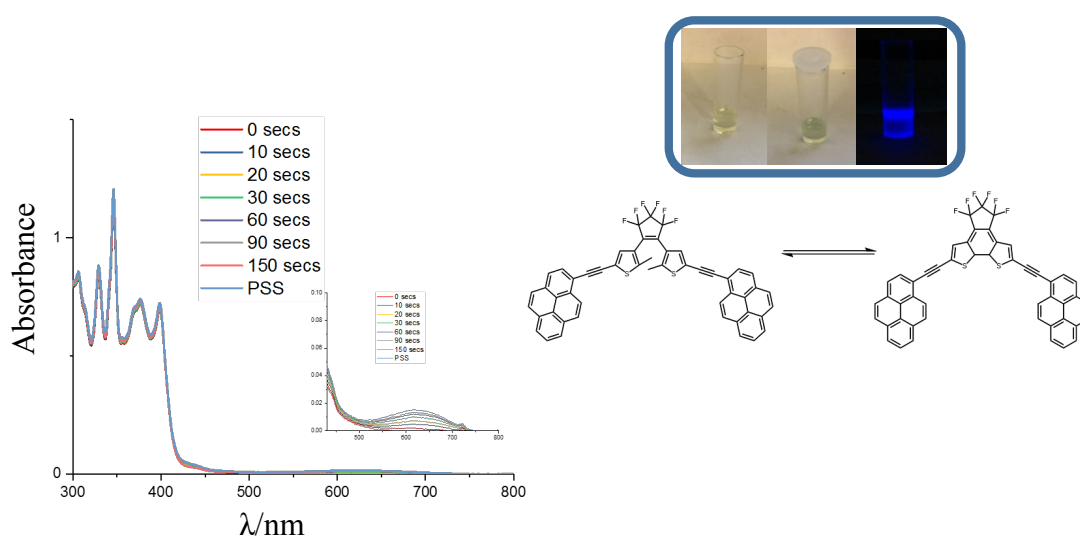


Figure 2.30. UV-Vis absorption of compound **11**

Figure 2.31 (b) shows an extremely interesting feature of compound **11**, which occurs at higher concentrations. The unique profile exhibited is normally associated with excimer formation due to the stacking nature of the cyclic aromatic group. This stacking shows a unique luminescent spectra when compared to the more simple one of the low concentrated sampled (showing the typical double-peak emission seen in dithienylethene switches thus far). Due to pyrene's complex nature, numerous transitions, and as such, numerous deactivation pathways may exist. Pyrene has a potential to emit both phosphorescence as seen in Figure 2.31. The presence of air in a sample should quench the triplet-accessed phosphorescent path, and only measurable fluorescent peaks may be seen. The growth of the sharp peak at 420 nm under argon atmosphere suggests a triplet character to this emission, as does its sharp decrease upon exposure to air. The peak at 395 nm remains completely unchanged. However, it is the blue-shift and slight decrease in intensity of the broad peak at

480 nm that is the most interesting photophysical property of this compound, one that is still not fully understood.

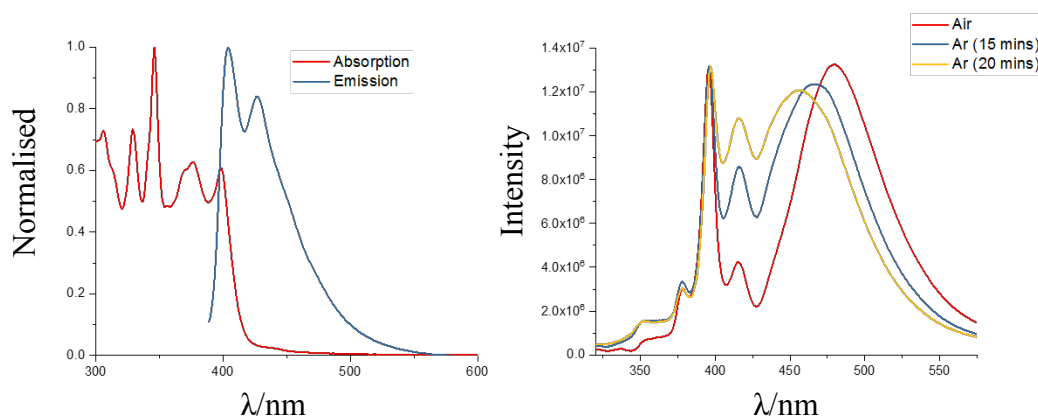


Figure 2.31 a) the absorption and emission spectra of compound **11** ($1 \times 10^{-6} M$) and (b) emission of compound **11** at higher concentrations under Argon and in air ($1 \times 10^{-4} M$)

2.7.1.8 Photochemical properties of Compound 12

Figure 2.32 highlights the main photochemical and photophysical processes occurring in compound 12, showing the UV-Vis absorption and the dual-wavelength-dependent emission that occurs. As seen, this is a common absorption pattern for these larger polyphenylene type systems, and what attracts their use in material chemistry. Photocyclisation may induce complete quenching within the system through intermolecular overlap, or may impede only one type of emission over the other. Due to the numerous substitution sites and ability of heteroatom introduction available to these π -platforms, tuning of these photophysical properties would prove invaluable in the fields of chemical sensing, upconversion and photodynamic therapy. However, as evidenced by the results seen in Figure 2.32, the photocyclisation reaction is extremely negligible in the case of compound 12. The PSS was reached after shining light for 2 hours on a sealed cuvette and subsequently measured. Though at higher concentrations a drastic visual affect is seen to occur from yellow to green, this is of little use to modern material science research. The evidence of stacking in the proton NMR spectrum may also be a valuable factor, due to the alternate deactivation pathways these excimer formations present. The broad absorption pattern also stumps the direct absorption into the thienyl transition itself, and the HOMO of the compound can be theorised to sit on this thienyl-core. Due to this, the use of the HPB-based antenna is also called into question, a problem which becomes more apparent in these types of systems. The photocyclisation that is seen to occur for the compound does not show a noticeable impedance of emission band intensity.

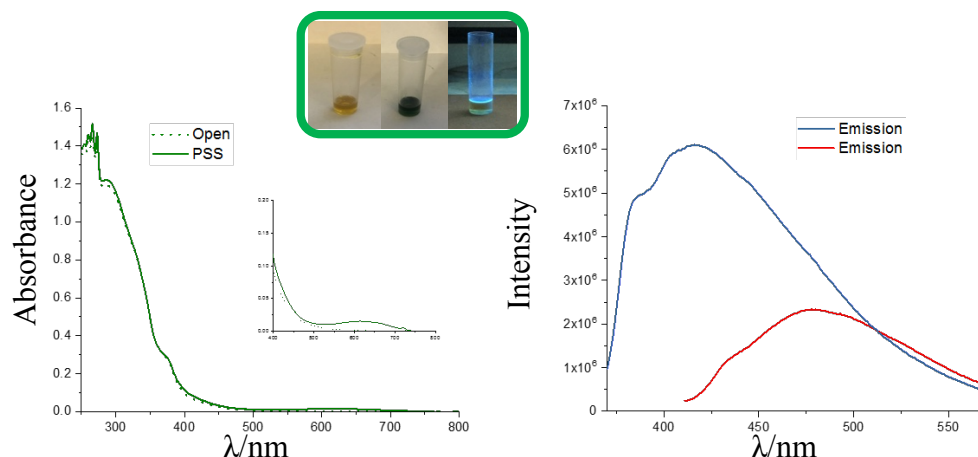


Figure 2.32 Normalised UV-Vis absorption spectrum ($2 \times 10^{-5} M$) and emission spectrum ($1.5 \times 10^{-6} M$), run in CH_2Cl_2 , RT. Inset shows photochromic activity of compound in solution and its emission under UV light.

2.8 Comparative photophysical properties

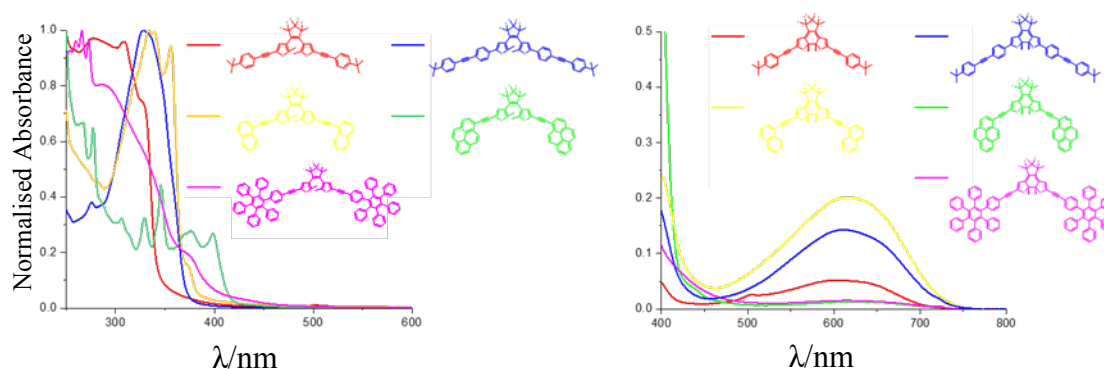


Figure 2.33. Normalised UV-Vis of open and closed form isomers (CH_2Cl_2 , $1 \times 10^{-5} M$)

Figure 2.33 shows the comparative absorption patterns of switches **8-11**, with (a) plotting the absorption of the open form and (b) the selected window of wavelength maxima in the closed form. The open forms have extremely varied absorptions within the UV range of the spectrum, due to the assortment of transitions that occur not just with the thienyl π - π^* bands, but in each of the appendages. For **9o**, **10o** and **11o**, a noticeable absorption peak between 320-350 nm is extremely prominent and correlates with the overlapping absorption patterns of the appendages and the ethynylthiophenes absorbing individually, with a pseudo-addictive effect thus represented in the spectrum. Switch **12** shows a mostly featureless absorption, though its thienyl absorption shoulder is more red-shifted than that of **9**, **10** and **11**.

The absorption maxima of the closed forms of **8c-12c** all occur within the same range, 600-620 nm. Instead, it is the intensity of these absorptions that are note-worthily different. **11c** and **12c** fail due their large variation of competing deactivation pathways. Though **9c** also retains a degree of independence due to its emissive profile, it shows a strong hyperchromic shift compared to **8c**, which performed surprisingly poorly in terms of efficiency and photocyclisation quantum yield. Compound **10c** lies at the perfect “Goldilocks” intersection of polycyclic aromatic hydrocarbon conjugation, and the ability undergo independent luminescence.

2.9 Fatigue resistance in compounds **8**, **9** and **10**

The fatigue resistance describes the number of cycles a photochromic switch can undergo. The repeatable number of cycles was previously defined as the number of photochromic cycles at which the absorbance change of the observed PSS “closed ring” isomer decreases to 80 % of the first cycle. One cycle is composed of four minutes irradiation with UV light and four minutes irradiating with light from the visible region. This operation was completed multiple times, and the UV-Vis spectrum was recorded after each 100 cycles over a 14-hour period. The decomposition products showed some absorbance within the absorption bands of the open-ring isomer and as such the absorbance of the coloured closed-ring isomer was monitored at λ_{608} nm. The test was repeated twice, initially with a similar process as before, and yielded an average result of an absorbance of 79 % of the PSS. Conditions were replicated and the experiment again repeated, however a UV-Vis spectrum was taken every 10 cycles and the absorbance at $\lambda = 608$ nm was recorded and graphed as a function of time, the cycle number, as shown in Figure 2.34. The plot shows an initial drop in the performance of **8** after the first 10-20 cycles, but gradual degradation of performance is maintained for the remaining course of cycles. Low durability and degradation of molecular switches have been attributed to the formation of endoperoxides.²⁰³ In systems lacking oxygen, this is due to the formation of six membered thienyl rings, caused by the absence of steric groups at the 4- and 4'-thienyl positions, or by using small aryl groups such as thiophene instead of its much more sterically hindering analogues, e.g. benzothiophene.¹³⁴

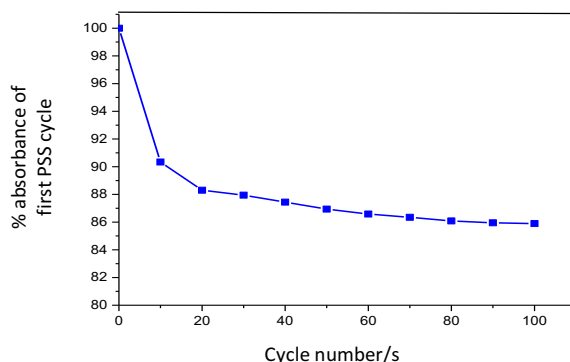


Figure 2.34 Fatigue resistance of **8** in hexane solution. Percentage absorbance of first PSS cycle at $\lambda = 608 \text{ nm}$ plotted against cycle number, showing the cycle number dependence of absorbance of irradiated samples.

The fatigue resistance of **9** was quantified by measuring the number of open/close cycles that could be carried out before the absorbance of the closed isomer diminished to 80 % of the initial absorption intensity of **9** at the PSS. The absorption spectrum of **9c** was initially measured in CH_2Cl_2 ($1 \times 10^{-5} \text{ M}$) before beginning the cycles, and again after every tenth cycle for a total of 40 cycles over a 6 hours (Figure 2.5).

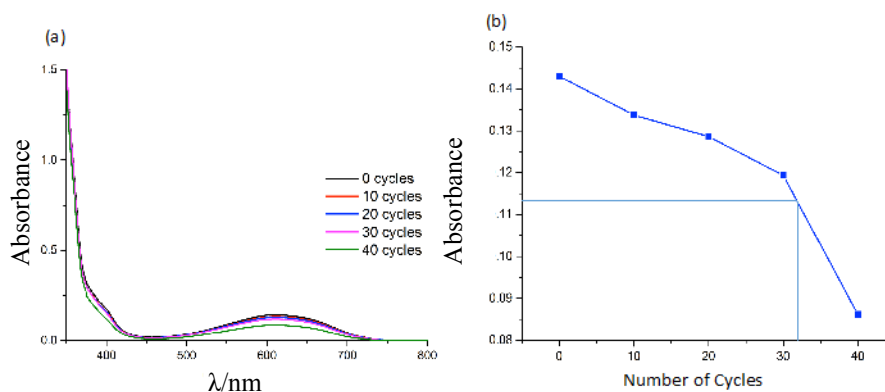


Figure 2.35 (a) absorption spectra of **5** recorded after 0 cycles (—), 10 cycles (—), 20 cycles (—), 30 cycles (—) and 40 cycles (—); (b) plot of absorbance at 613 nm vs. number of cycles to find the number of cycles needed to decrease the absorbance to 80 % of its initial value.

The absorbance before starting the cycles was valued at 0.143. After 40 cycles, the absorbance at 613 nm had dropped to 60 % of its initial value. By plotting a graph of absorbance versus number of cycles and extrapolating a line from 80 % of the initial absorbance it could be calculated how many cycles it took to diminish the absorbance to 80

% of the initial value. It was found that this happened after 32 cycles. This result was very poor considering that in the literature it has been reported that some diarylethene-based molecule switches have shown fatigue resistance for up to 10^4 cycles²⁰⁴, however it could be explained, in part, by the intense fluorescence emitted from the compound, as well as the formation of side products due to the unhindered 4- and 4'- positions.

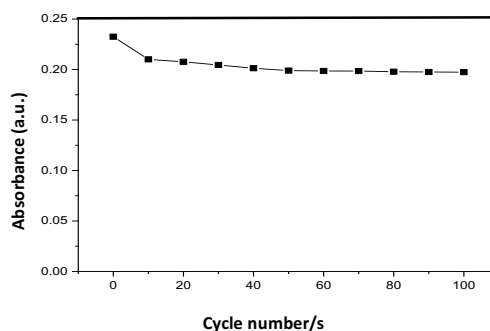


Figure 2.26 Fatigue resistance of **10** in hexane solution. Absorbance at $\lambda = 620$ nm plotted against cycle number, showing the cycle number dependence of absorbance of irradiated samples.

2.10 Thermal conversion

Compound **8-12** did not show any thermochromism at room temperature, due to the stability of the closed ring isomer, based on the state correlation diagrams. Raised temperature experiments were undertaken by heating compounds **8-12** in CHCl_3 at reflux for 12 hours and recording of the absorption spectrum to ascertain if high temperatures can cause thermal photocycloreversion. A UV-Vis spectrum taken after this time showed a distortion from the closed or open forms, and suggests degradation of the product during this time and possible reactivity with the solvent at elevated refluxing temperatures. The photochromic switches were dissolved in CHCl_3 solution and left overnight in a sealed cuvette in an oven at 90°C , covered and in the dark. The spectrum obtained did not show a decrease in the absorption maximum of the PSS at $\lambda = 608$ nm after 12 hours. This shows that at elevated temperatures, there is no thermal disrotary cyclisation occurring as was expected.

2.11 Quantum Yield

To determine the quantum yield of the photocyclisation reaction, the following equation is used:

$$\phi = \frac{\# \text{ of photons emitted}}{\# \text{ of photons absorbed}}$$

Equation 3

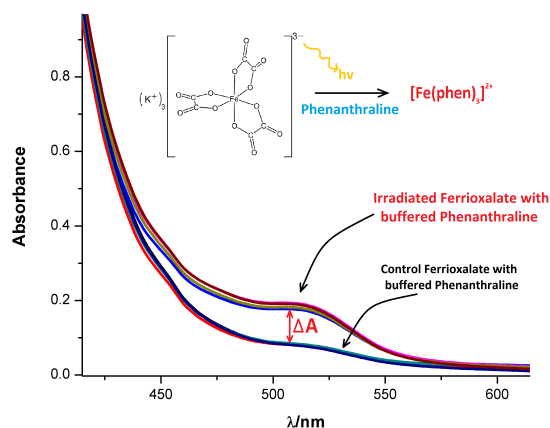


Figure 2.37 Observed absorption change in potassium ferrioxalate upon exposure to UV light. This change in absorption allows the photon flux of the irradiating light source to be calculated ($\lambda = 330 \text{ nm}$)

Measurements were only carried out for the beginning of the photochromic process to ensure that only the required form of the molecule was absorbing at the wavelength being monitored (Figure 2.38). This requirement for the measurement of photochemical quantum yields avoids the plots from leveling off from linearity due to the build-up of the other absorbing species. Measurements were carried out in the dark to avoid undesired photochromic switching of the compound.

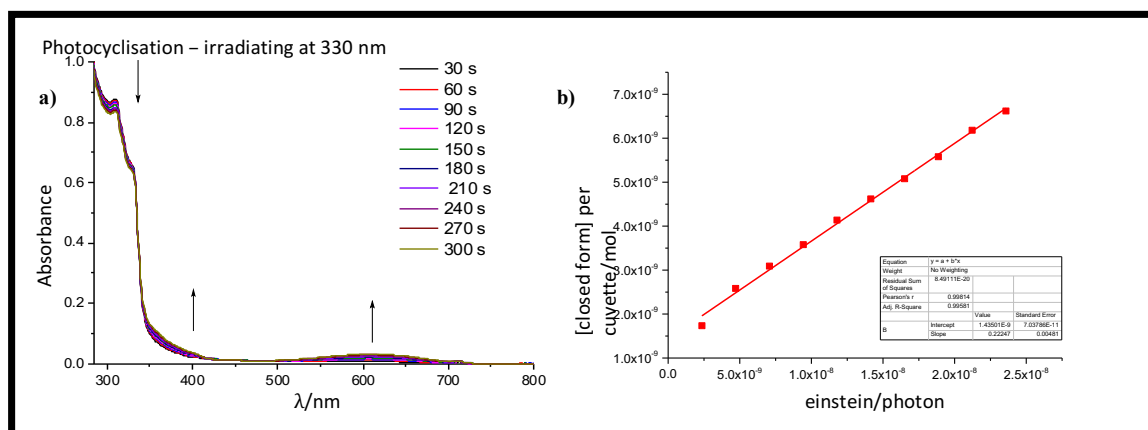


Figure 2.38 Photocyclisation quantum yield measurements for compound **8**, in CHCl_3 at RT. a) irradiating with $\lambda = 330 \text{ nm}$ for 5 minutes and b) plot of closed form concentration vs photon dose with respect to time.

Compound **8** was then irradiated with a Xeon lamp, $\lambda = 330$ nm, for 5 minutes, with absorbance spectra taken at 30-second intervals. Plotting closed-ring concentration per 2.7 mL cuvette against photon dose generates a linear plot (Figure 2.38 b)), and the intercept was allowed to deviate from zero in order to facilitate best-fit data. This allows for small deviations due to instrumental and random variation factors. An intercept point of 1.43×10^{-9} was recorded, and a high-adjusted R^2 value of 99.6 %, indicates a very good correlation of the obtained data. The slope of the straight line represents the quantum yield of photocyclisation of the switch, and thus $\Phi_{o \rightarrow c} = 0.22$. This quantum yield result is quite low for dithienylethene based molecular switches. Quantum yield is affected by the energy spent on bond closing/opening, and is competed with by molecular fluorescence and vibrational dispersion of the intaken energy. Compound **8** is quite strongly fluorescent in solution, and so this may account for the low quantum yield observed due to the competing pathway singlet-singlet emission represent. Quantum yield of fluorescence has yet to be undertaken and analysed.

2.11.1 Quantum Yield of switch **9** and **10**

The absorption spectrum of **9o** was recorded and then the sample was irradiated with 365 nm light from the Xe lamp and absorption spectra were recorded every thirty seconds. A graph of the concentration of the closed form per cuvette versus the number of photons emitted as a with respect to time was plotted. A straight line of best fit was applied to the data set and the slope of this line, 0.28, was taken to be the percentage value of Φ_{PC} .

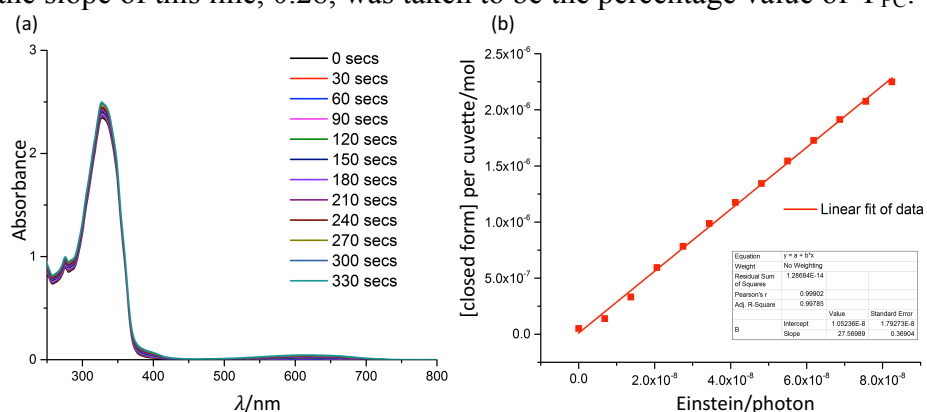


Figure 2.39 (a) absorption spectra of **9** recorded at 30 second intervals when irradiated with 365 nm light from a Xe lamp; (b) plot of concentration of cuvette versus photon dose with respect to time

In a similar method for switch **10**, By inducing the PSS of the switch and recording a UV-Vis spectrum, absorbance at the 620 nm peak can be recorded. ϵ value of $24525 \text{ dm}^3 \text{ mol}^{-1} \text{ cm}^{-1}$ for PSS. ^1F NMR was analysed for the PSS form, and a conversion of 90 % was calculated. Therefore $\epsilon = 27\,250 \text{ dm}^3 \text{ mol}^{-1} \text{ cm}^{-1}$ for a fully closed solution of **10**.

$$\frac{A_{0,1,2,\dots}}{\epsilon_{620(c)}} V_{\text{cuvette}} = \text{conc. of closed form per 3 mL cuvette}$$

$$\frac{A}{\epsilon_{620(c)}} V = \phi_{o \rightarrow c} [\text{incident photons}]$$

$$y = mx$$

Plotting closed-ring concentration per 3 mL cuvette against photon dose generates a straight line. An intercept point near 0 (4.404×10^{-10}) and an R-squared value of 0.997 were recorded. The slope the linear graph is 0.415 which is the quantum yield of the switch **10**. Quantum yield is affected by the energy spent on bond closing/opening, and is competed with molecular fluorescence and vibration. In 2004 Morimoto *et al* developed naphthalene based switches without an acetylene moiety between the aryl thiophene group and the naphthalene, with a quantum yield of 0.99 for the photocyclisation reaction. This has a higher value than that of the switch generated here, though a lower value of **10b** is also due to the fluorescence of the switch.

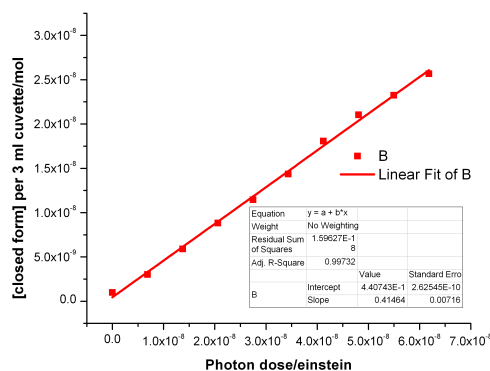


Figure 2.40 Linear graph of $y = mx$, where the slope is the quantum yield, Φ

2.12 Electrochemical analysis of **10**

A voltammogram of the switching compound **10** is shown in Figure 2.40 (0.1 V/s). This study was carried out in a dry CH_3CN 0.1 M TBAF_6 (tetrabutylammonium hexafluorophosphate) solution, which acted as a supporting electrolyte for the experiment. A Pt wire and a glassy carbon electrode were used as the working and counter electrodes

respectively, while Ag/AgCl was initially used as reference electrode. Ferrocene was used as an internal reference.

The spectrum shows two irreversible oxidations at $E_p^{ox} = 1.36$ V vs Fc/Fc⁺, and $E_p^{ox} = 1.53$ V vs Fc/Fc⁺, which can be ascribed to the oxidation of the thiophene components. Also displayed in the voltammogram is the singular irreversible reduction at $E_p^{ed} = -2.15$ V. This may be attributed to the reduction of the naphthalene of the molecule. Reversibility was not observed even at higher scan rate. Continuous scanning did not show evidence for electrocycloisation, however spectroelectrochemical analysis is required to address this fully.

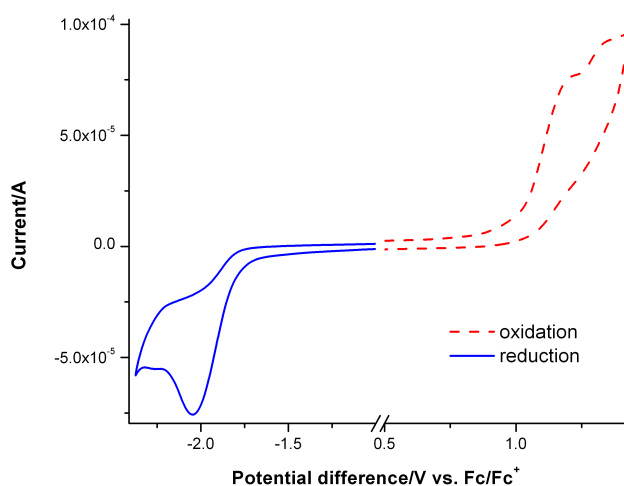


Figure 2.41 Cyclic voltammogram carried out in dry, degassed CH₃CN on compound **8**, at a scan rate of 0.1 V/s.

2.13 Conclusions & Future Work

2.13.1 Computational Analysis

Initial computation analysis was undertaken on brominated thienyl appendages **2**, **3** and **5**. Understanding the electronic pathways in compounds such as these is a key step in continued work to produce more efficient reaction pathways. Figure highlights the optimised geometry coordination, and the HOMO and LUMO of compounds **2**, **3** and **5**.

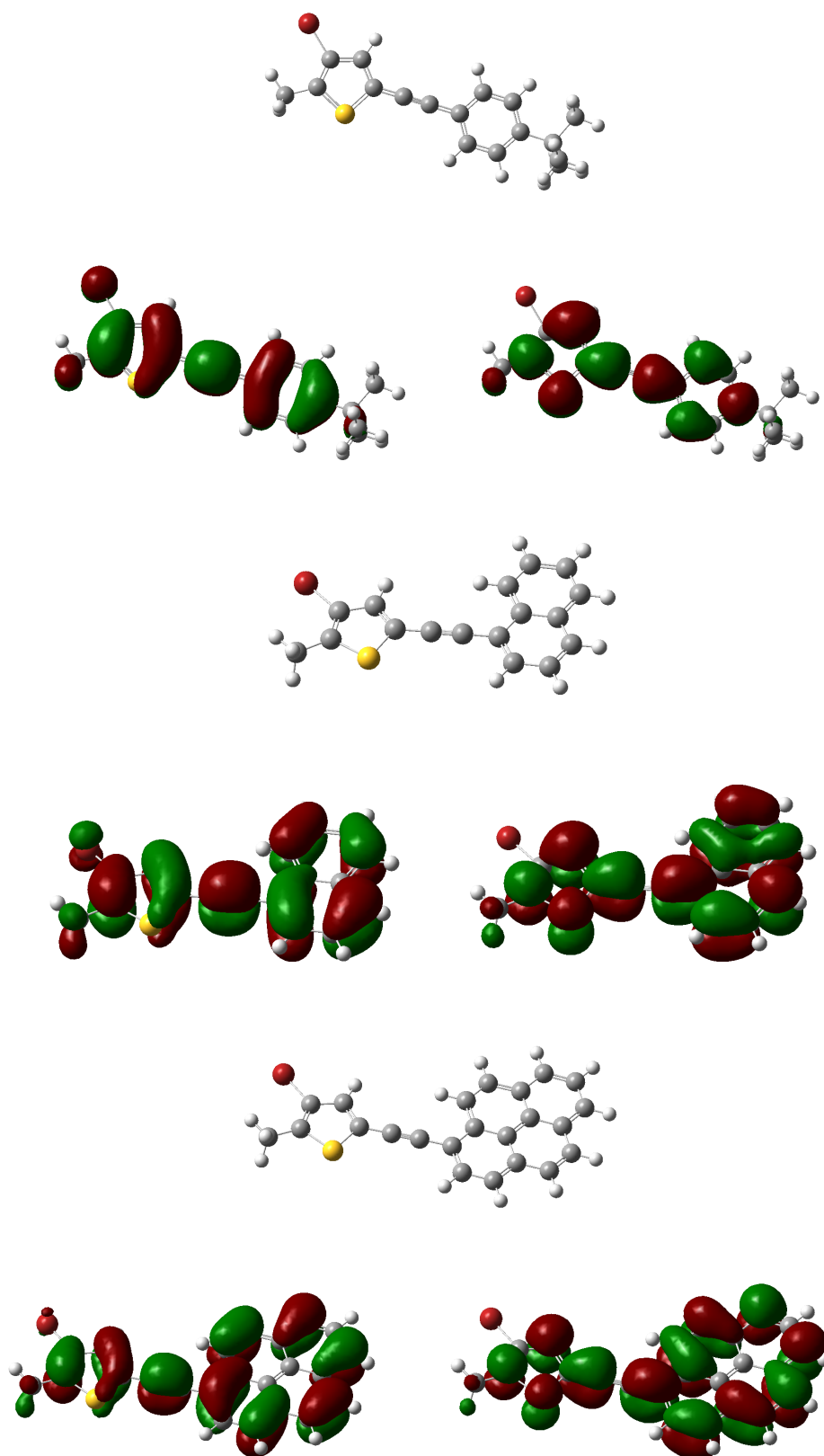


Figure 2.42 DFT calculations for compounds 2, 4 and 5. Assessment of the orbitals involved in the extended π -structures offers details on the chemical properties of the switching analogues. (B3LYP, 6-31g basis set)

It was hoped that these brominated fragments would yield insight into the photophysics of the much more complex and conjugated molecular switch systems of which these are the precursor analogues, especially for that of the open forms, which are usually thought of in terms of two uncommunicating appendages. As seen in each case, the HOMO and LUMO orbitals of each compound are spread almost evenly. The HOMO appears across the conjugated double bonds in each case, as expected. Continued work in this area of computational analysis is hoped to shed more light on the intricacies of these system and how they behave chemically.

The molecular switches synthesised, compounds **8-12**, has been assigned through NMR spectroscopy and its photochemical properties analysed. The addressability of the switches using UV and visible light allows conversion between open and closed forms of the isomers, with a clear absorption peak absorption maximum in the red region of the closed form. Interconversion between parallel and anti-parallel isomers could be addressed through the steric limitations of one form in preference to another. Energy of the emitting wavelengths of the compound occur within a portion of the absorption spectrum that the compound does not strongly absorb, and thus photocyclisation/photocycloreversion reactions are minimal, but still not wholly addressed. There is a good correlation between the calculated on/off quenching ratio and that measured with fluorescence spectroscopy with most of the fluorescence originating from the open form. Initial electrochemical analysis is non-indicative of electrochromic activity, though further analysis is required through spectroelectrochemical measurements. The quantum yield value is quite low for such a strong class of photochromic compounds, which may be due to the strong fluorescence observed. Optimisation of the aromatic appendages, with modulation of the excitation and emission bands is a key component of non-destructive fluorescence readout capability. Compound **12** has shown preliminary photochromic ability, with large PAH moieties.

Design of symmetric and non-symmetrical dithienylethene switches, based on past work done by the Draper group in polycyclic aromatic hydrocarbons, (hexabenzocoronene's (HBC) and their nitrogen doped analogues (N-HSB)) is currently underway. This has initially involved the Diels-Alder reaction of thienylactylene compounds with compound, 2,3,4,5-tetra-(4-*tert*-butylphenyl)cyclopenta-2,4-dienone. Work in this area in this area can allow the design and optimisation of larger and more electronically delocalised aromatic structures, and addition of ligand functionality.

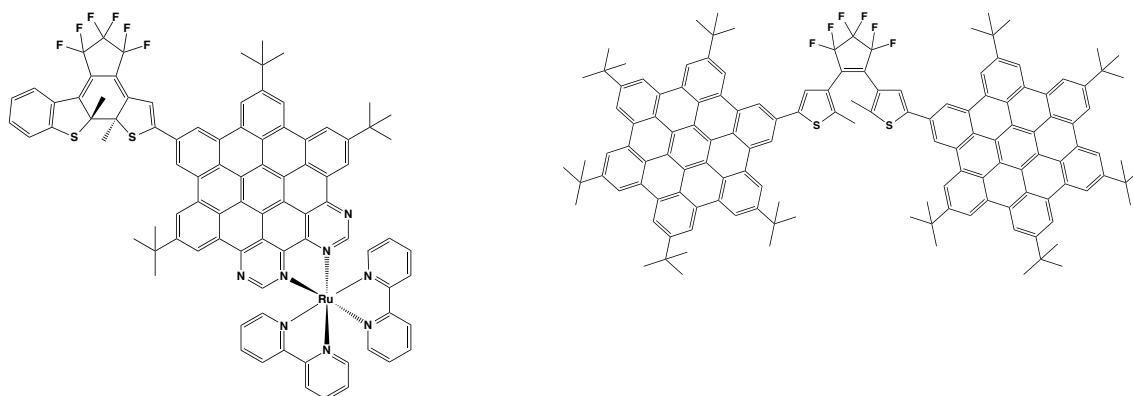


Figure 2.43 HBC and N-HSB based molecular switches

Fluorescent photoswitching using conjugated PAH's with fluorescent moieties that overcome destructive readout capabilities is also a primary focus. The emissive properties of these compounds is still in its infancy (Figure 2.43). The emission of these large hexa-peri-hexabenzocoronene's (HBC) is found in the green portion of the visible spectrum, which allows modulation of molecular synthesis to avoid destructive photocyclisation and photocycloreversion reactions. In 2009, Aida *et al.*,²⁰⁵ reported a novel semiconducting organic nanotube with DTE pendants, whose photoconducting output could be modulated by the photochromic nature of DTE. A semiconducting organic nanotube composed of a graphite-like bilayer of columnarly assembled hexabenzocoronene units changes its photoconductivity in response to photoisomerisation of the photochromic dithienylethene pendants on the surface. The photochromic activity was reported for both the HBC type platform and when self-assembled into the carbon-nanotubes. Under an applied electric field of +2 V, the film exhibited a photocurrent, which was 15 times greater than the dark current. When the open-form DTE pendants on the surface of nanotube 1NT/open were fully converted into the closed form, the photocurrent was enhanced by a factor of 5 from 0.033 to 0.15 nA. Photoisomerisation to the closed form also induced a significant luminescence quenching when compared to its open component. They concluded that in relation to the energy diagrams of HBC and DTE suggest that the electron transfer from photoexcited HBC to the closed form of DTE is energetically much favored over the electron transfer to its open form. This work builds on the foundations that accessibility of molecular switching process through the use of molecular graphenes have an extremely attractive potential, and the plausibility to the use of heteroatoms is an urgent area of exploration.

The efficiency of these systems and the modulation of their spectroscopic characteristics is key towards optimizing the structures for beneficial applications. PAH's such as these are known for their π -stacking and self-assembly in solution and how these this affects the photophysical properties of photochromic molecular switches will be an extremely interesting avenue of research.

3. Hexaphenylbenzene and polyphenylene π -platforms with thienyl substituents, synthesis and photochemical properties

This chapter of work attempted to incorporate thiophene rings into polyphenylene type structures and explore their potential as both delocalised 2D graphene-like platforms and as switching structures. Polycyclic aromatic hydrocarbons were explored in the previous chapter as a gateway to offer optimal π -delocalisation and subsequent switching properties. However, work in this area involved the deliberate incorporation of a ethynyl bridging unit, which served the functions of extending this already massive electron network, but also to analyse the optimum appendage distance, the difference between a single switching unit, or two photophysically independent moieties.

Here, work set out to explore the idea of having the dithienylethene central moiety sit within, or just along the periphery, of much larger polyphenylbenzene structures. Having the thiophene units sit within the extensive π -cloud observed in these graphene-like structures, may allow for previously inaccessible photochemical and electrochemical pathways to be accessed. Again, much like in Chapter 1, both the brominated precursors and the final switching products were synthesised and compared, in terms of their spectroscopic characteristics. Due to the large nature of these substituents, new or alternate pathways were sometimes provided (due to steric environments, solubility etc.). Most products in this chapter explore the possibility of large, extensive and delocalised dithienylethene based switches, however not all of these platforms could be successfully used in the final switching reactions. An inherent problem with these hydrocarbon sheets is their preference to stack in solution. An investigation between the location of the thiophene subunit to the periphery and the extension of stacking seen in solution via ^1H NMR was also undertaken. The absorption profile of these hexaphenylbenzene photochromic products showed a surprising blue-shift in terms of maximum absorption wavelength, however, further exploration into the photophysics of these larger platforms may correlate with these findings.

Synthetic routes in this area revolved around the substitution of phenyl rings with thienyl-analogues in previously reported dynamic pathways, specifically focusing on the Diels-Alder cycloaddition of 2,3,4,5-tetraphenylcyclopentadienone and 2-methyl-3-bromo-5-ethynylthiophene groups. The photophysical and photochromic possibilities of these systems are discussed, with particular emphasis, however, on the NMR spectroscopic characterisation of these isomers. Hexaphenylbenzene platforms, and their mono-, di- and poly- substituted thiophene counterparts were analysed in depth, and a comparative synopsis was drawn for each unique system. The second half of this work into extensive platforms specifically dealt with the photochromic activity of some of these synthesised

switches and how incorporation of the dithienylethene backbone *into* the rotating ring system effects overall switch performance.

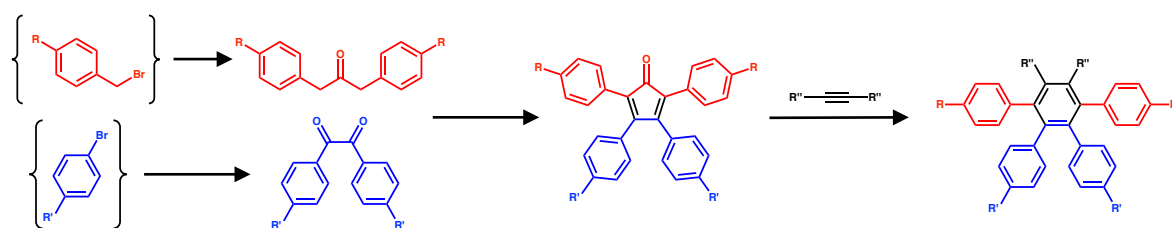
3.1 Tetraarylcyclopentadienone systems, synthesis and characterisation

As discussed in the Introductory chapter, there is great interest in the development of large polycyclic aromatic hydrocarbons, due to their thermal stability and interesting optoelectronic properties, as a result of the π -delocalisation around the aromatic framework. The synthesis of these systems has been developed and subsequently significantly expanded upon in recent years, most notably through the use of polyphenylene precursors. The introduction of the nitrogen heteroatom into these frameworks has, in the past, allowed for the synthesis of a new family of compounds, the nitrogen heterosuperbenzenes (N-HSB).²⁰⁶ In these systems, nitrogen atoms have been placed at the periphery of the coronene framework. The fully cyclised N-HSB product is prepared through the cyclodehydrogenation of the polyphenylene precursor. Nitrogen substitution means that the compounds are now more polar, having lost the C_6 symmetry of the coronene systems. Resulting from this is an increase in the solubility compared to the all carbon analogues, along with an observed increase in the electron accepting ability; a significant increase in the charge carrying ability of these systems is also observed. The coordinating nature of these ligands provides an opportunity to study the N-HSB systems both in terms of their metal coordination properties and their π -stacking ability.

Here, thiophene is used in the synthesis of new polyphenylene derivatives to incorporate sulphur into these conjugated platforms. This chapter discusses a series of sulphur containing polyphenylenes which were synthesised in order to study the effect this heteroatom incorporation would have on both the core ligand, and on switching processes through further chemical reaction. It was hoped that new possibilities would arise for the use of such systems, including the possibility of polymeric thiophene-thiophene bond formation, significant shifts in the ground and excited state dipoles and properties induced by the lone pair of electrons on the sulphur, as the optoelectronic and physical properties of the switches open form and its brominated precursor are remarkably similar. This overlap would allow at least partial control of any unique photoactive properties found in the precursor when developed into an operational switching moiety.

Scheme 3.1 shows the general synthesis of a hexaarylpolyphenylene in which, through design of the substituents (R, R', R'' and R'''), at least four different substituents can be placed on the periphery. Using 1,2-diarylacetonone, **a**, made using the method of des Abbayes²⁰⁷, and 1,2-diarylketones, **b**, from the method of Muller-Westerhoff²⁰⁸, it is possible to synthesis 2,3,4,5-arylcyclopentadienones, **c**. These can then be further reacted with diarylacetylenes, **c**, in [4+2] cycloadditions to give a range of cycloaddition products. Although the Knoevenangel condensation used in the synthesis of cyclopentadienones is well known,¹¹⁴ it was found that the synthesis of cyclopentadienones where the aryl groups of the mono- and diketone reactants are substituted with strong electronic groups such as thiophene, the classical condensation reaction failed. As such, it was utilised that varying the acetylene moiety was the simplest way by to moderate the substitution of the final polyphenylene.

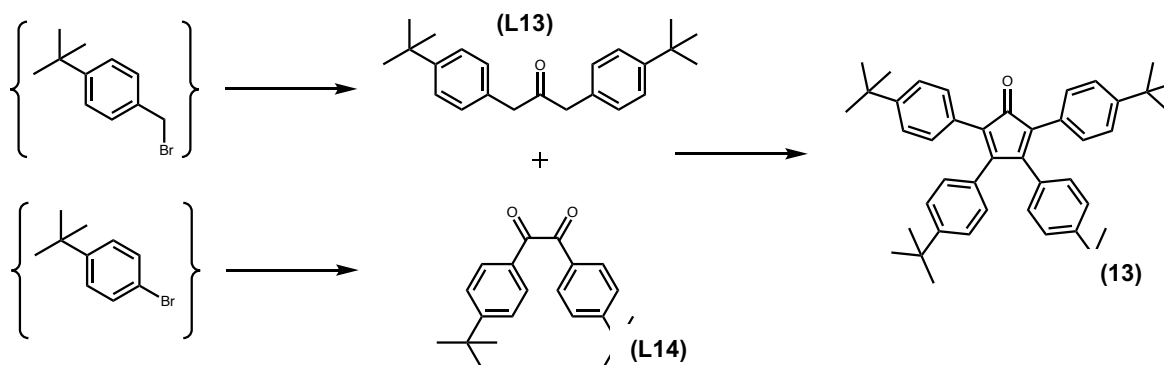
However, modulation of compounds **a** and **b** were still undertaken, with a variance in the substituent groups R and R' (R= Me, Br, R'= Me, Br). Methyl groups at these periphery positions allow for increased solubility of the products, a problem addressed for the coronone analogue in Chapter 2. Substitution with bromine, however, allows for potential further reactions, such as Suzuki cross-coupling reaction with a suitable boronic acid. This step-wise synthesis would instead allow the incorporation of thienyl-units *outside* of the classic hexaarylcore, and observe the consequent effect this may have on the overall system. As shown in Section 3.1, this may also be achieved through the use of cobalt carbonyl as catalyst in a cyclotrimerisation reaction of varying substituted acetylenes, appearing in both the asymmetric and symmetric analogues. Combination of these techniques allow for the study mono-, di- and trithienyl-hexaarylbenzenes, both within the core framework and as strong electronic components outside on the periphery.



Scheme 3.1 Synthetic route for the formation of substituted hexaphenylbenzenes, divided into constituent parts: (i) procedure of des Abbayes to synthesise 1,3-diarylacetonones (red); (ii) procedure of Mueller-Westerhoff for the synthesis of 1,2-diketones (blue); (iii) two-fold Knoevenagel reaction for the synthesis of tetraphenylcyclopentadienones.

Based on these initial modifications, and to further optimise overall photochromic potential and ability, a new family was developed. 1-(3-bromo-2-methylthiophene)-2,3,4,5,6-penta(4-*tert*-butylphenyl)benzene (**17**) and 1-(3-bromo-2-methylthiophene)-2,3,4,5-tetra(4-*tert*-butylphenyl)benzene (**18**) were the target molecules, themselves concurrent appendages of novel dithienylethene based switches. These novel platforms were also studied independently towards understanding their photophysical and photochemical properties. The dienophile stereospecifically adds 1,4 to a conjugated diene component, to generate a six membered ring through the formation of two C-C bonds. The resulting extended π -conjugation allows for extensive delocalisation of electrons throughout the photochrome.

3.1.1 Synthesis and ^1H NMR of 2,3,4,5-tetra-(4-*tert*-butylphenyl)cyclopenta-2,4-dienone, **13**



Scheme 3.2. Synthetic route and reactions of **13**, with **L13** and **L14**, (i) in the presence of *KOH* in ethanol at 95 C for an hour (81 %)

Scheme 3.2 shows the proposed synthesis of compound **13** (2,3,4,5-tetra-(4-*tert*-butylphenyl)cyclopenta-2,4-dienone), developed from synthesised precursors **L14**, a *tert*-butylsubstituted diketone, and **L13**, a *tert*-butylphenyl substituted diketone, which had previously been developed within the group in the synthesis of N-HSB. The *tert*-butyl groups were added for increased solubility of the conjugated systems. The monoketone, 1,3-bis-(4-*tert*-butylphenyl)propan-2-one, was prepared via a liquid-liquid phasetransfer carbonylation reaction, with $\text{Fe}(\text{CO})_5$ as the source of CO and $\text{tBuN}^+(\text{HSO}_4)^-$ as a phase transfer catalyst. The diketone, 2,5-bis-(4-*tert*-butylphenyl)ethane-1,2-dione, was prepared by lithiation of 4-*tert*-butylbromobenzene with *n*-BuLi at -78°C in THF, followed by reaction with DMPD (1,4-dimethylpiperazine-2,3-dione) and subsequent quenching with aq. HCl (10 %). Finally the cyclopentadienone, 2,3,4,5-tetra-(4-*tert*-butylphenyl)cyclopenta-2,4-dienone was

synthesised by a two-fold Knoevenagel condensation reaction between the monoketone and diketone, in the presence of KOH (0.5 eq.) in ethanol with the loss of two molecules of water. The tetraphenylcyclopentadienone was obtained as a dark purple solid, with no further purification required. The generation of this reactive diene would allow for a wide range of reactions with dienophiles and the subsequent compilation of a thienyl-HPB compound library.

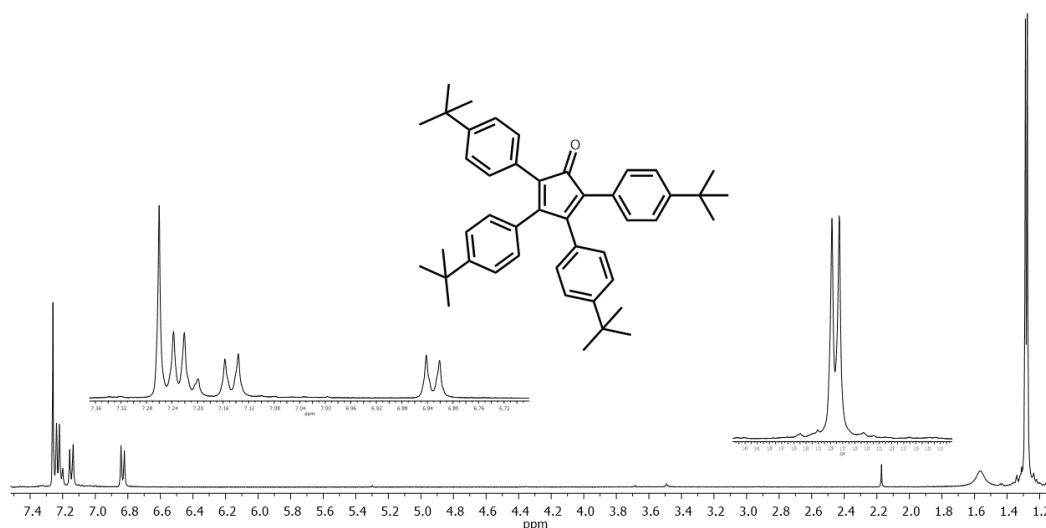


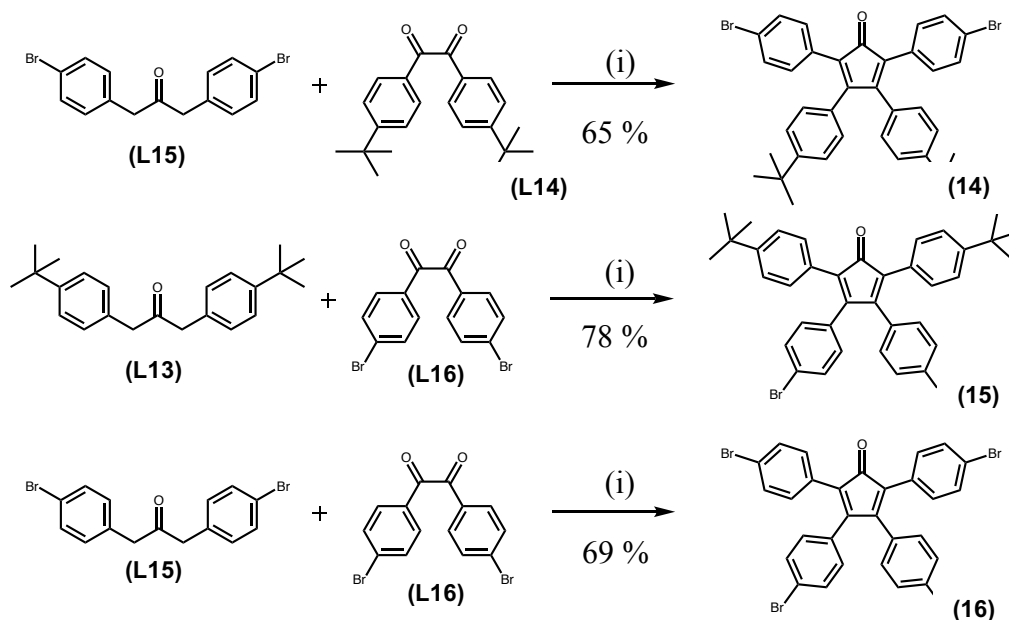
Figure 3.1 ^1H NMR of 2,3,4,5-tetra-(4-tert-butylphenyl)cyclopenta-2,4-dienone in CDCl_3 (400 MHz, RT).

However, it was upon extraction of the target purple compound that it was clear that varying substituted mono- and diketones could also be used, namely brominated adducts. These various products could potentially be used in the reactions of larger, more intricate systems, and allow for thienyl substitution beyond the hexaaryl-core.

3.1.2 Synthesis of tetraarylcyclopentadienones 14-16

Synthesis of tetraarylcyclopentadienones was carried out identically for all three products, and in a similar manner to the synthesis of **13**, with only variances in the starting materials used. 1,2-Diphenylethane-1,2-dione (**L16**), commonly known as Benzil, is commercially available, 2,5-bis-(4-tert-butylphenyl)ethane-1,2-dione was synthesised and described previously. 1,3-Bis(4-bromophenyl)-2-propanone (**L15**) was prepared according to literature procedures; a solution of dicyclohexylcarbodiimide and 4-(dimethylamino)pyridine in CH_2Cl_2 was stirred at 25 °C under dry N_2 and treated dropwise with a

solution of 4-bromophenylacetic acid. The reaction was allowed to proceed overnight and the resulting product was purified via column chromatography, and recrystallised with ethanol.



Scheme 3.3 The syntheses of tetraarylcyclopentadienones, **14-16**, (i) KOH, $\text{CH}_3\text{CH}_2\text{OH}$, 90 °C.

These products were then reacted with KOH as basic catalyst in accordance with the scheme above, and produced compounds **14**, **15** and **16** in moderate to well yields (65 %, 78 % and 69 %). The yields may reflect how the reaction suffers from the low boiling point of the alcohol and the limited solubility of both potassium hydroxide and the reaction product in this solvent. Triethyleneglycol has shown more success as a solvent and permits operation at a higher temperature, usually used with benzyltrimethylammonium hydroxide, a strong base readily soluble inorganic solvents, which serves as catalyst. However, due to the high yields and readability of the starting materials, alternative methods were not immediately sought after in the course of this research. All tetraarylcyclopentadienone products are a variance of purple. The five conjugated aromatic rings create a delocalised π -electron system. These electrons are excited by radiation in the visible region. However, a prominent feature of all of their structures is the carbonyl group, namely the non-bonding electrons of the oxygen. These $n \rightarrow \pi^*$ transitions occur within the visible portion of the UV-Vis spectrum, usually around 500-560 nm, and are responsible for the intensity of the colour observed. The higher energy $\pi \rightarrow \pi^*$ transitions usually only occur with the UV portion of the spectra.

3.1.3 ^1H NMR spectra of tetraarylcyclopentadienones **14**, **15** and **16**

The ^1H NMR of compounds **14**, **15** and **16** are shown in Figure 3.2. The proton phenyl peaks lie in the region typical of aryl substituted groups. The protons nearest to the bromine remain largely unaffected by the surrounding environment in each case, however the *tert*-butyl substituted phenyls have a proportional relationship with their position in relation to the middle cyclopentadiene ring.

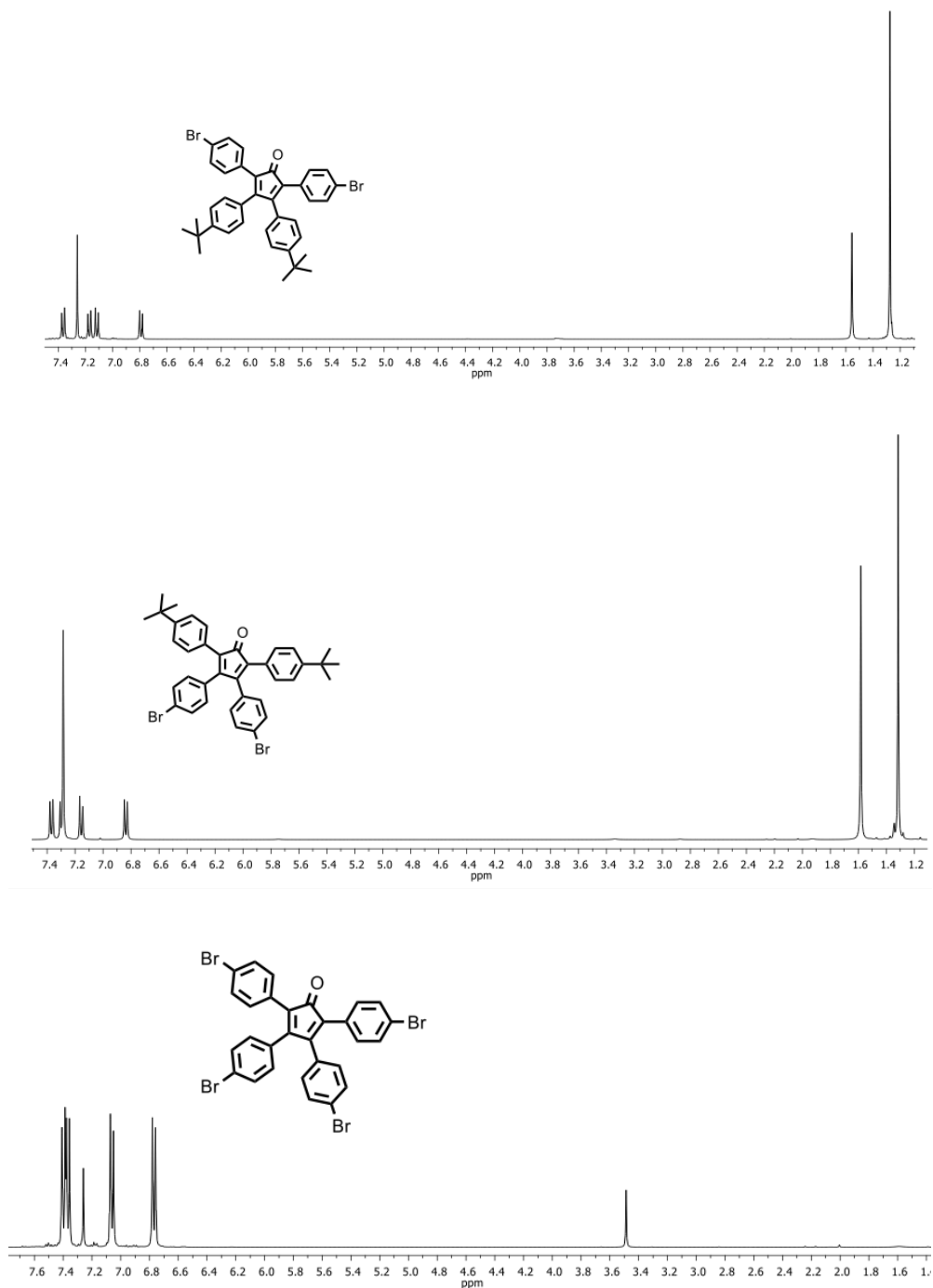


Figure 3.2. ^1H NMR spectra of tetraarylcyclopentadienone compounds **14**, **15** and **16** in CDCl_3 (400 MHz, R.T.)

A comparative look at each of these systems and their respective proton signals makes this clearer. There is no direct overlap between any of the proton signals between compounds **14**, **15** and **16**. This would suggest a level of conjugation in the system that was not expected. The top-most rings appear analogous with the central ring system, and shifts appear at similar ppm in all cases, including that of model compound **13**. The bottom rings, however are influenced much more by substitution, and act almost as independent phenyl systems. This may be a factor of the reactivity of the central diene, with its orbitals equally spread across the top half of the compounds. The protons nearest to the para-substituents are the most influenced by this environment, with all other signals relatively unchanged in each case.

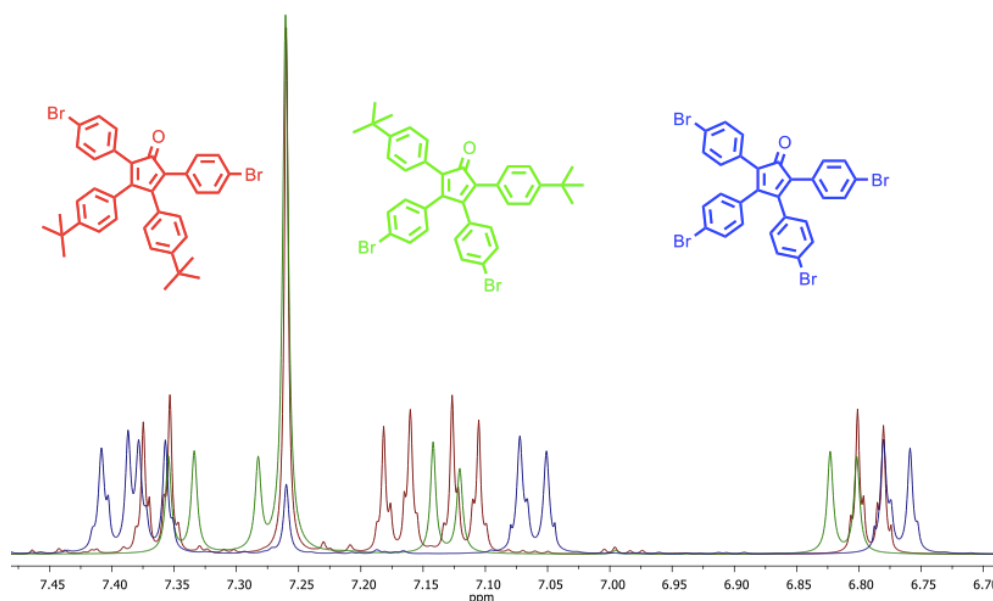
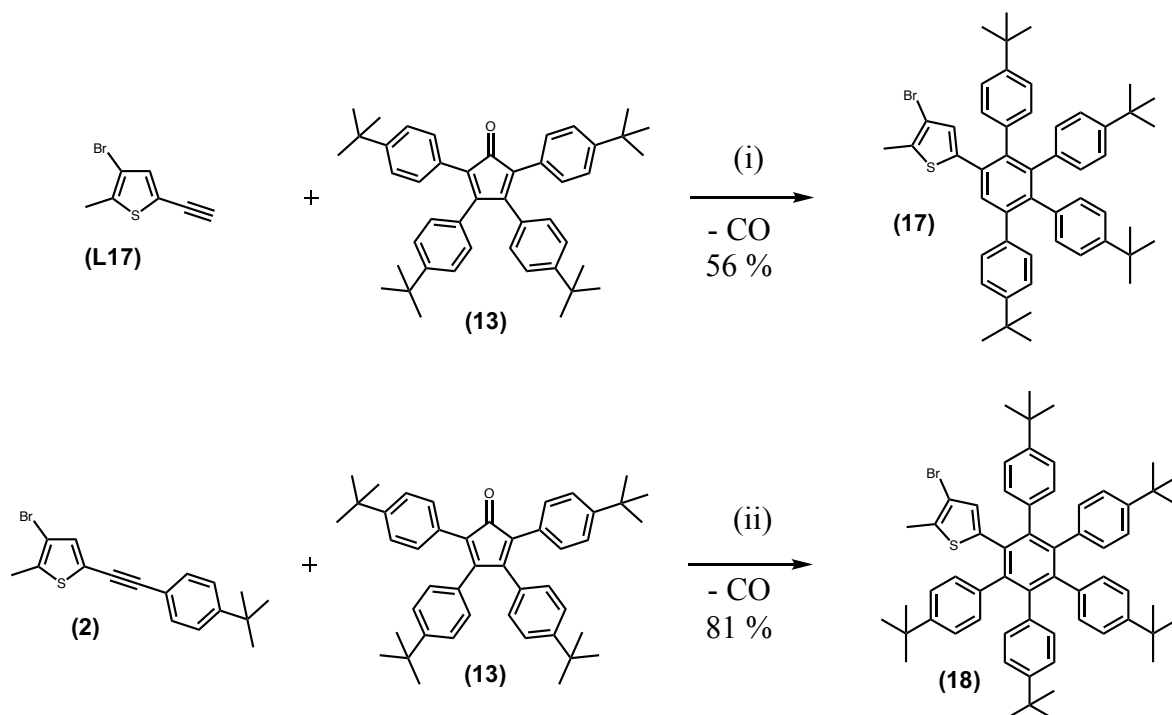


Figure 3.3 Comparison of ^1H NMR spectra of compounds **14**, **15** and **16**

3.2 Synthesis and characterisation of polyphenylene appendages

The novel compound **17** was synthesised using [4+2] Diels-Alder cycloaddition from 3-bromo-5-ethynyl-2-methylthiophene and tetraarylcyclopentadienone, which were heated in benzophenone in a sandbath at elevated temperatures for 6 hours. The reaction was monitored with TLC chromatography. The instability of compound meant the use of a shorter reaction time, as the product was seen to decompose upon previous iterations of this reaction. The product was obtained as a pale brown solid after purification by column chromatography on silica eluting with CH_2Cl_2 : hexane (1: 5 v/v), with a second column with

a similar packing and eluent used to further purify the final product from unreacted benzophenone (56 % yield)



Scheme 3.4. Syntheses of thienyl-HPB compounds 17 and 18, (i) Benzophenone, 250 °C, 6 hours, Ar (ii) Benzophenone, 300 °C, overnight, Ar

Product **18** was prepared using a [4+2] cycloaddition reaction between **2** and cyclopentadienone in a benzophenone melt at high temperatures overnight. Though the reaction required longer reaction times and higher temperatures, it proceeded in a more facile manner to **17**. Purification was achieved via column chromatography, eluting first with hexane and then CH₂Cl₂: hexane (1: 9 v/v), to remove unreacted benzophenone, side products and cyclopentadienone. CH₂Cl₂: hexane (1:4 v/v) was gradually added as the solvent system and the target compound was obtained as a dark yellow powder in 81 % yield.

3.2.1 Characterisation of polyphenylene compounds 17 and 18.

Polyphenylene compounds **17** and **18** were fully characterised using ¹H, ¹³C, and 2D (HH-COSY, HSQC, HMBC) NMR spectroscopy infrared spectroscopy and mass spectrometry. The NMR of known reactants, monoketone, diketone and cyclopentadienone were in excellent agreement with literature, as shown. Reactants **2** and **L17** were also solved via ¹H and ¹³C{H} NMR due to their simplified spectra. Chemical shifts and certain multiplicities of the NMR spectra are discussed in the following section, and full details are provided in Chapter 5.

The electrospray mass spectra of the two products **17** and **18**, recorded in methylene dichloride, reveal the major peak in each corresponds to the $[M]^+$ molecular ion, where the compound has become charged upon ionisation in the mass spectrometer. The values are in excellent agreement with the values calculated for the molecular ion. The mass spectral data is summaries in Table 2.1

Compound	Molecular Ion	Formula	Found m/z	Calculated m/z
17	$[M+H]^+$	$C_{61}H_{69}BrS$	912.4349	912.4303
18	$[M+H]^+$	$C_{51}H_{57}BrS$	780.3399	780.3364

Table 3.1

3.2.1.1 1H NMR of polyphenylene compounds **17** and **18**

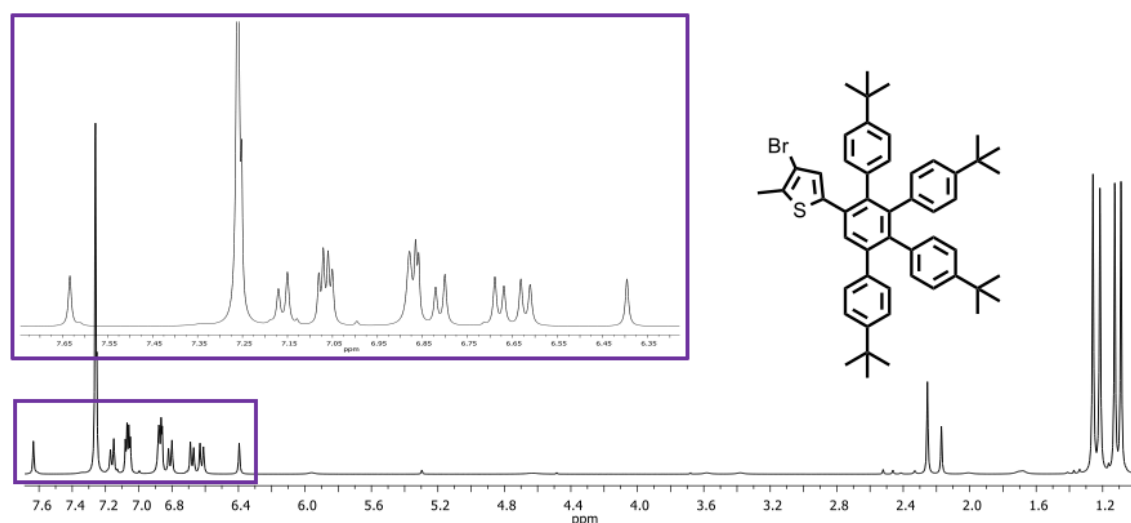


Figure 3.4 (a) 1H NMR spectra of compound **17** in $CDCl_3$ (400 MHz, RT) showing magnification of the aromatic region. Atom labelling as per figure inset.

The 1H NMR spectrum of **17** is shown in Figure 3.4. The most prominent feature both in terms of the spectrum and that of the synthetic structure is probably the singular proton and its associated peak of the core benzene. It's highly downfield and shielded rather play into the theory of continuous conjugation across the system via the central benzene, with the extension of the electron cloud afforded from the funnelling from each aryl electron cloud,

despite the rotation each observes around the single bond. As such, the central ring is afforded much more nuclear shielding compared to a standard phenyl ring.

The most upfield signal in comparison, is that of the thiophene ring. The electron density within the ring affords a level of shielding due to its pseudo- aromaticity, however this is much lower than that of benzene, and as such appears much more upfield as a singlet. The remaining signals

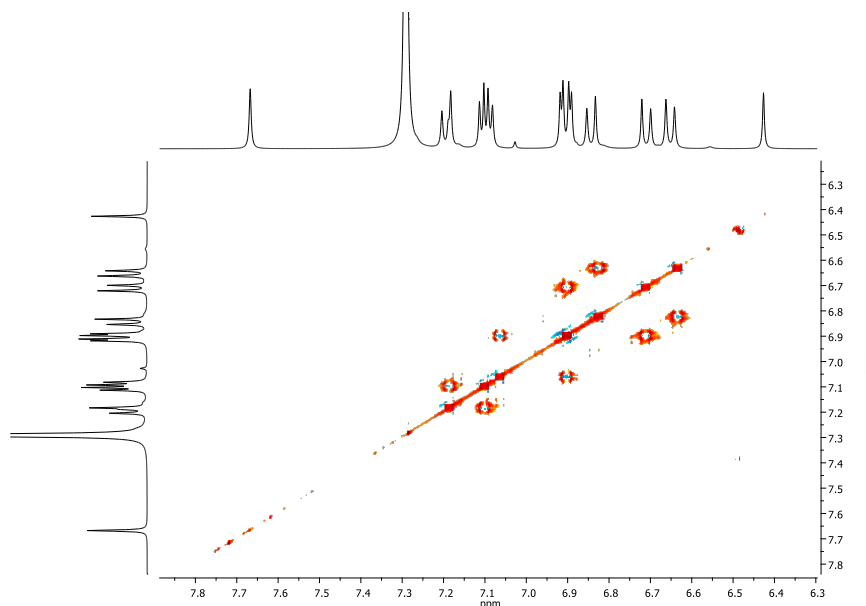


Figure 3.5 ^1H -COSY experiment for compound **17**.

The ^1H NMR spectrum of thienyl-HPB **18** is shown in Figure 3.6. The compound possesses a C_2 axis of symmetry through the thiophene. The aromatic region of compound **18** is much more simplified in nature due to this symmetry, compared to that of **17**. The signals for the aromatic protons occur as a series of overlapping AB splitting patterns for each of the phenyl rings located $\delta = 6.64$ and 7.03 ppm. The thienyl proton is also noticeable at $\delta = 6.13$ ppm, with its notable upfield shift when compared to that of **17**, analogous of either an extension of the π -cloud observed in the system, or the division it now faces between two equally rotating phenyl rings. Interestingly, the *tert*-butyl signals, which usually appear in these systems as a singlet integrating for 18 protons and a signal integrating for 27, such as seen for iodo-hexaphenylbenzene, instead here appear much more defined, with two singlets integrating for 18 each, and the last singlet, seen to be the *tert*-butyls of the phenyl ring para to the thiophene, integrating for 9 protons. This may be due to the upsetting nature of the thiophene itself, and allows the removal of the usual degeneracy observed in these platforms.

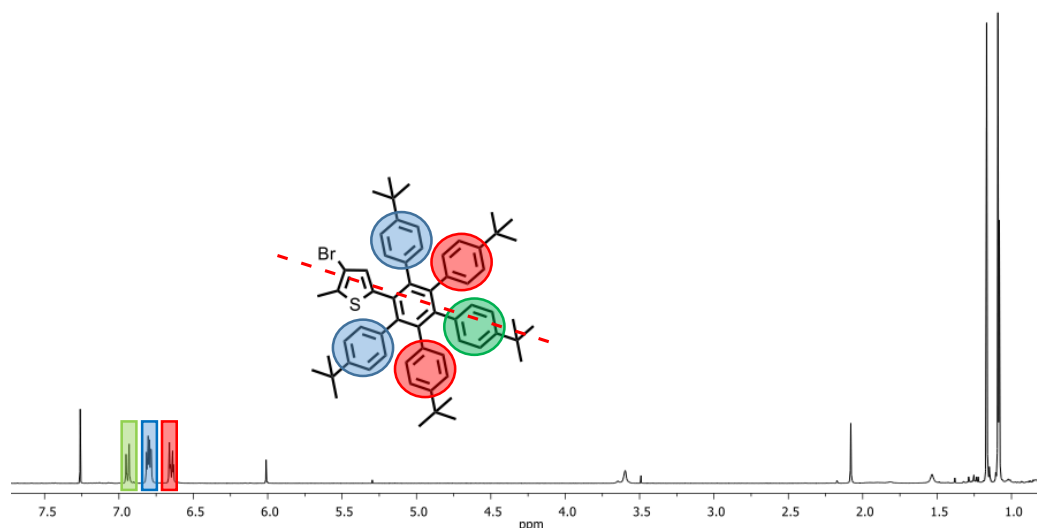


Figure 3.6 ^1H NMR of **18** in CDCl_3 (400 MHz, RT), with inset showing symmetry of compound and also splitting pattern observed in the aromatic and aliphatic regions.

In general, it is possible to identify the aromatic phenyl ring signals that are closest to the *tert*-butyl functional groups using selective NOE (Nuclear Overhauser Effect) experiments. By this method, selective irradiation of an individual *tert*-butyl resonance will see a NOE enhancement on adjacent spins through space. For example, irradiation of the smallest of the *tert*-butyl groups in **18** results in a positive signal for the more downfield multiplet (6.82–6.88 ppm). This indicates that H₁, H₃ and H₅ spins occur within this multiplet which integrates for 12 protons. A HH-COSY experiment is then used to find the adjacent proton on each phenyl ring, such that H₂, H₄ and H₆ (integral value 10) found to occur in the more upfield multiplet.

3.2.2 Synthesis of symmetric dithienyl compound, DTR.

Due to the properties substitution of a singular thienyl-unit had afforded the HPB-based systems, integration of further units and the synthesis to obtain these products was established. Initially, similar reaction steps similar to those discussed previously were thought to be viable, such as using bromo- or iodoacetone as the monoketone and a subsequent suitable diketone, in the double aldol condensation reaction to produce, the 1,4-dihalo-2,3,5,6-tetraarylbenzene. This could then be further reacted through Suzuki cross coupling and produce the relevant symmetrical final product. However, this method proved unviable and so an alternate route was sought.²¹⁰

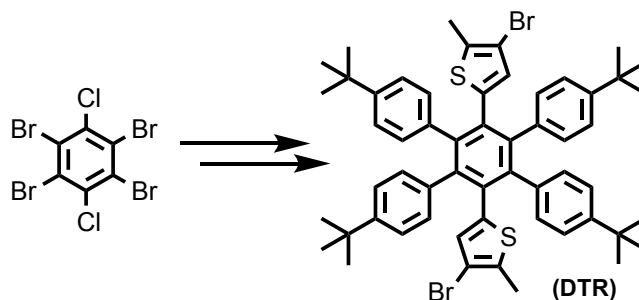
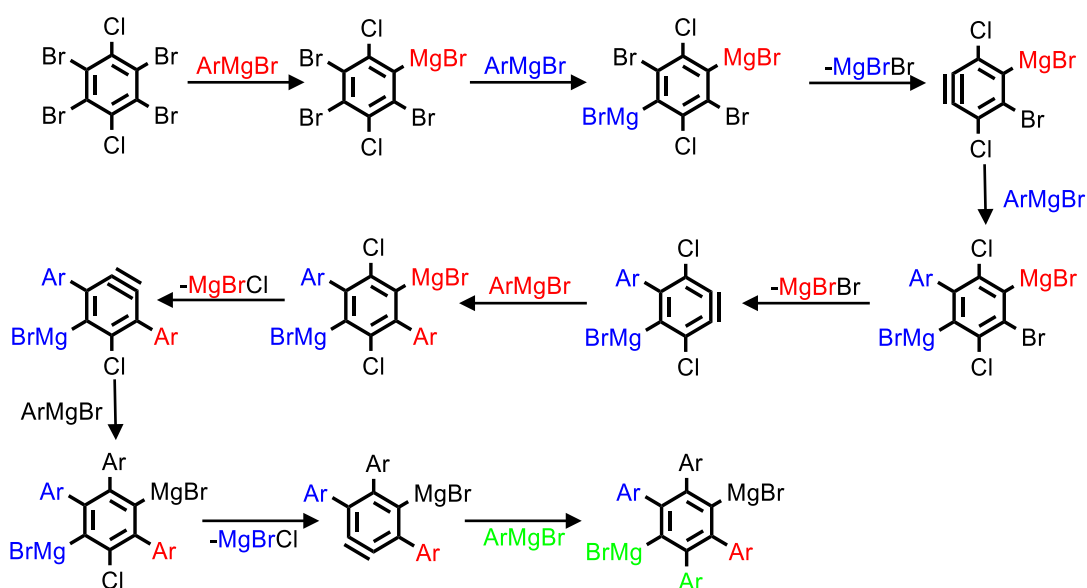


Figure 3.7 Overall synthetic pathway from starting material to final product.

Durand reported that hexabromobenzene reacts with phenylmagnesium bromide to give hexaphenylbenzene,²¹¹ but shortly afterwards, Dilthey showed²¹² through independent synthesis that the product was in fact 1,2,4,5-tetraphenylbenzene. Geiasman²¹³ confirmed these results and showed, through obtaining 1,2,4,5-tetraphenylbenzene-3,6-dicarboxylic acid on carbonation, that the actual reaction product was the tetraphenyl 1,4-di-Grignard. In these early studies, the solvents were ether, in which the starting materials is nearly insoluble, or benzene, a poor Grignard solvent. Product yields were well below 10 % and considerable tars were formed. Hart *et al.*,²¹⁴ proposed the reaction scheme seen in Scheme 3.5. Through the use of excess phenylmagnesium bromide, and halting before hydrolysis, the reaction could be halted. Treatment of 1,2,4,5-tetrabromo-3,6-dichlorobenzene with various arylmagnesium bromides in THF at room temperature for 12 h led to the formation of dimagnesium inter-mediate. Its direct reaction with iodine provided diiodobenzene as a white powder in 62 % yields.



Scheme 3.5 Mechanism proposed by Hart *et al*, using excess phenylmagnesium bromide and showing key intermediates.

The Suzuki–Miyaura coupling was chosen because it is one of the most powerful biaryl C–C bond-forming transformations available to synthetic organic chemists. This transformation enjoys a broad scope and wide functional-group tolerance. Usually, in the case of sterically hindered aryl or alkenylhalides, limited success has been realised and special ligands and harsh reaction conditions are often required. However, here this was not the case.

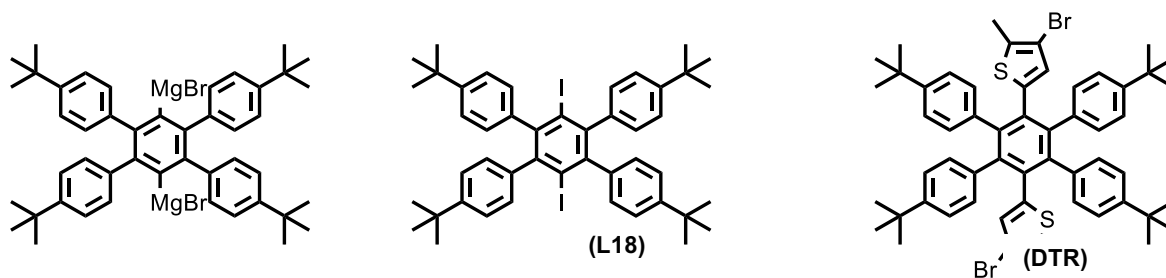


Figure 3.8. The two intermediates in the reaction pathway to compound **DTR**

The boronic thiophene was reacted in excess with the diiodobenzene product, with $\text{Pd}(\text{PPh}_3)_2\text{Cl}_2$ as catalyst, and produced compound **DTR** as a brown solid. The product was dissolved in CH_2Cl_2 and repeatedly crashed out of methanol.

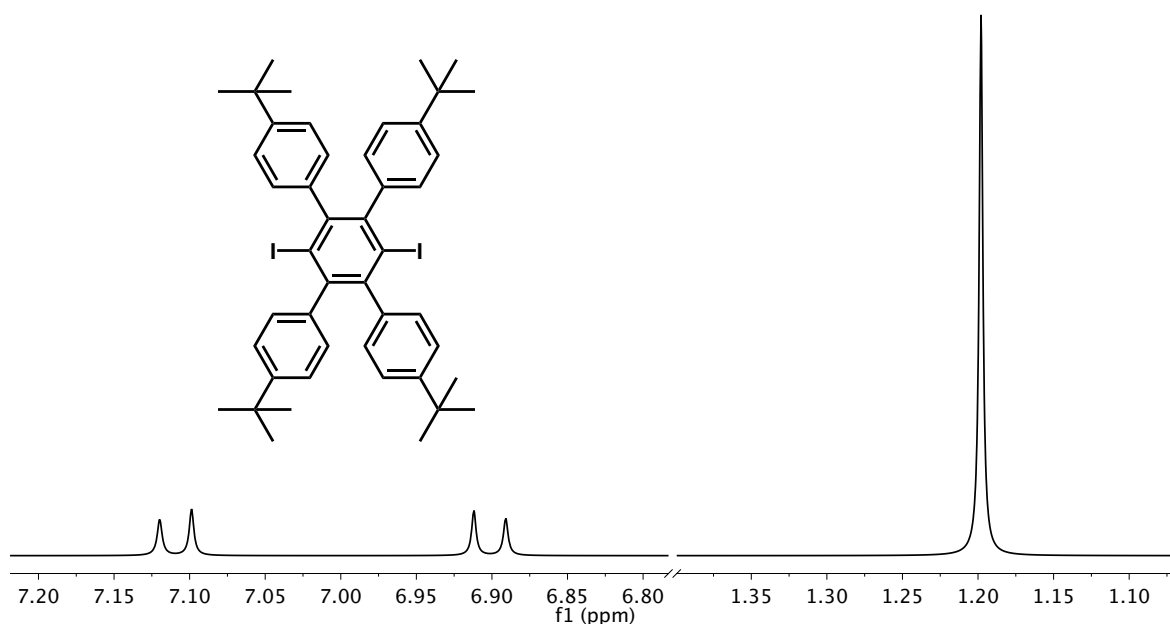


Figure 3.9. ^1H NMR of **L18**. The intermediate precursor displays an almost identical proton spectrum to the final compound **DTR**, though slight more upfield (CDCl_3 , 400 MHz, RT)

3.2.2.1 ^1H NMR spectra of compound **DTR**

Like its diiodo-precursor, compound **DTR** produces a very simplified NMR spectrum. This is due to the high level of symmetry within the system. The thienyl proton presents at 6 ppm, a value typical of thiophenes substituted at the 2-position and incorporated into these large delocalised systems. The rotating phenyl rings appear in the range typically seen of aromatic groups, though slightly more upfield than in free benzene or phenyl-substituted systems. The inner most protons are shielded, likely due to the extension of the electron cloud of the central benzene ring.

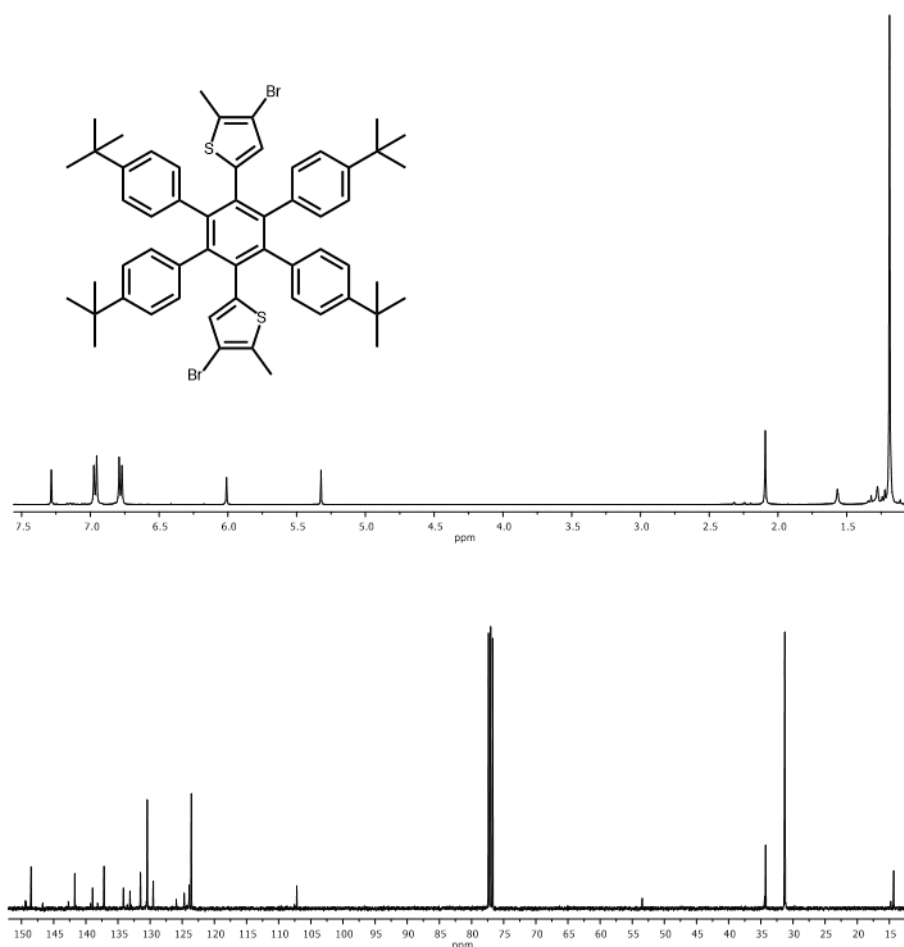
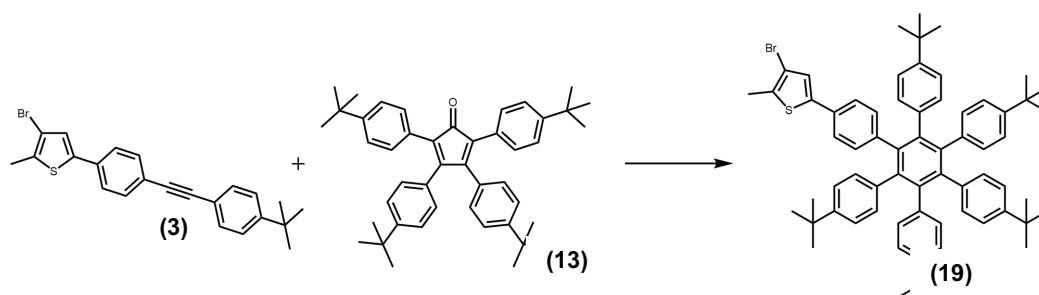


Figure 3.10 ^1H and ^{13}C NMR of **18**

3.2.3 Synthesis of 3-bromo-5-(4''-(*tert*-butyl)-3',4',5',6'-tetrakis(4-(*tert*-butyl)phenyl)-[1,1':2',1''-terphenyl]-4-yl)-2-methylthiophene, **19**



Scheme 3.6 Synthesis of **19**, benzophenone, 300 °C, 5.5 h, 19 %.

19 was prepared via a Diels Alder reaction between **3** and **13**. The reaction mixture was refluxed at a temperature of approximately 300 °C for 5 hours. The crude product was a brown solid which was purified by column chromatography to yield an off-white powder. Preliminary photophysical measurements were carried out on **19** in order to compare the properties of **10**. Understanding of the dynamics of the brominated appendages

3.2.3.1 NMR Characterisation of **19**:

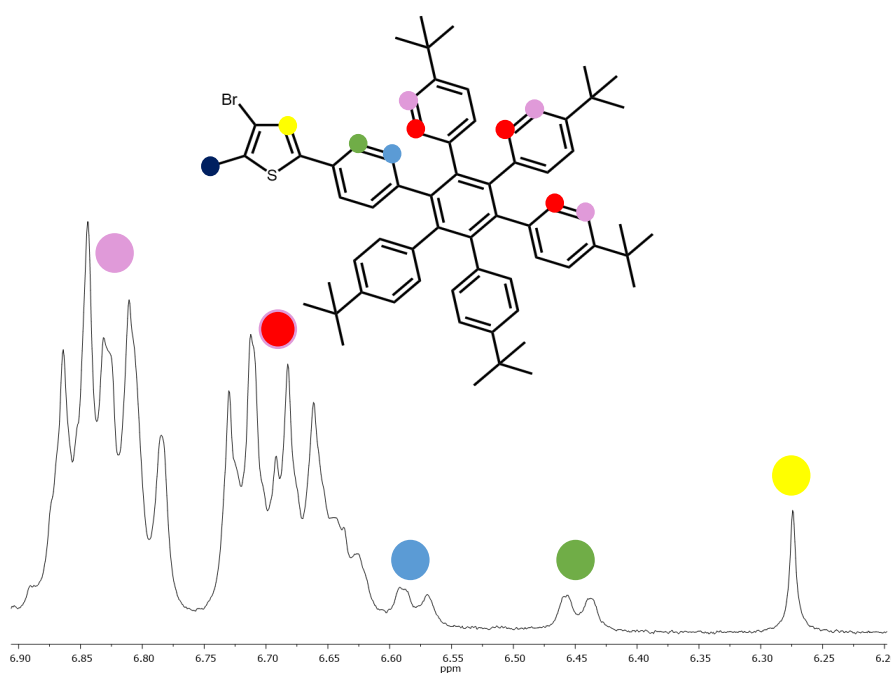


Figure 3.11 ^1H NMR of compound **19** (CDCl_3 , 400 MHz, RT)

19 was fully characterised by using NMR spectroscopy and mass spectrometry. On the ^1H NMR, the aromatic protons on the phenyl rings were represented by two multiplets present at 6.83-6.78 ppm and 6.70-6.63 ppm. The integration of each of these signals corresponded to twelve protons. The signal at 6.24 ppm appeared as a singlet with an integration value of

one proton and this was assigned to the aromatic proton on the thiophene ring. The singlet at 2.34 ppm integrated to three protons and represented the protons on the methyl group attached to the thiophene ring. The signals for protons on the *tert*-butyl groups appeared as two singlets at 1.21 ppm and 1.09 ppm. The signals allowed for the differentiation between the *tert*-butyl protons on the phenyl rings closest to the thiophene moiety (1.21 ppm integrated to eighteen protons) and those further away (1.09 ppm integrated to twenty-seven protons). The ^{13}C NMR spectrum was resolved with the aid of HSQC and HMBC two-dimensional spectra to identify the carbon signals attached to protons and quaternary carbons, respectively. The carbon signals at 131.13 ppm and 123.16 ppm each represented twelve aromatic carbons which had protons attached. These signals represented the aromatic carbons on the six peripheral phenyl rings. The peak at 130.52 ppm corresponded to one aromatic carbon nucleus which had a proton attached and this was assigned to the only carbon on the thienyl ring which had a proton attached. The resonance at 31.32 ppm represented fifteen carbon nuclei and this corresponded to the fifteen methyl carbons on the *tert*-butyl groups. The quaternary signal at 34.17 ppm corresponded the five quaternary carbons on the *tert*-butyl groups. The peak at 14.91 ppm was assigned to the methyl carbon attached to the thiophene ring. The quaternary carbon adjacent to the methyl on the thiophene was represented by the signal at 132.88 ppm. The resonance at 109.68 ppm was representative of the quaternary carbon on the thienyl ring attached to the bromine atom. The quaternary signal at 136.81 ppm represented the carbon on the thiophene ring which was attached to the phenyl ring and the carbon on the phenyl ring attached to the thienyl ring was represented by the peak at 139.35 ppm on the spectrum. The signal at 129.84 ppm was representative of the second quaternary carbon on this phenyl ring. The signals at 147.53 and 147.85 ppm were assigned to the five quaternary carbons on the five other peripheral phenyl rings that were attached to the *tert*-butyl side groups. The other quaternary carbon on these five peripheral rings was represented by the resonances at 140.82 and 140.27 ppm. The six quaternary carbons on the central phenyl ring corresponded to the peak at 137.93 ppm.

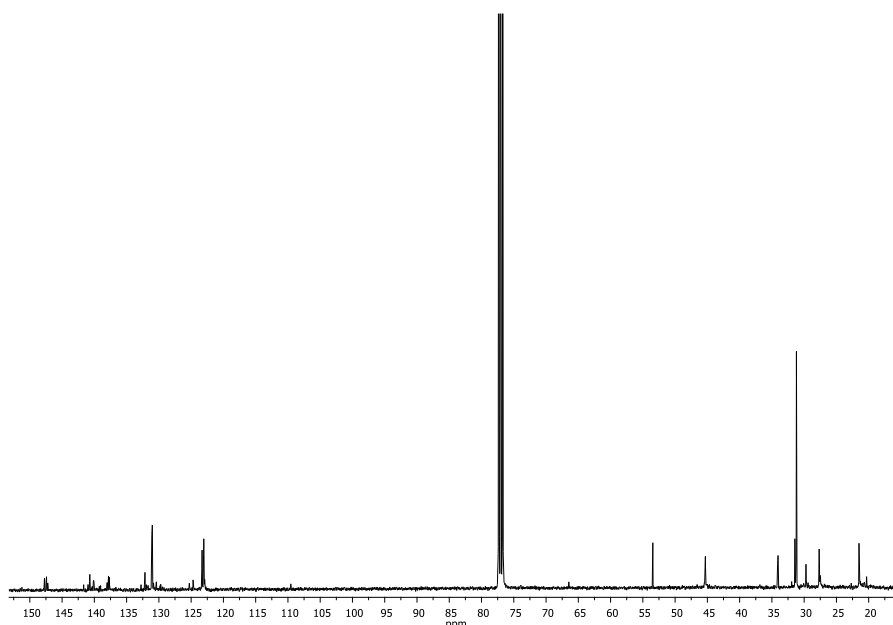


Figure 3.12 ^{13}C NMR spectrum of compound **19** (101 MHz, CDCl_3 , RT)

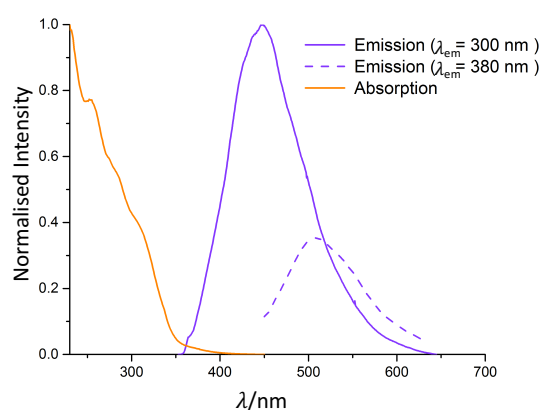


Figure 3.13 Absorption and emission spectrum from compound **19**, run in CH_2Cl_2 (1×10^{-5} M). Spectra are normalised to show the difference in emission between high- and low-energy excitation wavelengths.

The absorption and emission of compound **19** was run in CH_2Cl_2 solvent. The absorption pattern is not dissimilar to that already observed in this types of π -platform, with a generally featureless absorption pattern, and a slight shoulder at 324 nm due to the thienyl transitions already noted. The emission spectra were also recorded and was shown to be dependent on excitation wavelength. Excitation at high energies induces strong emission. This emission band is usually attributed to fluorescence derived from the polyphenylene chromophore. This high energy emission is a feature of propeller-like polyphenylene emission. The recorded excitation spectra also match the absorption spectrum, indicating the absence of

intermolecular aggregates or interactions. Interestingly, a series of polyphenylene dendrimers composed of tens or hundreds of out of plane twisted phenyl units display an analogous strong emission profile with fluorescence centred at 365 nm. Upon excitation at lower wavelengths, a less-intense red shift is observed. Again, this emission occurs as generally quite broad and featureless.²¹⁵

3.3 Synthesis of polyphenylene based switches.

Performing a Diels-Alder reaction of **L** with **13** for 3 hours at 300 °C yields (1,2-bis(5-(2,3,4,5,6-penta(4-*tert*-butylphenyl)benzene)-2-methylthiophen-3yl)perfluorocyclopent-ene) compound **20**. The novel switch under short wave UV light, demonstrates a conversion to purple whilst in solution, and photocycloreversion upon irradiation with visible light. The product was positively identified by mass spectrometry and NMR spectroscopy. It's photochromic ability was also tested under a range of conditions.

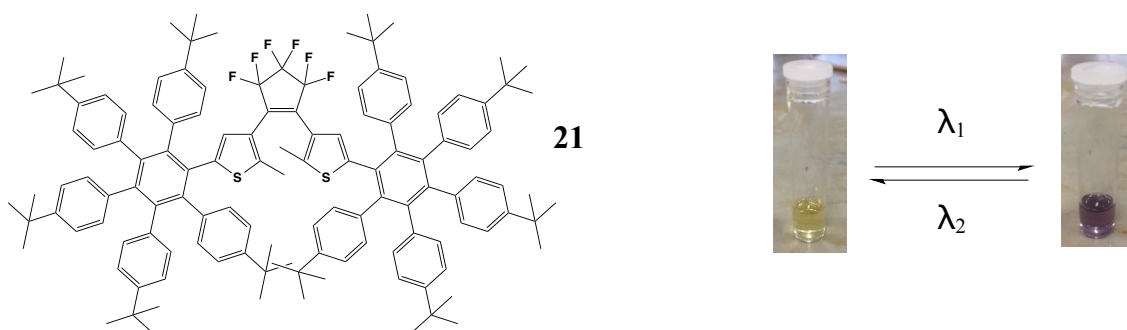


Figure 3.14 Photochromic ability of proposed compound **21**

As with the reaction to produce product **20**, performing a Diels-Alder reaction of **8** with **13** for 3 hours at 300 °C yields (1,2-bis(5-(2,3,4,5,6-penta(4-*tert*-butylphenyl)benzene)-2-methylthiophen-3yl)perfluorocyclopent-ene) compound **21** (Figure 3.14). However, instability in terms of the diene was less significant in this reaction and so higher temperatures were used. The switch demonstrated photochromic ability under UV upon purification, and corresponding photocycloreversion under normal lighting conditions. The product was positively identified by NMR spectroscopy and analysed in terms of its photophysics.

3.3.1 Characterisation of polyphenylene switches **20** and **21**

Figure shows the ^1H NMR of the compound **20**. Due to the unsymmetric nature of the molecule, each proton signal was quite easily defined. Assignment of the benzene proton, and the thienyl proton at 6.5 ppm allowed for the assignment of all other classical phenyl signals through the use of HH-COSY, HSQC and HMBC NMR experiments.

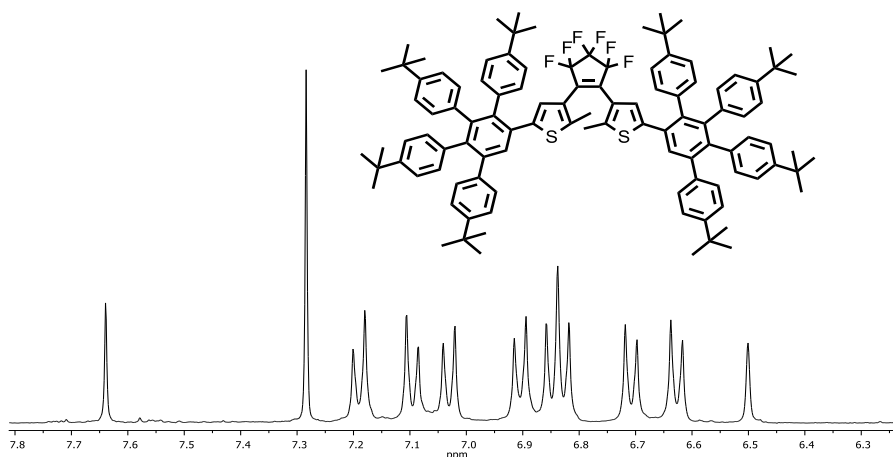


Figure 3.15 ^1H NMR of **21**, with a focus on the aromatic region (CDCl_3 , 400 MHz, RT)

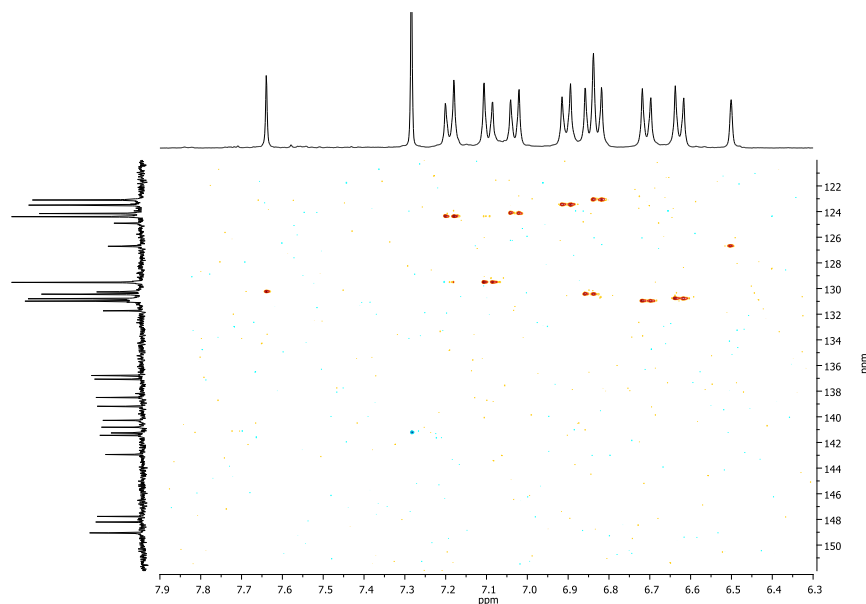


Figure 3.16 HMBC NMR experiments run on compound **21**

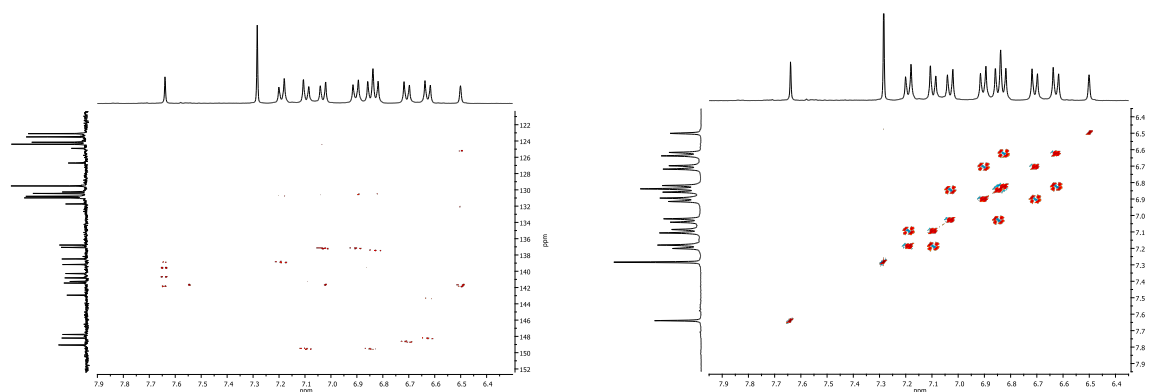


Figure 3.17 HSQC and ^1H - ^1H COSY experiments of compound **21**.

Due to the much more symmetrical nature of switch **21**, the proton signals were a lot less defined. All four protons on each phenyl ring appeared as a cluster of multiplets, and the phenyls position around the central benzene corresponded in such a way that they act like ortho-, meta- and para-protons of a substituted phenyl ring. As such, the signals for each pair of protons is again split further by the chemical environment of the ring systems. The *tert*-butyl groups appear as two singlets, integrating for 18 and 27 protons, respectively, their less defined nature suggests they are not split as equally as the protons of the phenyl groups and thus appear as an overlapping singlet, due to their chemical environment. This in contrast to the unsubstituted state of precursor **18**, which shows three sets of signals for this groups.

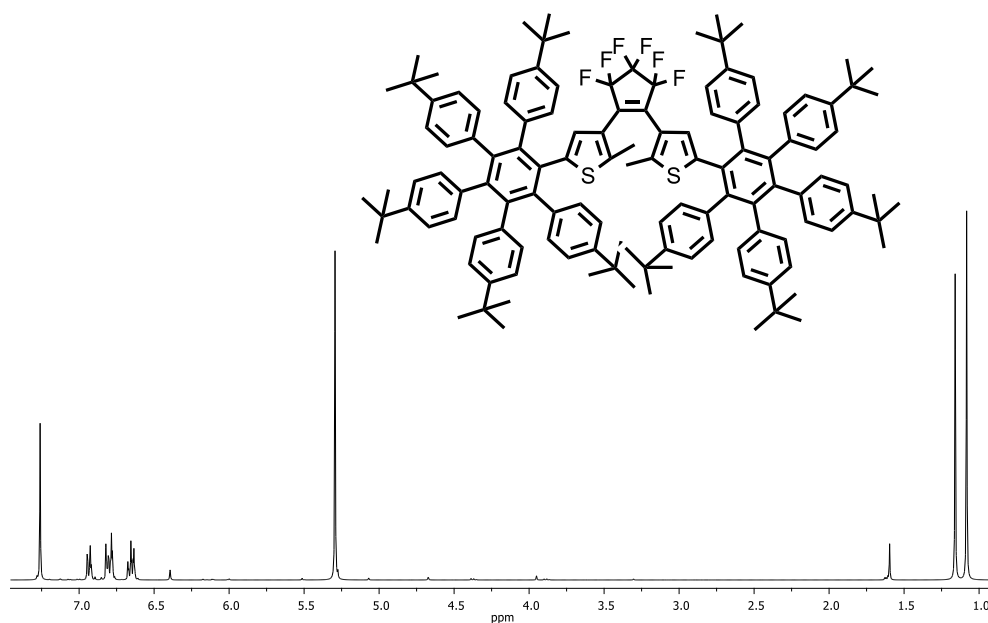


Figure 3.18 ^1H NMR of compound **21** (CDCl_3 , 400 MHz, RT)

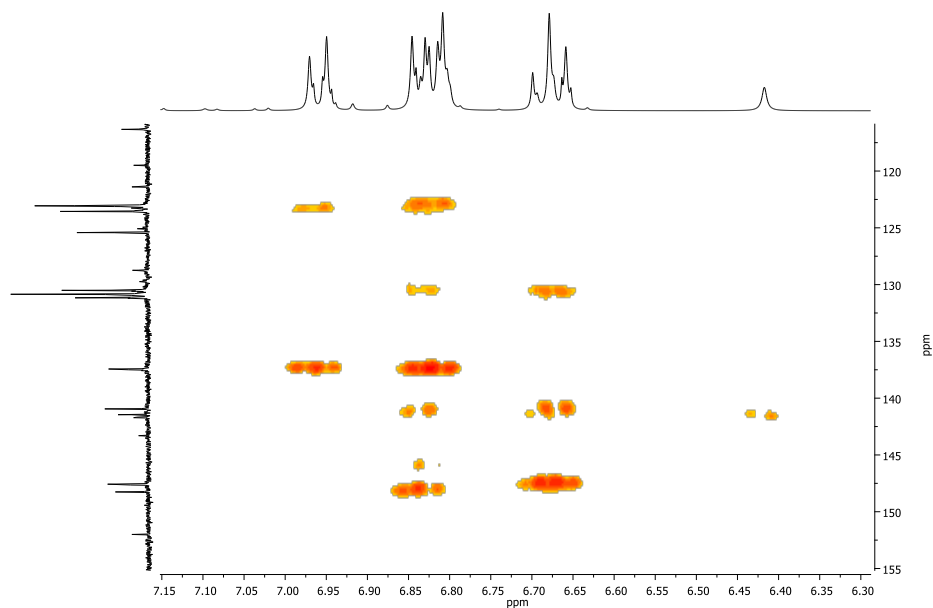


Figure 3.19 HMBC assignment of compound X

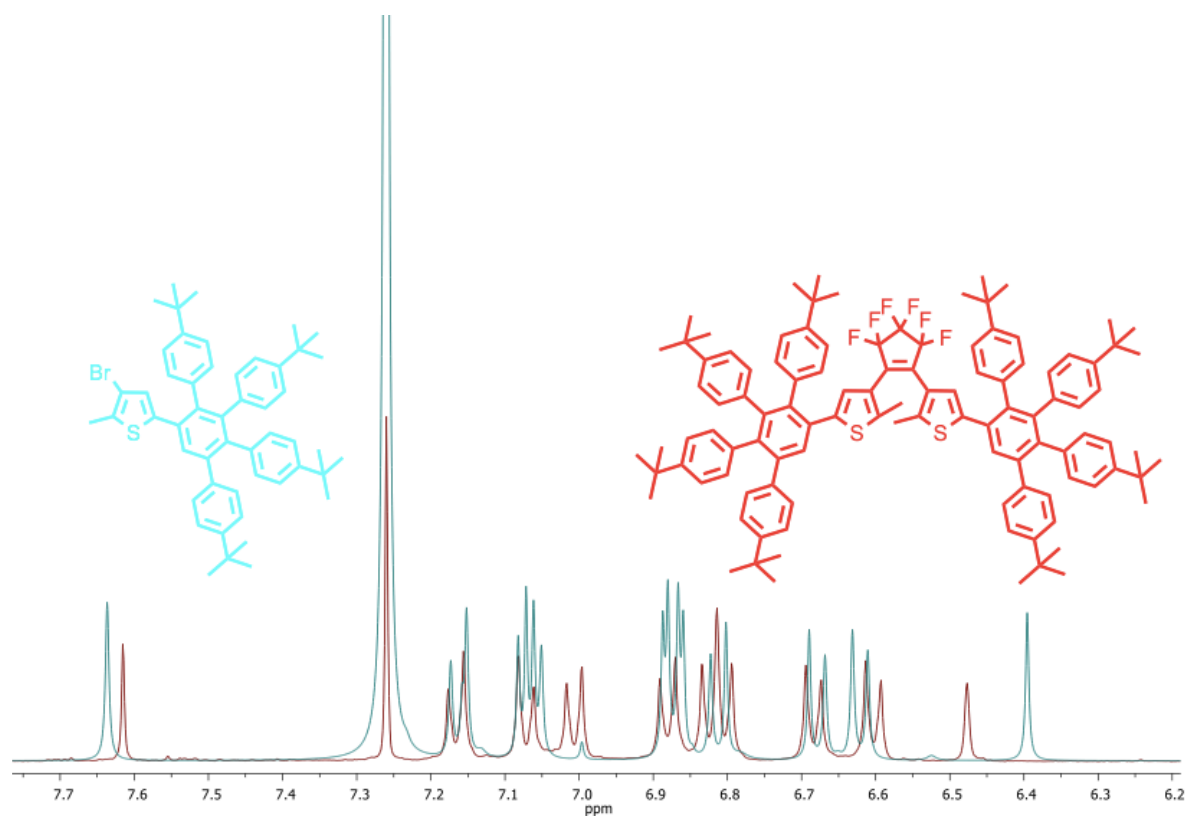


Figure 3.20 Comparison of the relative shifts seen in the **17** and **20**

The most noteworthy shifts in the NMR spectra of **17** and **20** above is that of the thienyl proton, which as is usually seen in these types of systems, has been deshielded due to a decrease in the electron cloud. Notable however, is the relative minor shift that is seen, less

than 1 ppm. This is an interesting occurrence, as a much more substantial shift would be expected in a system such as this. The NMR of both **17** and **20** are therefore almost identical, and as such exist in a similar electronic environment. The rotating phenyl rings act independently of the extension of the system. This substitution only seems to remove some of the degeneracy felt by protons on one of the phenyl rings (7.05 ppm), perhaps a combination of the electronegativity of the fluorines and the new steric environment of the platform. A cause of this may be due to the nature of the unsymmetrical central benzene ring. With a free proton on this phenyl, steric or electronic effects may be promoting as less deshielded signal than usually observed. The affinity for the phenyl system to act as a pseudo-aromatic platform with free rotation may hinder the extension of the electron cloud within the system, as the central delocalisation is not unilaterally dispersed. With this, the thiophene rings are chemically similar to their brominated counterparts, despite the new conjugated system. This unequal dispersion may also account for the opposite affect that is observed for the central phenyl's singular proton, which has become more shielded from the magnetic force. A more conjugated system would push density from the central ring to the thiophenes and across the ethene moiety. However, NMR data suggests there is instead stabilisation of this central benzene ring upon forming the switch from the thiophene rings and as such there is even less of an extension in the open form than normally observed.

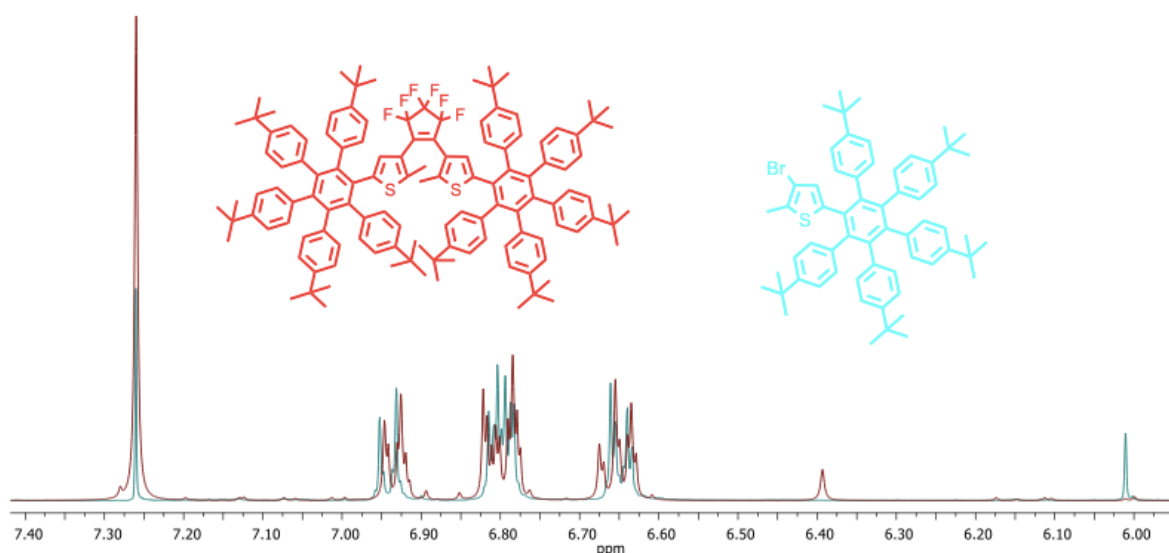


Figure 3.21 Comparison of the relative shifts seen in the **18** and **21**

Notably, there is very little comparative difference in the proton signals between compounds **18** and **21**. The most significant shift is seen in that of the proton of the thiophenes, with a much more deshielded signal appearing downfield upon substitution with the

octafluorobackbone, a difference of almost 4 ppm. Though photophysically, the two appendages are suggested to act independently, and almost analogously to their brominated counterparts, this deshielding suggests that there is an extension of the electron cloud through the ethene bond, and as such partial communication via an electron source may be plausible even in the open form. The overlap of the *tert*-butyl groups of the outermost rings could be instigating a steric effect on the aromaticity of the system, both of the rings individually and the overall platform. The large shift could be due to a two-fold electron cloud extension in the thienyl rings, both towards the central benzene and back through the ethene backbone.

3.4 Trimerisation of asymmetric thienyl-phenyl acetylenes

A series of polythienyl substituted benzenes were synthesised via a [2+2+2] cyclotrimerisation of the relevant thienyl acetylenes using dicobaltoctacarbonyl as the catalysts. The thienylacetylene starting products were allowed to react for three days and generated a mixture of isomers of cyclotrimerised products. The first unsymmetrical diarylacetylene reacted was compound **2**. Isolation of a mixture of the two polyphenylene products was possible by column chromatography using dichloromethane: hexane (1: 9) as eluent; however unlike in some other systems reported, it was not possible to separate the two isomers chromatographically. This may be due to the thienyl substituents themselves, which were observed to greatly increase the rate of flow of the products when compared with similar all carbon analogues previously reported in the group. Separation of cyclotrimerisation isomers may be best achieved in systems containing groups such as methoxy groups, which have been shown to slow the rate in the chromatography in the polphenyl systems. Purification of the crude material resulted in the extraction of a yellow powder in 76 % yield.

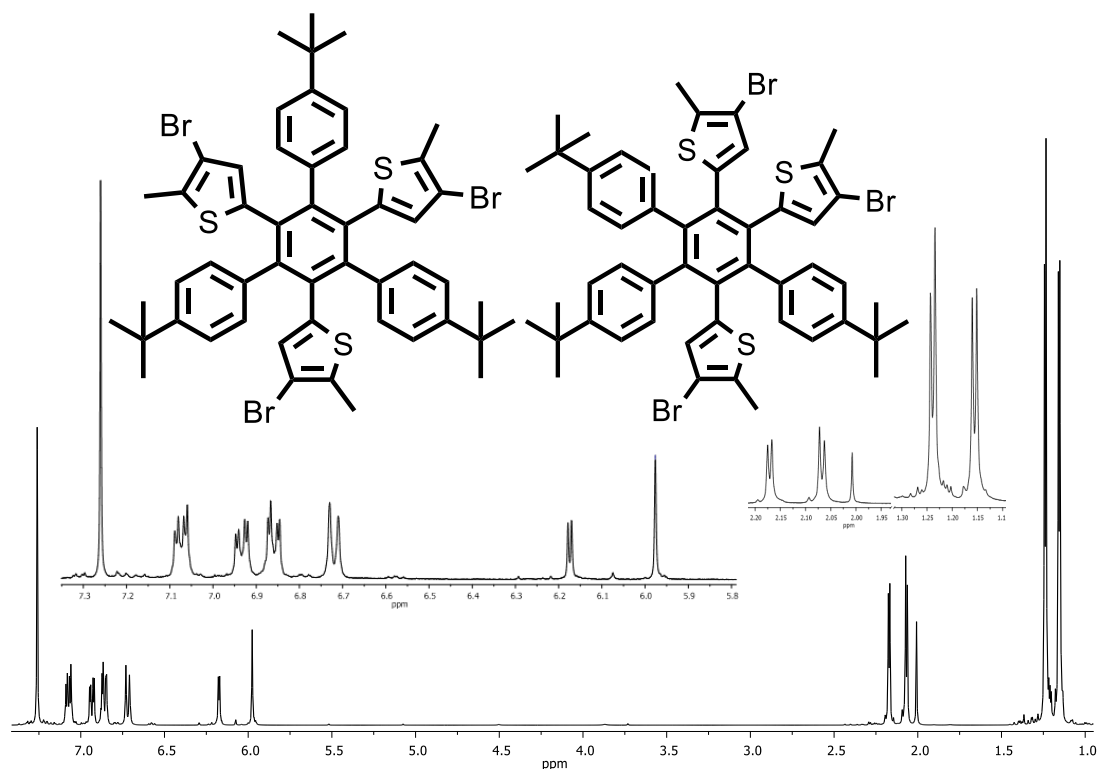


Figure 3.22 ^1H NMR of the sym and anti-isomers of **22** (CDCl_3 , 400 MHz)

As a result of the inability to separate the sym- and anti-isomers, *in situ* interpretation of the spectroscopic data was required. Looking at the ^1H NMR of the cyclotrimerised product of 3-bromo-5-((4-(*tert*-butyl)phenyl)ethynyl)-2-methylthiophene to give the mixture of polyphenylisomers (Figure 3.22), a number of interesting features can be observed. Firstly, looking at the upfield portion of the spectrum, a total of eight signals can be seen. Four sharp peaks integrating for roughly nine protons each are observed between 1.1 and 1.3 ppm, the position and relative size of these peaks suggests they are the methyl signals substituted with the phenyl ring. In the trimerisation of the precursor acetylene, a 1:3 ratio of the symmetric:antisymmetric isomer is predicted. As such, a three times excess of the antisymmetric isomer, in which all phenyl-substituted methyl groups are inequivalent, over the symmetric isomer, is expected. However, in the symmetric isomer, a C_3 axis of symmetry is present, so the three phenyl-substituted methyl signals are equivalent in NMR analysis. As such, three of the four signals for the phenyl-substituted *tert*-butyl groups, represent the antisymmetric isomer, and the fourth for the symmetric isomer.

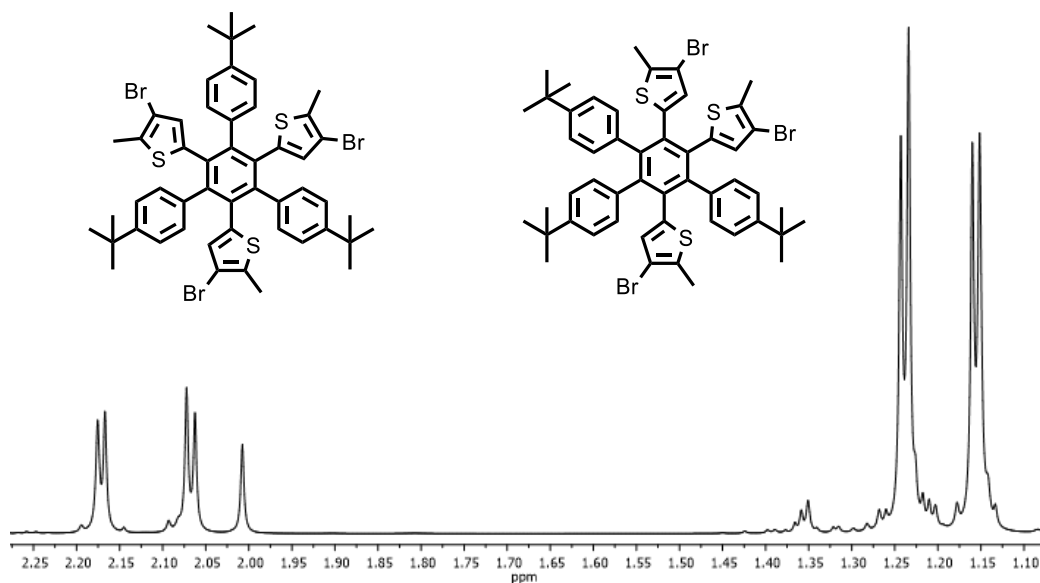


Figure 3.23 Examination of the aliphatic region of the ^1H spectrum of **22**.

There is however, a notable increase in the integration of one of the signals relative to the others. This indicates there has been an increase in the relative concentration of the symmetric isomer, as only one of the signals has increased in intensity. Using a difference between the two integration values, a sym: anti ratio may be calculated. Due to these methyl signals usually appearing as a singlet in ^1H NMR spectra, a minimal amount of overlap is to be expected and as such a reliable interpretation of these ratios may be undertaken.

$$3x = 1.36 \quad y = 1.00$$

$$x = 0.453 \quad y = 1.00$$

$$x: y = 1: 2.21$$

Looking at the ^{13}C NMR spectra for this substituted trimer (Figure 3.24), a change in isomeric ratio from that usually expected is again observed, with an increase in the intensity of the quaternary carbon signals for the symmetric isomer. This can be seen in both the quaternary core phenyl signals located alpha to a thiophene and those located alpha to a phenyl ring.

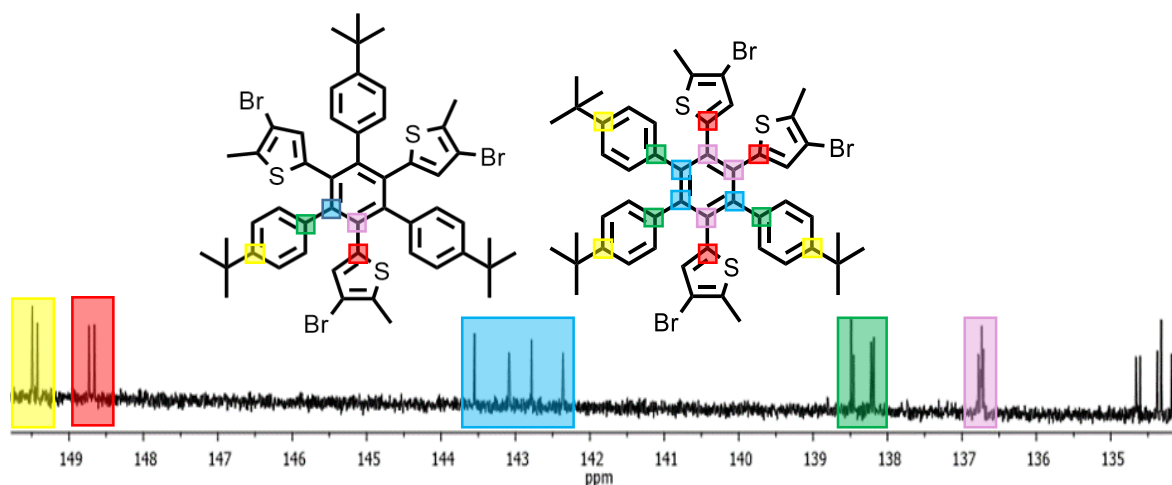


Figure 3.24 The aromatic region of the ^{13}C spectrum of trimer **22**.

This relative increase in symmetric isomer concentration was unexpected, as according to Hilt a change in the substituent groups of the precursor alkyne should result in an increase in the relative concentration of the antisymmetric isomer and not the symmetric one. The use of a bulky 2-thienyl substituent may be a prominent factor in this shift, due to the steric and electronic character of the thiophene, with the sulphur atom and its accompanying lone pair pointing toward the central benzene ring. In the 3-thienyl cases described by Hilt²¹⁶⁻²¹⁸, this change in relative position of the sulphur atom was not investigated, and it is likely that the effect of this increased electron density due to the sulphur, as well as owing to its bulky methyl and bromine substituents, has resulted in a shift from the norbornene like trimerisation usually associated with these reactions, to a metallocycloheptatriene intermediate. This intermediate may minimise both the sulphur interactions with the cobalt catalyst and the energetically unfavourable sulphur-sulphur interactions by allowing the substituent groups to alternate around the seven-membered ring. The more sterically demanding *tertiary* butyl groups have also been previously investigated and further suggest this metallocycloheptatriene intermediate formation, allowing for favourable alternation of the substituent groups around the ring and an increase in the symmetric isomer concentration.

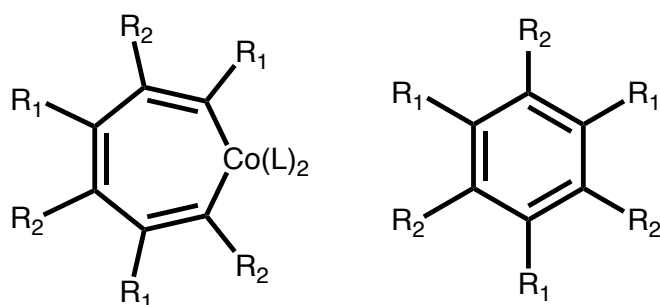


Figure 3.25 A hexasubstituted metallacycloheptatriene and the resulting hexasubstituted phenyl product.

Along with these methyl signals, four sharp peaks appear 2.18 ppm, each integrating for 3 protons. The four phenyl rings appear as four sets of AB signals, each integrating for 6 protons.

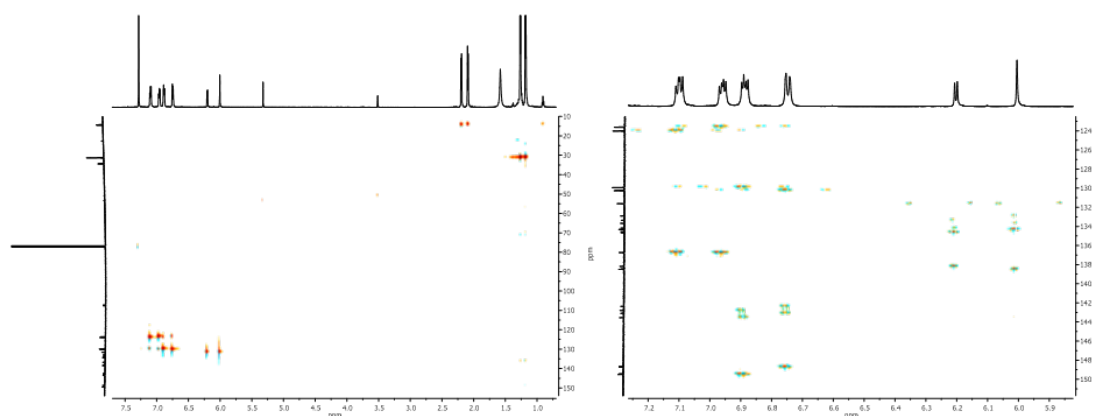


Figure 3.26 HMBC and HSQC experiments performed on trimer **22** (CDCl₃, 600 MHz, RT)

3.5 Photochemical measurements of switches **20** and **21**

Photocyclisation of switch **20** is shown in Figure 3.27. The molecular switch was irradiated with monochromatic light and the change in absorption maxima was noted. The open form shows a typical absorption pattern of that seen in free-delocalised pi systems, generally featureless. The absorption spectrum is quite broad, as is typical of polyphenylene derivatives, with little effective conjugation between rings, though an extension of this π cloud system is evident from NMR spectroscopic data. In the ground state, sterics are expected to impose a non-planar configuration on the chromophore, resulting in a mostly structureless absorption.

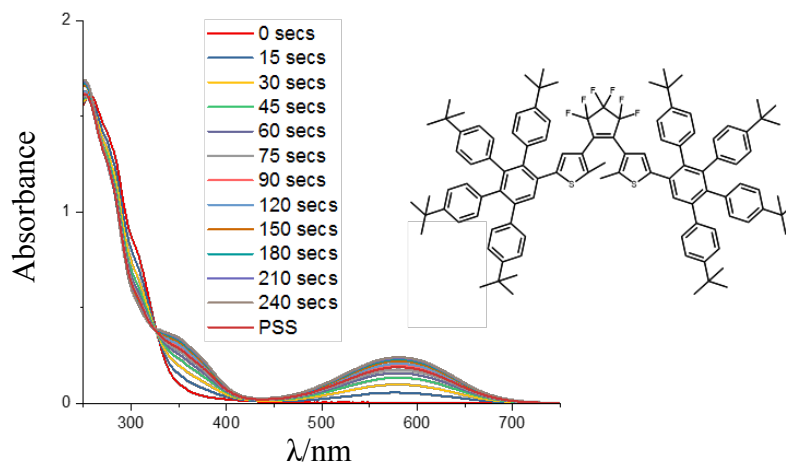


Figure 3.27 UV-Vis absorption spectrum for the photocyclisation of switch **20**. Irradiation wavelength $\lambda = 320$ nm. (CH_2Cl_2 , 1×10^{-5} M)

Upon excitation and subsequent photocyclisation, a much more structured absorption pattern is observed, with a single isobestic point seen at 340 nm. The slight increase in planarity and rigidity results in this UV-Vis absorption, with the increased conjugation of the system spreading between both appendages.

In contrast, switch **21** shows a similar fine structure in both the open and closed states. This may be due in part to the sterics of the overlapping *tert*-butyl groups, which enable much more structured and defined transitions to occur.

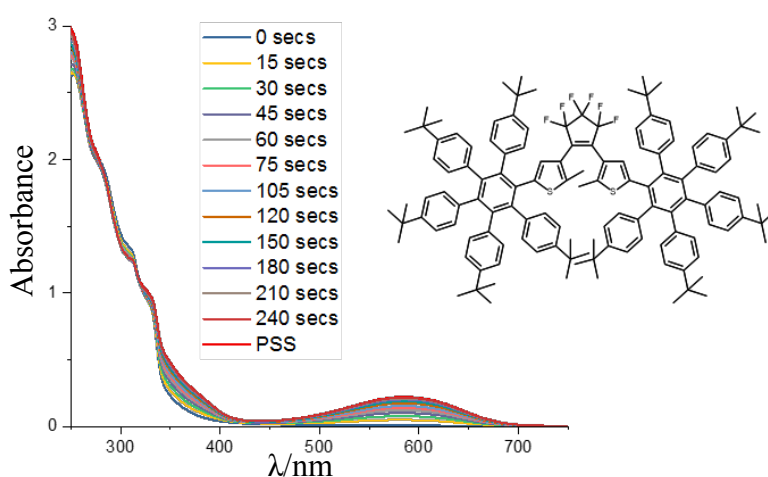


Figure 3.28 UV-Vis absorption spectrum for the photocyclisation of switch **21**. Irradiation wavelength $\lambda = 330$ nm. (CH_2Cl_2 , 1×10^{-5} M).

Figure 3.29 shows the absorption maxima for the open and closed forms of switches **20** and **21**. Due to the steric nature of switch **21**, especially in its closed analogue, its full cyclisation is hindered, and as such, a more hypochromic intensity is observed in comparison to switch **20**. However, the absorption maximum of switch **21** is more red-shifted than that of switch **20**, owing to the slightly more delocalised nature.

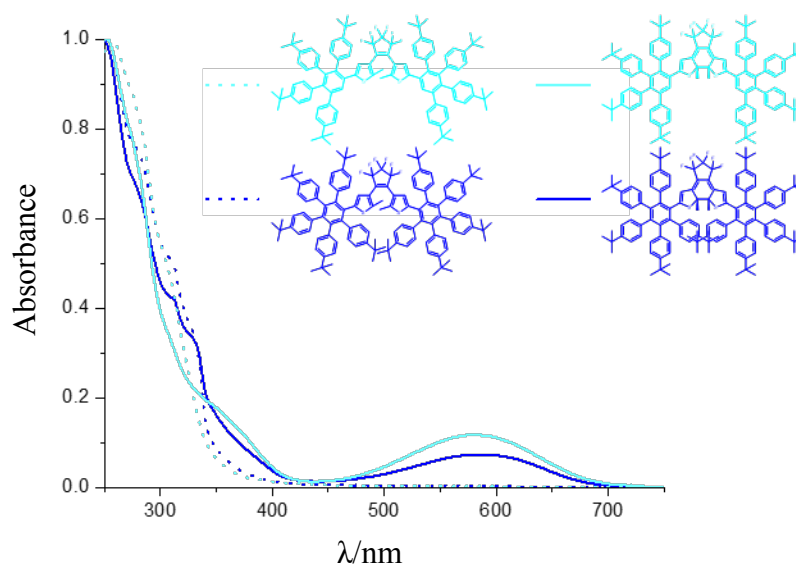


Figure 3.29 Normalised absorption spectra of compounds **20** and **21**.

It should be noted that molecular switches **20** and **21**, though perform relatively well in terms of photocyclisation ability, are much more blue-shifted due to their hindered nature in comparison to the ethynyl-PAH based switches discussed in Chapter 2. Irie et al. investigated the photophysical properties of compound DAE, and observed an absorption maxima at 575 nm. This is consistent with the absorption maxima observed for both switch **20** and **21**. This is consistent with the theory that due to the rotating phenyl rings, the extension of the dithienylethene moiety into the appendages only proceeds to the middle benzene ring. However, DAE shows more fine structure in comparison to switch **20** and **21**, in the region of 200-400 nm, with a more defined thiophene absorption seen at 360 nm. This feature is lost in compounds **20** and **21**, due to their polphenylene nature.

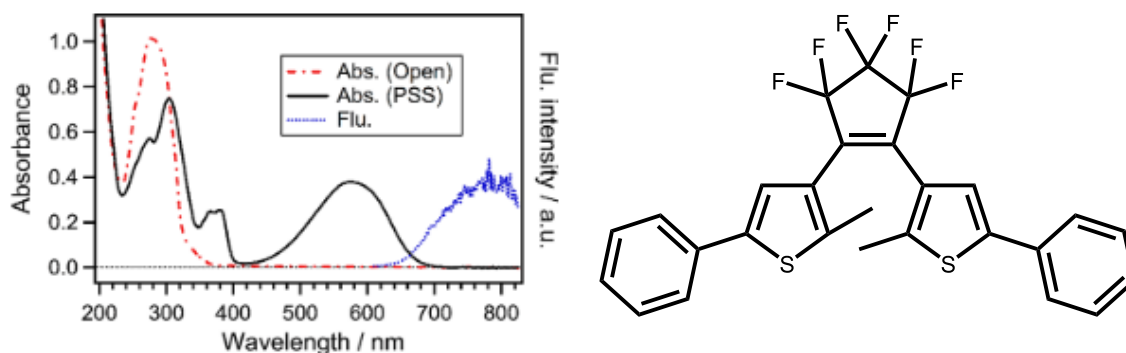


Figure 3.30. Photophysical absorption of compound DAE.

The more efficient switching nature of DAE is also owed to the simplicity of the system. The addition of ethynyl moieties was seen as a way to extend the conjugation of the π -system, and allow to absorption maximum of the closed/PSS form to be more red-shifted. However, the spacer group also had the effect of allow a degree of independence in certain systems, allowing them to luminesce, even when in this photo-inactive form. As such, emission became a competing process with that of photocyclisation in certain systems.

3.6 Conclusion and Future Work

3.6.1 Retrosynthetic Analysis of the DTE-based Switches

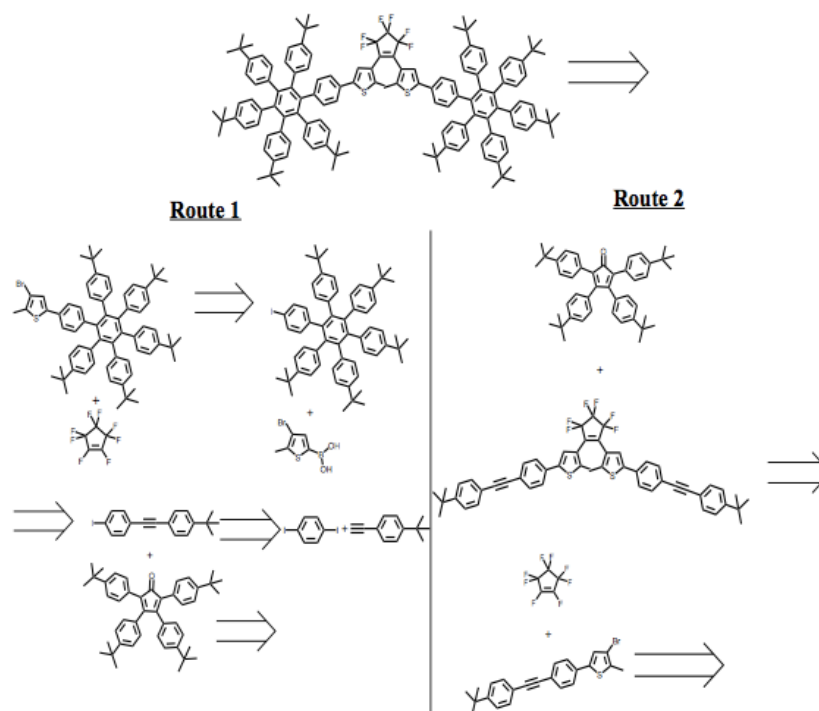


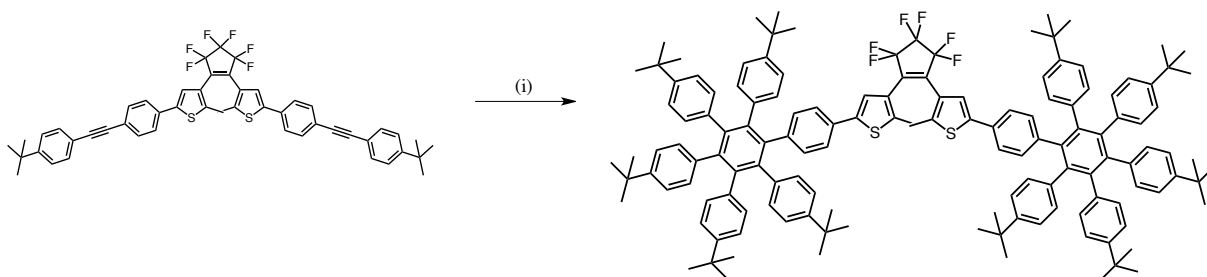
Figure 3.31 Retrosynthetic approach towards the synthesis of conjugated switch 23

In order to synthesise the DTE-based switches with an extension of the thienyl moieties from the π -platform, use of a phenylspacer compared to an acetylene spacer was initially proposed to circumvent the strong luminescent properties of the free appendage. Though the freely rotating phenyls would affect the quantum yield of the system, cyclodehydrogenation of such a platform seemed more viable, due to the thienyl ring existing on the periphery rather than as a substituent of the central benzene.

A number of precursor molecules had to be synthesised first including diphenylacetylene, **13** and a substituted thiophene moiety. The synthesis of 4-Iodo-4'-*tert*-butylphenylacetylene was carried out using a Pd-catalysed Sonogashira cross-coupling reaction. 2,3,4,5-tetra-(4-*tert*-butylphenyl)cyclopenta-2,4-dienone, **13**, was previously synthesised. 3-bromo-5-(4-((4-*tert*-butyl)phenyl)ethynyl)phenyl)-2-methylthiophene, **3**, and 3-bromo-5-(4''-(*tert*-butyl)-3',4',5',6'-tetrakis(4-(*tert*-butyl)phenyl)-[1,1':2',1''-terphenyl]-4-yl)-2-methylthiophene, **19**, were synthesised via a Suzuki cross-coupling reaction with a thienyl boronic acid. There were then two possible routes for the synthesis of the hexaphenylbenzene-substituted switch. In the first option, a [4 + 2] Diels-Alder cycloaddition reaction between 4-iodo-4'-*tert*-butylphenylacetylene and 2,3,4,5-tetra-(4-*tert*-butylphenyl)cyclopenta-2,4-dienone could be carried out, followed by a Suzuki coupling to give 3-bromo-5-(4''-(*tert*-butyl)-3',4',5',6'-tetrakis(4-(*tert*-butyl)phenyl)-[1,1':2',1''-terphenyl]-4-yl)-2-methylthiophene. This could then be lithiated and reacted with octafluorocyclopentene to yield the HPB-substituted dithienyl-based switch. The second option was to do the Suzuki coupling and the reaction with octafluorocyclopentene *before* the Diels-Alder. It was this latter route that proved more successful of the two, due to the small nature of the octafluorocyclopentene backbone and the 0.5 mole ratio that was required stoichiometrically in these switch reactions.

The use of a phenyl spacer would allow the free rotation of the inward phenyl rings without a steric overlap of the solvating *tert*-butyl groups. End-to-end, a phenyl spacer is longer in molecular length than an acetylene spacer, however the conjugation acts non-linearly, as well as the phenyl groups ability to rotate which the acetylene group cannot. Disruption in this rigid linearity and its affect on the complimenting system was hoped to be well studied, however, as shall be seen, work with large platforms of these molecular weights usually requires numerous steps and low yields. The possibility of stacking between the systems was also known to be a viable occurrence.

3.6.1.1 Synthesis of 3,3'-(perfluorocyclopent-1-ene-1,2-diyl)bis(5-(4''-(*tert*-butyl)-3',4',5',6'-tetrakis(4-(*tert*-butyl)phenyl)-[1,1':2',1''-terphenyl]-4-yl)-2-methylthiophene), **23**



Scheme 3.7 Synthesis of **23**, (i) benzophenone, **9**, 300 °C, 5.5 h, 3.2 %.

Compound **23** was prepared via a Diels Alder reaction between **5** and **9**, which resulted in a bicyclic intermediate followed by the immediate extrusion of carbon monoxide in a cheletropic reaction to give the hexa-substituted phenyl moiety. The refluxed reaction required a temperature of approximately 300 °C for 5.5 hours, and was monitored by TLC.

3.6.1.2 Characterisation of Compound **23**

23 was characterised by mass spectrometry and NMR spectroscopy. The ^1H NMR initially proved very difficult to fully assign, due to harsh and laborious separation techniques and low reaction yields. The singlets at 1.08 and 1.24 ppm integrated to thirty-six and fifty-four protons respectively. These peaks were assigned to the *tert*-butyl protons. The signal at 2.17 ppm, which appeared as a singlet, integrated to six protons and corresponded to the protons on the methyl groups attached to the thiophene rings. The signals for the fifty aromatic protons, the forty-eight protons on the phenyl rings and the two thienyl protons, overlapped extensively and appeared as two multiplets at 6.87-6.78 and 6.71-6.63 ppm on the ^1H NMR spectrum. For this reason, the aromatic signals could not be definitely assigned to any particular protons. However, these multiplets confirmed the presence of the final product, which displays a much more complex NMR spectrum compared to that of starting material **9** and analogous to that of the brominated analogue **19**. Whilst the bulk of the proton signals appear in an identical range for **19** and **23**, there is a significant downfield shift of the thienyl proton and the phenyl protons most adjacent to the substituted thiophene moiety. Due to the now more expansive molecular orbital cloud within the system, the central benzene ring may be directing more electron density towards itself to maintain aromaticity, with an inductive

electron-withdrawing effect occurring from the dithienyl backbone and towards the central appendage. What was also quite surprising was the lack of apparent stacking seen for the compound. No immediate broadening of the signals was observed, and numerous proton signals occurred as defined peaks. This may be due to the high level of tert-butyl groups on the central platform, impeding stacking formation in favour of free rotation as a monomer.

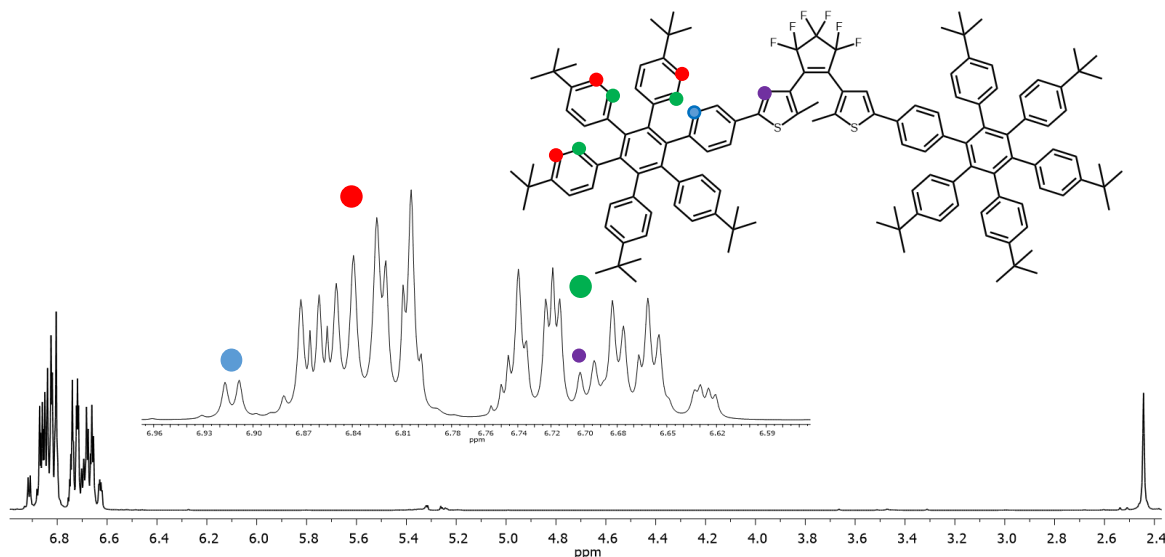


Figure 3.32 Preliminary ^1H NMR of compound **23**

3.6.1.3 Preliminary Photophysical Analysis **23**

A 5×10^{-6} M solution of **23** in CH_2Cl_2 had a blue colour which intensified when irradiated with UV light. The colour of the solution disappeared when visible light was shone on the sample. This confirmed that the sample in solution was photochromic. Preliminary photophysical measurements were recorded for **23**; absorption spectra were recorded for the open isomer of **23**, **23o**, and the switch in the PSS, **23c** (Figure 3.33 a). The spectrum for **23o** had an absorption maximum $\lambda_{\text{max}} = 315$ nm ($\epsilon = 128,574$ $\text{dm}^3 \text{mol}^{-1} \text{cm}^{-1}$). This absorption band was assigned to the $\pi\text{-}\pi^*$ interactions, as before, of the individual thiophene rings. Upon irradiation of UV light for 1 hour ($\lambda_{\text{ex}} = 365$ nm), the absorption spectrum of **23c** had an absorption maximum of $\lambda_{\text{max}} = 315$ nm ($\epsilon = 110,742$ $\text{dm}^3 \text{mol}^{-1} \text{cm}^{-1}$) and 591 nm ($\epsilon = 9760$ $\text{dm}^3 \text{mol}^{-1} \text{cm}^{-1}$). This latter band represents the $\pi\text{-}\pi^*$ transition of the thiophene rings in the conjugated closed ring system and also corresponds to the decrease of the absorption maximum at 315 nm. Comparing the absorption spectra of **23c** with those of **9c** (Figure 3.35), it was observed that the absorption maxima for **23c** was blue shifted relative to the absorption maxima for **9c**, which appeared at longer wavelengths. There was a slightly larger spectral shift between the open and closed isomers observed in the spectra for **9**

compared to **23** (285 nm vs 276 nm). By comparing the absorption spectra of **9c** and **23c**, it could be postulated that **9c** was potentially the better switch; however additional photophysical analyses on **23c** would be required to confirm this.

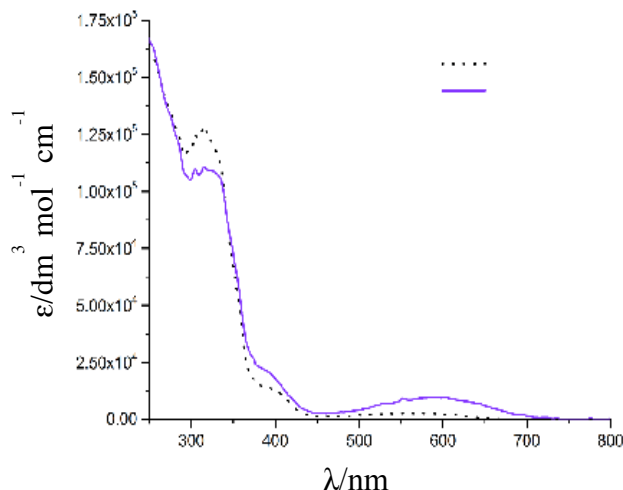


Figure 3.35 Absorption spectra of **23o** (.....) and **23c** (—).

3.6.2 Cyclodehydrogenation of aromatic π -platforms.

In order to combat the lack of delocalisation within the systems, and to slow the formation of unwanted side products, cyclodehydrogenation procedures were seen as an efficient and effective strategy. Not only would this allow for the carbon-carbon bond formation between the central thiophenes and the adjoining phenyl rings, thereby negating the formation of hexatriene side products (Figure 3.36), but the large delocalisation across the system was hoped to extend the closed form absorption maximum, and further red-shift it.

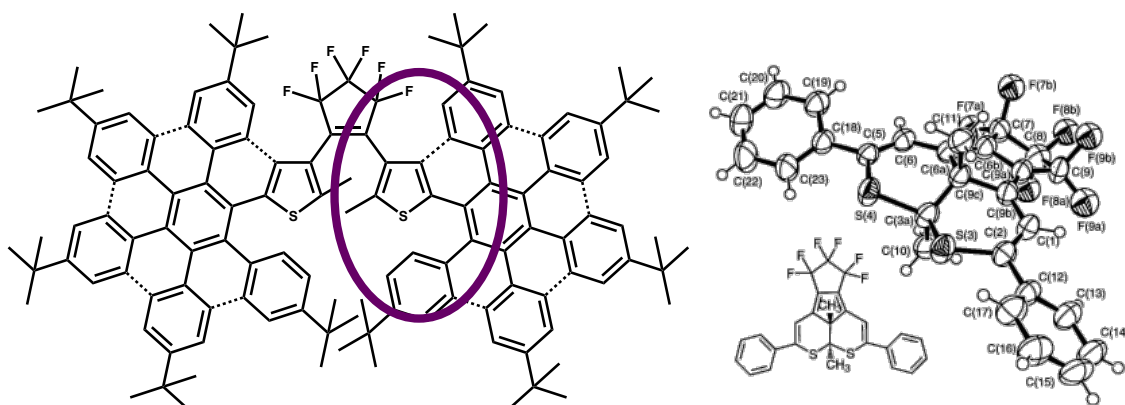


Figure 3.36 (a) cyclodehydrogenation attempts using molecular switch **21** would allow a carbon-carbon bond formation between the 4-position carbon and the adjacent phenyl ring. This coupling was hoped to hinder the formation of stable side products (b) and also allow a more conjugated absorption pattern in the closed form isomer.

Rathore and co-workers have recently used 2,3-dichloro-5,6-dicyano-1,4-benzoquinone (DDQ) in the presence of acid to perform oxidative cyclodehydrogenation on fused aromatics, such as naphthalene and anthracene, with oxidation potentials up to 1.7 V.²¹⁹ Interestingly, through observation and radical trapping using hydroquinone, the authors were able to confirm that the reaction proceeds via a radical-based mechanism in yields up to 97%, for isoalkyl substituted HBCs. A useful comparator for these reactions is the smallest of the polyaromatic family; triphenylene, first studied by Allen and Pingert in 1942. Several kinetic and computational studies present the mechanism of its cyclodehydrogenation, with the rate determining step believed to be the formation of the radical cation intermediate, upon removal of an electron from the reactant. Negri and co-workers have recently published a very comprehensive Density Functional Theory (DFT) analysis for triphenylene using the B3LYP/3-21G function.²²⁰ By optimising geometries of the ortho-terphenyl ($C_{18}H_{14}$) precursor molecule and subsequent intermediates, an analysis of the cyclodehydrogenation is performed, paying particular attention to steric factors, spin and charge distribution. They found that the cation radical $C_{18}H_{14}^{\cdot+}$ exhibits dihedral angles between the pendant phenyls and central ring which are reduced by more than 20% from the neutral starting material. Additionally, the distance between carbon atoms at the ortho positions on these pendant phenyls decrease from 3.331 Å in o-terphenyl to 2.949 Å in the intermediate. Both of these rearrangements would result in considerably stronger interactions between adjacent rings. Analysis of spin and charge density distributions show that both orthocarbons behave as feasible centres for bond formation and that subsequent formation of a σ -bond between phenyl rings is likely. The release of the second proton to produce the fully aromatised triphenylene requires the removal of another electron. This is calculated to require a lower energy than for the generation of $C_{18}H_{14}^{\cdot+}$ as it is associated with a singly occupied molecular orbital.

The work of Negri has circumvented the laborious task of using computational models coupled with practical observations, to shine light on the cyclodehydrogenation of the more complex PAH system, namely hexaphenylbenzene (HPB). Not only do they evaluate the likelihood of potential mechanisms but they also present useful predictions for the formation of partially fused products, which have been supported by synthetic observations. As in the case for o-terphenyl, Negri assesses the formation of the cationic radical and computationally shows that the symmetry of the intermediate is lowered to different degrees

around the molecule. In accordance with the Jahn-Teller effect, this results in two adjacent phenyl rings being brought into close proximity. Calculation of the electrochemical nature of the radical-generating reaction shows a low oxidation potential and therefore gives support to the thesis of a radical cation route. Consideration of the locality of charge shows that this reaction exhibits a less dramatic geometry change than for small PAH analogues.

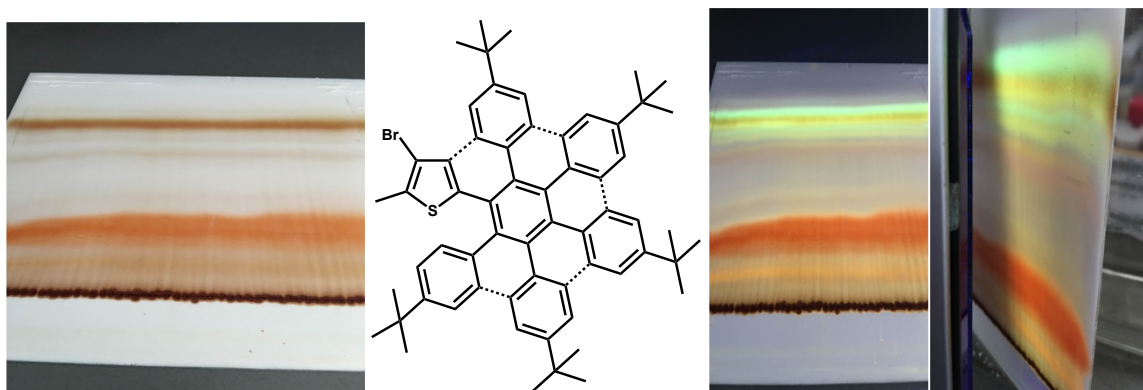


Figure 3.37 Initial cyclodehydrogenation attempts using DDQ in acidic conditions resulted in a plethora of luminescent compounds from precursor 17.

An all-compassing method for cyclodehydrogenation still does not exist. Methods using Lewis acids, such as FeCl_3 and AlCl_3 have been shown to fall short in the controlled cyclisation of polyphenylenes with heteroatom or electron-withdrawing substituents. Similarly, more recent systems such as the use of DDQ in acidic conditions, which successfully cyclise halogenated hexaphenylbenzenes, induce no response whatsoever for nitrogen substituted systems. This is the case here, though cyclisation of the polyphenylene systems using DDQ in acidic conditions failed to produce the fully cyclised product, it did produce an array of luminescent side products which are still being analysed (Figure 3.35). A plethora of reaction conditions, change of solvent, temperature, reaction times, use of microwave synthesis and pressure-tube reactions have all thus far failed to produce a cyclodehydrogenated product with any of the products of the chapter. Due to the inability to cyclise these bonds in situ, an alternate method of approach, whereby the rings already exist in a semi-cyclised nature, was seen as a viable method. Work in this area is continuing.

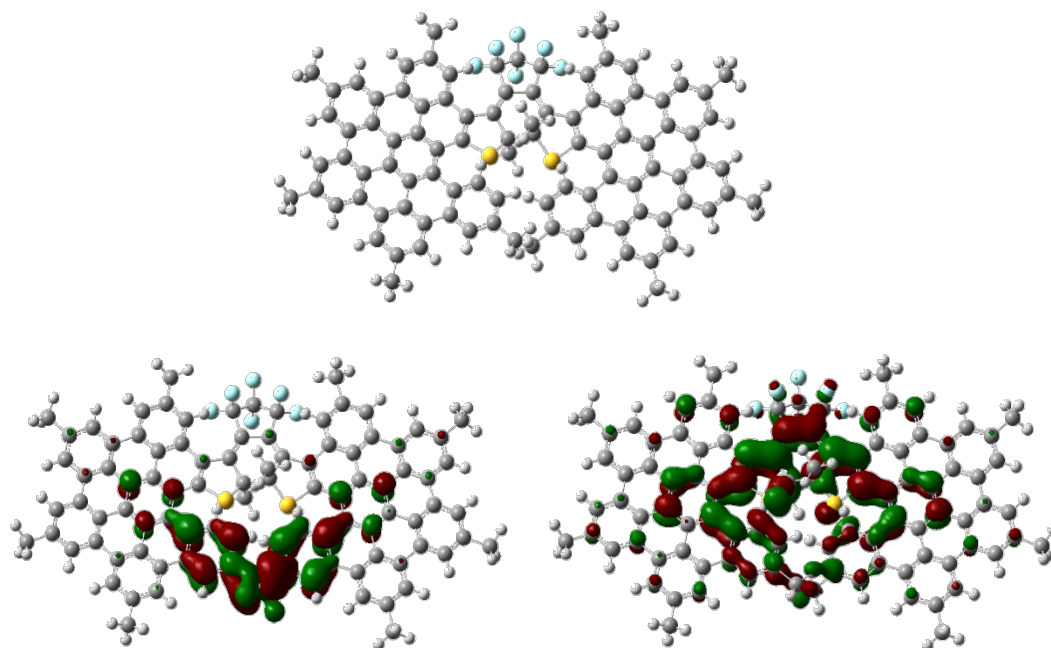


Figure 3.38 DFT calculations for future HBC-based dithienylethene switches. HOMO of compound lies across the sterically hindered and overlapping *tert*-butyl groups of the inner phenyls, whilst the LUMO sits slightly more spread across the dithienylethene-octafluorocyclopentene core.

In attempt to understand the potential conjugation and subsequent electronic delocalisation that was plausible in switches that had undergone cyclodehydrogenation, initial DFT analysis was undertaken. Owing to the large sterics involved in the overlapping *tert*-butyl groups, it is of no surprise that the HOMO sits at this periphery. The LUMO is also spread congruently where expected, mostly located around the dithienyl-moiety and the fluorinated ethene backbone. It is surprising, however, that there is a much less equivocal spread of the atomic orbitals across the system as would be suspected. This may be hindered by the overlapping *tert*-butyl groups and thus the representation of the electronic delocalisation may be negated by the large energies involved in this overlap. Experimental data in this area will be of significant interest, especially in terms of switch complex **24**. In contrast to broad and generally featureless absorption patterns seen in HPB-systems, the increased planarity and rigidity of cyclised ligands results in the appearance of well-resolved bands with significant fine-structure, characteristic of hex-*peri*-hexabenzocorones, with a max at 350-370 nm. According to the nomenclature employed by Clar to describe the electronic transitions of HBCs and of polyaromatic hydrocarbons in general, this max can be assigned at the B-band, which corresponds to the interaction between benzenoid rings. Another transition, usually

centred at 380-400 nm, is designated the p-band, and involves the delocalisation of electrons in the excited state.

3.6.3 Cyclotrimerisation of more extended linear-thienyl acetylenes, compound 25

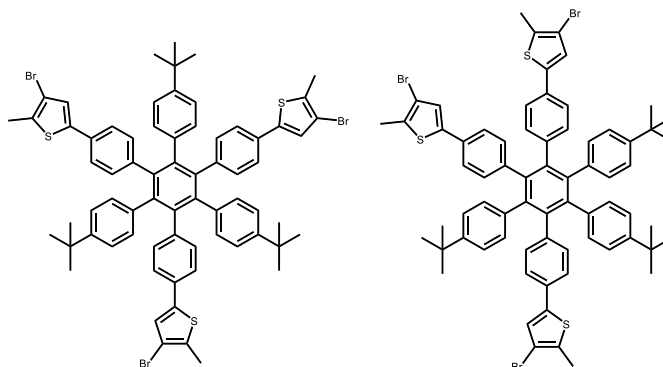


Figure 3.39 The symmetric and antisymmetric isomers of trimerised product 25

Figure 3.39 shows the product of the cyclotrimerisation reaction of compound 3 to produce the anti- and symmetric isomers. Again, this was done using a cobalt catalyst, heating for three days at 140 °C in dioxane. Both isomers were unable to be separated using a range of solvents and TLC chromatography. In solution NMR analysis of both isomers was then hoped to be performed analogously and simultaneously as done for previous systems. However, unlike compound X, which showed little to no stacking in solution, all ^1H NMR features of compound X were extremely broad and indistinguishable. Variable temperature NMR studies were performed on the spectroscopic sample, and though at higher temperatures certain features began to appear in a more structured manner, the individual peaks could not be completely resolved.

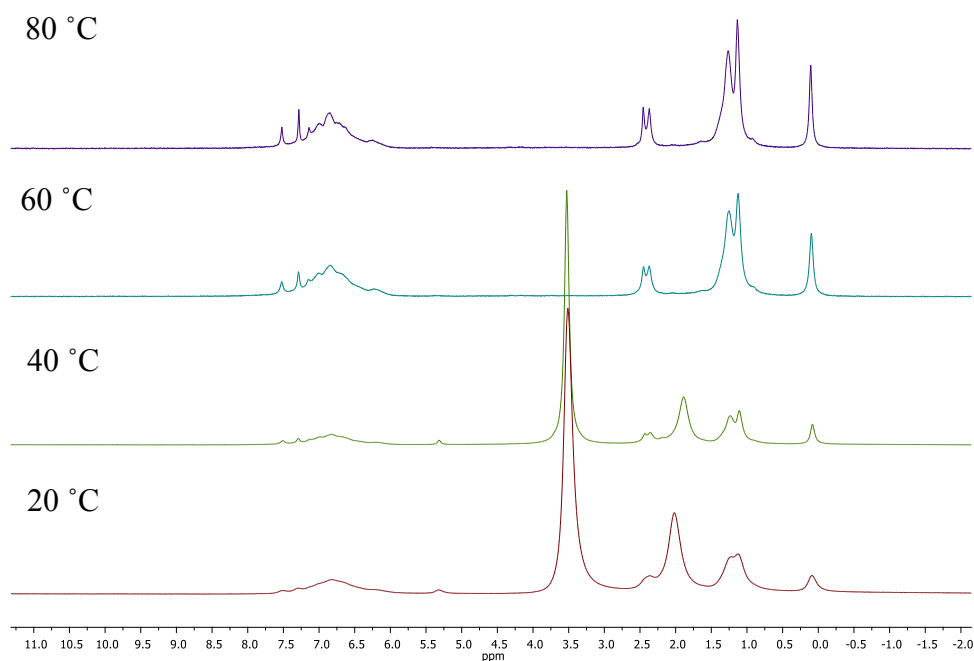
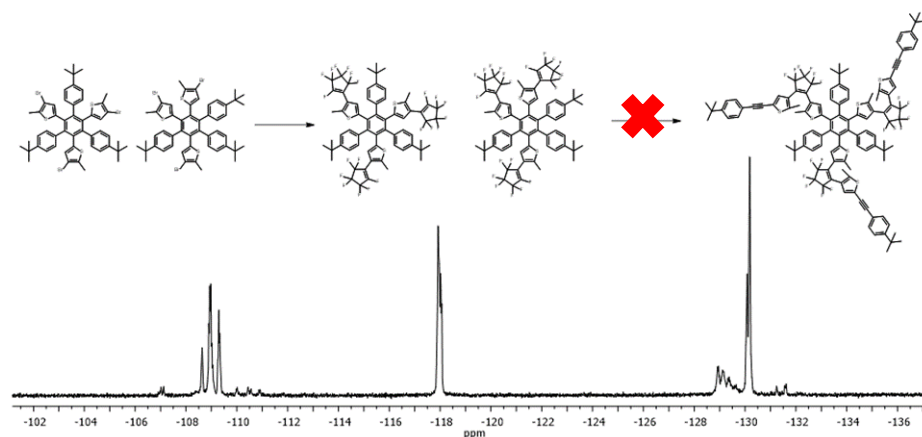


Figure 3.40 Variable temperature NMR studies of compound **25** (20 °C, 40 °C, 60 °C, 80 °C, CDCl_3 , 400 MHz, RT)

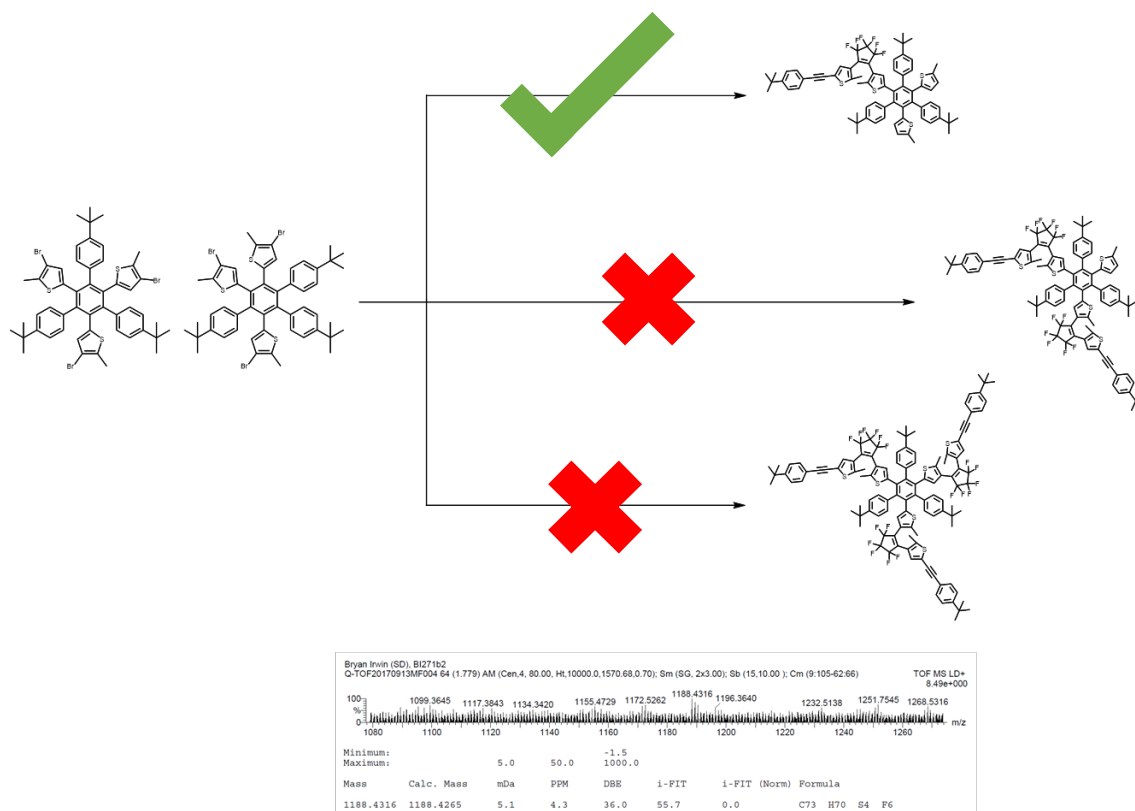
It is suspected that conformity of the middle hexaphenylbenzene core is what causes this stacking in solution. In compound **25** this issue is circumscribed due to the lack of side central phenyl rings in the compound. For the case of compound **25**, however, the thienyl rings lie outside of this homogenous core and this π - π^* stacking interactions are much more readily available.

As such, compound **25** was hoped to be further reacted to create the tri-(ditheinylolethene)-hexaarylbenzene molecular switch, **26**, shown in Figure 3.8. The perfluorinated intermediate precursor was generated upon $n\text{-BuLi}$ addition to compound **25**, in both its symmetric and antisymmetric forms. After two hours, a small sample was neutralised, **26**, and sent for NMR and mass spectrometry analysis to confirm the formation of this intermittent species. Compound **2** was then lithiated in a separate reaction vessel and cannulated across to hopefully form final compound **27**. However, upon subsequent work upon and analysis, the final product was found not to have been generated and the intermediate product was lost in the reaction process. Scheme 3.8 shows the preliminary ^{19}F spectrum of the intermediate isomers.



*Scheme 3.8 Synthetic route towards compound 27, through intermediate isomers 26s and 26a (i) *n*-BuLi (x 5 equiv), octafluorocyclopentene (in xs) in THF at -78 C, 4 hrs, under Ar (ii) *n*-BuLi, 2, overnight, under Ar. 27 is shown as 27s only for simplicity.*

To circumvent these unreactive fluorinated isomers of compound 27, an alternate route was then proposed, instead reacting one equivalent of octafluorocyclopentene directly with compound 2 in *n*-BuLi. The unsymmetrical fluorinated intermediate used in the reaction is now much smaller and was hoped to proceed with greater efficiency than the previous fluorinated platform. This was left to stir at low temperature at two hours before it was added directly to a solution of *n*-BuLi and compound at -78 °C. The solvent was a mixture of THF: diethyl ether (1: 1) and was shown to have limited success towards a final product. Mass spectrometry analysis has shown the presence of one reactive isomer in solution, however, the reaction proceeded in such low yields that further NMR and photochemical studies could not be undertaken. Towards a more efficient reaction pathway, and generation of all six products (symmetrical and anti-symmetrical mono-, di- and tri- substituted dithienylethene platforms, Figure 3.15), harsher reaction conditions may be required.



*Scheme 3.9 An alternate pathway to product 27A (27As and 27Aa isomers), 27B (27Bs and 27Ba isomers) and 27C (27Cs and 27Ca isomers), with *n*-BuLi, octafluorocyclopentene and compound **2** in THF: diethyl ether at -78 °C, under Ar.*

Study in this area could prove extremely promising, due to either the competing nature of the dithienylethene appendages or the additive nature of their absorptions. The low yields and lack of di- and tri-substituted products in the initial reaction attempt may indicate high energy barriers towards the formation of these products. Whilst extended π -platforms offer an extension of the conjugated system.

This chapter saw the design, synthesis, analysis and theoretical approach to a family of novel thienyl-based polyphenylene systems. The photophysics of the freely rotating platforms is analogous with mono-substituted phenyl DTE switches, and so cyclodehydrogenation was seen as a logical step forward. Use of these platforms requires harsher reaction conditions and longer relative steps than may be plausible, however work is being continued in this area to understand the dynamic relationship thiophene centres play in the photochemistry of molecular switches and HPB systems.

**4. Investigating 1,10-phenanthroline based Ir(III) complexes
and their potential use as photochromic molecular
switches**

This final chapter explores recent work involved the synthetic exploration of Ir(III) and Ru(II) based molecular switches, initially via 1,10-phenanthroline precursors and eventually through their pseudo-delocalised hexaphenylbenzene analogues. 1,10-phenanthroline was chosen due to its commercial availability and its viability in a wide range of reactions, as well as its ease of substitution, however its extreme difficulty in subsequent purifications reactions hindered fast-paced results. For metal centre binding, 1,10-phenanthroline also exhibits lower LUMO energy than most corresponding bidentate ligands¹³⁸ and so transitions between the metal and the ligand can be much more easily analysed. An extension of this simple planar platform via Diel-Alder reactions to form larger π -platforms was investigated, due to the previous failed attempts at cyclodehydrogenation in Chapters 2 and 3. 1-10-phenanthroline provides analysis of partially fused platforms and their effect on photochromic switching ability, as well as allowing for the incorporation of a metal centre via its bidentate binding sight. Co-analysis of these metallated and non-metallated systems side by side afford unique insight into the role metal centres may play in future switching products.

Initial work involved the synthesis of a novel series of 3- and 3,8-aryl-1,10-phenanthroline ligands and their corresponding Ir(III) complexes. Ethynyl linkers were again chosen due to their red-shifting ability seen in Chapter 2. Even a slight extension of the MLCT or IL transition ($\lambda = 470$ nm) was hoped to be seen, however this red-shift was not a crucial component in the brominated counterparts of the metal complexes, only in their switching prologues. The NMR shifts between species were analysed, and the photophysical properties of the complexes were explored for potential future applications. The second part of this research explored the theoretical investigation of compound, and precursor, 1,2-bis(5-phenylacetylene)-2-methylthiophen-3-yl)perfluoro-cyclopentene, and a review of the crystallographic viewpoint of the molecular switch in the solid state. The compound shows a high degree of thermal stability, and a substantial hyperchromic intensity shift when compared to much more complex systems. Most interesting, however, was the switches ability to perform complete photocyclisation and photocycloreversion whilst in the solid state. This may afford an alternate avenue of research not usually explored.

Lastly, in depth work involved the amalgamation of the three areas briefly explored in the previous three chapters. Various Ir(III) and Ru(II) complexes were synthesised, with a dithienylethene core, an extensive herteroom π -platform ligand and a transition metal centre. The photophysical properties of these complex were explored, with an analysis of its overlapping triplet energy levels and their affect on the photophysical properties.

4.1 Substituted 1,10-Phenanthroline With Acetylenic Tethers as Linkages

Tor and co-workers¹³⁸ successfully explored the effect of electron-donating substituents on 3,8-substituted 1,10-phenanthroline ligands functionalised with acetylenic linkers. To achieve tunable fluorescent chromophores, the conjugated derivatives were assembled using Sonogashira cross-coupling reactions between 3,8-dibromo-1,10-phen and substituted phenylacetylenes.

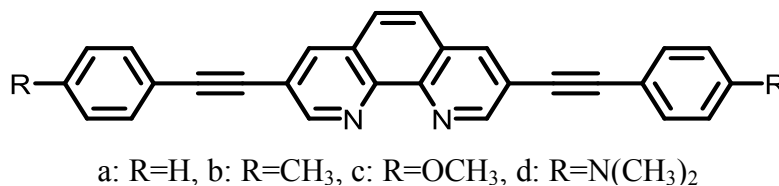


Figure 4.1 Conjugated 1,10-phenanthroline derivatives.

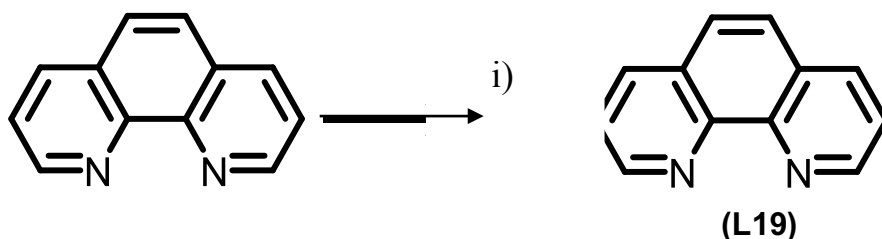
By increasing in the electron donating ability of the substituent, a corresponding shift in the peak maxima of both the absorption and emission spectra to longer wavelengths was observed. Solvent polarity also exerted a more significant effect on the emission maxima than the absorption maxima. This can be explained by the greater stability of the excited state e.g., the -N(CH₃)₂ derivative displays the most prominent red-shift of the emission into the visible range ($\lambda_{em} = 600$ nm). Both the methoxy and the -N(CH₃)₂ derivatives demonstrate a bathochromic shift in emission with increasing solvent polarity, while the parent ligand displays a blue shift under the same conditions. This can be attributed to energetically close $\pi-\pi^*$ and $n-\pi^*$ singlet excited states. Tor and co-workers also prepared a series of homonuclear and heteronuclear multimetallic complexes by using the “chemistry-on-the-complex” method.²²⁰⁻²²² These metal complexes exhibit interesting photophysical properties which could have promising applications in molecular devices with light-induced functional capabilities. Using acetylenic tethers as connecting bridges provides control over the distance between the coordinated metal centre and its chromophores. This also infers rigidity and linearity on the resulting ligand while offering a synthetic handle which can be used to generate sophisticated molecular structures. Furthermore, inclusion of acetylene linkers can also generate molecular wire-like behaviour by providing effective pathways between substituents and central ligand for electron and energy transfer. The electronic delocalisation in the excited state of conjugated systems can also be noticeably increased by appending acetylene functionalities. This results in a significant red-shift in emission wavelength, and increasing emission intensity. The combination of these features made

acetylenes the optimal functionality so that the effect of ligand modification on emission properties can be explored. Sonogashira cross-coupling reaction is found to be the most prevalent method for alkylation between a terminal alkyne and an oligopyridine bromide or triflate. The same approach, can be applied to 1,10-phenanthroline. Even though the reaction's success can be unpredictable, it can generate a stable framework from which to construct firm structure/property relationships.

4.2 Synthesis of Ir(III) 1,10-phenanthrolines complexes

4.2.1 Synthesis of 1,10-phenanthroline ligand

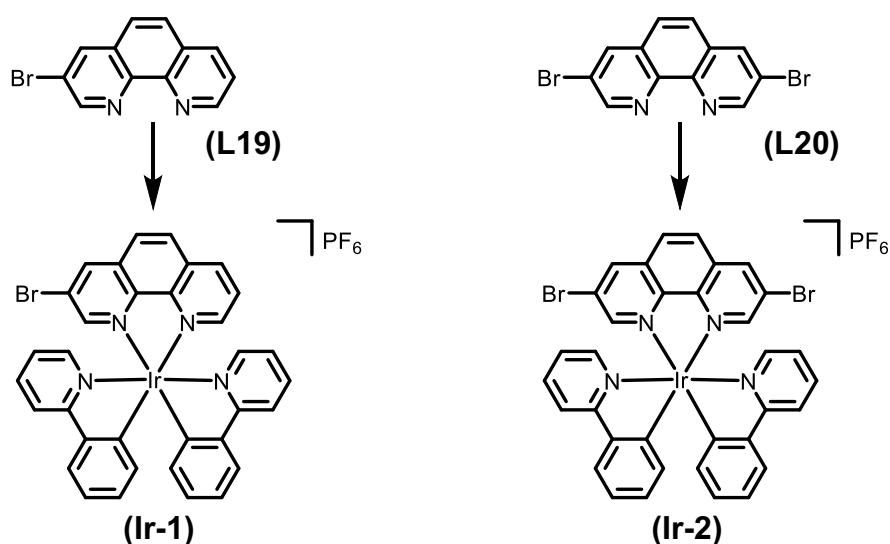
Procedures for the bromination of 1,10-phenanthroline have previously been reported for the 3-, 3,8- and 5-positions.^{223,224} The procedure reported by Saitoh *et al.* for the bromination of the 3,8-positions was modified for this work to reduce the amount of Br₂ used to 0.5 equivalents, in an attempt to drive the reaction towards monobromination. S₂Cl₂ was used as solvent, and the reaction was heated to 80 °C for 12 h. The crude product was purified by column chromatography using dichloromethane (CH₂Cl₂) and methanol (MeOH) (100:1) as the eluent, and crashed from CH₂Cl₂ using diethylether to give a white product **L19** with a yield of 50%. The structure was assigned using ¹H NMR spectroscopy. The ¹H NMR spectrum shows six doublet peaks and a quartet, each integrating to 1 proton, at 9.24 (d), 9.21 (d), 8.43 (d), 8.30 (d), 7.86 (d), 7.75 (d), and 7.70 (q) ppm. Though reaction conditions were modified to allow monobromination to proceed, a second product of the reaction was isolated from the crude reaction mixture. This isolated side product was purified by silica gel chromatography and precipitated from cold MeOH. The compound was assigned by NMR spectroscopy and identified as 3,8-dibromo-1,10-phenanthroline. The ¹H NMR spectrum shows three distinct peaks at 9.22 (d), 8.45 (d) and 7.79 (s) ppm, each integrating for two protons. This product would also be used in later work to analyse the spectroscopic differences between mono- and di-metallic molecular structures and their potential use as switching complexes.



Scheme 4.1. Synthesis of 3-bromo-1,10-phenanthroline .(i) Br₂, S₂Cl₂, pyridine, 1-chlorobutane, 80°C, 12 h, yield: 50%.

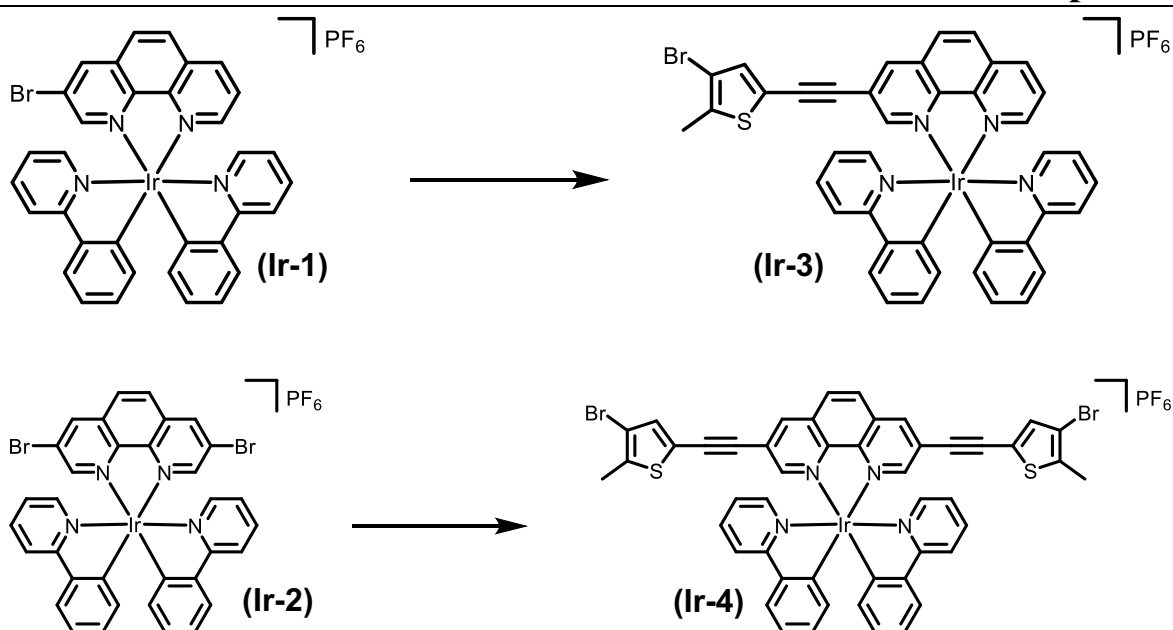
4.2.2 Coordination of Iridium centres

All three brominated ligands were coordinated to an Ir(III) centre using similar reagents. The ligand was dissolved in CH_2Cl_2 (25 ml) and heated to 40 °C. The dimer $[\text{Ir}(\text{ppy})_2(\mu\text{-Cl})]_2$, which was previously prepared, was similarly dissolved in minimal CH_2Cl_2 and added to the solution dropwise *via* the condenser over several minutes, and the reaction was allowed to proceed for 4 hours. In both cases the yield was notably high for the precursor complexes, $[\text{Ir}(\text{ppy})_2(3\text{-bromo-phen})](\text{PF}_6)$, **Ir-1**, and $[\text{Ir}(\text{ppy})_2(3,8\text{-bromo-phen})](\text{PF}_6)$, **Ir-2**. (96 % and 94% for the 3- and 3,8-positions respectively.) The structure of each complex was assigned using ^1H NMR, ^{13}C NMR and 2D long range NMR spectroscopic methods, and confirmed by HRMS.



*Scheme 4.2 The coordination reactions of brominated ligands using the same reagents to form complexes **Ir-1** and **Ir-2** (i) $[\text{Ir}(\text{ppy})_2(\mu\text{-Cl})]_2$, CH_2Cl_2 , 40 °C, 16 h. Yields: 96 % **Ir-1** and 94 % **Ir-2**.*

Further to this, 3-bromo-2-methyl-5-ethylthiophene (ET) was then attached to the 3- and 3,8-positions of phen respectively via single or double Sonogashira cross-coupling reactions, using the “chemistry-on-the-complex” method. Excess amounts of the thienyl starting material were added to favour the completion of the reaction. $[\text{Ir}(\text{ppy})_2(3\text{-ET-phen})](\text{PF}_6)$, **Ir-3**, and $[\text{Ir}(\text{ppy})_2(3,8\text{-diET-phen})](\text{PF}_6)$, **Ir-4**, were formed via these successful Sonogashira cross-coupling reactions, and the full reaction scheme is presented in Scheme 4.3. Each Ir(III) complex is fully characterised by multinuclear NMR spectroscopy, and high resolution mass spectroscopy.



Scheme 4.3 The Sonogashira cross-coupling reactions towards final Ir(III) cyclometallated complexes **Ir-3** and **Ir-4**, (i) 3-bromo-2-methyl-5-ethynylthiophene, $\text{Pd}(\text{PPh}_3)_2\text{Cl}_2$, PPh_3 , CuI , $\text{Et}_3\text{N}/\text{DMF}(2:5)$, 60°C , 24 h and (ii) 3-bromo-2-methyl-5-ethynylthiophene, $\text{Pd}(\text{PPh}_3)_2\text{Cl}_2$, PPh_3 , CuI , $\text{Et}_3\text{N}/\text{CH}_3\text{CN}(2:5)$, 60°C , 17 h.

4.3 Structural Characterisation of Ir-1 - Ir-4

4.3.1 NMR Spectra Analysis of Ir-1 - Ir-4

The ^1H NMR spectra of **Ir-1** - **Ir-4** were fully assigned with the assistance of ^1H - ^1H COSY, HSQC and HMBC, and are presented in Figure 4.2 and Figure 4.3. The assignment of proton signals for **Ir-1** and **Ir-3** was more complicated due to their asymmetrical structures. The most deshielded peak for all of the complexes studied is the proton signal originating from the 4-position of the phenyl fragment. It appears as a pseudo-singlet at $\delta = 8.90$ ppm for **Ir-3**, as a doublet with J values around 8.5 Hz in those Ir(III) complexes substituted at the 3- and 3,8-positions of the phenyl fragment with Br, and as a singlet at $\delta = 8.86$ ppm in **Ir-4**. Slight shifts upfield were observed for this 4-position proton by the substitution of the respective Br with the thienylacetylene moiety in the 3- or 3,8-positions of the phenyl fragment. For example, the resonance located at $\delta = 8.81$ ppm in **Ir-1** was shifted to $\delta = 8.68$ ppm in **Ir-3**, and that located at $\delta = 8.83$ ppm in **Ir-2** was shifted to $\delta = 8.65$ ppm in **Ir-4**. The remaining proton signals from the phenyl fragment are coloured with different circles for the identification of their positions (Figures 4.2, 4.3 and 4.5).

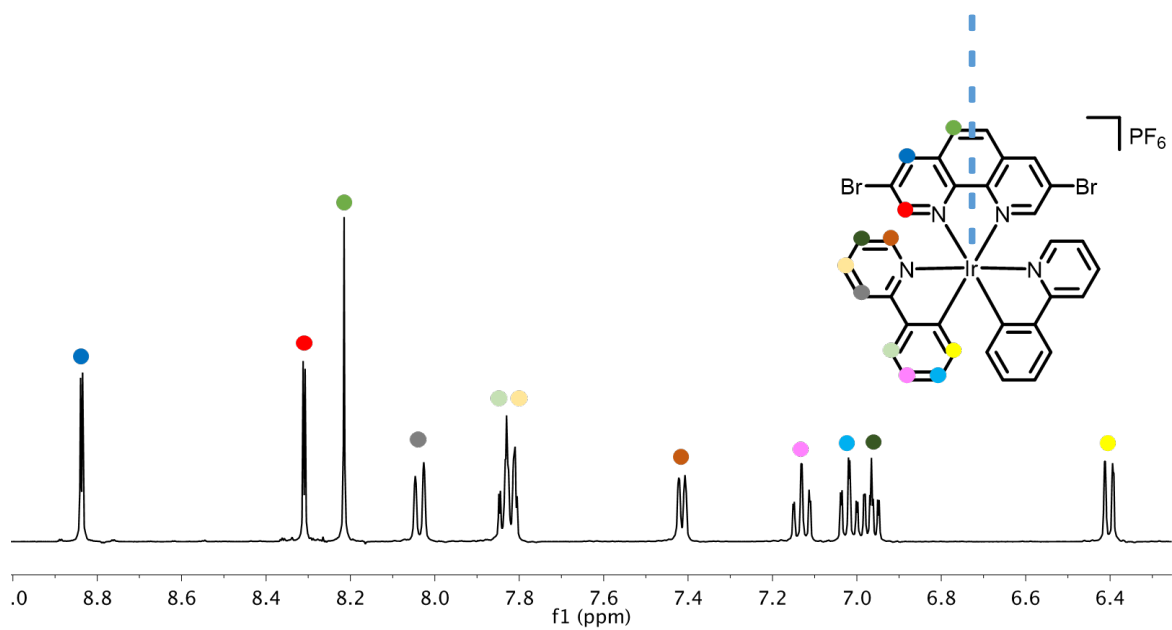
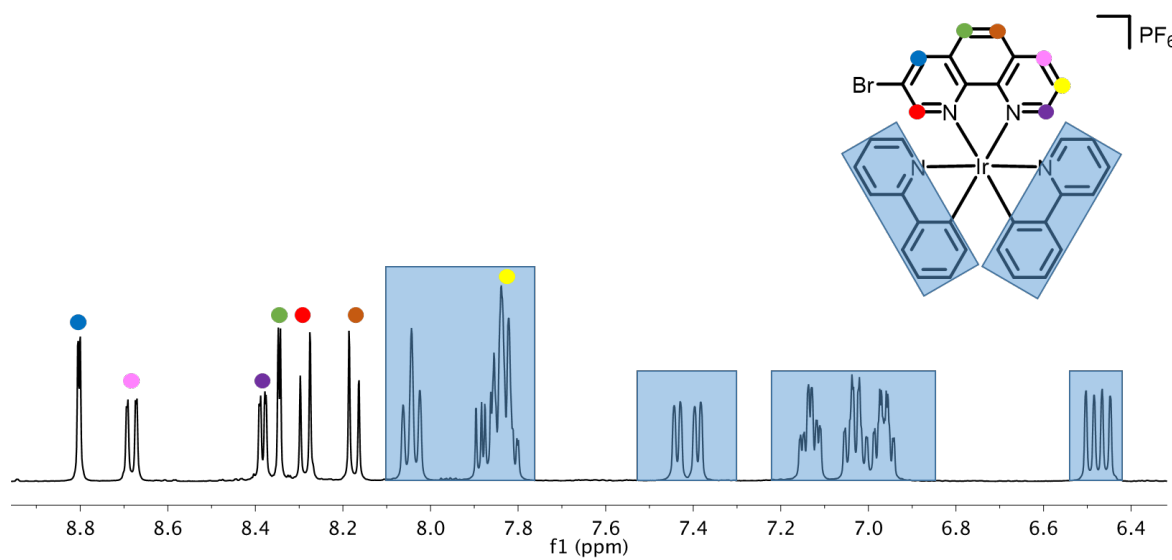


Figure 4.2 ^1H NMR spectrum of **Ir-1** and **Ir-2** showing complete assignment of the proton signals (400 MHz, CD_2Cl_2 , RT)

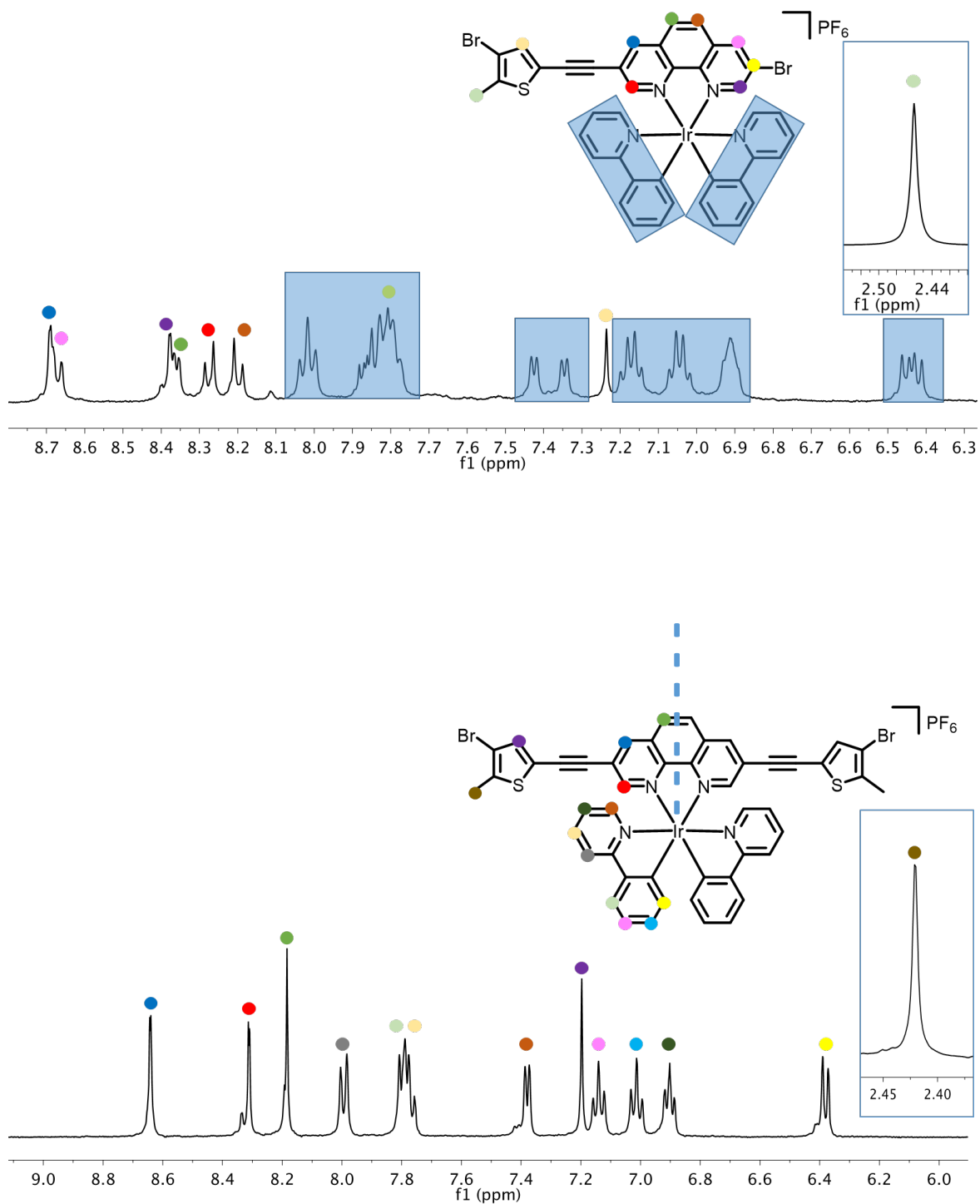


Figure 4.3 ^1H NMR spectrum of **Ir-3** and **Ir-4** showing complete assignment of the proton signals, with inset showing methyl signals present further upfield (400 MHz, CD_2Cl_2 , RT)

In Ir-1 and Ir-3, the four π^* n system was identified as the 7,8,9-positions of the phenfragment, and the two-spin system with well-split doublets, was attributed to the 5,6-positions. Ir-2 and Ir-4 the signals from the 2,4,5-positions of phen appear as singlets. An analysis of the well-resolved ^1H - ^1H COSY experiments revealed the presence of four-spin systems, attributed to the remaining ppy auxiliary coordinating ligands. The proton signals from ppy appear in the region $\delta = 8.3$ - 6.3 ppm, and are visualised with light blue rectangles in Ir-1 and Ir-3, but full characterisation of their signals was viable in Ir-2 and Ir-4 due the more symmetrical nature of the system. The thienyl proton signal in Ir-3 and Ir-14 are visualised in both spectra and remain relatively unchanged in both.

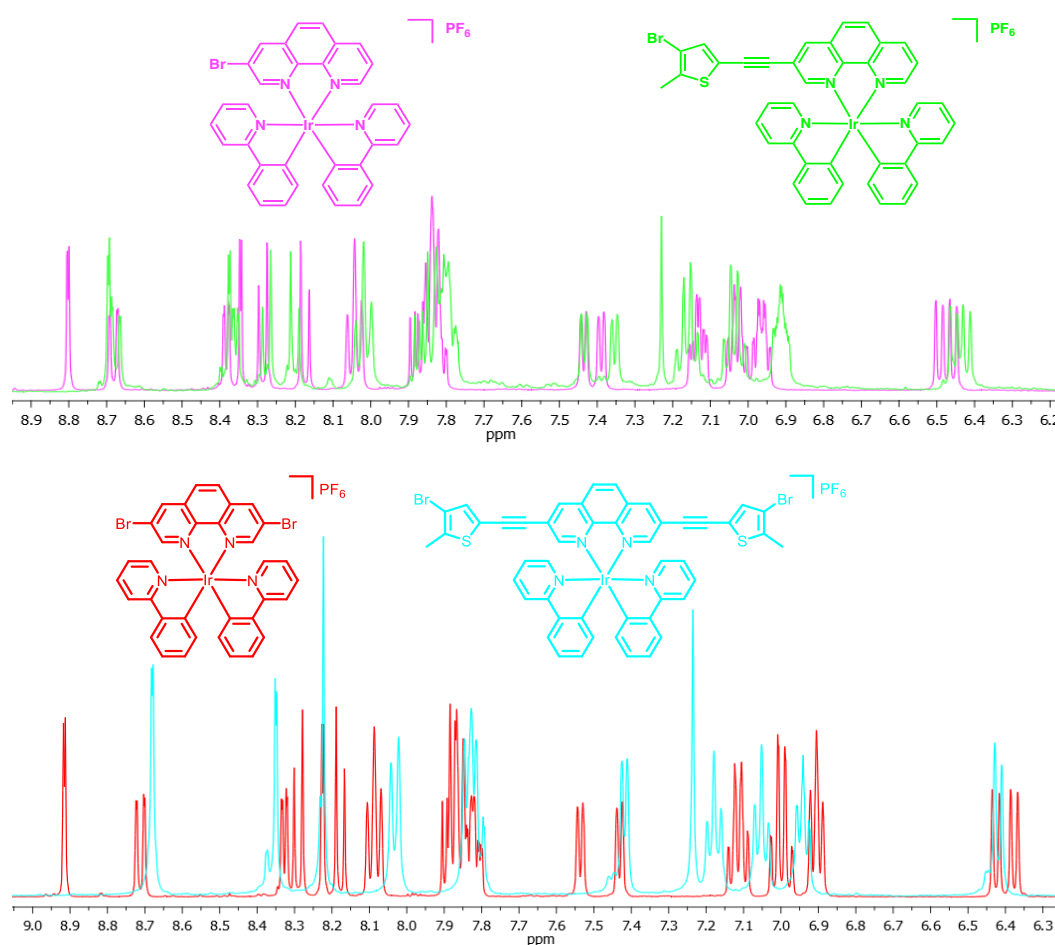


Figure 4.4 (a) Overlapping ^1H NMR spectra of (a) **Ir-1** and **Ir-3**, (b) **Ir-2** and **Ir-4**

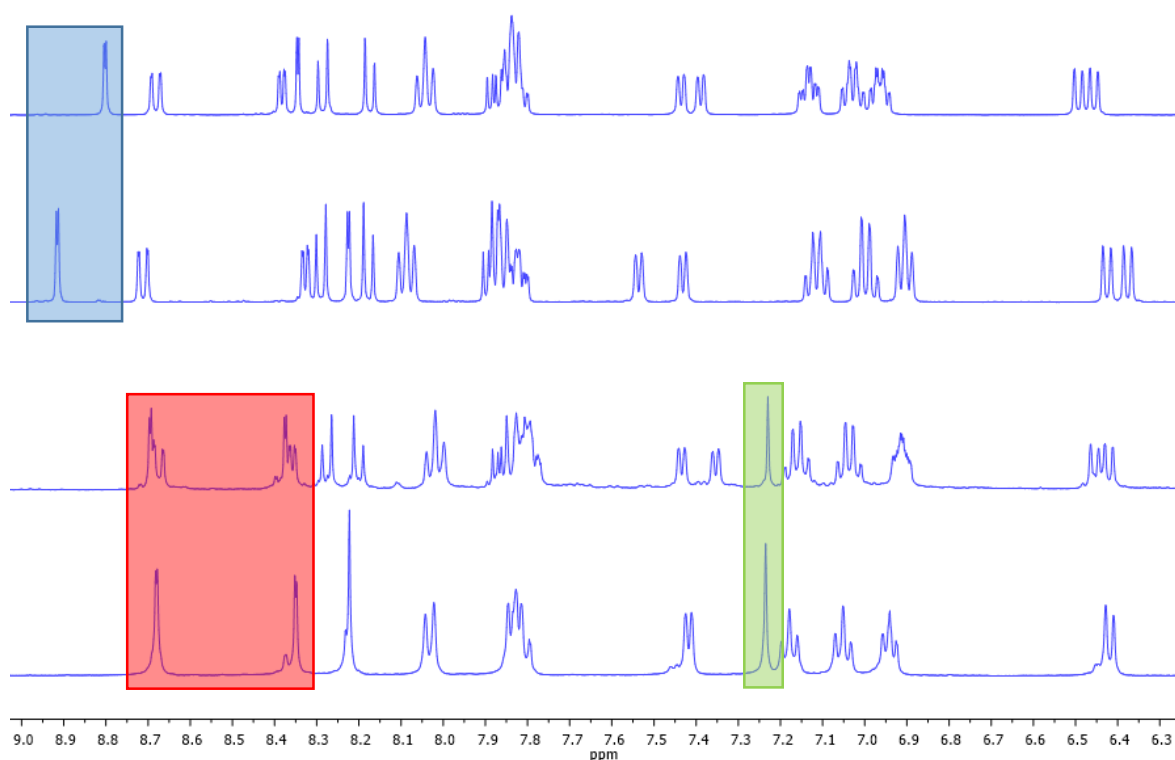


Figure 4.4(b) ^1H NMR of **Ir-1** – **Ir-4** stacked showing downfield phen-singlet in bromine substituted complexes (blue), the thienylacetylene substituted complexes (red), and the growth of the thienyl proton signal in **Ir-3** and **Ir-4**.

The spectra of **Ir-1** and **Ir-2** overlap more readily as brominated ligand complexes, compared to an expected overlap of **Ir-1** and **Ir-3** as mono-substituted ligand complexes. This is most notable for the phen-ligand signals, as shown in Figure 4.5. Though **Ir-3** is more complex and has more signals than **Ir-4**, due to its unsymmetrical nature, all peaks within the spectra appear at very similar positions. The phenylpyridine peaks remain relatively unchanged between both, as expected, but those of the symmetrical and unsymmetrical phen-ligand also remain relatively unchanged, seen here as the singlet thienyl peak and the singlet peaks of the phen itself.

4.3.2 Crystallographic analysis of Ir-1

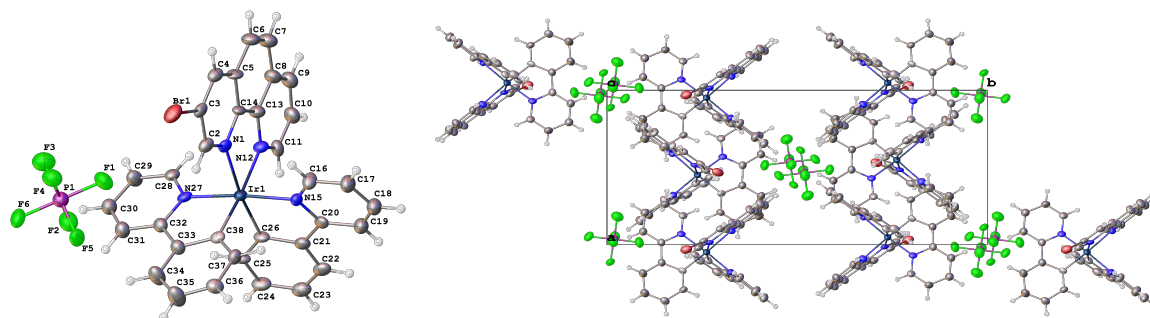


Figure 4.5 Asymmetric unit of **Ir-1** with atomic displacement parameters shown at 50% probability and (b) Packing structure diagram of **Ir-1** viewed along the *b*-axis

Crystals of **Ir-1** suitable for single crystal X-ray diffraction were obtained by the slow evaporation of CH_2Cl_2 (in a mass spec tube sample). A translucent orange needle-like specimen of the formula unit $\text{C}_{34}\text{H}_{23}\text{BrF}_6\text{IrN}_4\text{P}$ was determined to have crystallised in the P21/c space group, with four formula units in the unit cell. The asymmetric unit is presented in Figure 4.5. The unit consists of one $[\text{Ir}(\text{ppy})_2(3\text{-bromophen})]^+$ cation and one PF_6^- anion. The Ir(III) centre is coordinated by four nitrogen atoms and two carbon atoms from one bidentate 3-bromo-phen and two bidentate ppy ligands, in a distorted octahedral configuration. The dihedral angles between the phen plane and the two ppy rings in **Ir-1** are ca. 84.8° and 85.2° , respectively, and the dihedral angle between the two ppy rings is ca. 88.8° . The dihedral angles between the 2-phenylring and pyridine ring of two bidentate ppy ligands are ca. 12.4° and 3.7° , respectively. The packing structure diagram of **Ir-1** is presented in Figure 4.4, viewed along the *b*-axis. The phen-units interdigitate and overlap with neighbouring phen moieties to give an interplanar distance of approximately 3.43 \AA .

4.3.3 Spectroscopic analysis of compounds Ir-1 and Ir-2

The UV-vis absorption spectra were collected for **Ir-1** and **Ir-2** in different polarity solvents; Hexane (for **Ir-1**), CH_2Cl_2 , MeOH and CH_3CN (Figure 4.6 (a)). No solvent dependence was observed for each complex with a change of solvent polarity. The spectral profiles of both complexes are also quite similar to each of the other complexes. The absorption spectra show two main features in the UV-Visible region. The intense absorption below 350 nm are assigned as ligand centred $\pi \rightarrow \pi^*$ transitions within the ppy and the phen fragments. The

much weaker absorption bands at lower energies are typical of spin-allowed metal to ligand charge-transfer (MLCT) transitions. In this case, mostly of $[d(\text{Ir}) \rightarrow \pi^*(\text{phen})]$ character.

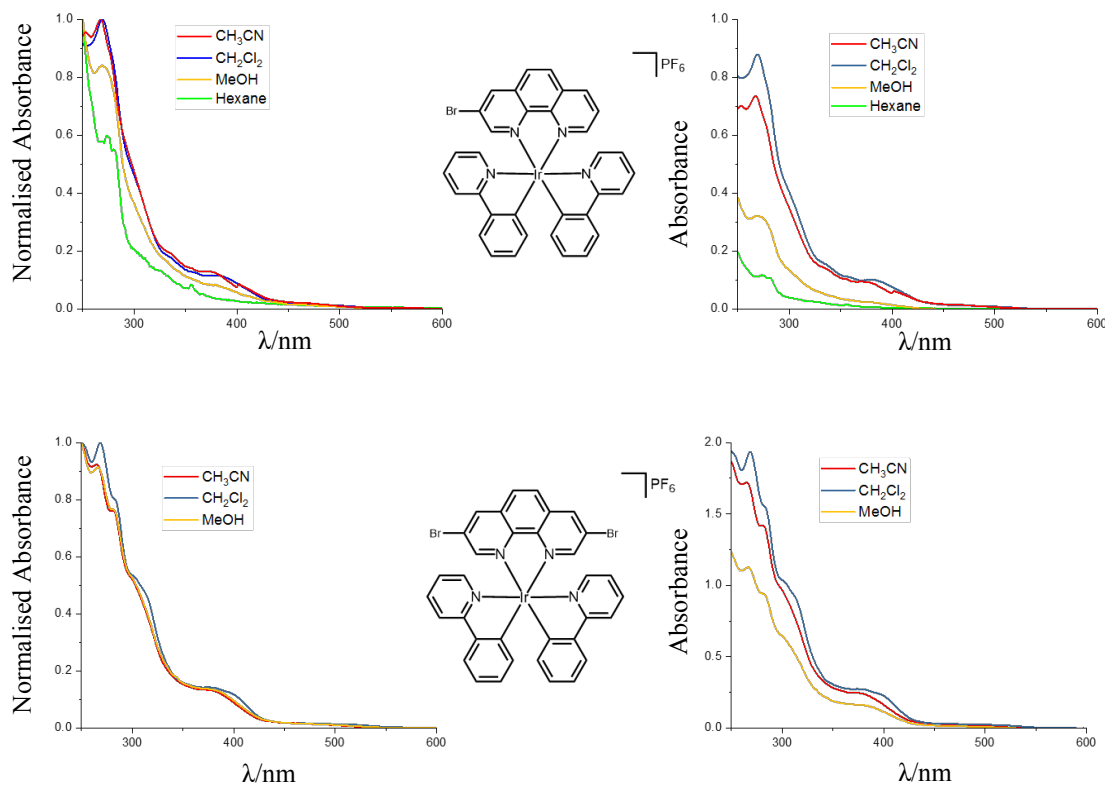


Figure 4.6(a) Absorption spectra of complexes **Ir-1** and **Ir-2** in varying solvents ($1 \times 10^{-5} M$), showing both normalised and unaltered transitions.

The emission spectra of **Ir-1** and **Ir-2** were collected in CH_2Cl_2 purged with Ar atmosphere. Single broad and featureless emission peaks were observed at $\lambda_{\text{em}} = 594 \text{ nm}$ and 605 nm respectively (Figure 4.6(b)). The parent Ir(III) complex, $[\text{Ir}(\text{ppy})_2(\text{phen})]^+$, reported by Wilson *et al.*²²⁵ shows an emission band centered at 584 nm . Considerable red-shifts in the emission peaks were achieved by comparing **Ir-1** and **Ir-2** to this parent Ir(III) complex. These shifts can be attributed to the narrowed energy gap between the Ir(III) t_{2g} ground state and the phen π^* excited state after bromination of the phen moiety. These emission bands at $\sim 600 \text{ nm}$ are typical of the $^3\text{MLCT}$ emission character for this type of Ir(III) complexes, and is further supported by their featureless appearance. Significant quenchings were observed when the solutions were exposed to air, further indicating phosphorescence character.

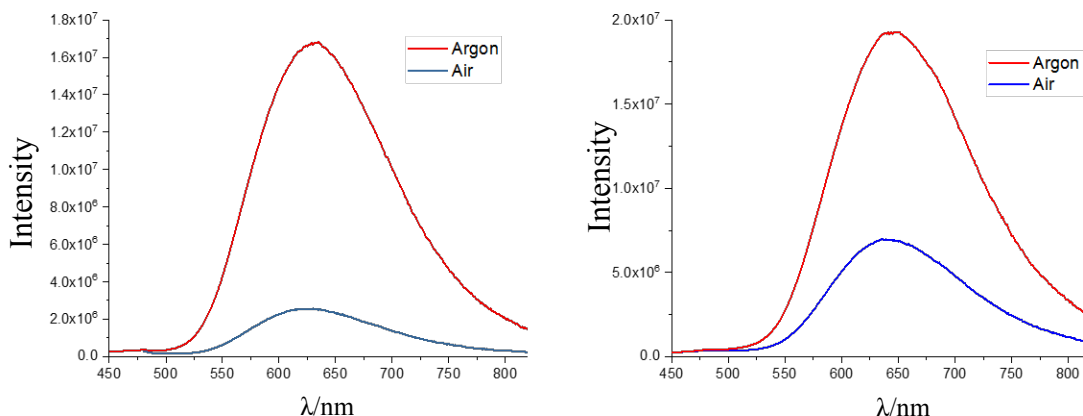


Figure 4.6 (b) Emission studies of **Ir-1** and **Ir-2**, carried out in air and under argon (1×10^{-6} M). Both solutions showed significant emission quenching when exposed to air.

4.3.4 Spectroscopic analysis of compounds **Ir-3** and **Ir-4**

The UV-vis absorption spectra of **Ir-3** and **Ir-4** were collected in three different polarity solvents (CH_2Cl_2 , MeOH and CH_3CN), and are presented in Figure 4.7. Minor solvent dependence was observed with a change of the solvent polarity. For example, **Ir-3** shows absorption peaks at 414 nm in CH_3CN and 417 nm in MeOH. The most red-shifted absorption peak was observed in CH_3CN at 440 nm. However, for **Ir-4**, the most red-shifted peak occurred in CH_2Cl_2 . For both Ir(III) complexes, measurements in toluene and hexane produced negligible results and therefore disregarded, owing to the extreme insolubility of the products in these solvents.

Also notable in both of these spectra is the hyperchromic shift observed in relation to these MLCT based absorptions in CH_3CN compared with MeOH and CH_2Cl_2 . Due to the presence of the lone pair of electrons on the sulphur atom, and the high levels of conjugation with the substituted phen system, the brominated thiophenes may be acting in an auxochromic nature, which is most stabilised in CH_3CN . The increased absorption in this region of both **Ir-3** and **Ir-4** compared to **Ir-1** and **Ir-2** is naturally ascribed to thienyl absorption patterns previously noted.

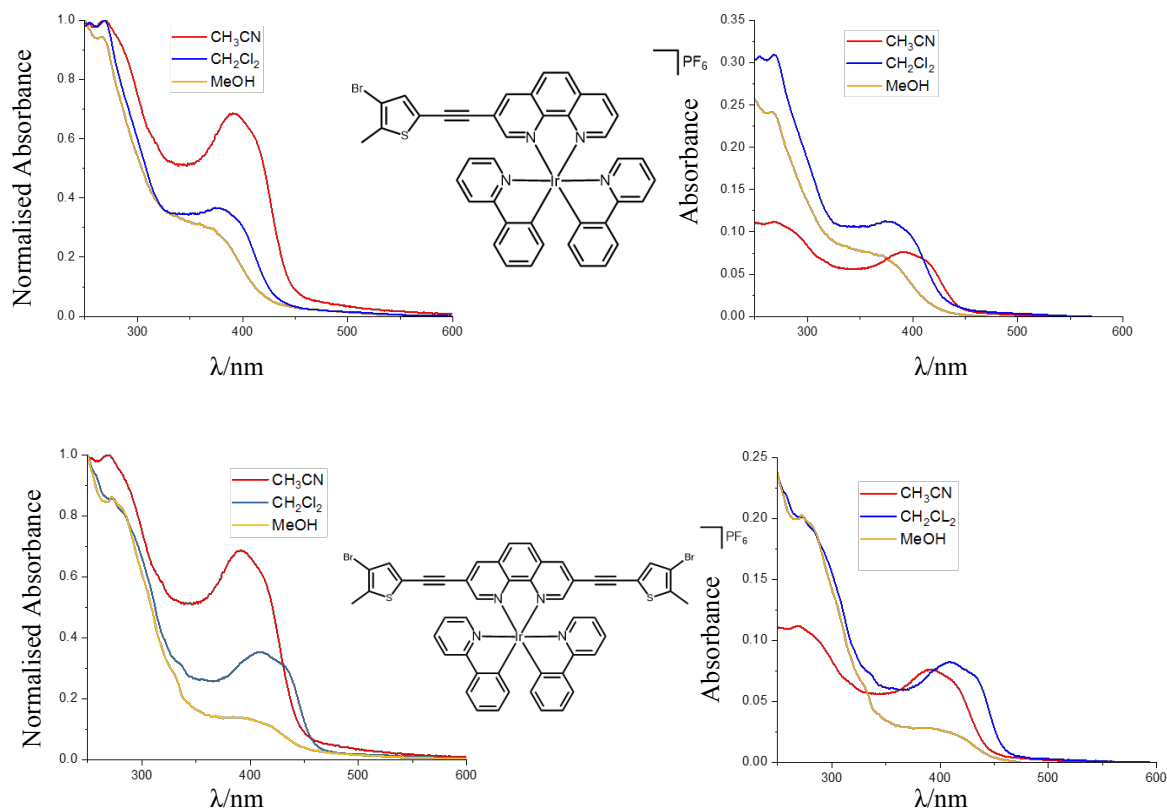


Figure 4.7 Absorption spectra of complexes **Ir-1** and **Ir-2** in varying solvents (1×10^{-5} M), showing both normalised and unaltered transitions.

The photoluminescence of each complex was measured under an Ar atmosphere at RT. The normalised emission spectra are compared and shown in Figure 4.8. Both emission profiles feature a broad featureless phosphorescence, at wavelengths comparable to those of **Ir-1** and **Ir-2**, suggesting a similar T_1 energy level for all four complexes. Conjugation with the brominated thienyl moieties and lowering of the LUMO as seen in the absorption spectra imply only the $^1\text{MLCT}$ is lowered upon substitution and the $^3\text{MLCT}$ is relatively unchanged for all four complexes.

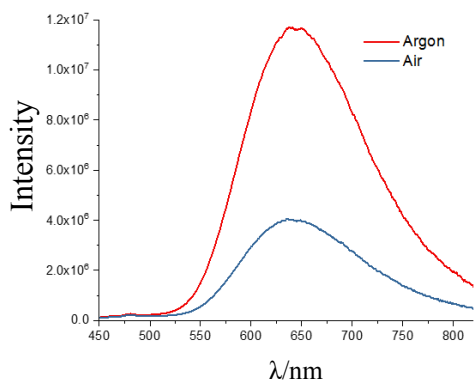


Figure 4.8 Emission of **Ir-3** and **Ir-4** carried out in air and under an argon atmosphere.

4.3.5 Comparative analysis of UV-Vis absorption patterns of Ir-1 – Ir-4

The UV-Vis absorption spectra of all the generated Ir(III) complexes are compared in CH₂Cl₂ (Figure 4.9). The absorption spectra of the parent Ir(III) complex, and that of the free ethynyl-thiophene, greatly aids in the assignment of the transitions observed in each of the four complexes of this study. The absorption band structure in the region of 250-400 nm is virtually the superposition of the spectra of the parent Ir(III) complex and pyrene moiety. However, most notable in the spectra is that of the hyperchromic shift seen upon substitution from brominated phen, to its ethynylthiophene counterpart. This is due to the absorption of the free thiophenes, which occur in a range of 330-370 nm, as well as their potential auxochromic nature. Also interesting to note is the broadening and subsequent red-shift of the dithienyl **Ir-4** compared to **Ir-3**. This extensive bathochromic shift could also suggest a potential MLCT/IL mixed absorption in this region, due to the increased conjugation along the phen ligand, as it has a much more extensive delocalisation between the two thiophenes than in one. This conjugation lowers the energy of the LUMO, and a red shift is observed.

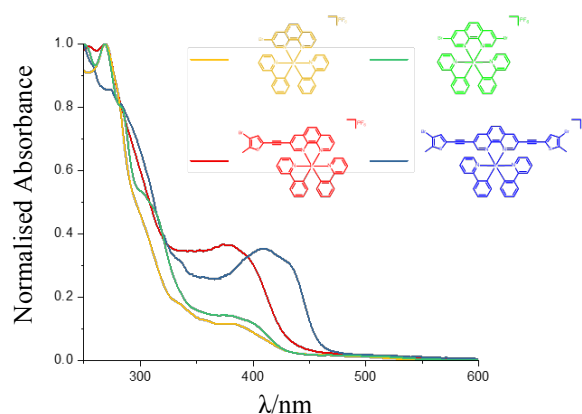
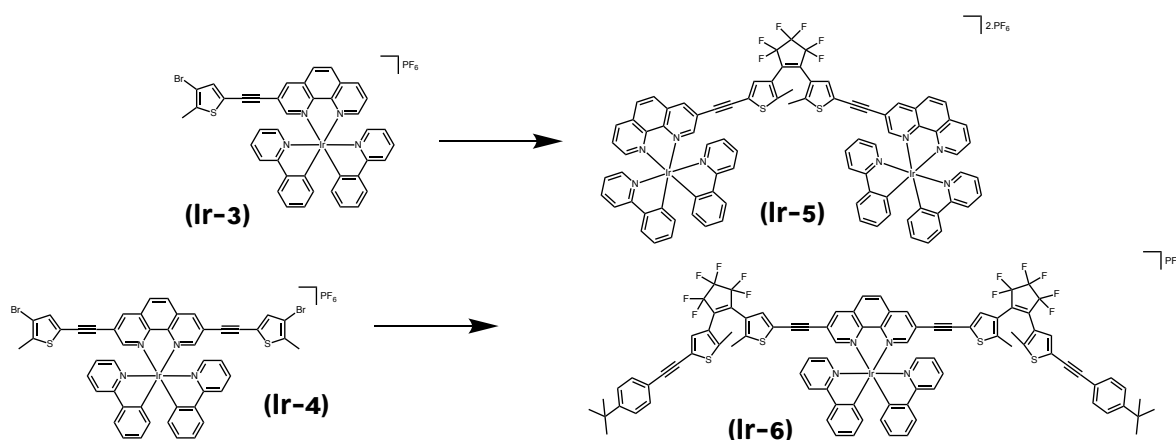


Figure 4.9 Normalised UV-Vis absorption of **Ir-1**, **Ir-2**, **Ir-3** and **Ir-4**

4.3.6 Further reactivity of Ir-3 and Ir-4

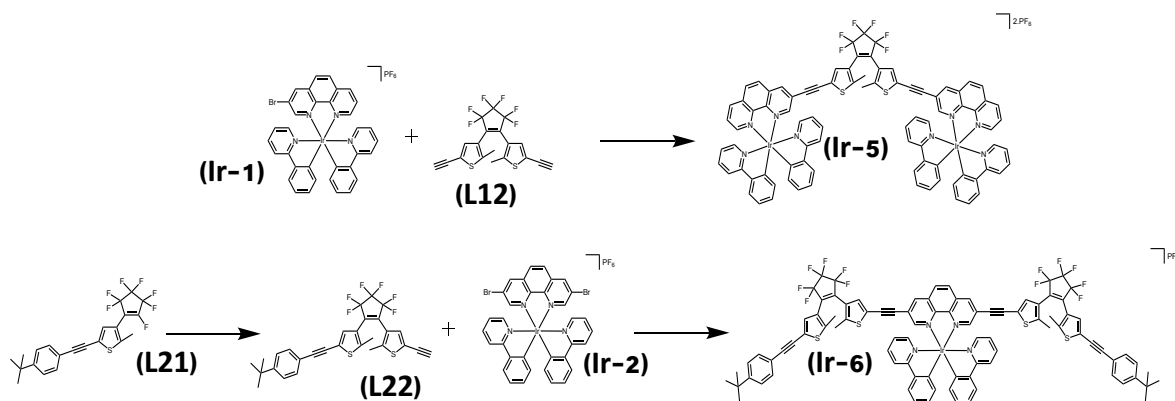
Scheme 4.X shows the synthetic route opted to be taken to further the reactivity of complexes Ir-3 and Ir-4 towards functionality as switching compounds. Reaction of Ir-3 in dry MeTHF at -78 C was treated with an excess of n-BuLi and allowed to stir for four hours at low temperature. MeTHF was chosen as an optimal solvent to to the insolubility of the complexes in THF and diethyl ether. Octafluorocyclopentene was then added at a stoichiometric ratio and the reaction allowed to stir for a further six hours at this temperature, (-78 – -90 C). The reason for this 1:1 addition of the perflourinated backbone was due to the relative size of the the reacting iridium metal complex. The solvents were removed at reduced pressure following two days of stirring at room temperature and the products purified by column

chromatography. No photochromic switching under UV light was immediately evident. TLC chromatography analysis indicated at least one phosphorescent spot, and so the crude was purified with CH_2Cl_2 : MeOH as eluent. However, mass spectrometry and NMR analysis only revealed the presence of starting material **Ir-3**, and of its unbrominated analogue. The reaction was repeatedly completed numerous times, with varying reaction conditions and solvent systems tried, however they did not proceed to completion. A similar method was tried using **Ir-4**, and **L21**, however this also failed to produce **Ir-6** in any of the tried reaction conditions. Though the complexation reaction of the iridium dimer to phen is quite facile, it is the strenuous purification of 3-bromophen that meant repeat reactions often occurred at varying points in time, and reactions proceeded sparingly.



Scheme 4.10 Further synthetic routes towards Ir(III) dithienyl switches, **Ir-6** and **Ir-7**.

As such, a second alternate route was proposed, using the more readily accessible **Ir-1** and **Ir-2**, shown in Scheme 4.10. Unfortunately, these reactions also did not proceed, and neither the symmetric or unsymmetric products were found in both cases. The lack of reactivity of these complexes towards a lithiating reaction such as this is intriguing. Evidence of the unbrominated products in the case of route one suggests at least partial lithium-halogen exchange occurring, but the occurrence of the unreacted starting material, even in conditions with excess *n*-BuLi is a cause for further research into the area. Higher reaction temperatures and longer reaction conditions had a negligible effect on the forward reaction. A lithiation reaction with the unchelated phen-ligand was also briefly considered, however, there is a high risk of Cu(I) coordination with phen derivative during the Sonogashira cross-coupling reactions, and even when these can be avoided in copper-free reactions using $\text{Pd}(\text{PPh}_3)_4$, use of *n*-BuLi in conditions involving free nitrogens was decided to be too unviable.

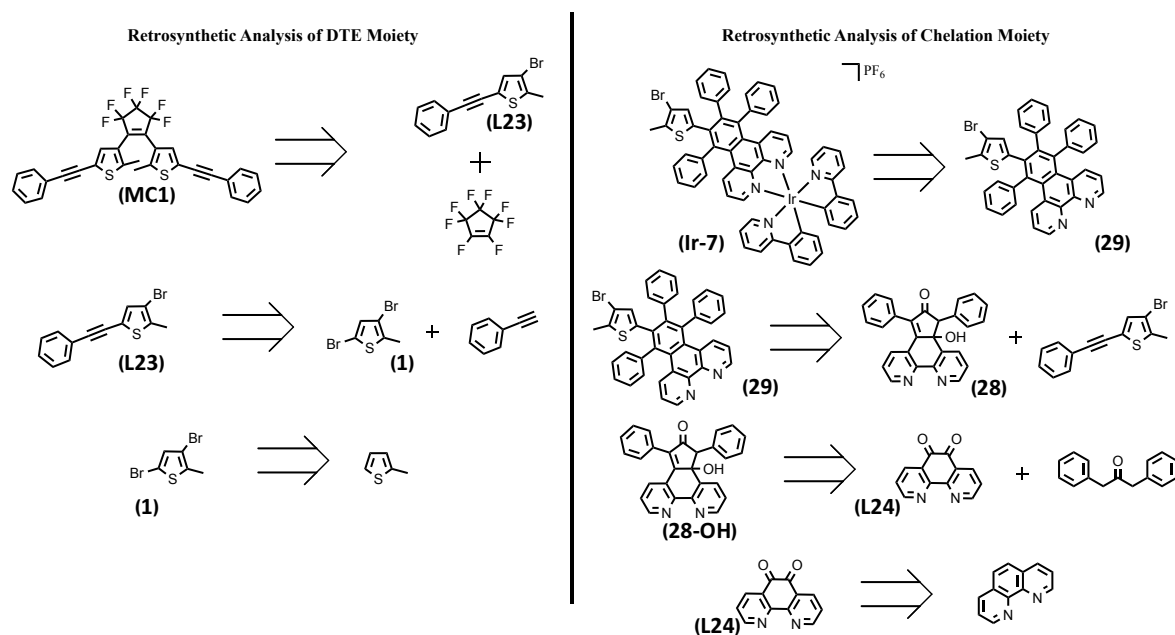


Scheme 4.11 Alternate synthetic routes towards Ir(III) dithienyl switches, **Ir-6** and **Ir-7**.

Work on much larger derivatives, with a funnelling platform between the metal and the switching centre, one with much more delocalisation than the linearity seen in 3- and 3-8-substituted acetylenic phen compounds. This work is detailed in the following sections.

4.4 Ir(III) 1,10-phenanthroline platform molecular switch

4.4.1 Synthetic Route



Scheme 4.4 Retrosynthetic analysis towards (a) precursor compound **MCI** and (b) **Ir-7**.

The synthetic routes optimised and undertaken during this research allowed for the individual characterisations of components that would later be integrated into the DTE molecular switch ligand of the iridium metal centre. The initial reaction methods are shown in Scheme 4.4. By evaluating the components individually and analysing their photochemical impact on the overall properties of the switch, it could be determined for future work whether alterations to existing moieties should be made, and if so, in what way

could they could be functionally altered. Full details pertaining to reactants, solvents, other reagents and reaction conditions may be found in the experimental section. All starting materials were prepared according to literature methods. The main compounds necessary for complete characterisation were compounds **MC1** and **Ir-7**. The examination of **MC1** in detail is imperative as it serves as a good basis and source of information for the standard molecular framework seen in dithienylethene based molecules, as well as serving as a precursor for later chelating moieties. **29** and **Ir-7** yield insight into the photochemical effect of Ir(III) incorporation; **29** as a semi-delocalised platform capable of chelation and **Ir-7** as the corresponding system with the iridium centre. The synthesis of the final products was achieved via a Diels-Alder [4+2] cyclisation reaction between compounds **MC1** and **28**. Route B of the synthesis outlined above was undertaken to gain insight into each individual component, and yielded valuable information on the types of transitions seen in the final complex.

4.4.1.1 Synthesis and NMR analysis of 3,3-(perfluorocyclopent-1-ene-1,2-diyl)bis(2-methyl-5(phenylethynyl)thiophene), model compound **1** (**MC1**)

Several precursors were required for the synthesis of the first DTE molecular switch to be characterised. The synthesis of 3,5-dibromo-2-methylthiophene, **1**, was achieved through the allylic bromination of 2-methylthiophene with N-bromosuccinimide, and in acidic conditions the solution was left to stir at room temperature for 12 hours to yield the desired product. The selective dibromination of the thiophene moiety allowed for the synthesis of 3-bromo-2-methyl-5-(phenylethynyl)thiophene, **L23**, via a Sonogashira cross-coupling reaction³⁰ between **1** and phenylacetylene, carried out at 120 °C overnight. The reaction was facilitated by through use of a Pd(II)-catalyst and co-catalysed by CuI and PPh₃. N-butyllithium was used as the lithiating agent of compound **L23** and stirred at -78 °C for a period of 2 hours. Octafluorocyclopentene was then added directly to the reaction whilst maintaining the low reaction temperature, to yield the final precursor product, the symmetrical 3,3-(perfluorocyclopent-1-ene-1,2-diyl)bis(2-methyl-5(phenylethynyl)thiophene), **MC1**, *in situ*.

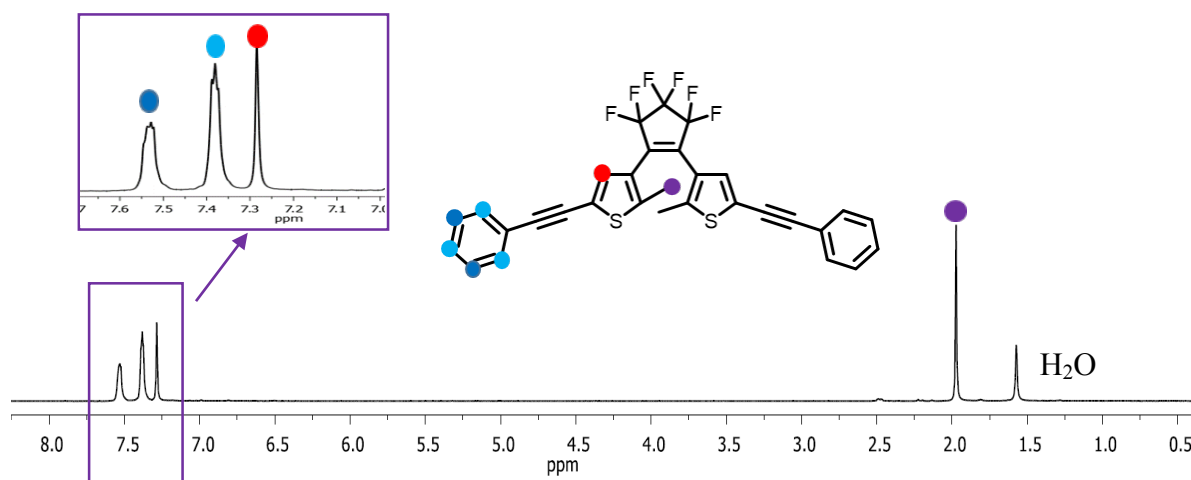


Figure 4.12 ^1H NMR (400 MHz) of Compound MCI in CDCl_3 with aromatic region magnified.

Assignment of the geometric structure of compound **MCI** was achieved using ^1H NMR, ^{13}C NMR, HSQC and long-range HMBC experiments. Initial assignment through the use of the ^1H NMR spectrum of the open isomer confirmed the presence of the expected number of proton signals. (Figure 4.12). The signal due to the methyl protons is observed upfield as a singlet integrating for 6 protons, with a chemical shift of 1.97 ppm. This chemical shift is due to the inductive nature of the thiophene ring onto which the methyl group is substituted. The protons at the 4/4' position of the thiophene ring is obscured by the solvent peak (CDCl_3 at 7.26 ppm) and as such its integration and multiplicity was indiscernible from this spectrum. The signal was resolved using HSQC NMR spectroscopy and is deshielded due to the delocalisation of the aromatic system. The final signals to be assigned correspond to the phenyl groups which present with characteristic splitting patterns and chemical shifts for aromatic protons, at 7.54 ppm corresponding to the orthoprotons with an integration of 4 and the remaining signal at 7.40 ppm to the meta- and paraproteons whilst integrating to 6.

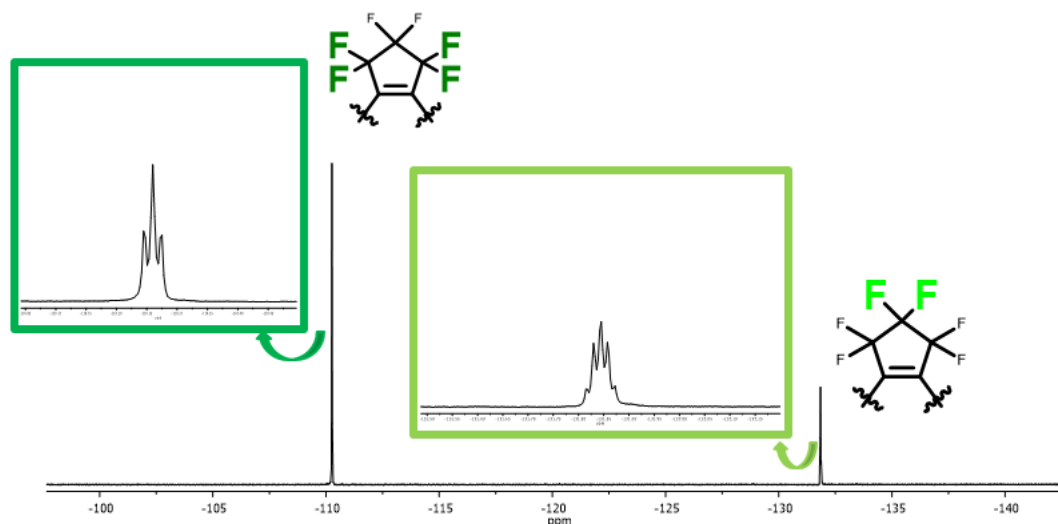


Figure 4.13 ^1F NMR, showing the splitting pattern of the fluorinated backbone.

The fluorinated NMR shown in Figure 4.13 shows the splitting pattern observed for the six fluorine atoms in the final compound. A triplet integrating for four fluorine at -110.03 ppm and a quintet integrating for the two remaining atoms -132.21 ppm.

4.4.1.2 Photochemical Analysis of Compound MC1

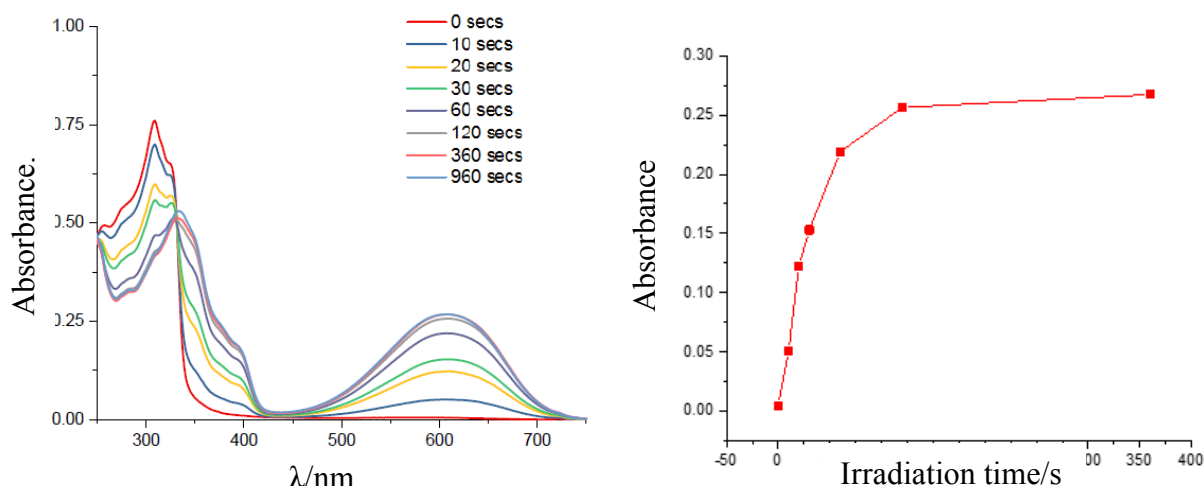


Figure 4.14 UV-Vis Spectra of Compound MC1 in CH_2Cl_2 with conc. $1 \times 10^{-5}\text{M}$ when irradiated with UV light with time intervals of 30 seconds and plot showing the increase in absorption at 603 nm with respect to exposure time.

The UV spectrum of MC1 presents with two absorbance maxima (Figure 4.14). The peak at 310 nm corresponds to the $n \rightarrow \pi^*$ and the $\pi \rightarrow \pi^*$ transition of open isomers (MC1o) thiophene rings. Upon ring closure via photocyclised rearrangement, this transition is

bathochromically shifted into the visible region which gives the compound its blue colouration, corresponding to the closed form (**MC1c**) $\pi \rightarrow \pi^*$ transition at 603 nm. The large difference in absorption maxima may be attributed to the reduction of the HOMO-LUMO gap as conjugation is extended into the phenylacetylene groups in the closed form, whereas in the open form electrons are localised mainly within the ring system. The UV-Vis spectrum displays the changes in absorption intensities of the closed and open form isomers as a result of exposure to UV light. Fatigue resistance was also evaluated and the switch performance was shown to decay by 20% after only 10 cycles. This may be due to the lack of functional groups that could prevent photo deactivation of molecules. The excitation and emission spectra were also recorded, the excitation spectrum aligned well with the main absorption peaks, and when coupled with the initial NMR spectrum, indicates a high degree of sample purity. Upon comparing the emission and absorption spectra, a Stokes shift of 42 nm was noted.

4.4.1.3 DFT Analysis of Compound MC1

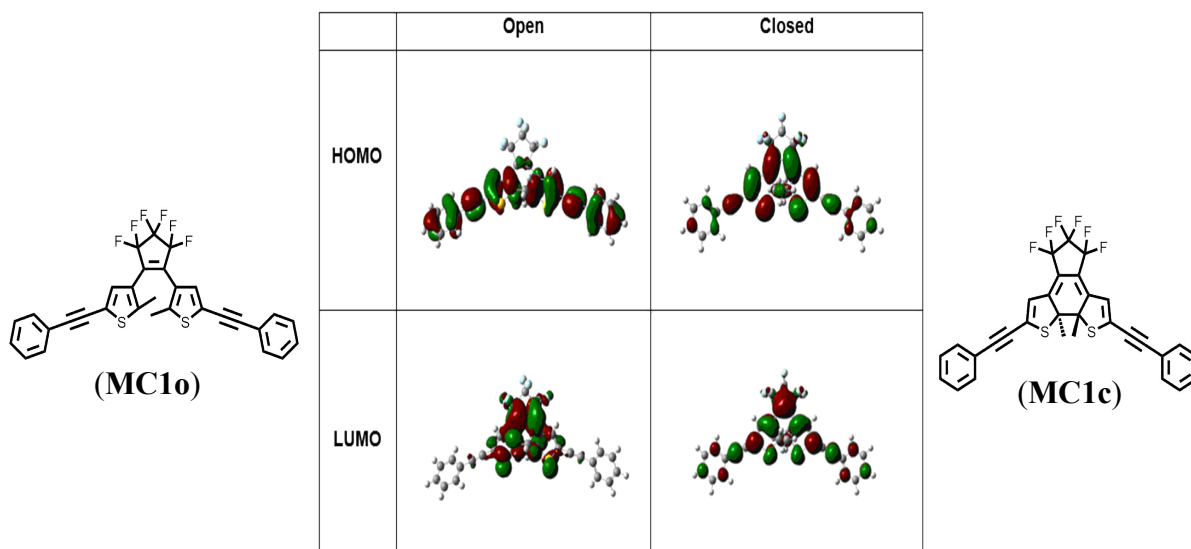


Figure 4.15 DFT (B3LYP, 6-31g basis set) visualisation of compound **MC1**'s MOs, displaying the HOMO and LUMO orbitals of both photoisomers.

DFT (B3 LYP) was used in the energetic optimisation and visualisation of both switch isomers (Figure 4.15). CH_2Cl_2 was employed as solvent in the calculation. Calculated by CAM-B3LYP/6-31G(d)/genecp, based on the optimised ground state geometries. The LUMO of **MC1o** was observed to be localised on the thiophene rings as expected, while the HOMO is spread evenly throughout the phenylacetylene framework of the compound. This

insulation of both phenylacetylene appendages overlaps well with the strictly higher energy transitions seen in the open form absorption pattern. In **MC1c**, both the HOMO and LUMO display a large degree of delocalisation with a similar distribution of orbital density suggesting a similar energy quantisation of molecular orbitals (MOs). This is confirmed through evaluation of the energies of each of the MOs. The open form isomer's HOMO-LUMO gap of 361.94 kcal/mol is much larger than that of the closed isomer; 200.55 kcal/mol. The lowering of the HOMO-LUMO gap observed is due to the extension of delocalisation to the phenyl moiety of the compound in the closed form. The high degree of accuracy in the DFT is confirmed by its approximation of the $\pi \rightarrow \pi^*$ transitions in the isomers, which were within 12 nm of the experimentally recorded values. The visualisation of the orbitals also allows for rationalisation of isomer interconversion as the HOMO of the open form displays electron density evenly throughout the molecular framework, however the lack of conjugation near the octafluoro-backbone means this electron density is contained within the substituted thienyl moieties. The $S_0 \rightarrow S_1$ transition which results in promotion of an electron into the LUMO via irradiation with UV light centralises electron density to the thiophene rings, encouraging bond rotation and the consequent [4+2] electrocycloisomerisation reaction towards the closed form. A similar trend is observed in **MC1c**, and passing through a higher energy transition state situated between the two isomers is avoided through electron promotion to an antibonding orbital.

The DFT optimisation of compound **MC1** provides valuable insight of the reaction coordinates of photoisomerisation associated with the DTE derivatives worked with over the course of the project and their classification as P-type photochromic compounds. It also serves as a precursor and model compound for much for intricate systems. Orbitals of the most allowed transitions are shown for both the open and closed isomers (Figure 4.16).

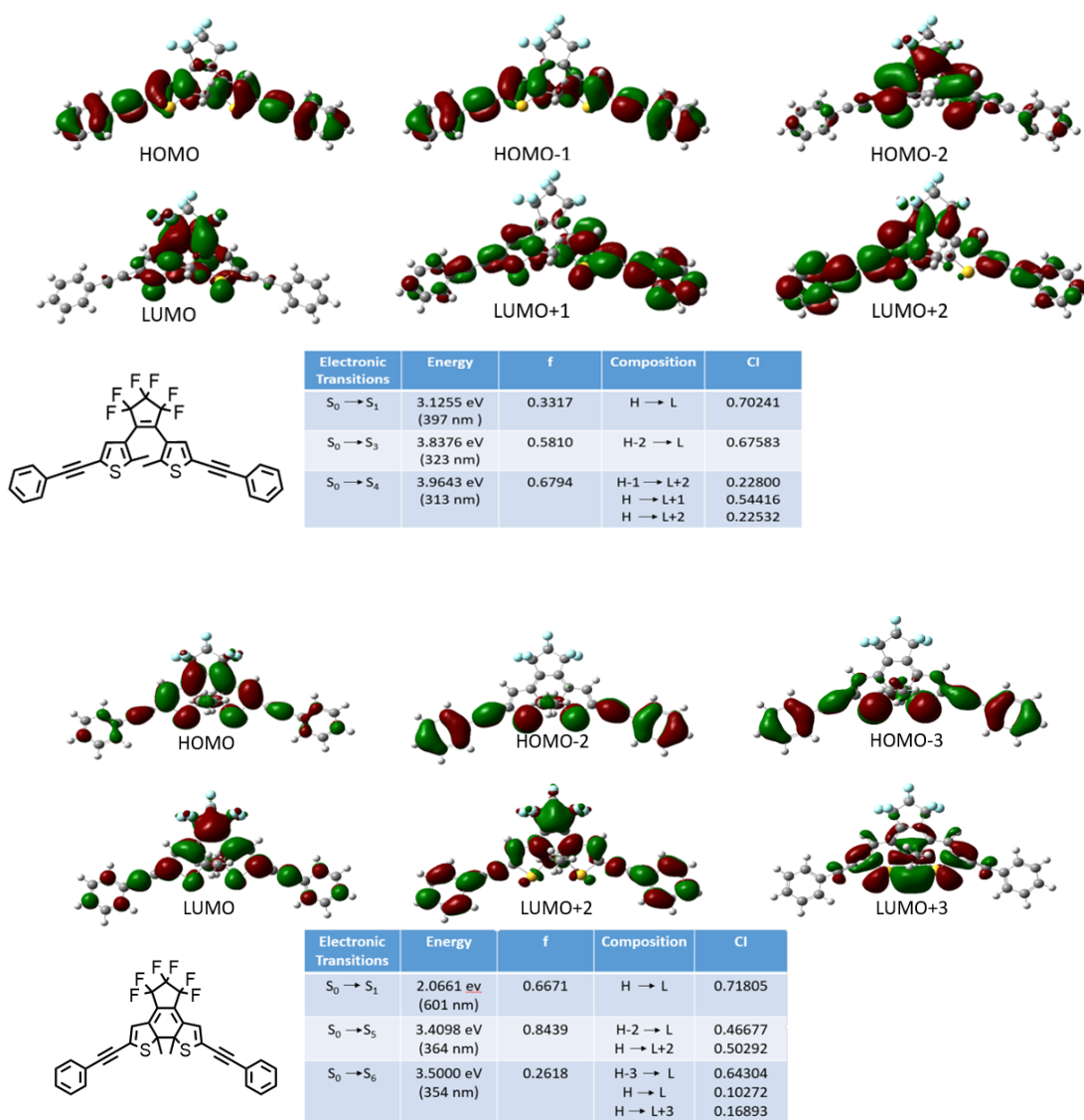


Figure 4.16 TD-DFT calculations for compound MClO/c. ^aOnly selected excited states were considered. The numbers in parentheses are the excitation energy in wavelength. ^bOscillator strength. ^cH stands for HOMO and L stands for LUMO. Only the main configurations are presented. ^dcoefficient of the wavefunction for each excitations. The CI coefficients are in absolute values.

4.4.1.4 Quantum Yield of MC1

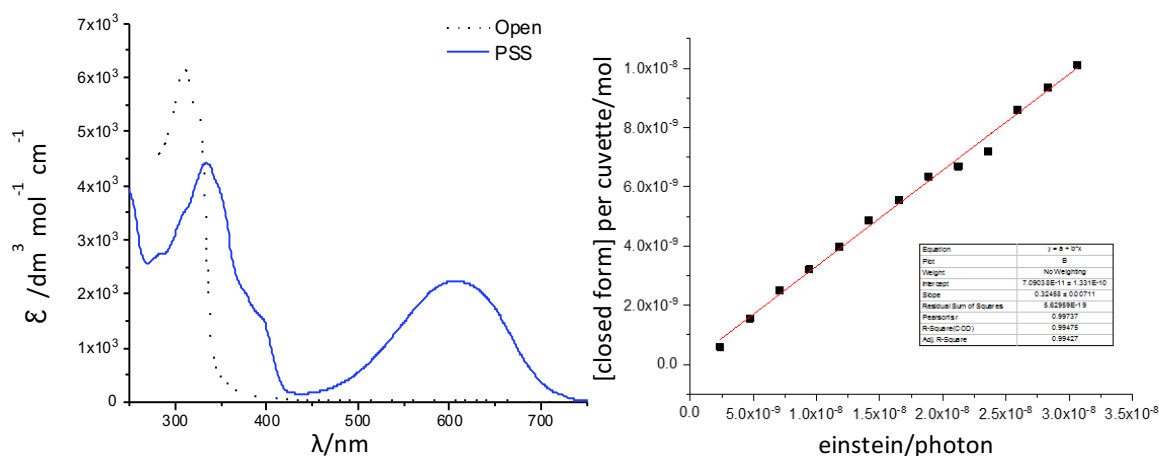


Figure 4.17 (a) UV-Vis Spectra of MC1 displaying the large differences in the absorption between the PSS and open states at 603 and 310 nm (b) displays the plot used in the evaluation of the quantum yield of 5 through establishing a ratio between reacted molecules and photon flux.

The method used for the calculation of quantum yield of isomer interconversion is outlined in Section 1.7 (Chemical Actinometry). The photon flux of the lamp was evaluated through monitoring the decomposition of potassium ferrioxalate. With the photon flux determined, the ratio of reacted molecules to total lamp emitted photons is evaluated by plotting the values in a linear form and determining the slope which corresponds to the quantum yield as per Figure 4.17(b). This resulted in a quantum yield of **MC1_o** to **MC1_c** ($\Phi_{o \rightarrow c} = 32\%$). The high R^2 of 99.475% indicated that the model and therefore the quantum yield value was of high accuracy. In solution, the quantum yield is limited to roughly 50% depending on the sterics of the R groups at the DTE 2/2' positions and their effect on the molecules preponderance for the photoinactive parallel conformation. Taking this into consideration a value of 32% suggests the interconversion of isomers is fairly facile. This may contribute to the switches poor fatigue resistance i.e. if more photoisomerisation reactions are taking place per cycle there may be a larger proportion of photoinactive molecules formed per cycle.

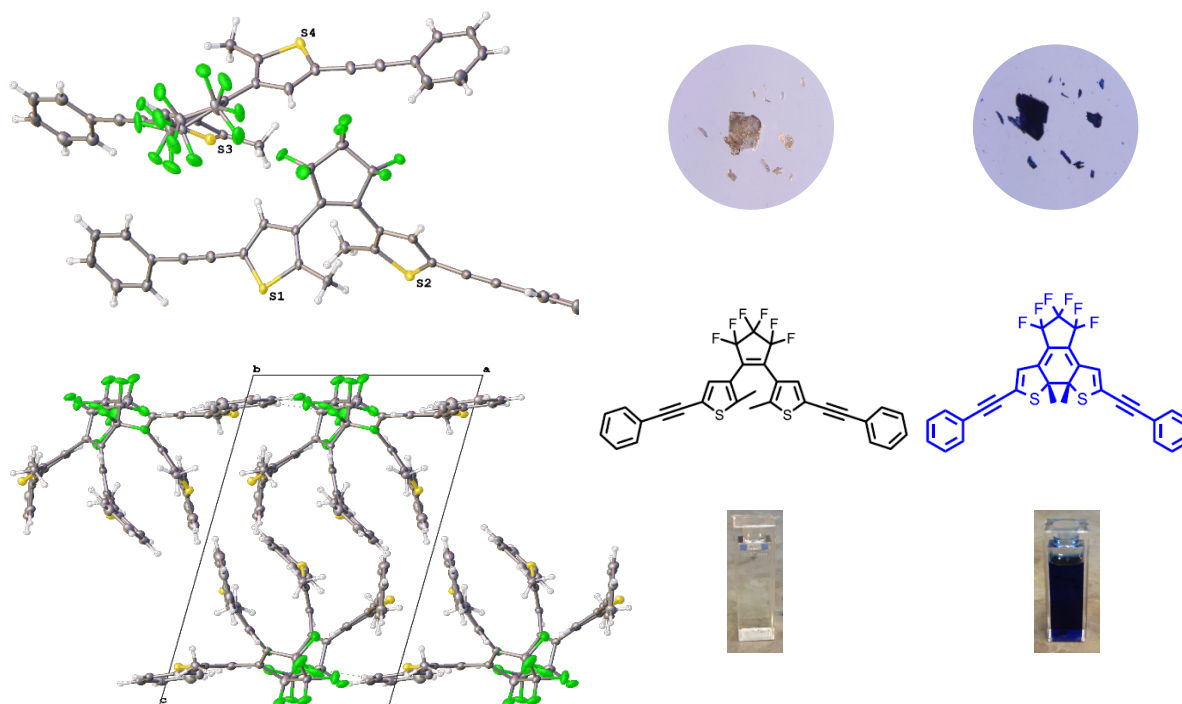
4.4.1.5 X-Ray Crystallography Analysis of Compound **MC1**

Figure 4.18 X-ray crystallographic analysis of **MC1**. A clear, pale-blue rod-like crystal of **MC1**, approximate dimensions 0.060 mm x 0.080 mm x 0.320 mm, was used analysis and yielded the shown unit cell and packing structure. Compound showed photochromic switching capability in both solid and whilst in solution.

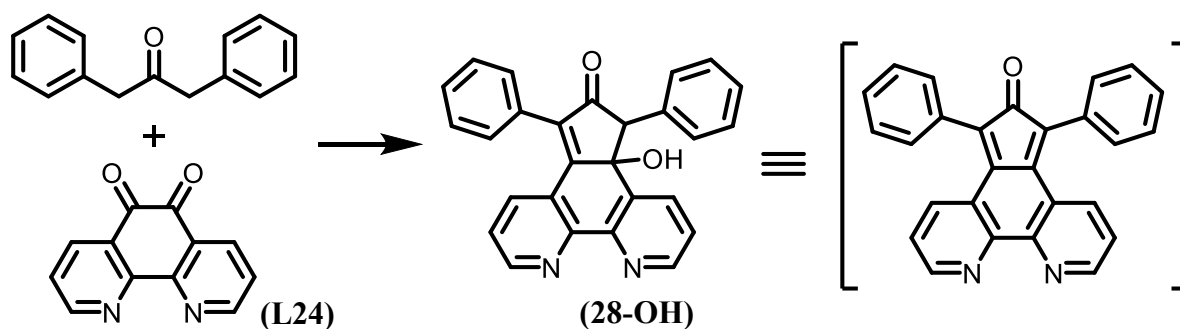
Single crystals of compound **MC1** which were adequate for X-ray diffraction study were isolated through slow evaporation from a hexane:CH₂Cl₂ solvent system over a period of four weeks. The open isomer's structure parameters shown at 50% probability. One fluorinated ring shows some disorder and is thus modelled in two positions with 68:32% occupancy. This disorder is most likely due to the presence **MC1c** during initial analysis, due to the presence of light within the machine. The compound retained its photochromic behaviour even in the solid phase (Figure 4.18), due to the anti-parallel stacking of molecules in the unit cell. The quantum yield of the product in this solid state is intended to be included in future work.

Compound **MC1** is a simple example of a DTE molecular switch of high purity, as indicated by the resolution of the ¹H NMR spectrum, the overlap of the excitation and absorbance spectra and the isolation of crystals that were suitable for X-ray diffraction. The compounds lack of intricacy in its molecular framework resulted in poor fatigue resistance (10 cycles to 80% conc.) but the quantum yield ($\Phi_{0 \rightarrow c} = 32\%$) is within a good range for potential use in

a system. Compound **MC1** allowed for initial analysis of spectral evaluation techniques associated with molecular switches and serves as a benchmark with which consequent switches synthesised could be compared. It also acted as a precursor for much more extensive molecular frameworks.

4.4.2 Retrosynthetic Route 2

4.4.2.1 Synthesis of of 5,7-diphenyl-6H-cyclopenta[f][1,10]phenanthrolin-6-one, **28**



*Scheme 4.5 Optimised synthetic routes to **28**. i) MeOH, KOH, rt, 12 h, 56 %. ii) Al₂O₃, chlorobenzene, 130 °C, 24 h. iii) Microwave assisted synthesis; Al₂O₃, 1:9/CH₂Cl₂:THF, 125 °C, 150 W, 0.5 h.*

Heteroatom “doping” of PAHs permits the ability for complexation to metal centres with the heteroatoms acting as donor atoms. Though not doping in the traditional sense, exchanging carbon atoms for specific heteroatoms in the initial synthetic stages allows for a potential systemic framework to be realised, with properties of both π -frameworks and metal-chelation sites. Indeed, the extent of heteroatom incorporation allows for changes in the coordination environment of the metal centre, with the added ability to control mono vs. multidentate binding, depending on the metal of choice. This allows for the rapid generation of a number of different but similar ligand systems which would display different opto-electronic properties.

For this work, interest was primarily focused on expansion of the 1,10-phenanthroline moiety to act as a cyclopentadienone type reactant. Scheme 4.5 shows the final synthetic pathway developed by the Draper group towards this final product. Due to the ineffective synthetic routes attempted to generate the desired a reactive aryne type ligand, a new approach was needed to reach the ultimate goal of synthesising the novel diene. Unfortunately, **28** was known to be a challenging ligand to work with due to its moderate

sensitivity to atmospheric conditions, preferring to exist as the air stable 4b-hydroxy-5,7-diphenyl-4b,5-dihydro-6H-cyclopenta[f][1,10]phenanthroline-6-one, **28-OH**. Compound **28** was previously fully characterised by members of the group. A full NMR characterisation of the compound was undertaken and experimental spectra are consistent with the air stable hydroxyl product. **28** is a dark, intense blue, which is in stark contrast to the pale translucent yellow of the **28-OH**. Optimisation of the dehydration reaction and novel workarounds developed to counteract these synthetic challenges are now discussed.

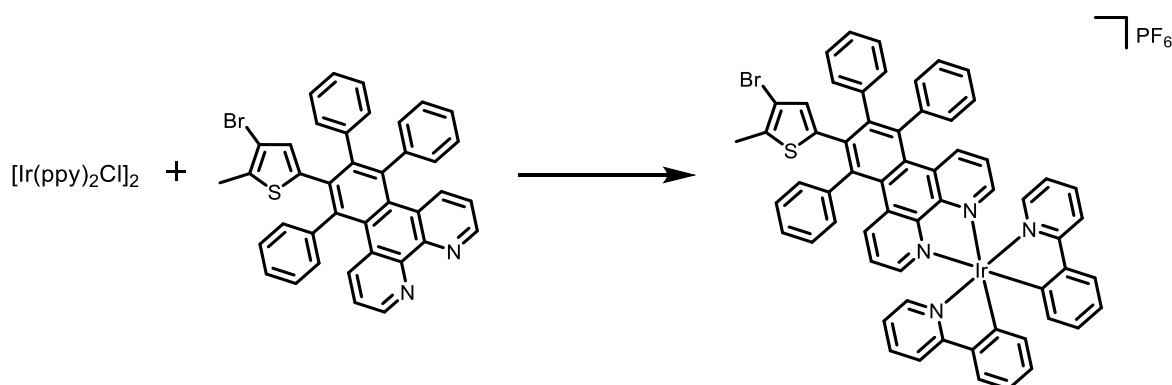
28 is a cyclopentadienone type ligand with a desirable 1,10-phenanthroline moiety as its core ring system. The synthesis of **28** was expected to be completed in a similar synthesis to that of the commercially available tetraphenylcyclopentadienone, with **L24** and 1,3-diphenyl-2-propanone, in a KOH catalysed Knoevenagel-like condensation in EtOH.²²⁶ Surprisingly, the sole product of this reaction is **28-OH**. In the synthesis of tetraphenylcyclopentadienone, the similar hydroxyl-product is reported but only in negligible quantities. Before the undertaking of this report, **28-OH** could be dehydrated to **28** using two methods, the first being a high temperature dehydration (280 °C) in a benzophenone melt, the second being an acid catalysed dehydration at lower temperatures (120-130 °C) in 1,2-dichlorobenzene. Both of these methods were considered undesirable, as at high temperatures, the rate of side product formation is expected to increase dramatically. The risk of Diels-Alder reactions occurring between two molecules of starting material is also increased. At lower temperatures, the use of acid was not welcome due to the potential for co-reagent acid-sensitivity. For the successful use of **28** as an attractive ligand system precursor, optimisation of the dehydration reaction at lower temperature and without acid was at first deemed necessary. An optimised route to **28** was thus presented in high yield with the novel use of alumina, Al₂O₃, as a dehydrating agent. As the intermediate is sensitive to atmospheric conditions, and appears to only be present as the cyclopentadienone product in solution, subsequent reactions must be carried out immediately. Product yield in subsequent reactions of **28** offer a determination of conversion to the cyclopentadienone product. Whilst not ideal, the high yields found with further reaction indicate very high conversion to the cyclopentadienone intermediate.

For both reactions, a microwave assisted process and a conventional style synthesis, the use of solvent was found to be extremely important. As the microwave assisted synthesis was attempted first, a very large number of solvents were tested in the optimisation process for

this reaction. It was found that the poorest results were found in polar solvents like MeOH and EtOH. These were initially chosen as they are known to be ideal solvents for microwave synthesis, due to their high dielectric constants. A 1: 9 mixture of CH₂Cl₂: THF was found to be a highly successful solvent system for conversion when combined with a small arbitrary amount of alumina. The moderate dielectric constant of THF allows for the required temperature to be reached, while the small amount of CH₂Cl₂ aids in the solubility of **28-OH**. With this in mind, the method was optimised for conventional synthetic means, retaining the use of alumina in refluxing chlorobenzene.

However, it was quickly realised that due to the dehydration occurring more readily at higher temperatures, reacting in benzophenone at 280 °C would allow the concurrent Diels-Alder reaction to occur. Despite the need for this activation of the hydrocyclopentadienone, this method allowed for the procedure of the retrosynthetic analysis towards the unabridged switch appendages, and how the study of these individual moieties can lead to a great understanding of similar processes in the final products. The risk of coupling with another molecule of **28** was also a notable risk, however for the purposes of these reactions it was deemed a viably worth option due to it enabling a direct Diels-Alder reaction compared to trying to isolate the phen **28** intermediate.

4.4.2.2 Synthesis and NMR characterisation of Ir-7



Scheme 4.6 Synthesis of Ir-7 through complexation of 29 to Ir(ppy)₂ following heating for 12 hours at 45 °C and consequent exposure to a source of the counterion PF₆⁻.

The retrosynthetic analysis of Ir-7 is detailed in Scheme 4.6. As described previously, in the highly acidic conditions provided by a combination of sulfuric and nitric acid and in the presence of KBr, 1,10-phenanthroline yielded phendione **L24** following reflux at 130 °C for

4 hours. The diketone is thus suitable for a subsequent double Knoevenagel reaction. **L24** is stirred for 2 hours at room temperature with 1,3-diphenylpropan-2-one in the presence of KOH causing the production of the tetraarylcyclopentadione, 4b-hydroxy-5,7-diphenyl-4b,5-dihydro-6H-cyclopenta[f]-[1,10]phenanthroline-6-one, **28**.²²⁶ The presence of the ethylene moiety of 3-bromo-2-methyl-5-(4-*tert*-butylphenyl-acetylene)thiophene, **L23**, enables it to act as a dienophile and undergo a [4+2] Diels-Alder cycloaddition²²⁶, with **28** acting as the diene. This yields 6-(4-bromo-5-methylthiophen-2-yl)-5,7,8-triphenylbenzo[f][1,10]phenanthroline, **29**, and is driven to completion by heating to 280 °C for 2 hours, the shorter reaction time than normally attributed to these reactions due to the decomposing nature of the phentetracyclone.²²⁶ While purification of the compounds along this route proved extremely difficult due to cationic binding abilities of the aromatic nitrogen containing rings, this moiety would prove to be perfect for chelation to an iridium metal centre. The synthesised dimer $[\text{Ir}(\text{Ppy})_2\text{Cl}]_2$ served as a source of iridium, and generates complex Ir-7 under mild reaction conditions, 45 °C for 12 hours in CH_2Cl_2 , in moderate yields. Addition of NH_4PF_6 in methanol and purification using TLC chromatography on silica (MeOH: CH_2Cl_2 , 2: 98) separated the product as a bright orange solid.

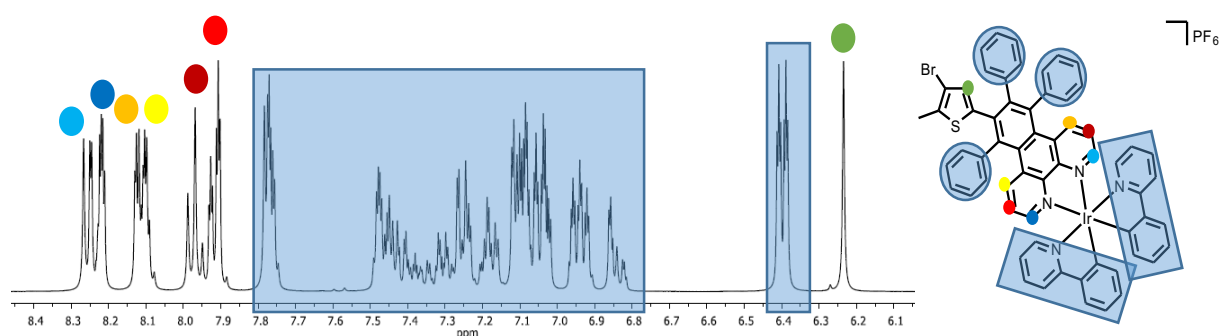


Figure 4.19 ^1H NMR of **7** in CD_2Cl_2 displaying large amounts of non-first order coupling in the aromatic region. Upfield methyl signals not shown for clarity. (400 MHz, RT)

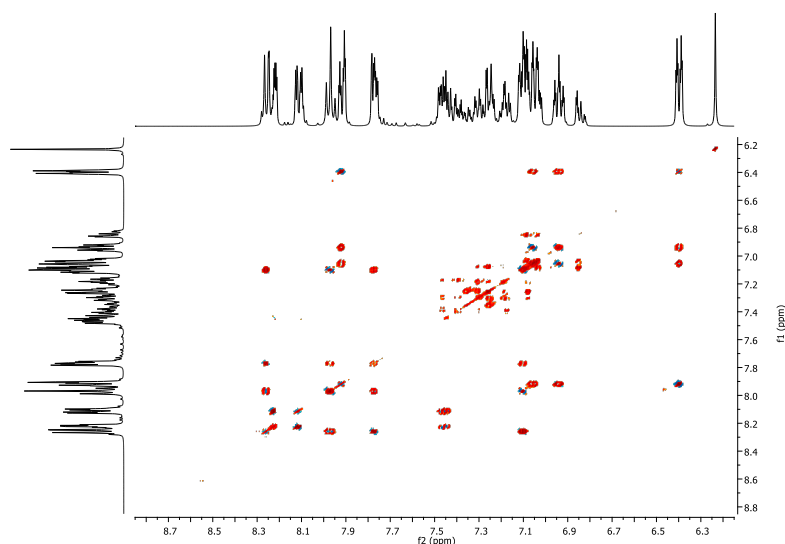


Figure 4.20 H-H COSY of the aromatic region of complex **Ir-7**.

The phenanthroline protons are unevenly split, due to the unsymmetric nature of the chelating platform (Figure 4.19 and 4.20). Due to the constrained nature of the phenanthroline moiety, this type of π platform is twisted and has much less rotational freedom than the HPB moieties explored thus far. The single bond “cyclodehydrogenation” inherent in phenanthroline substituents compared to their bipyridial and phenylpyridal counterparts, may allow a degree of conjugation in the system not yet explored in this work, and the twisted nature of the entire ligand has as of yet unexplored effects. The phenyl and pyridal protons appear as a series of peaks from 6.8 – 7.5 ppm. Assignment of these peaks proved difficult due to the similar yet slightly distorted nature of the complex. The phen and thienyl signals, however, proved much more analogous and easier to assign. The singlet at 6.23 ppm, assigned to the thiophenes single proton, appeared at similar shift other thienylsubstituted HPB platforms. There is a large and noticeable shift of the phen protons, comparing the ^1H NMR of compound **29** and that of **Ir-7**. The phen protons appear as much more shielded signals upon chelation to the metal centre. This may be explained by the large extension of Ir(III) molecular orbitals, much spread from the metal to the surrounding chelation sites. Thus to the molecular orbitals of the complex **Ir-7** shows much more metal and ligand character, than analogous 1st or 2nd row transition metals would.

4.4.2.3 Photochemical Analysis of Ir-7

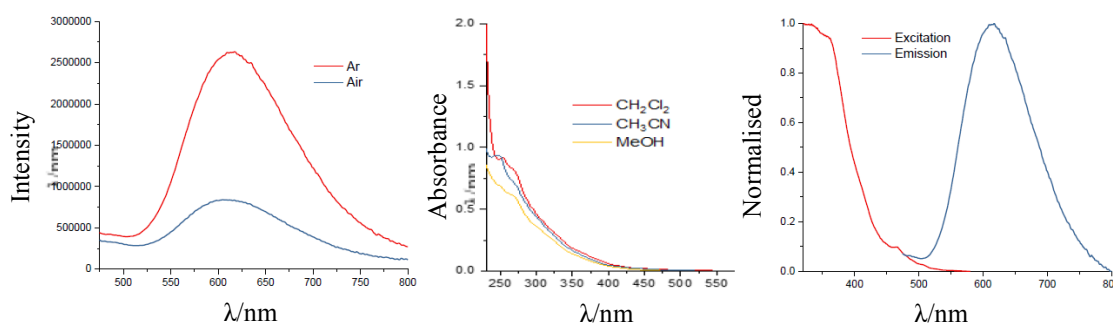


Figure 4.21 Photochemical analysis of compound **Ir-7** showing (a) increased luminescent intensity upon degassing with Ar, suggesting strong phosphorescent character, (b) solvation studies of **Ir-7**, and (c) excitation and emission spectra under Ar ($\lambda_{exc} = 440$ nm, $\lambda_{em} = 610$ nm, 1×10^{-6} M).

The absorbance spectra of **Ir-7** was recorded using solution of 1×10^{-6} M in various solvents, however no immediate comparatives could be noted as solvent polarity was increased (Figure 4.21). Two strong bands are observed at 250 nm and 275 nm which correspond to ligand centred transitions arising between the phenylpyridine and phenanthroline moieties of the complex. The spectra gradually trails off from the shoulder present at 275 nm. The continuous low absorbance associated with this region, $\lambda > 500$ nm, may be assigned to an aggregate of mixed spin character excited state transitions which are characteristic of the spin-orbit coupling associated with iridium complexes.²²⁷ However, within this region there are two absorbance bands of note, the first is that of the mostly spin-allowed MLCT transitions, which corresponds to transitions from 300 to 440 nm. The second corresponds to that of the ³MLCT which are responsible for a large proportion of absorbance in the region of to 440 nm to 480 nm, the low intensity of these transitions may be ascribed to their spin-forbidden nature and would not be observed if the ligands were chelated to a metal-centre with a lower spin-orbit coupling affect. Iridiums spin-orbit coupling character facilitates these spin-forbidden transitions between singlet and triplet states via intersystem crossing. These transitions and their effect on the complexes optoelectronic properties are more apparent from the excitation spectra. A strong decrease in luminescent intensity upon exposure to air further suggests the strong role and triplet character of the compound.

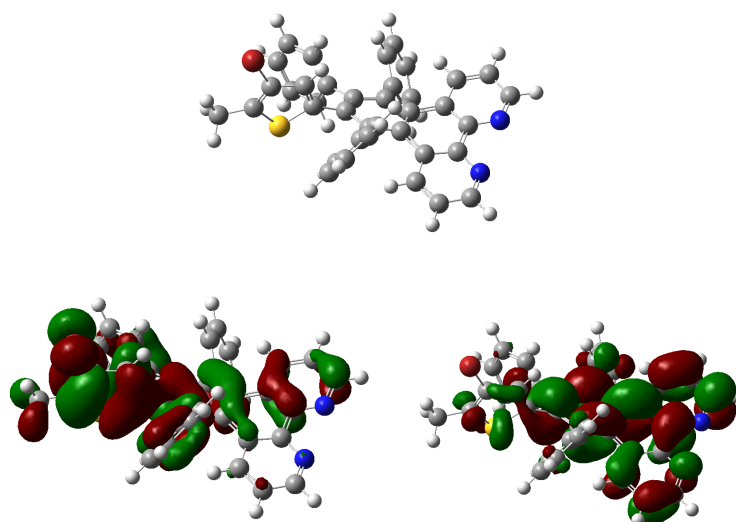


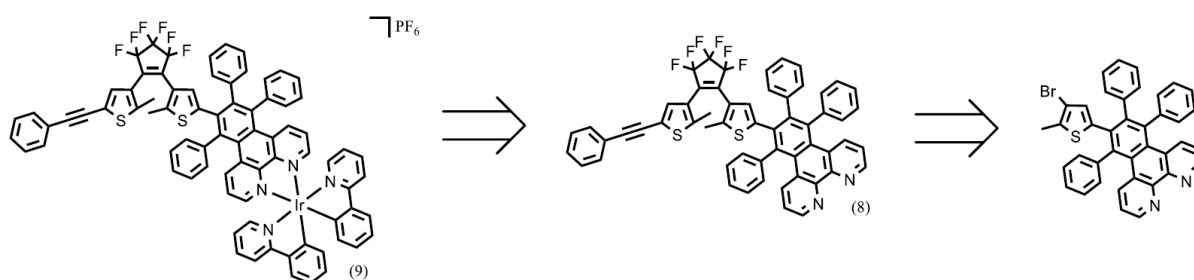
Figure 4.22 Initial computational experiments show (a) the selected orientation of the organic π -platform, (b) the HOMO character of the ligand which exists mainly on the thienyl moieties and (c) the LUMO which is delocalised across the phen moiety and through the spinning triphenyl groups.

Before the 1990s, a few quantum chemical investigations of ruthenium complexes had been published, and for most of them, the semi-empirical calculation methods, such as EHMO, INDO, SINDO, MNDO, AM1, etc. were applied.²²⁸ One of the problems in applying an ab initio quantum chemistry method to the polypyridyl complexes of second- or third-row transition metals is that such systems are too large to computations, and the other one is the considerable effects of electron correlations on binding energies, which is usually not accounted for in a traditional Hartree-Fock calculation, except for applying configuration interaction (CI) methods, and Møller-Plesset perturbation theory²²⁹ needing a terrible computational expense. Since the 1990s, in particular, recently, with the high-speed development of computer technology and the wide applications of G94/G98 program packages,^{230,231} it becomes possible to calculate strictly some bigger transition metal complexes. Some computations applying density functional theory (DFT) method²³² and using LanL2DZ basis set²³³ have been reported²³⁴, because of their accounting better for electron correlation energies and reducing greatly the computation expenses.

However, so far, the reports of studies on transition metal polypyridyl complexes (especially those of second-row and third-row transition metals) with DFT method are still less found, and maybe some computational works on this field have escaped our attentions. When quantum chemical computations are applied to transition metal polypyridyl complexes with

a relatively large size, undoubtedly the computations of energies and spectrum properties of complexes in an absolute meaning still have some disparities, but the most important thing is to obtain some regularities on the electronic structures and related properties of the complexes with similar structures. For this purpose, the DFT method maybe the most suitable. Calculations with the inclusion of the metal centre and/or the switching moiety could not be performed at the time due to the time-scale and resources involved. However, DFT calculations on the tetraaryl-substituted 1,10-phenanthroline, **29**, allow for a comparative study towards understanding the orbital energies of complex **29** and subsequent switches, **30** and **Ir-8** (Figure 4.22). With the HOMO located on the thienyl moieties and the LUMO delocalised across the phen-platform, electron traffic seems to proceed in the opposite direction initially hoped. Due to the predicted low-lying nature of the $^3\text{MLCT}$, the absorption of energy via the thienyl moieties may funnel electron density toward the metal, and thus be lost radiatively or non-radiatively via this energy pathway. Analysis of the photophysical properties of switches **30** and **Ir-8** seemed to later confirm this.

4.3 Ir (III) based molecular switch



Scheme 4.7 Retrosynthetic analysis of molecular switches **30** & **Ir-8**.

4.3.1 Synthesis and NMR analysis of 6-(4-(3,3,4,4,5,5-hexafluoro-2-(2-methyl-5-(phenylethynyl)thiophen-3-yl)cyclopent-1-en-1-yl)-5-methylthiophen-2-yl)-5,7,8-triphenylbenzo[f][1,10]phenanthroline, **30**

The synthesis of compound **30** was achieved through the [4+2] Diels-Alder cycloaddition of 4b-hydroxy-5,7-diphenyl-4b,5-dihydro-6H-cyclopenta[*f*][1,10]phenanthroline-6-one **28-OH** and the previously characterised compound **MC1** using similar reaction conditions discussed for the synthesis of product **29**. The diene **28-OH** was added in 1.5 molar excess to the switching compound. This was due to the potential for both a single and double Diels-Alder reaction to occur, and the subsequent purification of compound **30** and **31**. However, though

both **30** and **31** were found by mass spectral analysis, compound **31** was only found in very low yields, and proved extremely difficult to purify. This was due to the two nitrogen-containing appendages available on this novel moiety, as well as its overall molecular size. The instability of **28** at higher temperatures also impacted these results and even multiple repeats of this reaction did not result in sufficient product **31**. As such, the unsymmetrical compound **30** was chosen for study and participation in on-going metallating reactions with an Ir(III) metal centre.

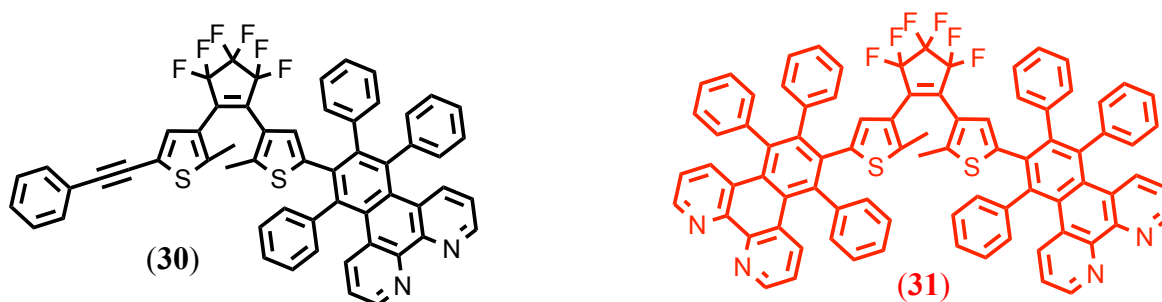


Figure 4.23 Products of reaction between **28** and **MCl**. Product **30** was collected in substantial yield, however, product **31** was only recorded via mass spectrometry and could not be separated.

4.3.1.1 NMR Analysis of Compound **30**

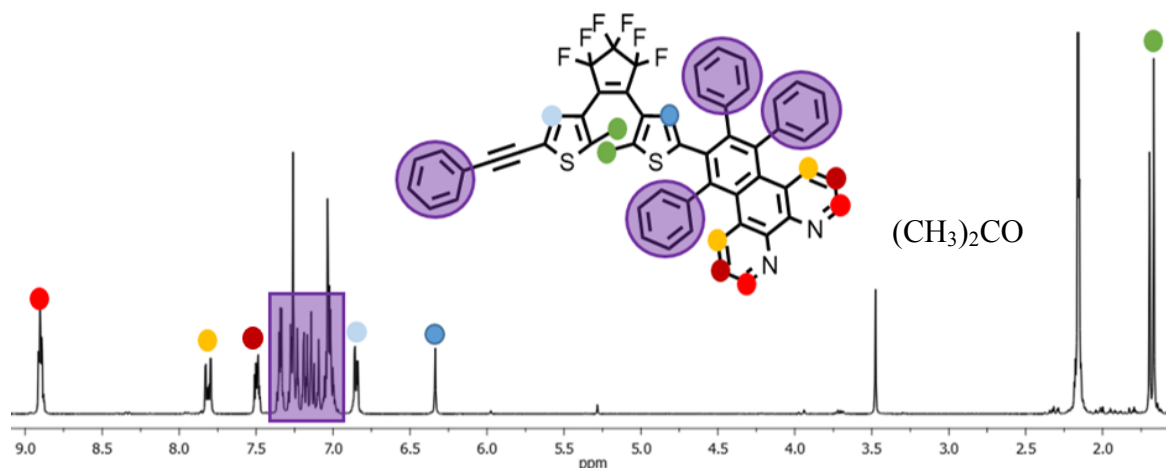


Figure 4.24 ^1H NMR of Compound **30** in CDCl_3 with overlapping phenyl signals highlighted

The three most downfield resonance signals of the ^1H NMR (Figure 4.24) of compound **30** confirms the incorporation of the 1,10-phenanthroline moiety into the DTE derivative via the Diels-Alder cyclisation reaction. Each of the phenanthroline proton signals (●, ●, ●) were observed at their expected positions with correct integration values. The protons of the

4 and 4' positions of the thiophene rings are observed as a singlet at 6.34 ppm and 6.75 ppm (●, ●), considerably more upfield relative to their positions in compound **MC1** (7.26 ppm). This is a result of introducing the highly electron rich delocalised platform associated with these phen-based compounds. The protons of the phenyl rings responsible for the electron richness of this system have been indicated and the resonances can be seen between 7.0 ppm and 7.4 ppm, within the expected region of aromatics, as a cluster of multiplets. The chemical environment of the phenyl ring bonded to the DTE moiety via the acetylene spacer, as expected, has experienced little to no change in its NMR pattern and the signals are observed in a very similar position in both compounds **MC1** and **30**. The direct assignment of the aromatic signals proved to be difficult due to the non-first order coupling occurring between the protons. However, the phenanthroline signals experienced a much less severe splitting pattern than that observed for **29**, though they appeared at similar positions. This is mostly due to the removal of degeneracy of the thiophene rings, and an extension of their internal electronic back through the ethane backbone and less through the central benzo[f][1,10]phenanthroline moiety. This returns the symmetry to this part of the switch and the proton signals appear less overlapped. This also has interesting properties for the thienyl protons, which show a large chemical shift due to the nature of their environment. HSQC of compound **30** (Figure 4.25) was also used in the assignment of appropriate proton signals.

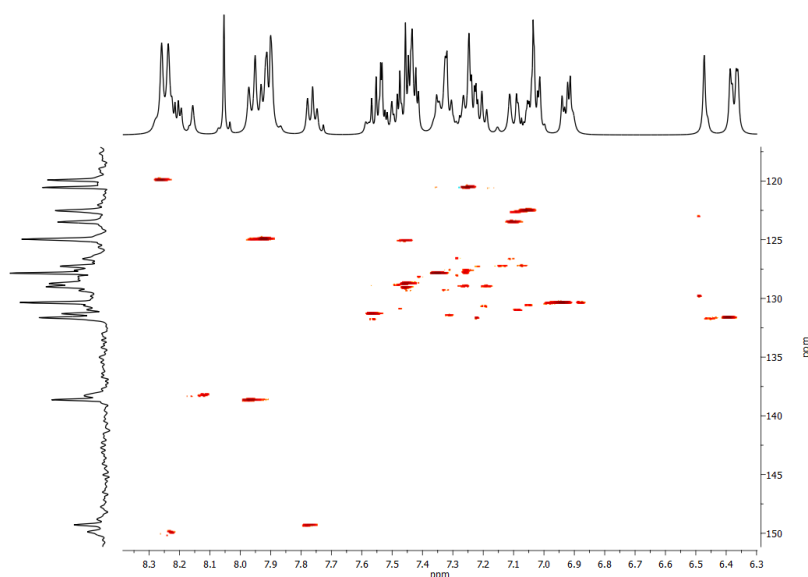


Figure 4.25 HSQC of compound **30**.

4.3.1.2 Photochemical Analysis of Compound 30

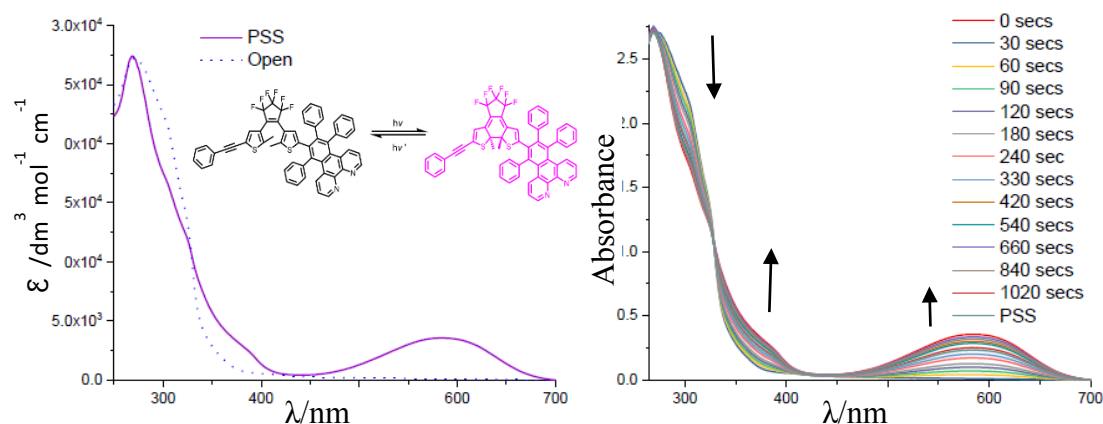


Figure 4.26 (a) UV-Vis Spectrum of **30** (b) UV-Vis Irradiation Spectrum of **30**

Figure 4.26 (a) displays two spectra recorded with a 2.5×10^{-5} M concentration in acetonitrile, the open form, **30o** (---) and the photostationary state PSS, **30c** (—), which describes the concentration at which the photoisomers are in dynamic equilibrium. The open form absorbs strongly in the UV region of light with an absorbance maxima of 250 nm while the closed photoisomer corresponding to the PSS also absorbs in this region, though not as strongly. The lack of absorbance in the visible range of the open form results in its clear colour. The PSS is observed as a dark blue solution due to strong absorbance of light of red wavelength, centred at 583 nm. The photochemically driven cyclisation reaction that results in the closed form extends conjugation into the π conjugated groups at the 2/2' positions of these thiophene rings. However, the slight blue-shift relative to the less conjugated switch **MC1** may be attributed to the increased delocalised anti-bonding character of the orbitals. Figure 4.22(b) displays the large variance observed in the transitions associated with the closed and open form isomers as solution is irradiated with UV light ($\lambda_{\text{exc}} = 360$ nm). As the exposure time increases, the absorbance maxima of **30o** (315 nm) decreases and the absorbance maxima of **30c** (583 nm) shows the observed increase. The opposite trend is observed when the solution is exposed to light in the visible region. While it is possible to cause all photoactive molecules to theoretically assume the open form as shown in Figure 4.22(b) (0 sec), it is much harder to ensure complete isomerisation of photoactive molecules in solution to the closed form due to the competing nature of the absorption patterns of the two isomers.

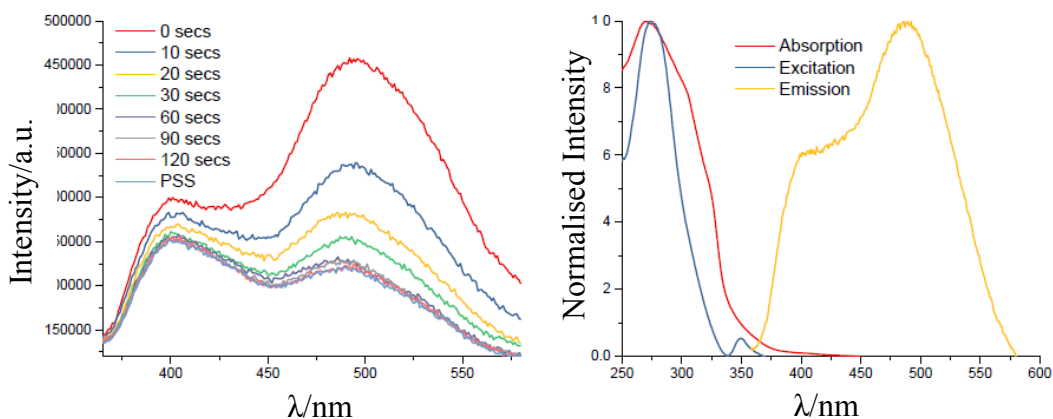


Figure 4.27 (a) Luminescence quenching of **30o** and (b) emission, excitation & absorption spectra of **30**

The emission spectra Figure 4.27 (a) displays the fluorescence quenching that occurs upon photoisomerisation from the open to the closed state recorded using a 1×10^{-5} M solution in CH_3CN . The chemical equilibrium is pushed as far as possible towards the open form isomer through bleaching with visible light, yielding the 0 second emission spectra. The solution is then irradiated with UV light $\lambda = 330$ nm, the absorbance maxima of the open form in order to drive forward the population of the closed isomer. As the concentration of closed isomer increases the fluorescence of the of the solution drops. The sharpness of this drop is due to the energy that is lost in the non-radiative isomerisation of the molecules and due to the fact that it is unlikely that the closed form fluorescence. Once the PSS is reached i.e. the concentration of closed form isomers has reached its maximum value, irradiation with UV no longer causes a decrease radiative emission. The remaining open form molecules are free to undergo emissive relaxation following irradiation. The closed form isomers populating the solution, due to the lowering of the HOMO-LUMO energy gap via an increase in conjugation, undergo a relaxation pathway which seems to occur non-radiatively. The excitation and emission spectra obtained were recorded using a 1×10^{-6} M solution in CH_2Cl_2 via irradiation with UV radiation, $\lambda_{\text{exc}} = 315$ nm, $\lambda_{\text{em}} = 500$ nm (Figure 4.23(b)). The excitation spectrum corresponds to the transitions directly responsible for emission from the S_1 energy level, while the absorption corresponds to all $S_0 \rightarrow S_n$ transitions, where S_n represents all excited states with wave functions of suitable overlap relative to S_0 . In theory, the spectra obtained should overlap well, as any excess energy gained in the promotion of an electron from $S_0 \rightarrow S_n$ should be lost in the non-radiative vibrational relaxation from $S_n \rightarrow S_1$, the consequent $S_1 \rightarrow S_0$ emissive decay should then be identical to that of the excitation spectra. The spectra did align well for their absorbance maxima. However the

broadness of the absorption spectrum may imply that some non-radiative deactivation pathway exists for the relaxation from S_1 , or relaxation may occur directly from higher energy levels directly to S_0 . A large Stokes shift of 45454.55 cm^{-1} is observed, this is most likely due to the large amount of vibrational energy used in relaxation from high energy transitions introduced by the 1,10-phenanthroline moiety.

4.3.1.3 Synthesis and analysis of Ir (III) complex Ir-8

Compound **30** and the dimer $[\text{Ir}(\text{Ppy})_2\text{Cl}]_2$ were heated to $45\text{ }^\circ\text{C}$ for a period of 12 hours. NH_4PF_6 in methanol was consequently added as a source of counterion²³⁵ and yielded **Ir-8** as an orange solid. The switch complex was then purified using TLC chromatography, with CH_2Cl_2 : MeOH (100: 3.5) as eluent. Numerous purification methods were employed towards the final purified product. This was seen mostly due to the creation of iridium based side products, and the slow retention factor of Ir-9 in most solvent systems. Upon purification, Ir-9 was yielded as a dark solid, which displayed slight photochromic behaviour and exhibited strong red emission.

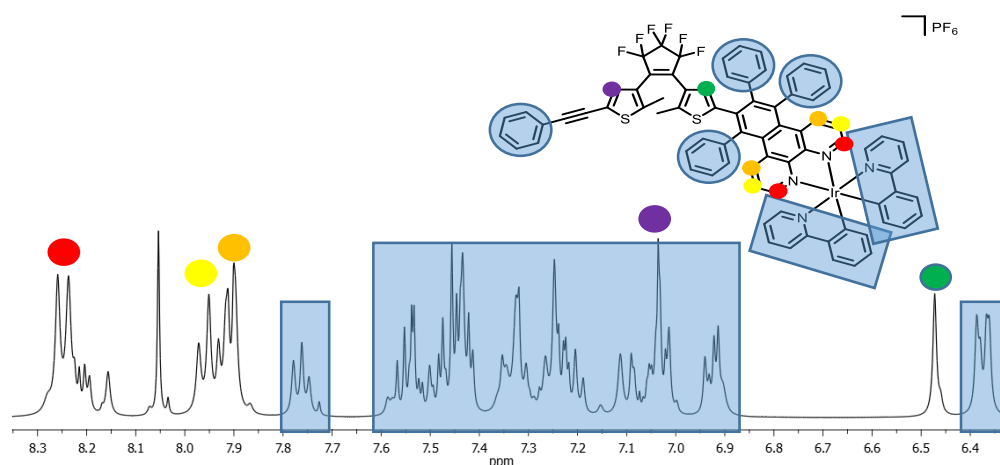


Figure 4.28 ^1H NMR of Ir-8 displaying a very similar spectral pattern to that of **8**, however with the additional signals corresponding to ppy ligands and subsequent shielding of the phenanthroline protons upon complexation.

Assignment of the geometric structure of compound **Ir-8** (Figure 4.28) was achieved using ^1H NMR, ^{13}C NMR (Figure 4.29), ^1H - ^1H COSY, ^{13}C - ^1H HSQC and long range HMBC (Figure 4.30) experiments, and confirmed by mass spectrometry, a technique that helps identify the amount and type of chemicals present in a sample by measuring the mass-to-charge ratio and the abundance of gas ions present.

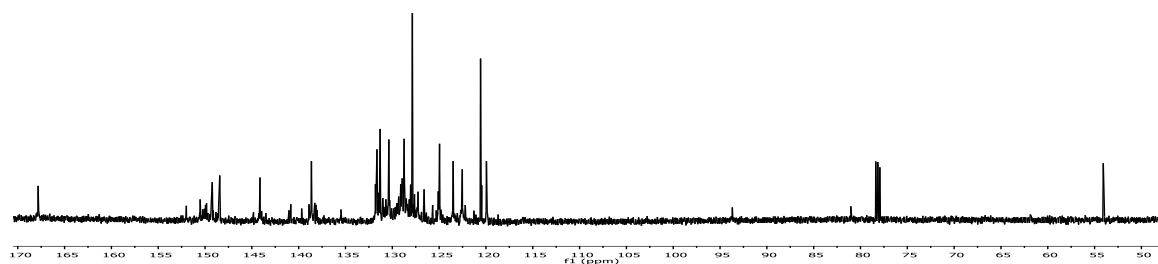


Figure 4.29 ^{13}C spectrum of **Ir-7**

As with **Ir-7**, the protons nearest the nitrogens of phenanthroline moiety are more upfield compared to their non-chelated counterparts. This may be due to the fact that due to the size of the iridium nucleus, its orbitals extend much further outwards than is seen in metals such as ruthenium, most notably the LUMO. As such, the electron cloud extends into the surrounding ligands, including the phen-ligand, and offers more shielding of the surrounding protons. The thienyl protons also experience a similar shift to that seen in **Ir-7**. Unsurprisingly, **Ir-8** exhibits properties in the range seen of **Ir-7** and compound **30**, both in terms of chemical shifts in carbon and proton spectra, and its photochemical ability.

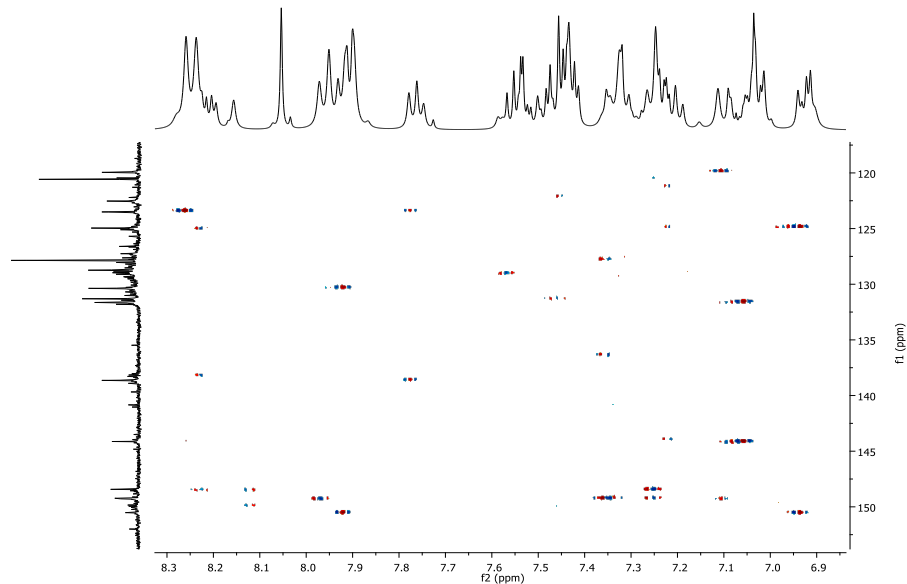


Figure 4.30 HMBC of Ir(III) switching complex **Ir-8**

4.3.1.4 Photochemical analysis of Ir-8

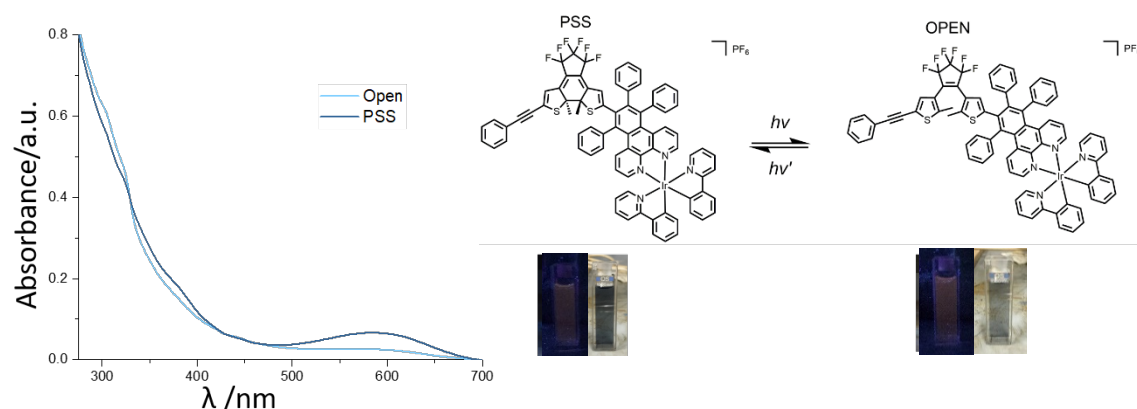


Figure 4.31 (a) Absorption spectrum of open and PSS states of **Ir-8** (2.5×10^{-5} M) and (b) isomer interconversion and phosphorescence of **Ir-8** in air.

The absorption spectra of **Ir-8** (Figure 4.31) was recorded in CH_3CN at a concentration of 2.5×10^{-5} M. It exhibits the characteristic absorbance maximas of a DTE based molecular switch, with the intense band in the visible region at 330 nm corresponding to the $\pi \rightarrow \pi^*$ transitions of the open form, **Ir-8o**, and that of the closed form, **Ir-8c**, occurring at 583 nm. The relative intensities of the thiophene centred transitions are far more skewed towards the visible region relative to the non-chelated switches examined thus far. This is as a result of the metals dominance on the photochemical properties of the molecule. As seen in the case of compound **Ir-7**, there are intense absorbance bands in the UV region centred on LC transitions stemming from the phenylpyridine and phenanthroline moieties of **Ir-8** (370 nm). The range of particular interest, 500 to 700 nm, may be that of the nominally disallowed $^3\text{MLCT}$ transitions, and direct population of this orbital via the ground state upon excitation. In the case of the previous switch, **30** these transitions levelled off to zero, however upon chelation of a well conjugated dithienylethene moiety, these transitions maintain a base level of intensity within the region of visible light, resulting in a dark grey solution in the PSS and a black solution at high concentration of closed form isomers (Figure 4.31 (b)) due to increased absorption of visible light. As seen in the theoretical calculations of the delocalised platform **6**, the thienyl moieties lie at a higher energy than was expected, with the emissive pathway occurring via the phenanthroline ligand.

This suggests that switch and iridium absorptions are competing processes (with both the Ir(ppy) and thienyl absorption bands usually occurring within the 330-370 nm range), and

all deactivation passes through the MLCT band of compound **9**. Both **9o** and **9c** display minimal difference in phosphorescent intensity (luminescence observed in cuvettes of Figure 4.31 (b)).

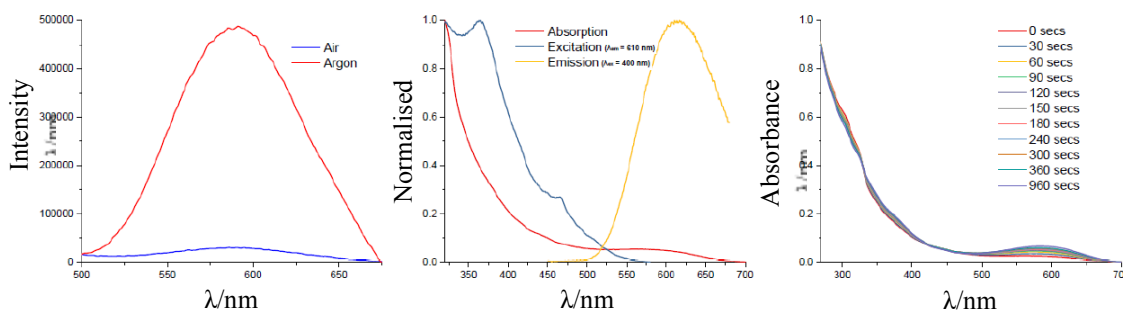


Figure 4.31 (a) comparison of the luminescence intensity under Argon and in air, (b) the excitation, emission & absorption in CH₃CN at $1.2 \times 10^{-5}M$ concentration and (c) UV-Vis irradiation spectrum of **Ir-8**.

The emission band at 590 nm (Figure 4.32 (b)) are typical of the ³MLCT for these type of Ir(III) complexes, further supported by the featureless appearance of the luminescence profile. Significant quenching was observed when the solutions were exposed to air (Figure 4.32), further indicating phosphorescent character. Future work of measuring phosphorescence lifetimes and their subsequent quantum yields should be undertaken to support this initial research. The excitation and absorption spectra offer the same relative profile, however the excitation profile suggests that nearly all excitation wavelengths between 250 and 450 nm result in phosphorescence from the switch, with the peak at 370 nm indicative of Ir(ppy) absorption, and the shoulder at 460 nm is a prominent MLCT absorption feature. The extension of the absorption of **Ir-8o** well into the visible region may suggest some direct population of the ³MLCT energy level, however with the strong absorption of such disallowed transitions, further study is required. Excitation into this absorption band produced negligible emission from the complex, and the strength of this band in the UV-Vis may indicate a radiationless decay from ³MLCT via this excitation. Emission in this region is common for phen-substituted Ir(III) complexes.

It was hoped that the iridium centre may act as an energy funnel to facilitate photocyclisation and photocycloreversion at lower energies, however the phosphorescent profile suggests that the complex is emitting this energy as a photon instead, and is in fact a competing process to the molecular switching, or is itself enhanced by the thienyl absorption bands. The

extension of the $^3\text{MLCT}$ absorption into lower wavelengths also suggests that the energy levels of the complex are lower than those of the switch, and is thus acting as an energy well for all switching processes. A small amount of photocyclisation is observed upon irradiation into the 410 nm MLCT band, however this may be direct absorption of the switching platform as a competing process to the iridium emission rather than direct conjugate communication. This is in agreement with the initial DFT calculations of the non-metallated platform **29**, with the HOMO existing on the aromatic thiophenes and the LUMO spread across the phen and phenyl substituents.

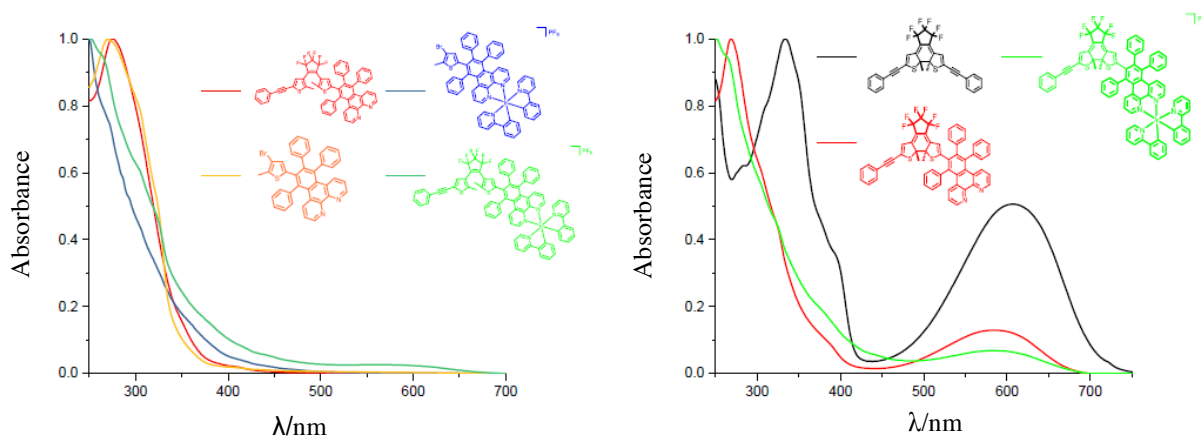


Figure 4.33 Comparison of absorbance spectra of (a) **29**, **Ir-7**, **30o** and **Ir-8o** and (b) **MC1c**, **30c** and **Ir-8c**

Through comparative normalised stacking of the absorbance spectra of the four synthesised compounds (Figure 4.33), it is apparent that the metal centre plays the largest role in determining the photochemical properties of the compounds synthesised. In the iridium complexes (**Ir-8** – green, **Ir-7** – blue) a steep decline is noted from the maxima. The transitions in this region correspond to spin allowed ligand centred transitions. While this does include the $\pi \rightarrow \pi^*$ transition of the open form DTE, it is obscured. **Ir-7** continues to absorb slightly in the visible region ($\lambda > 450$ nm), though this extension is a far more prominent feature of complex **Ir-8** ($\lambda > 700$ nm). Spin allowed MLCTs can be seen in the region of 300 to 440 nm. The lower ϵ values recorded are due to the disallowed nature of the MLCT based transitions and the subsequent ISC from singlet to triplet states. The intensity of **Ir-8** is higher relative to **Ir-7** throughout the visible region possibly due to an extension of the $^3\text{MLCT}$ from closed form DTE moiety to the Ir(III) centre, or due to the inability of the complex to exist as a fully open system. The high degree of overlap suggests the similarity of the photochemical properties of the non-chelated compounds (**29** – orange, **30** – red).

Past the visible region no notable absorbance maxima are observed, in the case of **30** this is due to the spectra being recorded in its open form. In compound **29** the lack of a second thienylethene unit prevents absorbance in the visible region associated with a closed form isomer. Upon comparison of the photochromic switch molecules (**Ir-8** – green, **30** – red) it is noted that the absorbance maxima corresponding to the $\pi \rightarrow \pi^*$ transitions of the open (315 nm) and closed isomer (583 nm) transitions have not been altered. This suggests that while the iridium uniquely impacts the quantum yield through MLCT transitions and consequent emission, it had little to no impact on the energy levels of the MOs associated with the open and closed form isomer excitations.

4.4 Conclusion and Future Work

Incorporation of a chelated iridium centre into the molecular framework of a DTE via a system of delocalisation was unfortunately found not to enhance the molecular switch specific photochemical properties. Instead, a competing photochemical process between radiative decay and photocyclisation is thought to occur, with a preferential pathway towards phosphorescence. The reaction pathways of isomer interconversion were largely unaffected by the presence of the Ir(III) as displayed by the lack of shifts of the absorbance maxima corresponding to the open and closed form transitions, as seen in the spectra of **30** & **Ir-8**. This suggests that the delocalisation and corresponding red shift of the spectrum, and as such, the colour of the complex, are controlled by the thienyl moieties, and partly through its extension into the π -platform. The iridium centre instead acted as an electron sink which funnels energy from the DTE moiety and may hinder isomer interconversion from the closed to open form. This resulted in consistent absorption in the visible region, thereby reducing the quantum yield.

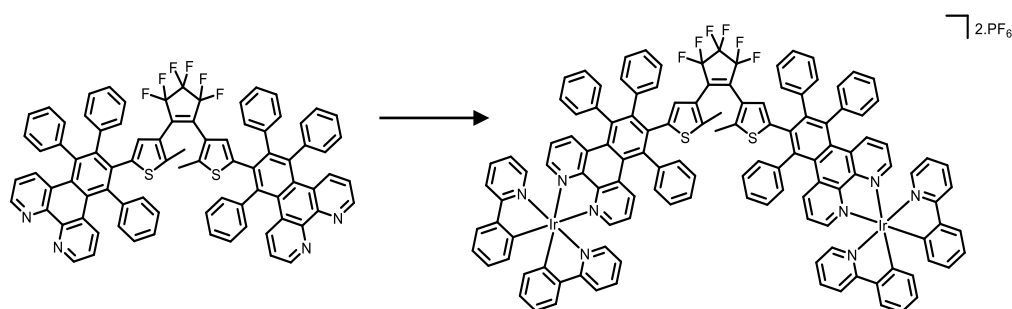


Figure 4.34 Symmetrical side product from the Diels-Alder reaction may be used to investigate unsymmetrical metallic system, or possibly in the use of cation capture.

The Diels-Alder reaction between **28-OH** and **MC1** yielded a secondary switch side product, the symmetrical version of **30**, confirmed by mass spectrometry. This compound possesses two chelation sites in the form of cation binding nitrogens. With this information that incorporation of iridium results in electron density being highly centred upon the phenanthroline ligand, metals centres such as ruthenium(II), osmium(II) and rhenium(III) could be trialled (Figure 4.34). This exposed chelation sites may also allow for a fluorescent probe for cations such as Zn^{2+} .

Aluminum is the third abundant element in the lithosphere, and it plays an important role in many fields, such as drinking water supplies, manufacturing industry, cookware, food packaging and soon.²³⁶ However, aluminum is a nonessential element in living organisms. Excess aluminum not only could influence the plant growth, but also damage the central nervous system and induce various neurodegenerative and neurological disorders including dialysis encephalopathy, Alzheimer's disease, Parkinson's disease, and problems in bone and muscles.²³⁷ According to the World Health Organisation (WHO) report, the average daily uptake of Al^{3+} ions for the human body is about 3-10 mg/day. Tolerable weekly aluminum dietary intake in the human body is estimated to be 7 mg kg^{-1} body weight.²³⁸ However, compared to transition metals, the detection of Al^{3+} has always been a problematic task due to its lack of suitable spectroscopic characteristics and poor coordination ability, and as a result only a few fluorescent chemosensors are available in the literature.²³⁹ Meanwhile, zinc is an essential element for life and plays critical roles in a series of biological processes such as neural signal transmission, gene expression, apoptosis and immune system responses.²⁴⁰ However, misregulation of Zn^{2+} is also implicated in human health disorders. It is believed that a lack of Zn^{2+} can result in an increased risk of several diseases such as those affecting stature, mental retardation and digestive dysfunction because the majority of biological Zn^{2+} are tightly sequestered by proteins.²⁴¹ Therefore, the effective and selective detection of Zn^{2+} and Al^{3+} ions are of great significance for biochemistry, environmental science and medicine. As well as known, fluorescent probes do offer the advantages of operation simplicity, adaptability, high detection sensitivity and selectivity has drawn much attention. Over the past two decades, photochromic compounds as fluorescent sensors for ions have attracted substantial attention.

Among the photochromic compounds for detection of ions, diarylethenes are the most promising materials because their excellent thermal stability, fatigue resistance and rapid

response.²⁴² Furthermore, many ions could induce them to undergo multi-addressable transformation, thus making them promising candidates for ion sensors and complex electronic components. Although some processes for ions recognition have been made,²⁴³ the sensor for Al^{3+} and Zn^{2+} based on multi-state diarylethenes under the same condition has not been reported. Alterations could also be made in earlier synthetic steps to allow for the introduction of electronegative functional groups which could possibly coax electron density to the π -system of the dithienylethene unit.

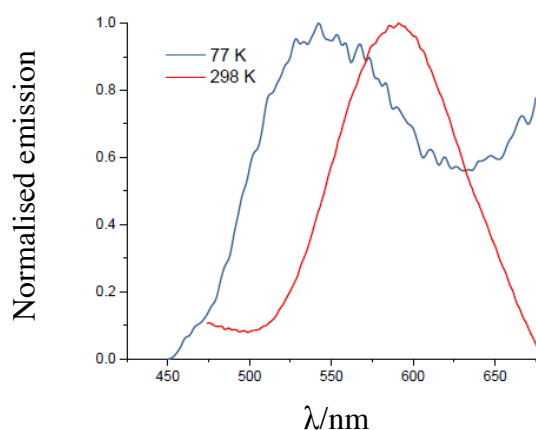


Figure 4.35 Low Temperature, 77 K, study of complex **Ir-8**, with a notable blue-shift occurring between the emission profiles.

Low temperature studies of switch **Ir-8** were also undertaken (Figure 4.35). A large blue-shift was observed, as well as an extension of the broad emission peak seen in the room temperature emissive state. Large ΔE values typically indicate $^3\text{MLCT}$ emissive states, whereas small ΔE suggests ^3IL emissive states. As discussed above, it is apparent that the greatest spectral changes that occur between a non-rigid and rigid environment involve MLCT states and, more specifically, triplet-centred $^3\text{MLCT}$ levels. Clearly, it is the relatively long-lived electronically excited states which are most perturbed by environmental and associated solvation changes. In contrast, the $^1\text{MLCT}$ excited states are relatively unaffected; these levels are anticipated to be extremely short-lived, as they are effectively deactivated by intersystem crossing mechanisms to the $^3\text{MLCT}$ excited states and rapid radiationless relaxation processes to the ground state.

Consequently, the luminescence rigidochromic effect can, to a large extent, be related to changes in the solvation environment. On excitation to the excited state, the complex will

possess a different dipole moment and will, thus, be destabilised compared to the ground-state molecule, until the solvent molecules are able to reorient and facilitate a more favourable electrostatic interaction. When the solvent viscosity is substantially increased (which is the case when the solvent passes through the glass transition point on freezing) the ability of the solvent molecules to rearrange the dipole-dipole interactions in the solvent sphere is hindered. Moreover, as a consequence of a reduced free volume in the frozen glass matrix, the solvent molecules can be considered to actually be closer to the excited-state complex, further enhancing the dipolar interactions. It is clear that changes in the solvation of the matrix environment will mainly influence the dipole-dipole forces of the long-lived $^3\text{MLCT}$ excited state because it is this level which is normally able to achieve a relaxed form through solvent rearrangement. In an extreme case, where the solvent forms a frozen glass, the motion of the solvent will be so restrained that the solvent dipoles will be unable to effectively reorient themselves about the $^3\text{MLCT}$ excited-state molecule. As a consequence, the $^1\text{MLCT}$ energy levels will be destabilised in a rigid solvent environment compared to those in a non-rigid one. In contrast, these solvation effects will be less influential on the short-lived $^1\text{MLCT}$ levels, which will experience much smaller energy perturbations. Using this interpretation makes it possible to explain not only the extent of rigidochromism on the luminescence ($^3\text{MLCT}$) and absorption ($^1\text{MLCT}$) bands but, also, the direction of the energy shift.

Thus, a larger rigidochromic effect between room temperature solution and frozen glass at 77 K was observed for $\text{Ir}(\text{ppy})_3$ than for other complexes exhibiting more vibronic structure in room temperature solution. For the series $\text{Ir}(\text{tpy})_2(\text{L}^\wedge\text{X})$,²⁴⁴ a smaller rigidochromic effect was observed the more blueshifted the emission was, correlating with other spectral features that indicated less MLCT and LC character. While the rigidochromic effect is usually encountered as a comparison of the emission energies in the room temperature liquid *versus* frozen glass, cases such as $\text{Ir}(\text{ppy})_2(\text{bpy})^+$ doped into crystals *versus* room temperature solution is a dramatic example of the rigidochromic effect in which the order of the two lowest excited states was switched. In related compounds, emission from states with a large amount of MLCT character exhibits greater solvatochromic effect, that is, greater stabilisation of the excited states in more polar solvents. This is concurrent with the absorption spectra seen for the complex, with the $^3\text{MLCT}$ situated on the phen-ligand acting as the lowest energy level across the compound.

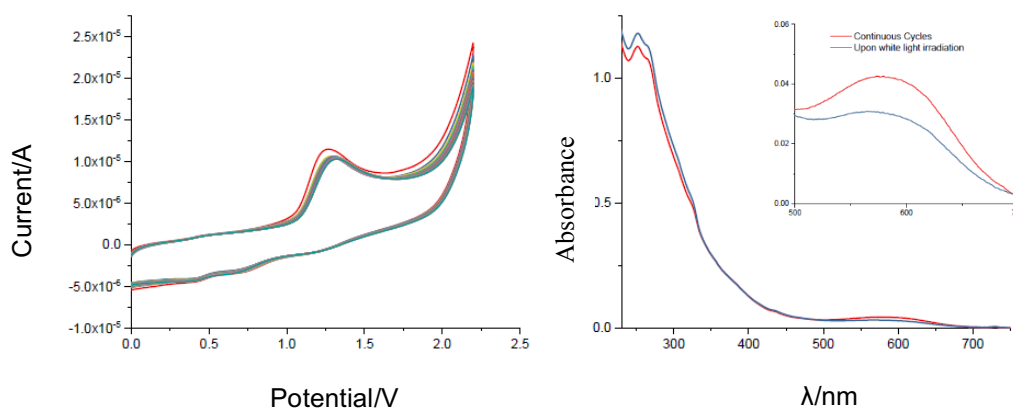


Figure 4.36 Cyclic voltammetry of complex **Ir-8** upon a continuous oxidation cycle and the corresponding change in absorption spectra indicating photocyclisation has occurred.

Initial electrochemical tests were also undertaken, to see if forced oxidation of the iridium core could instigate a photocyclisation of the switching thienyl groups and generate the C-C bond (Figure 4.36). 25 continuous cycles produced the cyclic voltagram shown and induced a photocyclisation of the product, albeit to an almost negligible effect. Further reactions and tests within the field of spectroelectrochemistry may yet yield interesting results in the future. Investigations into the extent of photocyclisation quantum yields and fatigue resistance, as well as photostability of these compounds, also needs to be undertaken.

The area of photocatalytic water-splitting also faces similar challenges, especially when both the photosensitiser and catalyst are coupled via an intramolecular pathway, such as a delocalised π -system.²⁴⁵ When combined with an electron sacrificial agent, the light harvesting centre may be coupled with the catalyst for the effective reduction of two protons into molecular hydrogen. This prevents to relaxation of the excited electron back towards the metal, and forces it forward through the molecular bridge. Though numerous viable sacrificial agents exist, triethylamine is one of the most well-known and universal. It's ease of access also allows initial studies into its use in molecular switching systems to be undertaken quite facily. 0.1 mL of triethylamine solution was added to the cuvette the dissolved Ir(III) switch and placed under UV light. Immediate quenching of the usually strong phosphorescence was noted. However, as the sacrificial agent was not indefinite, the switch was left under the UV lamp for ten minutes, hopefully to allow enough time for the usually competing emissive pathway to be negated, and allow for an efficient electronic transport system. Though the excitation with the lamp did allow for photocyclisation to occur, it was unfortunately of negligible consequence. As seen from the DFT calculations,

the energy pathways most likely still exist in the opposite to what is desired direction, and though the deactivation pathway back to the metal is now temporarily barred, a more non-radiative energy efficient pathway must exist in the compound. Though this result was ultimately unfortunate, it does offer insight into the viability of metal centres in this types of complexes.

Photon upconversion is a process in which the sequential absorption of two or more photons from a photosensitiser leads to the emission of shorter wavelength light than the initial excitation wavelength from an acceptor/emitting compound. It is an important process for luminescent bioimaging²⁴⁶ and photocatalytic hydrogen production²⁴⁷. Triplet–triplet annihilation (TTA) upconversion has attracted much attention owing to the advantage of low power and noncoherent excitation requirement (less than 100 mW cm^{-2} , solar light is sufficient), strong absorption of the excitation energy, and high upconversion quantum yields. Zhao *et al*²⁴⁸ have shown that the fluorescence of bodipy and other fluorophores, such as 9,10-diphenylanthracene (DPA) were controllable in solution by using an appended DTE unit, via the mechanisms of fluorescence resonance energy transfer (FRET), photoswitched electron transfer, or disruption of π -conjugation framework. The upconversion quantum yield (Φ_{UC}) of there DPA system was 1.2% when the switch was in its open form, and completely turned off when the switch underwent photocycloreversion. It is because of this that dithienylethene based compounds and metallic photosensitisers previously synthesised and characterised by the Draper Group may allow for the use of these systems in upconverting applications.

Molecular switches have already been shown to act quite similarly to the very unusual phenomom of upconversion; the open forms of 1-ethynyl naphthalene and 1-ethynyl-4-tert-butylphenyl DTE switches for example give absorption only in the UV spectral region, whereas the closed form DTE gives absorption at ca. 600 nm (620 nm and 608 nm respectively). As such the fluorescence emission of the covalently attached fluorophore (which gives emission length shorter than 600 nm in both cases) can be quenched by FRET. The reduction in fluorescence was shown to correlate with the system undergoing a photocycloreversion from open to closed, meaning that the closed form is able to quench fluorescence within the system, and this depended directly on the photocyclisation and photocycloreversion quantum yields, as well as the conversion rates between the isomers. However, the opposite is also true, using low-energy visible light, fluorescence in a system

could be “turned on” to a much higher blue-energy emissive light. Tuning of these systems, such as higher quantum yield efficiency, is underway, using smaller, more photoactive and highly fluorescent acceptor moieties like pyridazine-derived systems, in the hopes for allowing a greater triplet-triplet energy level overlap in upconverting systems in the closed form, which will effectively quench the emitting fluorescence. Tuning of the synthetic components of the closed form, the DTE moiety could exhibit a much lower T1 state energy level and therefore the triplet state of the photosensitizer would be able to be quenched by the closed form. Previously, the photoswitching of TTA upconversion was accomplished with only one mechanism, the triplet state quenching of the photosensitizer by closed form via either the intermolecular or intramolecular energy transfer.

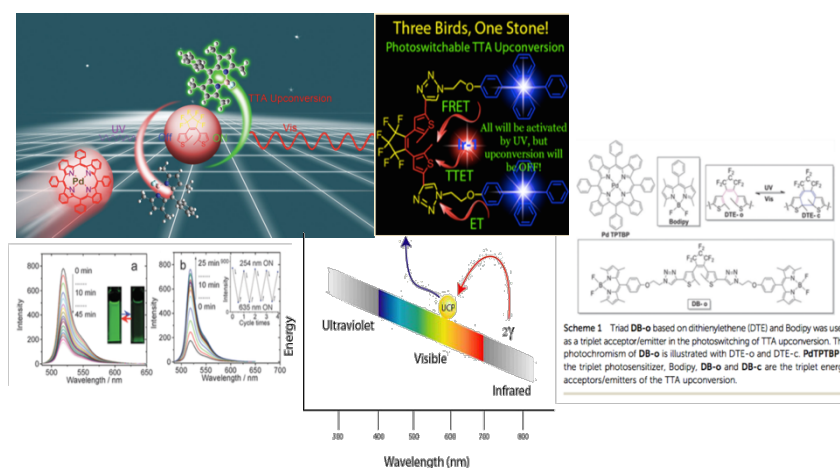


Figure 4.37 Upconversion complexes devised by the Zhao group, with control over the electronic pathways via dithienylethene based switches.

By using larger polycyclic aromatics, and continuing our work in this area, we hope to enable three different mechanisms for the upconverted fluorescence photoswitching effect: photoactivated fluorescence resonance energy transfer, the intramolecular electron transfer, as well as the photoactivated intermolecular triplet energy transfer between the photosensitizer and DTE closed moiety, as seen by the Zhao group (figure 4.37), but with a much higher upconverting quantum yield and greater overall efficiency. Photosensitising compounds, which accept the initial wavelength photons and are excited to a higher energy level, have been previously synthesised within the group, and current optimisation is still ongoing, compounds such as $[\text{Ru}_2(\text{bdp})(\text{bpy})_4]^{4+}$. In this way more efficient photoswitchable TTA upconversion could be achieved. The use of alkyl chain flexible linkages to the dithienylethene unit can also promote a fast, intramolecular singlet–triplet energy transfer,

which is essential for the efficient quenching of the fluorescence of the acceptor/emitter. Sulphur itself offers a dynamic range of properties, such as direct metal coordination which may prove viable, and allow a further avenue of study for these complexes.

5. Conclusions

Chapter 5: Conclusions

In summary, this work involves a vast array of organic synthesis and spectroscopic analysis, within one central core field of photochromic switching chemistry. Chapter 1 saw the synthesis and analysis of five novel molecular switches using ethynyl-based appendages, from the very simple 4-*tert*-butylbenzene, to the expansive and delocalised hexaphenylbenzene (HPB). Table 5.1 shows the results obtained in Chapter 1 in terms of photoactivity.

Compound	λ_{\max} (nm)/ ϵ_{\max} (dm ³ cm ⁻¹ mol ⁻¹)		$\Phi_{e\rightarrow c}$	α PSS (%)	P_{open} (%)	R_{calc}	R_{meas}	λ_{em} (nm)
	Open	Closed (PSS)						
8	276/33,000 311/32,000	608/5,700	0.22	44	56	1.78	1.7	395 415
9	328/262,000	613/18,000	0.28	89	11	-	-	458
10	335/92,000 360/88,000	620/24,525	0.41	67	33	1.56	1.49	380 405
11	Various	-	-	-	-	-	-	407 444
12	300/76,000 375/17,000	-	-	-	-	-	-	420 475

Table 5.1 Results of Chapter 1

Most notably from the table can be seen that compounds **11** and **12** could not be analysed in terms of photochromic performance. This was due to the intense nature of their luminescence profiles, and subsequent high fluorescence quantum yields, and their low switching ability. High performance of the molecular switch structure fell into the much more simple appendages, most notable is that of compound **10**, which contains naphthalene. The most red-shifted absorption was observed for the closed isomer, as well as the highest quantum yield for photocyclisation. It should be noted, however, that compounds **11** and **12** did offer rather unique photochemical activity themselves, which is currently being explored within the group. Excimer formation for compound **11** holds some interesting potential, and may be explored to understand the dynamics of the process. Compound **12** has dual emission depending on the excitation energy, a very unusual trait within the field of photophysics. Many more polycyclic aromatic hydrocarbons may be studied, as well as their photochemical properties on a surface and in solid state.

Chapter 2 dealt with much larger π -platforms, and investigated the effect the position of the thiophene in relation to the periphery of the central benzene rings had on the photochromic ability of the compounds. Incorporation of one of the thienyl units of the dithienyl core into

a polyphenylbenzene system caused a blue-shift in the absorption maximum of the closed form isomer. This was the case in all instances. Due to the lack of cyclohydrogenation, the phenyl rings were freely rotating and so the extension of the π -cloud from the thiophene only encompassed the central benzene. Sterics was also shown to have a negligible result on the absorption maxima, as seen by the overlapping *tert*-butyl groups in compound **20**. Much of this chapter involved heavy synthesis of these larger systems, to compare mono-, di- and polysubstituted hexaphenylbenzenes with thiophene units. Trimerised structures proved difficult to purify due to the presence of asymmetric and symmetric isomers, though a comparative analysis *via* NMR spectroscopy allowed for complete assignment of the signals, and provided information on preferentially synthesising a compound in either asymmetric or symmetric configurations. In the case of trimerised structures with a further phenyl spacer between the central benzene ring and the thiophene unit, extensive π -stacking is observed. This may be due to the much higher concentration of phenyl rings present compared to the smaller trimerised structures, which may combat stacking due to the thiophene rings. Various temperature studies were undertaken, which afforded some fine structure analysis, but prevented actually photochromic reactions from being performed.

Chapter 3 involved the incorporation of large metal centres into the dithienyl framework. Isolation of the MLCT state from the thiophene moieties seems a necessary next step to improve the efficiency of switching process in compounds containing metals. This may prove to be a potentially very strenuous activity. The metal centre and its accompanying HOMO and LUMO orbitals are difficult to configure, and only through the use of spacer groups or distance may this be achieved. This perfect “overlap” seems to exist in a goldilocks region that has not been much investigated thus far. As seen in **Ir-8**, the spacer group, an extensive π -platform, twisted out of plane, and provided a degree of decoupling between the MLCT accepting moiety, and still allowed some degree of energy transfer from this MLCT excited state to the switching thiophenes. However, the overlap was not great enough for this energy transfer to occur fluidly, and the system overpoweringly acted independently, with both the thienyl backbone and the metal absorbing energy without communication between the two. **Ir-8** did have an unusual feature in its absorption profile, with an extension of the MLCT well into the visible portion of the spectrum. This feature may be exploited and explored in our future work, but brings into question the idea of orbital overlap in switches containing metals.

To test this hypothesis about perfect spacer distance, the bimetallic product of switch **31** was

synthesised using ruthenium, and compared to ruthenium switches previously synthesised within the group, as well as those in literature.

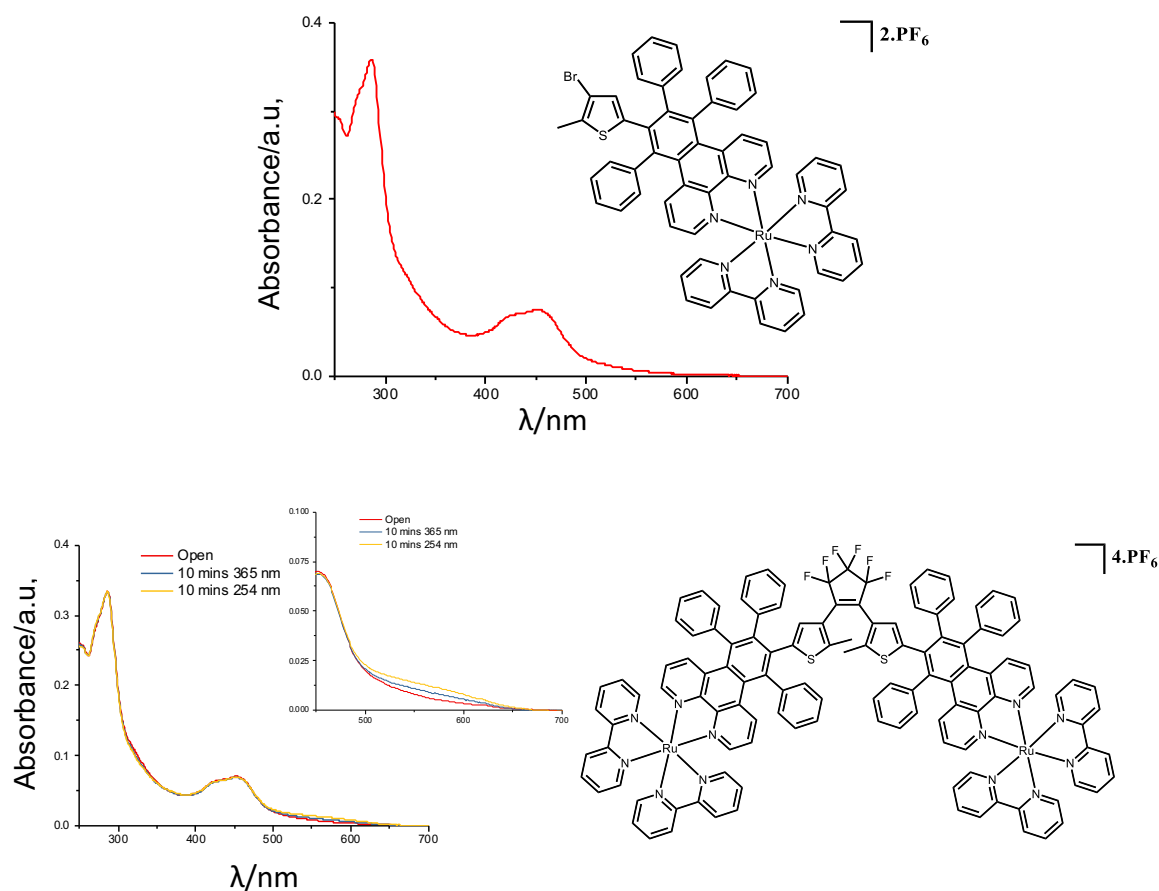


Figure 5.1 UV-Vis absorption spectrum of **Ru-1** and **Ru-2**

Figure 5.1 shows the absorption spectra of two synthesised Ru(II) compounds, **Ru-1** is the brominated analogue similar to **Ir-7**, and **Ru-2** is a novel bimetallic switch. Both products contain prominent MLCT peaks at 430 and 460 nm, indicative of ruthenium based complexes. Using **Ru-2**, we can further investigate the idea of a group spacer and how it affects photochromic performance. Figure 5.2 shows a comparative look at three similar metal based compounds, by DeCola²⁴⁹, Gearoid O'Maille¹⁶⁹ and **Ru-2**.

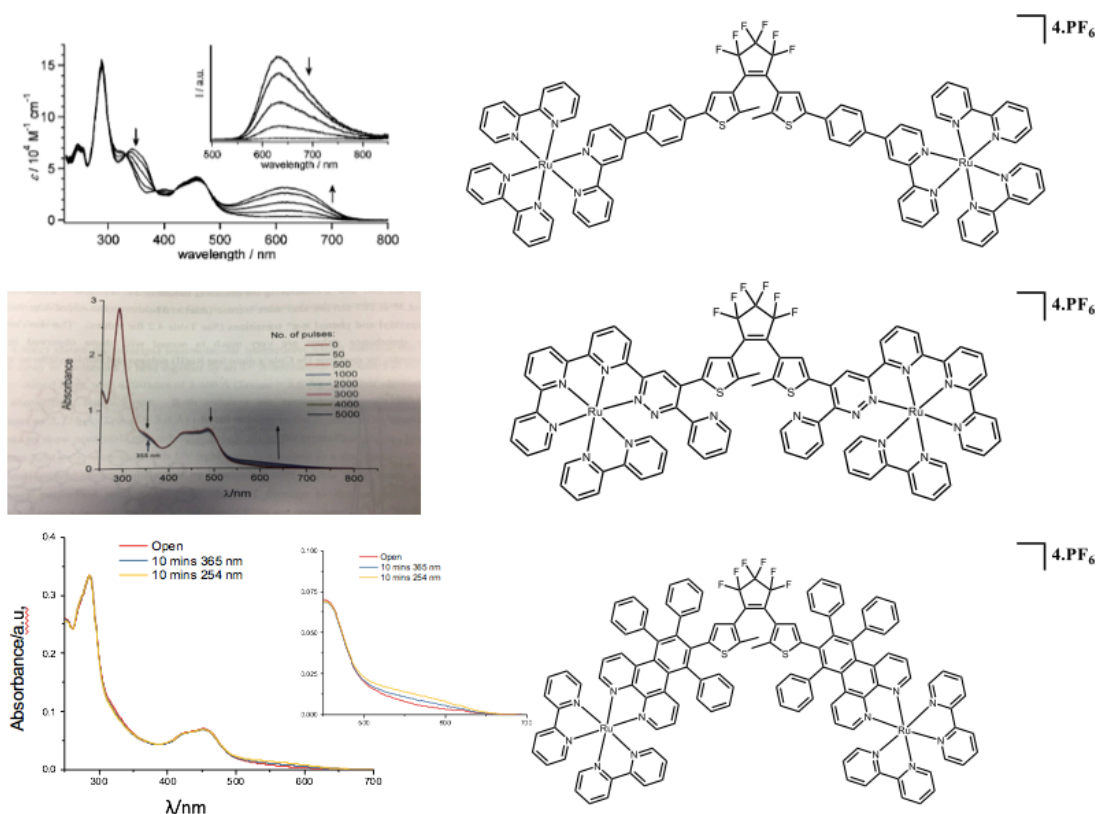


Figure 5.2 (a) DeCola's Ru(II) polypyridal switch, (b) O'Maille's unpublished bimetallic pyrizadine based switch and (c) **Ru-2**

De Cola's switch shows a drastic increase in performance compared to the other two, with a facile growth of an absorbance maximum in the red region of the spectrum. Interesting of note is that O'Maille's switch and **Ru-2** share an almost identical absorption profile, however **Ru-2** was photoswitchable using UV light, the O'Maille switch would only photocyclise after it had been irradiated with laser pulses. It is immediate evident that there is a correlation between the performance of the switch and how insulated the metal is.

Knowing this it may be postulated that based on the results seen here, metals be completely inhibit, or exponentially increase the photochemical properties of molecular switches, depending on the distance. Organic compounds, as seen in Chapters 2 and 3, exhibit beautiful switching properties, however they are harder to purify and crystallise. In comparison, metal containing switches offer an avenue of investigation of switches in solid and crystal form. Metals also allow other prospects to be explored, such as the idea of upconversion. The results of this chapter, however, suggest that metal-containing dithienylethene moieties must be synthesised in a way that allows expansion of the MLCT, which is controlled by the distance between the two.

In terms of using any of these compounds as actual molecular switches and incorporating

them into devices, there are a few strong candidates that stand out. Most notably, the smaller polycyclic aromatic structures, namely, compound **10**. Its structure allowed for a high quantum conversion, a strong absorption maximum and a large red-shift. The product was also able to be crystallised, though at the time they were unsuitable for XRD analysis. **MC1** was also crystallised, and though it performed poorly in terms of fatigue resistance, its smaller size meant it can undergo photocyclisation and photocycloreversion even in the solid state. Small to moderate tuning of the overall compounds, such as addition of functional groups, may improve performance even more. Metal centre complexes seem more suited for upconversion, affording some control in a new and highly prolific area of chemistry.

6. Experimental

6.1 Experimental Details

Unless stated, all reactions were performed under argon using standard schlenk techniques. All solvents were distilled using appropriate drying agents and degassed prior to use. Flash chromatography was performed using silica gel (Fluka 60) as the stationary phase; all separations were carried out in air. Chemicals were purchased from Sigma-Aldrich Chemical Ltd. and were used without further purification.

Electrospray mass spectra were recorded on a Micromass-LCT spectrometer. Electron impact mass spectra were measured on a Waters corp. GCT Premier electron impact mass spectrometer. MALDI-TOF mass spectra were recorded on a Waters MALDI-QTOF Premier spectrometer using an α -cyano-4-hydroxy cinnamic acid matrix. Accurate mass spectra were referenced against Leucine enkephalin (555.6 g/mol) or [Glue1]-FibrinopeptideB (1570.6 g/mol) and reported to within 5 ppm. All samples were dissolved in CH₂Cl₂ or CH₃CN unless otherwise stated.

NMR spectra were recorded in CDCl₃ with (i) a Bruker Avance DPX-400 MHz spectrometer at the following frequencies: 400.13 MHz for ¹H and 100.6 MHz for ¹³C (ii) an AV-400 MHz spectrometer at 400.23 MHz for ¹H and 100.6 MHz for ¹³C or (iii) an AV-600 MHz spectrometer at 600.13 MHz for ¹H and 150.6 MHz for ¹³C. The signals for ¹H and ¹³C were referenced to TMS at $\delta = 0.00$, coupling constants were recorded in hertz (Hz) to one decimal place. All 1-D ¹H and ¹³C spectra were recorded using a Bruker Avance 400 MHz spectrometer or an AV-600 MHz spectrometer and were employed to assign ¹H and ¹³C peaks. Homonuclear correlation spectroscopy was performed using ¹H-¹H COSY experiments and heteronuclear correlation spectroscopy was performed using HSQC, HMQC or HMBC (long-range experiments).

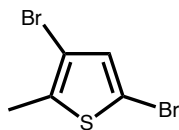
All photophysical measurements were carried out with solutions contained in 1 x 1 cm² quartz cuvettes in HPLC grade solvents. UV-visible absorption spectra were recorded on a Shimadzu UV-2450 spectrophotometer. Emission and excitation spectra were obtained on a Perkin-Elmer LS55 fluorimeter or on a RF5301 spectrofluorometer 145 (Shimadzu).

Computational Methods: Geometry optimisations were calculated by using the B3LYP or PBEH1PBE functional with the 6-31G(d)/LanL2DZ basis set with density functional theory (DFT). The vertical excitation energy was calculated with the time-dependent DFT (TDDFT)

method based on the optimised singlet ground state geometry. The spin-density of the triplet excited state was calculated with their energy-minimised triplet geometries. The solvents were used in the calculations (CPCM model). All calculations were performed with the Gaussian 09W software (Gaussian Inc.) in Trinity College Dublin.

Crystal and structural experimental data are summarised in the Annex. The single-crystal analysis was performed by Dr. Brendan Twamley in Trinity College with a Bruker SMART APEX CCD diffractometer using graphite monochromated Mo-K α ($\lambda = 0.71073 \text{ \AA}$) radiation at the temperatures given in tables. Data reduction was performed using SAINT. Intensities were corrected for Lorentz and polarisation effects and for absorption by SADABS. Space groups were determined from systematic absences and checked for higher symmetry. The structures were solved by direct methods using SHELX-97. All non-hydrogen atoms were refined with anisotropic displacement parameters. Hydrogen atoms were included in calculated positions with isotropic displacement parameters 1.3 times the isotropic equivalent of their carrier carbons. Absolute structure determinations were based on the Flack parameter. The functions minimised were $\sum w(F_o^2 - F_c^2)$, with $w = [\sigma^2(F_o^2) + (aP)^2 + Bp]^{-1}$, where $P = [\max(F_o^2) + 2F_c^2]/3$. In all cases, final syntheses showed no significant residual electron density in chemically sensible positions.

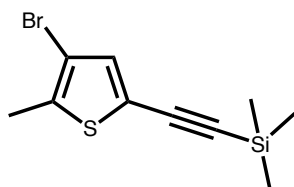
3,5-dibromo-2-methylthiophene, 1



2-methylthiophene (5 g, 0.051 moles) was added to a solution of N-bromosuccinimide (20 g, 0.112 moles) dissolved in hexane (60 mL) and left to stir in a three-necked round bottom flask. To this, perchloric acid (72 %, 0.1 mol %) and acetic acid (10 mL) were added and the solution was left to stir overnight at room temperature. Solution was neutralised with excess NaHCO₃ and water until there was no observable reaction. The mixture was extracted with diethyl ether and washed twice with water and brine. The aqueous layer was washed with diethyl ether and the organic fractions were collected and combined. The volume was reduced slightly in vacuo and a clear orange liquid collected. This was purified with column chromatography using hexane as eluent (R_f = 0.73). Yield: 6.99 g, 28 mmols, 54 %.

ESI-MS: (CNCH₃, m/z): Found: 253.8395 [M]⁺, calculated for [C₅H₄Br₂S]⁺: 253.8400.

3-bromo-2-methyl-5-trimethylsilyl ethynylthiophene



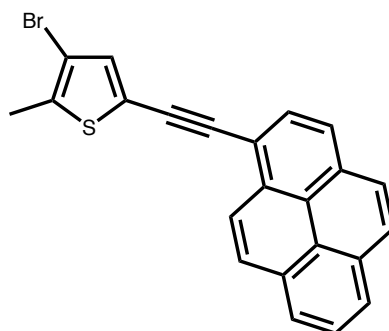
3,5-dibromo-2-methylthiophene (3.0 g, 11.7 mmol) was added to a stirred solution of DMF:NHEt₂ (3:7, 30 mL) in a 35 mL microwave vessel. The solution was bubbled with argon for half an hour. Bis(triphenylphosphine)palladium(II) dichloride (0.1042 g, 0.145 mmol) and copper iodide (0.071 g, 0.35 mmol) were added. This reaction mixture was continuously bubbled with argon for twenty minutes, after which trimethylsilylacetylene (0.99 g, 9.88 mmol) was added and the microwave vessel was sealed. An immediate colour change from yellow to dark orange-brown was noted. The mixture was heated in a microwave for 20 minutes at 125 °C. The solution, now dark brown, was added to aqueous HCl (100 mL, 2 M) and extracted with methylene dichloride. The organic layers were combined and washed with copious amounts of water and brine to remove any remaining

salts and DMF, and dried over magnesium sulfate. The organic solvent was removed in vacuo. The product was then purified using SiO₂ column chromatography (100 % hexane eluent). The resulting yellowing solid product was recrystallised from methanol to give a crystalline solid. Yield 2.3 g, 6.06 mmol, 62 %.

¹H-NMR: (400 MHz, CDCl₃, TMS) δ: 7.04 (s, 1H), 2.39 (s, 3H, -CH₃), 0.25 (s, 9H, Si-C).

ESI-MS: (CH₃CN, m/z): Found: 271.9652[M]⁺, calculated for [C₁₀H₁₃BrSSi]⁺: 271.9691.

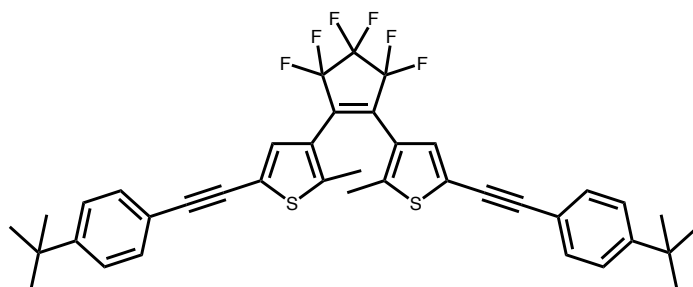
3-bromo-2-methyl-5-ethynlpyrenethiophene, 5



1-ethynylpyrene (2.81 g, 12.4 mmol) and 3,5-dibromo-2-methylthiophene (3.24 g, 12.8 mmol) were added dropwise to a degassed solution of DMF: NHEt₂ (2:5, 35 mL) in a microwaveable vessel. Bis(triphenylphosphine)palladium(II) dichloride (0.099 g, 0.14 mmol) and copper iodide (0.058 g, 0.3 mmol) were then added to the stirred solution, followed by triphenylphosphine (1 g, 3.81 mmol). This was placed in a microwave for 35 minutes at 120 °C. HCl (100 mL, 0.5 M) was used to quench the reaction. The product was extracted with diethyl ether and washed with a combination of water and brine. The organic layers were combined and dried with magnesium sulphate. The volume of the solution was then reduced under vacuum and the light powder product recrystallised using cold methanol to give a bright yellow product (R_f = 0.6 with hexane eluent). Yield: 3.41 g, 0.010 mol, 79 %.

¹H-NMR: (400 MHz, CDCl₃, TMS) δ: 8.54 (d, 2H), 8.20 (m, 4H), 8.14 (d, 1H), 8.11 (d, 1H, J = Hz), 8.03 (m, 2H), 7.25 (s, 1H), 2.47 (s, 1H).

1,2-Bis(5-(4-*tert*-butylphenylacetylene)-2-methylthiophen-3-yl)perfluorocyclopentene, 8



3-bromo-2-methyl-5-(4-*tert*-butylphenylacetylene)thiophene (1.5 g, 4.51 mmol) was dissolved in still dried THF (60 mL) and the solution was degassed by three cycles of freeze-pump-thaw. This was cooled down to -78 °C and *n*-BuLi (3 mL of 1.6 M solution in hexane) was added drop-wise. The reaction mixture was stirred at this temperature for an hour. Perfluorocyclopentene (0.42 g, 0.3 mL, 1.97 mmol) was then added directly to the reaction via gas-tight syringe which had been previously cooled, with the temperature maintained at -78 °C, and stirred for a further two hours. This was then left to warm to room temperature overnight. The reaction was then neutralised with 1 M HCl and extracted with diethyl ether. The solution was dried over MgSO₄ and reduced in volume under vacuum yielding a dark brown oil product. This was purified using column chromatography on silica with hexane as eluent. A portion of the product was also purified using TLC plates with same eluent for NMR analysis. Purification yielded a dark blue solid as product. Yield: 0.87 g, 1.28 mmol, 65 %.

¹H-NMR: (400 MHz, CDCl₃, TMS) δ: 7.44 (d, 2H, H12, 8Hz), 7.37 (d, 2H, H13, 7.6 Hz), 7.24 (s, 1H, H7), 1.93 (s, 3H, H6), 1.26 (s, 9H, H16).

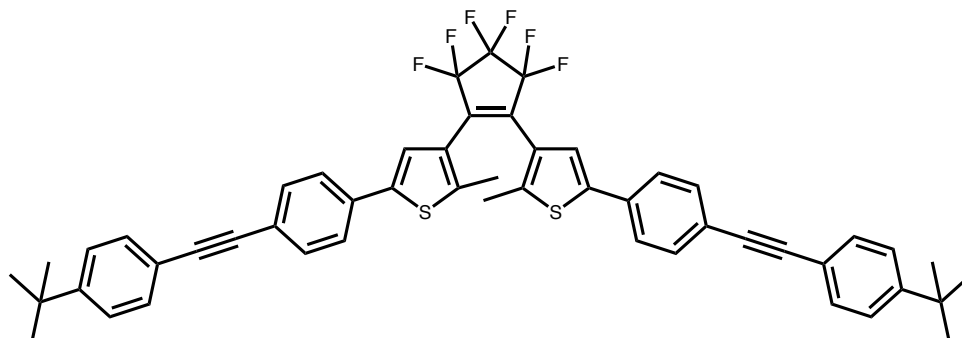
¹³C{¹H} NMR: (151 MHz, CDCl₃) δ: 152.25 (C14), 143.24 (C4), 131.85 (C13), 131.33 (C7), 125.60 (C12), 124.91 (C5), 122.24 (C8), 119.49 (C11), 94.31 (C10), 80.94 (C9), 35.02 (C15), 32.09 (C16), 31.30 (C2), 29.86 (C1), 22.86 (C3), 14.29 (C6).

¹⁹F-NMR: (400 MHz, CDCl₃, TMS) δ: -110.75 (s, 4F, C2-F), -132.34 (s, 2F, C1-F).

APCI-MS: (CH₃CN, *m/z*): Found: 681.2073 [M+H]⁺, calculated for [C₃₉H₃₅F₆S₂]⁺: 681.2078

IR ($\nu_{\text{bar/cm-1}}$): 3058, 3025, 2949 (C-H alkane), 2253, 1919, 1848, 1772, 1517 (C-C aromatic), 1453, 1421, 1374, 1228 (C-H rocking), 1131, 1042 (C-F alkane), 919, 886, 829 (C-H aromatic).

1,2-Bis(5-(4-*tert*-butylphenyl)ethynylphenyl)-2-methylthiophen-3-yl)perfluorocyclopentene), 9



4-Iodo-4'-*tert*-butylphenylacetylene (0.9803 g, 2.72 mmol) and Bis(triphenylphosphine) palladium(II) dichloride (0.0163 g, 0.0233mol) were added to a Schlenk flask containing dry THF (20 mL), ethylene glycol (1 mL) and aqueous sodium carbonate solution (2 M, 20 mL). The reaction mixture was heated to 40 °C under Ar and 3,5-dibromo-2-methylthiophene (0.4955 g, 2.25 mmol) was added. The reactants were stirred together at 80 °C under Ar overnight. Diethyl ether (30 mL) and water (40 mL) were added to the reaction mixture and the organic layers were collected. The aqueous layer was washed diethyl ether (30 mL) and the combined organic fractions were washed with brine (100 mL) and dried over magnesium sulfate. The solvent was then evaporated off at reduced pressure. The product was recrystallised using cold methanol to obtain the final product as an orange/brown solid (0.5335 g, 58 %)

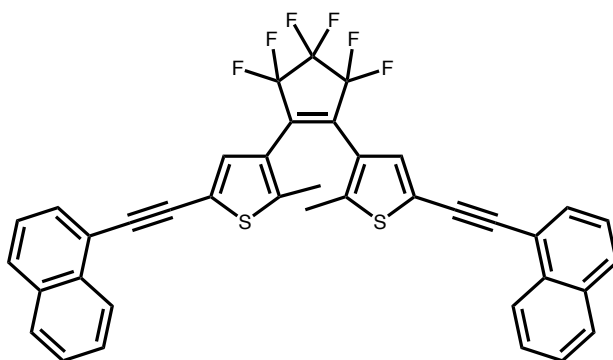
$^1\text{H NMR}$ (400 MHz, CDCl_3) δ : 7.50 (d, $3J = 2.28$ Hz, 2 H), 7.49-7.48 (m, 2 H) 7.47 (d, $3J = 8.60$ Hz, 2 H) 7.37 (d, $3J = 8.60$ Hz, 2 H), 7.14 (s, 1 H), 2.43 (s, 3 H), 1.33 (s, 9 H) ppm

$^{13}\text{C}\{^1\text{H}\}$ NMR: (151 MHz, CDCl_3) δ : 151.81 (1 C, quat., CAr), 140.54 (1 C, quat., CAr), 134.34 (1 C, quat., CAr), 133.11 (1 C, quat., CAr), 132.23 (2 C, CAr-H), 131.46 (2 C, CAr-H), 126.09 (1 C, CAr-H), 125.52 (2 C, CAr-H), 125.14 (2 C, CAr-H), 122.90 (1 C, quat., CAr), 120.21 (1 C, quat., CAr), 110.23 (1 C, quat., CAr), 90.87 (1 C, quart., $\text{C}\equiv\text{C}$), 88.59 (1

C, quart., C≡C), 34.95 (1 C, quat., -C(CH₃)₃), 31.31 (3 C, -(CH₃)₃), 15.05 (1 C, -(CH₃)₃) ppm

APCI-MS (CH₂Cl₂, m/z) Found: 409.061323 [M + H⁺], calculated for (C₂₃H₂₂BrS)⁺
Calculated mass: 409.062010;

1,2-Bis(5-(1-ethynynaphthalene)-2-methylthiophen-3-yl)perfluorocyclopentene, 10



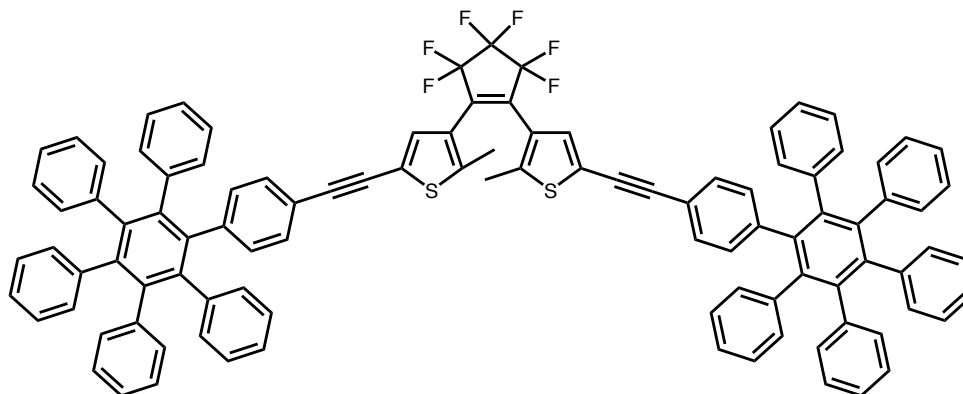
3-bromo-2-methyl-5-(1-ethynynaphthalene)thiophene (1.5 g, 4.58 mmol) was dissolved in still dried diethyl ether (50 mL) and the solution was degassed by three cycles of freeze-pump-thaw. This was cooled down to -78 °C and n-BuLi (3 mL of 1.6 M solution in hexane) was added dropwise. The reaction mixture was stirred at this temperature for 2 hours. Perfluorocyclopentene (0.49 g, 2.29 mmol) was then added, with the temperature maintained at -78 °C and stirred for a further hour and a half. This was then left to warm to room temperature overnight. Neutralised with 1 M HCl and extracted with diethyl ether. The solution was dried over magnesium sulphate and reduced in volume under vacuum yielding a blue oil product. This was purified using column chromatography with petroleum ether: dichloromethane as eluent (19:1). A portion of the product was also purified using TLG plates with same eluent for NMR analysis. R_f = 0.34. Yield: 800 mg, 1.2 mmol, 52 %.

¹H-NMR: (400 MHz, CDCl₃, TMS) δ: 8.28 (d, 1H, 3J = 8.16 Hz, H16), 7.95 (d, 1H, 3J = 8.36 Hz, H11), 7.92 (d, 1H, 3J = 8.32 Hz, H13), 7.79 (d, 1H, 3J = 7.44 Hz, H9), 7.68 (t, 1H, 3J = 7.00 Hz, H15), 7.61 (t, 1H, 3J = 8.08 Hz, H14), 7.52 (t, 1H, 3J = 7.44 Hz, H10), 6.62 (s, 1H, H4), 2.31 (s, 1H, H16).

$^{13}\text{C}\{^1\text{H}\}$ NMR: (151 MHz, CDCl_3) δ : 137.10 133.01 132.78 131.93 131.44 130.47 129.64 128.38 127.33 126.72 126.59 125.66 125.10 123.24 118.90 101.90 88.32 66.93 53.28 29.55

ESI-MS: (CH_3CN , m/z): Found: 668.1067 $[\text{M}]^+$, calculated for $[\text{C}_{39}\text{H}_{22}\text{F}_6\text{S}_2]^+$: 668.1063

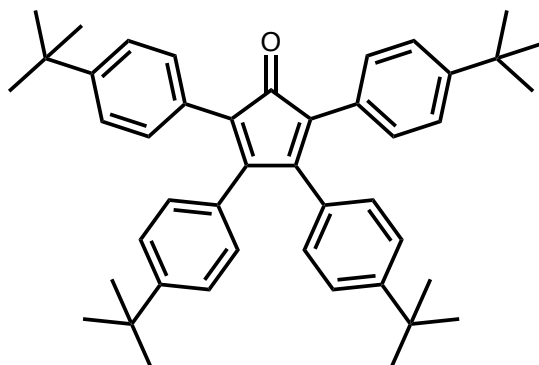
1,2-Bis(5-(1-hexaphenylbenzene)-2-methylthiophen-3-yl)perfluorocyclopentene, 12



Iodo-hexaphenylbenzene (0.1 g, 0.00016 mol) and 1,2-bis(5-ethynyl-2-methylthiophen-3-yl)perfluorocyclopentene) (0.032 g, 0.00009 mol) were dissolved in NH_4Et_3 and bubbled with argon for 30 minutes. The flask was slowly heated to 40 °C and $\text{Pd}(\text{PPh}_3)_2\text{Cl}_2$, CuI and PPh_3 was added. The reaction was allowed to stir for fifteen minutes before the temperature was slowly raised to 90 °C. The reaction was allowed to proceed at this temperature overnight. Upon cooling to room temperature, the solvents were removed in vacuo and the resulting product was dissolved in CH_2Cl_2 and washed with brine and water. These aqueous layers were extracted with CH_2Cl_2 and the organic phases combined and dried over MgSO_4 . The product was purified using column chromatography, using hexane and CH_2Cl_2 as eluent. Yield: (0.057 g, 25 %)

^1H -NMR: (400 MHz, CDCl_3 , TMS) δ : 6.82 (s, 2H), 7.17 (d, 1H), 7.25 (d, 1H), 7.69 (d, 1H)

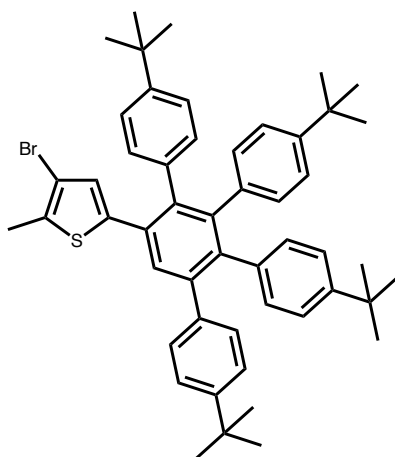
Double aldol condensation reaction example

2,3,4,5-tetra-(4-*tert*-butylphenyl)cyclopenta-2,4-dienone, 13

1,3-bis(4-*tert*-butylphenyl)propan-2-one (0.48 g, 1.380 mmol) and 1,2-bis(4-*tert*-butylphenyl)ethane-1,2-dione (0.47 g, 1.372 mmol) were dissolved in ethanol (3 mL) and heated to reflux for an hour. KOH (38.49 mg, 0.7 mmol) was dissolved in ethanol (3 mL) and added to the refluxing solution in 1 mL portions over the course of fifteen minutes. The reaction was then continued to be heated at reflux for a further hour. It was then left overnight and allowed to cool to room temperature. The purple precipitate was filtered off using methanol and the product collected. **Yield:** 0.81 g, 1.33 mmol, 97 %.

¹H-NMR: (400 MHz, CDCl₃, TMS) δ : 7.23 (d, 8H, ³H_{JJ} = 6.8Hz, H_{phenyl}), 7.15 (d, 8H, ³H_{JJ} = 8.4Hz, H_{phenyl}), 6.83 (d, 4H, ³H_{JJ} = 8.4Hz, H_{phenyl}), 1.29 (s, 18H, CH₃), 1.28 (s, 18H, CH₃).

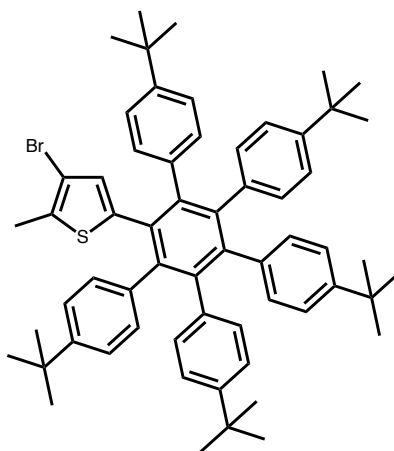
ES-MS: (CH₂Cl₂, m/z): Found: 780.3359 [M]⁺, calculated for [C₅₁H₅₇BrS]⁺: 780.3364.

1-(3-bromo-2-methylthiophene)-2,3,4,5-tetra(4-*tert*-butylphenyl)benzene, 17

3-bromo-5-ethynyl-2-methylthiophene (i), was synthesised in the lab using similar methods described previously. To this (0.12 g 0.66 mmol) compound 7 (0.3 g, 0.64 mmol) was added in a flask, and the reaction set to reflux in benzophenone at 280 0C under constant stream of argon for two hours. The reaction was monitored by TLC until completion. The reaction was allowed to cool overnight. Separation using column chromatography was employed, with petroleum ether as eluent, allowing the yellow poswer product to be extracted. Yield: 0.18 g, 0.23 mmol, 36 %. m.p. : > 360°C.

¹H-NMR: (400 MHz, CDCl₃, TMS) δ: 7.63 (s, 1H, H5), 7.16 (d, 2H, 3HJJ = 8Hz, Hphenyl), 7.07 (d, 4H, 3HJJ = 4.8Hz, Hphenyl), 6.87 (d, 4H, 3HJJ = 6.4Hz, Hphenyl), 6.81 (d, 2H, 3HJJ = 8Hz, Hphenyl), 6.68 (d, 2H, 3HJJ = 8.4Hz, Hphenyl), 6.62 (d, 2H, 3HJJ = 8Hz, Hphenyl), 6.40 (s, 1H, H4), 2.25 (s, 3H, H1), 1.26 (s, 9H, CH₃), 1.22 (s, 9H, CH₃), 1.13 (s, 9H, CH₃), 1.09 (s, 9H, CH₃).

1-(3-bromo-2-methylthiophene)-2,3,4,5,6-penta(4-*tert*-butylphenyl)benzene, 18



Compound 3 (0.17 g, 0.51 mmol) and compound 7 (0.3 g, 0.49 mmol) were added to a round-bottomed flask, along with benzophenone (1 g). The reaction vessel was set to reflux at 280 °C for three and a half hours under a constant stream of nitrogen. Upon completion, the reaction was allowed to cool down, before DCM (2 mL) was added, and the product extracted with cold MeOH (50 mL). The product was recrystallised with hexane to yield a grey powder product. Yield: 0.22 g, 0.26 mmol, 49 %. m.p. : > 360°C.

Chapter 6: Experimental

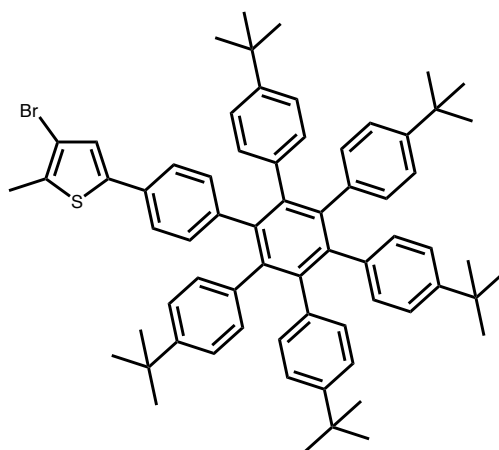
¹H-NMR: (400 MHz, CDCl₃, TMS) δ: 7.29 (d, 10H, 3H_{JJ} = 8Hz, H_{phenyl}), 7.14 (d, 10H, 3H_{JJ} = 7.6Hz, H_{phenyl}), 6.87 (s, 1H, H₄), 2.20 (s, 3H, H₁), 1.13 (s, 18H, CH₃), 1.03 (s, 27H, CH₃).

¹³C{¹H}-NMR: (400 MHz, CDCl₃, TMS) δ: 152.09, 141.49, 140.60, 140.23, 131.26, 130.85, 126.87, 126.62, 125.76, 125.33, 119.05, 83.82, 34.82, 31.36, 14.43.

ESI-MS: (CNCH₃, m/z): Found: 912.4309 [M]⁺, calculated for [C₆₁H₆₉BrS]⁺: 912.4303.

IR (v_{bar}/cm⁻¹): 3025 (C-H alkane), 1600, 1577, 1553 (C-C aromatic), 1495, 1441, 1396 (C-H rocking phen), 1079, 1071, 907, 843 (C-H aromatic), 791, 768, 720, 694, 594, 550

3-bromo-5-(4''-(*tert*-butyl)-3',4',5',6'-tetrakis(4-(*tert*-butyl)phenyl)-[1,1':2',1''-terphenyl]-4-yl)-2-methylthiophene



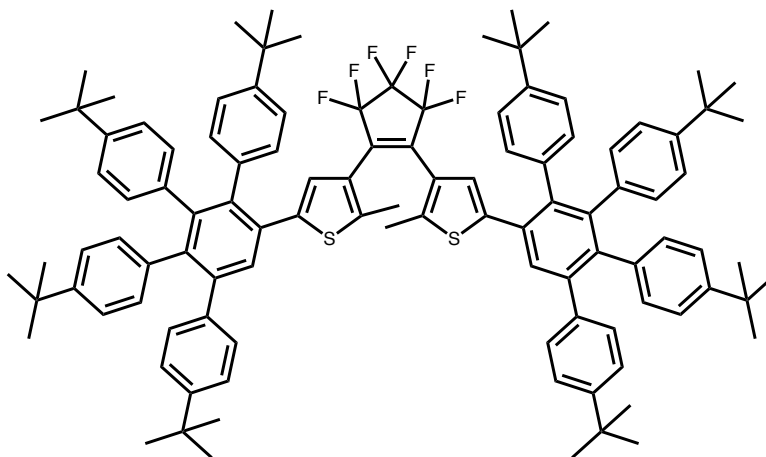
An oven-dried round bottomed flask, connected to a Schlenk line was a quarter filled with benzophenone and a stirrer was added. 3 (0.0814 g, 0.0014 mol) and 13 (0.1274 g, 0.0029 mol) were added to the reaction flask which was then lowered into a sand bath at 100 °C and the temperature was gradually raised to 300 °C and refluxed for 5 h under N₂. The reaction mixture was allowed to cool to room temperature and the brown product was purified by column chromatography on silica with a hexane/DCM mixture (7:3) to give an off-white powder (0.0183 g, 9 %)

^1H NMR: (400 MHz, CDCl_3) δ 6.83-6.78 (m, 12 H), 6.70-6.63 (m, 12 H), 6.24 (s, 1 H), 2.34 (s, 3 H), 1.21 (s, 18 H), 1.09 (s, 27 H) ppm;

$^{13}\text{C}\{^1\text{H}\}$ -NMR: (100 MHz, CDCl_3) δ 147.53 (5 C, quat., CAr), 140.82 (2 C, quat., CAr), 140.27 (3 C, quat., CAr), 139.35 (1 C, quat., CAr), 137.93 (6 C, quat., CAr), 136.81 (1 C, quat., CAr), 132.88 (1 C, quat., CAr), 131.13 (12 C, CAr-H), 130.52 (1 C, CAr-H), 129.84 (1 C, quat., CAr), 123.16 (12 C, CAr-H), 109.68 (1 C, quat., CAr), 34.17 (5 C, quat., -C(CH₃)₃), 31.32 (15 C, -CH₃), 14.91 (1 C, -CH₃) ppm;

MALDI-TOF: (m/z, CH_2Cl_2) Found: 988.4655 [M]⁺, calculated for [$\text{C}_{67}\text{H}_{73}\text{SBr}$]⁺ 988.4616

1,2-Bis(5-(4,4''-di-tert-butyl-3',6'-bis(4-(tert-butyl)phenyl)-[1,1':2',1''-terphenyl]-4'-yl)perfluorocyclopentene), 20

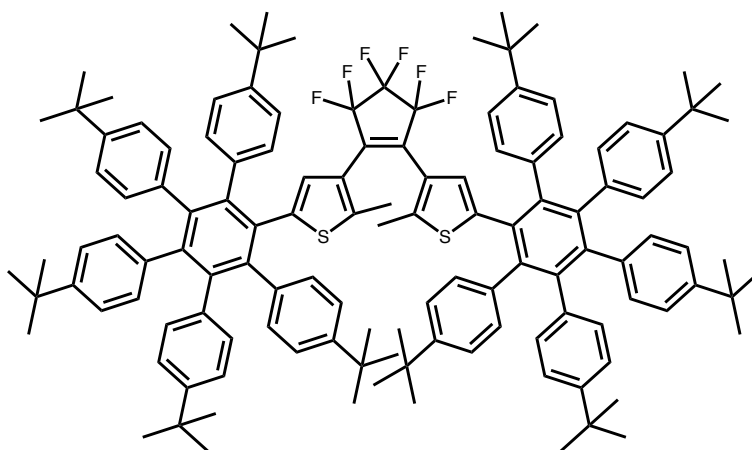


In a 10 ml oven-dried round-bottom flask, **13**, **L12** (0.1 g,) and benzophenone were added and allowed to stir under argon at room temperature for one hour. The flask was then heated in a sand-bath under a constant stream of argon, and covered in foil. Temperature was set between 290 and 310 °C. The reaction was allowed to proceed for four hours, with constant monitoring by TLC. Instability of **L12** led to its consumption in the reaction at faster reaction times, and leftover cyclopentadienone upon completion. Product was allowed to cool to room temperature and extracted with CH_2Cl_2 in MeOH. However further purification of this solid by silica chromatography (ethyl acetate as eluent) was required due to side products and unreacted benzophenone. Product was collected as a light purple solid. Yield: 0.05 g, 31 %

¹H-NMR: (400 MHz, CDCl₃, TMS) δ: 7.63 (s, 1H, H5), 7.16 (d, 2H, 3HJJ = 8Hz, Hphenyl), 7.07 (d, 4H, 3HJJ = 4.8Hz, Hphenyl), 6.87 (d, 4H, 3HJJ = 6.4Hz, Hphenyl), 6.81 (d, 2H, 3HJJ = 8Hz, Hphenyl), 6.68 (d, 2H, 3HJJ = 8.4Hz, Hphenyl), 6.62 (d, 2H, 3HJJ = 8Hz, Hphenyl), 6.40 (s, 1H, H4), 2.25 (s, 3H, H1), 1.26 (s, 9H, CH3), 1.22 (s, 9H, CH3), 1.13 (s, 9H, CH3), 1.09 (s, 9H, CH3).

MALDI-TOF: (CH₂Cl₂, m/z): Found: 1576.8257 [M]⁺, calculated for [C₁₀₇H₁₁₄F₆S₂]⁺: 1576.8266

1,2-Bis(5-(4,4''-di-tert-butyl-4',5',6'-tris(4-(tert-butyl)phenyl)-[1,1':2',1''-terphenyl]-3'-yl)-2-methylthiophen-3-yl)perfluorocyclopentene), 21

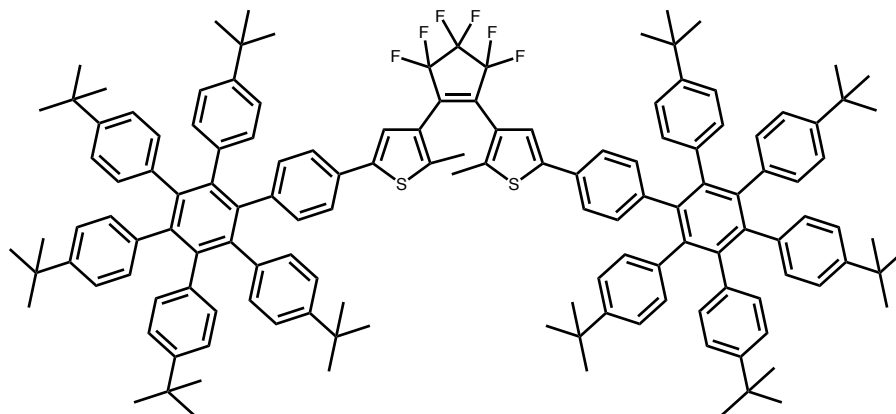


Due to the stability of compound switch **8** compared to **L12** this enabled longer reaction times and higher temperatures to allow for product formation. A flask was fitted with a magnetic stirrer and **13** (0.2 g,) and **8** (0.16 g,) were allowed to stir under N₂ gas for two hours before bezonphenone was added. Using a sand bath, The flask was heated to 330 °C, with a transitional period of 200 °C for 2 hours given initially. The reaction was allowed to proceed at 330 °C for eight hours, before allowing to cool overnight to leave a dark brown oil. This was purified by two silica columns (hexane: CH₂Cl₂ as eluent, 10:1), and a subsequent work up with a short plug run in straight CH₂Cl₂. Product was collected as a dark purple solid. Yield: 0.2 g, 45 % yield

¹H-NMR: (400 MHz, CDCl₃, TMS) δ: 1.58 (s, 27 H), 1.09 (s, 18 H), 1.13 (s, 3H), 6.65 (4H,

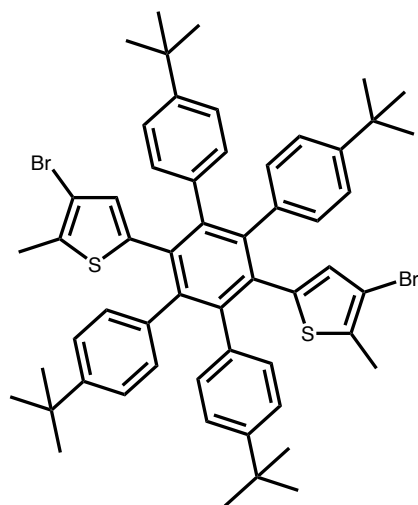
MALDI-TOF: (CH_2Cl_2 , m/z): Found: 1841.0149 $[\text{M}]^+$, calculated for $[\text{C}_{127}\text{H}_{138}\text{F}_6\text{S}_2]^+$: 1841.0144

1,2-Bis(5-(4''-(tert-butyl)-3',4',5',6'-tetrakis(4-(tert-butyl)phenyl)-[1,1':2',1''-terphenyl]-4-yl)-)perfluorocyclopentene)



A 10 mL round bottomed flask containing 5 (0.2588 g, 0.31 mmol) was connected to a Schlenk line and Ar gas was passed through it. The flask was then filled to the half-way mark with benzophenone and 9 (0.3812 g, 6.27×10^{-4} mol) was added to the reaction flask. The flask was then lowered into a sand bath at a temperature of 110 °C. The reaction temperature was gradually raised to 300 °C and refluxed for 5.5 h. The reaction mixture was then allowed to cool back to room temperature overnight and the product was extracted using DCM. The crude product was purified using a preparative TLC plate with a petroleum ether/DCM solvent system (9:1) to yield a blue product (0.002 g, 0.32 %)

MS (m/z - MALDI-TOF, CH_2Cl_2) ($\text{C}_{139}\text{H}_{146}\text{S}_2\text{F}_6$) Calculated mass: 1993.0770; Found: 1993.0806.

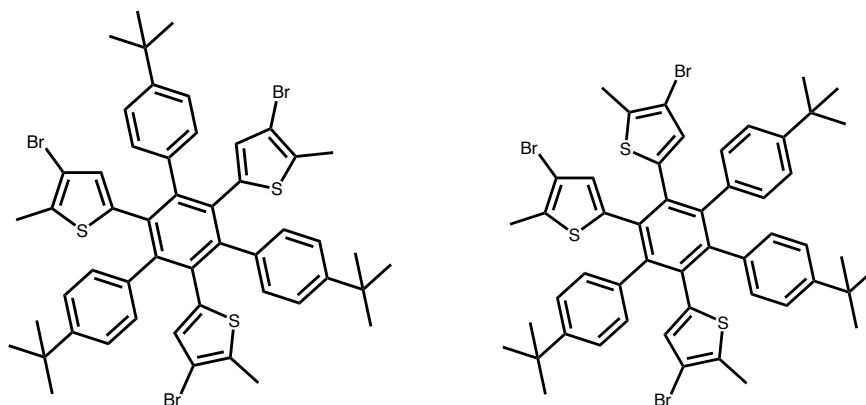
5,5'-(4,4''-di-*tert*-butyl-4',5'-bis(4-(*tert*-butyl)phenyl)-[1,1':2',1''-terphenyl]-3',6'-diyl)bis(3-bromo-2-methylthiophene)

A suspension of 1,2,4,5-tetrabromo-3,6-dichlorobenzene (2.2 g, 5 mmol) in 20 mL of THF was added slowly over 30 min to a solution of phenylmagnesium bromide (prepared from 6.28 g, 40 mmol, of bromobenzene, 0.92 g, 40 mmol of magnesium in 80 mL of THF) and the mixture was stirred for an additional 12 h at room temperature. I₂ (6.35 g, 25 mmol) was added directly to the reaction mixture at 0 °C, and the reaction was stirred at room temperature for 2 h. The reaction was quenched with water, and the resulting mixture was extracted with CHCl₃ (3 x 100 mL). The combined organic layers were washed with 2 M aqueous NaHSO₃ solution (2 x 200 mL), brine (50 mL), and water (50 mL) and dried with MgSO₄. After filtration of the MgSO₄, the solvent was removed in vacuo, and the resulting mixture was filtered. This was directly added to a 100-mL Schlenk tube equipped with a magnetic stirrer bar and a septum was charged with a suspension of 3-bromo-2-methylthienylboronic acid (1.5 mmol, 3.0 equiv), K₂CO₃ (10 mmol, 20 equiv), and aliquat 336 (0.01 mmol, 0.02 equiv) in toluene (15 mL). The mixture was degassed by “freeze–pump–thaw” cycles, and then [Pd(PPh₃)₄] (0.025 mmol, 0.05 equiv) was added. The resulting mixture was degassed again by three “freeze–pump–thaw” cycles. The mixture was warmed to 80 °C and left to stir overnight. The reaction mixture was quenched with water and extracted with CHCl₃. The organic extract was washed with brine, dried over MgSO₄, and concentrated in vacuo. Flash chromatographic purification on silica plates purified the final product.

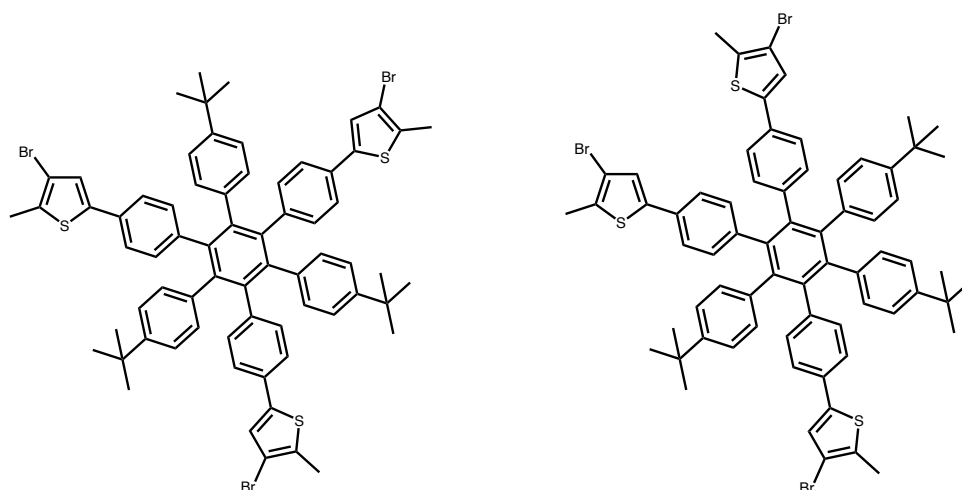
¹H-NMR: (400 MHz, CDCl₃, TMS) δ: 6.91 (d, 2H), 6.79 (d, 2H), 6.01 (s, 1H), 2.10 (s, 3H), 1.17 (s, 9H)

$^{13}\text{C}\{^1\text{H}\}$ -NMR: (150 MHz, CDCl_3 , TMS) δ : 150.82, 148.16, 146.91, 142.33, 141.19, 138.66, 18.14, 137.75, 134.89, 133.31, 131.14, 129.02, 126.10, 124.95, 124.36, 123.99, 106.75, 53.81, 34.81, 31.86, 14.87

Symmetric and antisymmetric isomers of 19



In dioxane (10 mL), acetylene **2** (0.50 mmol) was stirred at 115 C with dicobalt octacarbonyl (26.22 mg, 0.075 mmol, 0.15 eq.) for three days. The solution was cooled to room temperature and the solvent was removed to give a dark brown solid. The resulting compound was purified by column chromatography using dichloromethane: hexane (1: 5) as eluent.

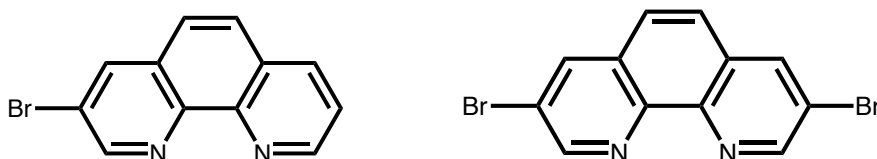


In dioxane (10 mL), acetylene **3** (0.50 mmol) was stirred at 115 C with dicobalt octacarbonyl (26.22 mg, 0.075 mmol, 0.15 eq.) for three days. The solution was cooled to room

temperature and the solvent was removed to give a dark brown solid. The resulting compound was purified by column chromatography using dichloromethane: hexane (1: 5) as eluent. Yield: (21 %)

Spectrum of ^1H displayed in Results. Due to stacking, accurate H NMR peaks could not be taken.

3-bromo-1,10-phenanthroline and 3,8-dibromo-1,10-phenanthroline



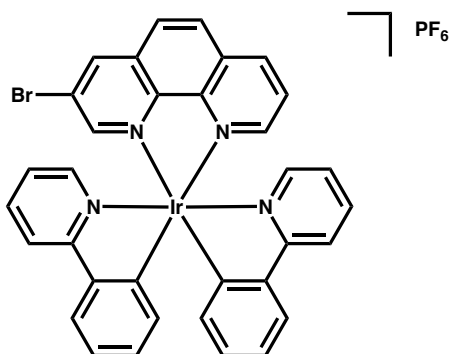
1,10-phenanthroline (2.5 g, 13.9 mmol), S_2Cl_2 (6.15g, 45.66 mmol) and pyridine (3.85 g, 3.9 ml, 48.67 mmol) were heated to 80 °C. Bromine (22.2 g, 13.9 mmol) was added dropwise, and the reaction was allowed to proceed at reflux for 12 hours. The solution was cooled, solvent removed under vacuum and the product purified using column chromatography (silica gel, DCM:MeOH ; 100:1). Both products were successfully isolated, concentrated and crashed out of solution using diethyl ether to give a white solids which were filtered off.

Yield: (2): 1.79 g, 50%, (1): 36%

(1): ^1H NMR (400 MHz, CDCl_3 , TMS) δ : 9.24 (d, 1H, $J = 4$ Hz), 9.21 (d, 1H, $J = 4$ Hz), 8.43 (d, 1H, $J = 2$ Hz), 8.30 (d, 1H, $J = 8$ Hz), 7.86 (d, 1H, $J = 8$ Hz), 7.75 (d, 1H, $J = 8$ Hz), 7.70 (q, 1H, $J = 4$ Hz).

(2): ^1H NMR (400 MHz, CDCl_3 , TMS): $\delta = 9.13$ (d, 2H, $J = 2.4$ Hz), 8.58 (d, 2H, $J = 2.4$ Hz), 7.75 (s, 2H) ppm.

Ir-1



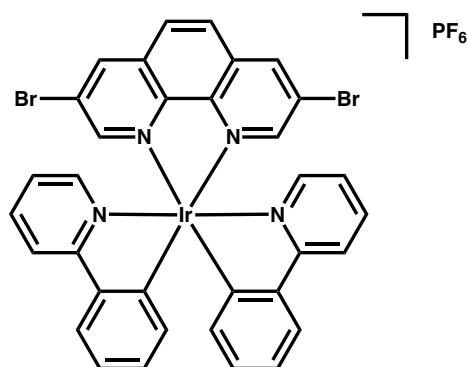
3-bromo-1,10-phenanthroline (2) (73.7 mg, 0.28 mmol) was dissolved in DCM (25 ml) then heated to 40°C. [IrCl(ppy)₂]₂ (151.0 mg, 0.14 mmol) was dissolved in DCM and a few drops of MeOH, and added dropwise down the condenser. The solution was allowed to react at reflux for 4 hours. The solution was allowed to cool, the solvent was removed under vacuum and NH₄.PF₆ (approx. 20 ml) was added to provide the counterion for the complex, which was then filtered from solution using water and diethyl ether to give a slightly pale orange solid. Yield: 247.0 mg, 96%.

¹H NMR: (400 MHz, CD₃CN, RT): δ: 8.92 (d, 1H, J = 4 Hz), 8.71 (d, 1H, J = 8 Hz), 8.32 (d, 1H, J = 4 Hz), 8.29 (d, 1H, J = 8 Hz), 8.22 (d, 1H, J = 2 Hz), 8.18 (d, 1H, J = 12 Hz), 8.09 (t, 2H, J = 8 Hz), 7.85 (m, 5H), 7.53 (d, 1H, J = 6 Hz), 7.42 (d, 2H, J = 8 Hz), 7.12 (q, 2H, J = 8 Hz), 7.00 (q, 2H, J = 8 Hz), 6.90 (t, 2H, J = 6 Hz), 6.41 (d, 1H, J = 10 Hz), 6.36 (d, 1H, J = 8 Hz).

¹³C-NMR (101 MHz, 20 °C, (CD₃)₂CO, δ in ppm): 168.6, 168.6, 153.0, 152.6, 150.6, 150.5, 150.5, 150.3, 148.6, 147.6, 145.2, 145.1, 139.5, 139.0, 138.8, 132.7, 132.6, 132.5, 132.4, 131.8, 131.3, 131.3, 128.9, 128.6, 125.8, 125.8, 124.4, 123.6, 123.5, 122.9, 120.7.

MALDI-TOF-MS: calc. for [C₃₄H₂₃BrIrN₄]⁺ m/z = 759.0735, found m/z = 759.0726.

Ir-2



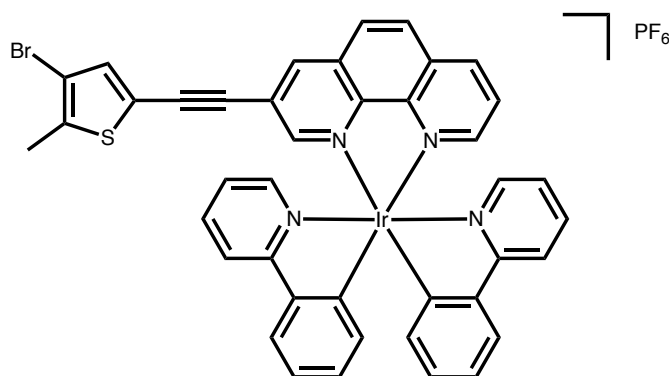
Tetrakis(2-phenylpyridine-C₂,N')(μ -dichloro)diiridium(III) (Ir-0) (200 mg, 0.187 mmol) was dissolved in CH₂Cl₂(5 mL) and MeOH (1 mL) and then added dropwise to a solution of 3,8-dibromo-1,10-phenanthroline (126 mg, 0.374 mmol) in CH₂Cl₂(5 mL). The mixture was heated to 40 °C for 24 h. Once the mixture had cooled after completion of the reaction, a saturated solution of ammonium hexafluorophosphate in MeOH was added dropwise to the mixture to give a precipitate which was isolated by filtration to give an orange solid. Yield: 285 mg, 78%.

¹H-NMR(400 MHz, 20 °C, CD₂Cl₂, δ in ppm): 8.80 (d, 2H, J= 1.0 Hz), 8.28 (d, 2H, J= 1.0 Hz), 8.17 (s, 2H), 7.98 (d, 2H, J= 8.2 Hz), 7.78 (m, 4H), 7.33 (d, 2H, J= 5.6 Hz), 7.14 (t, 2H, J= 7.5 Hz), 7.01 (t, 2H, J = 7.5 Hz), 6.91 (t, 2H, J = 6.7 Hz), 6.35 (d, 2H, J = 7.5 Hz).

¹³C-NMR (151 MHz, 20 °C, CD₂Cl₂, δ in ppm): 167.8, 152.7, 148.9, 147.7, 145.3, 143.9, 140.9, 138.8, 137.5, 131.2, 129.2, 125.4, 123.7, 123.6, 120.4.

MALDI-HRMS: calcd([C₃₄H₂₂N₄Br₂Ir]⁺)m/z= 836.9841, found m/z= 836.9843

Ir-3



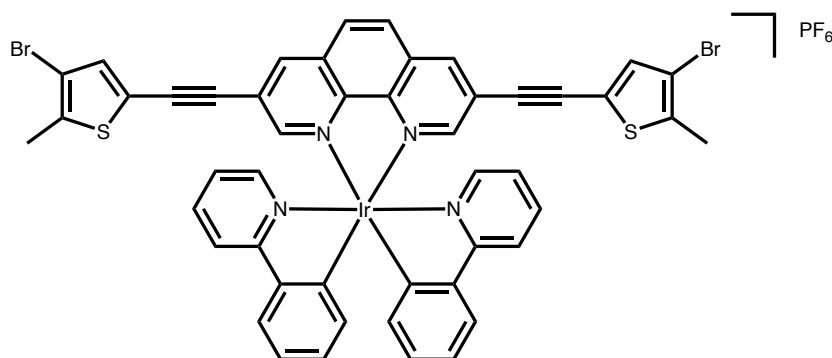
Ir(ppy)₂(3-bromo-1,10-phenanthroline)](PF₆) (99.7 mg, 0.11 mmol), 1-ethynylpyrene (50.2 mg, 0.22 mmol), CuI (2.1 mg, 0.011 mmol), PPh₃ (2.9 mg, 0.011 mmol) and Pd(PPh₃)₂Cl₂ (3.5 mg, 0.005 mmol) were mixed in a 25 mL round bottom flask and was deaerated with Ar. A 1:1 mixture of DMF (10 mL) and Et₃N (4 mL) was deaerated with Ar and transferred to the reaction flask under an Ar atmosphere. The reaction mixture was heated at 60 °C overnight. The reaction mixture was cooled and the solvent removed under vacuum. The product was purified by column chromatography (silica gel, CH₂Cl₂:MeOH, 100:1, v/v) to give an orange solid. Yield: 68.8 mg, 60%.

¹H-NMR (400 MHz, 20 °C, CD₂Cl₂, δ in ppm): 8.86 (s, 1H), 8.66 (d, 1H, J = 8.1 Hz), 8.54 (s, 1H), 8.46 (d, 1H, J = 9.0 Hz), 8.38-8.20 (m, 9H), 8.13-8.09 (m, 2H), 8.01 (t, 2H, J = 9.4 Hz), 7.89-7.75 (m, 5H), 7.49 (d, 1H, J = 5.7 Hz), 7.40 (d, 1H, J = 5.7 Hz), 7.26 (t, 1H, J = 7.4 Hz), 7.14 (m, 2H), 7.03 (t, 1H, J = 7.5 Hz), 6.91 (t, 2H, J = 6.4 Hz), 6.52 (d, 1H, J = 7.4 Hz), 6.45 (d, 1H, J = 7.4 Hz).

¹³C-NMR (101 MHz, 20 °C, CD₂Cl₂, δ in ppm): 168.1, 168.0, 153.3, 151.7, 149.3, 149.1, 149.0, 148.9, 147.0, 145.5, 144.3, 144.1, 139.8, 138.9, 138.6, 132.8, 132.7, 132.2, 132.1, 132.0, 131.4, 131.3, 131.2, 131.1, 131.1, 130.1, 129.6, 129.5, 128.4, 127.4, 127.1, 127.0, 126.7, 126.6, 125.4, 125.3, 125.0, 124.9, 124.6, 124.3, 124.0, 123.6, 123.6, 123.3, 123.3, 120.4, 120.2, 115.3, 96.7, 90.1.

MALDI-TOF-MS: calcd([C₅₂H₃₂N₄Ir]⁺)m/z = 905.2256, found m/z = 905.2284.

Ir-4

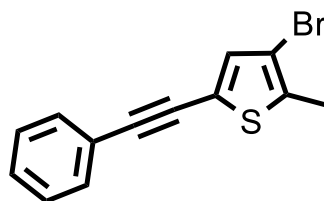


[Ir(ppy)₂(3,8-dibromo-1,10-phenanthroline)](PF₆) (101.5 mg, 0.1 mmol), 1-ethynylpyrene (91.7 mg, 0.41 mmol), CuI (2.1 mg, 0.011 mmol), PPh₃ (2.9 mg, 0.011 mmol) and Pd(PPh₃)₂Cl₂ (3.5 mg, 0.005 mmol) were mixed in a 25 mL two-necked round bottom flask which was subsequently degassed with Ar. A mixture of still-dried degassed CH₃CN (10 mL) and Et₃N (4 mL) was added via cannula and the reaction was left to stir at 60 °C overnight. The mixture was allowed to cool and the solvent was removed under vacuum. The product was purified by column chromatography (silica gel, CH₂Cl₂:MeOH, 100:1, v/v) to give a red solid. Yield: 80.5 mg, 63%. 163

¹H-NMR (400 MHz, 20 °C, CD₂Cl₂, δ in ppm): 8.88 (s, 2H), 8.57 (s, 2H), 8.47 (d, 2H, J = 9.1 Hz), 8.35 (d, 2H, J = 7.7 Hz), 8.32-8.27 (m, 6H), 8.22-8.19 (m, 6H), 8.14-8.10 (m, 4H), 8.06 (d, 2H, J = 8.3 Hz), 7.91 (d, 2H, J = 7.8 Hz), 7.81 (t, 2H, J = 7.8 Hz), 7.56 (d, 2H, J = 6.5 Hz), 7.29 (t, 2H, J = 7.6 Hz), 7.16 (t, 2H, J = 7.4 Hz), 6.97 (t, 2H, J = 6.6 Hz), 6.55 (d, 2H, J = 7.5 Hz).

¹³C-NMR (101 MHz, 20 °C, CD₂Cl₂, δ in ppm): 167.8, 153.3, 148.8, 148.5, 145.0, 143.9, 139.5, 138.5, 132.6, 132.5, 131.9, 131.3, 131.2, 131.0, 130.9, 129.9, 129.3, 129.0, 127.2, 126.8, 126.4, 126.4, 125.2, 124.7, 124.6, 124.3, 124.0, 123.9, 123.4, 123.2, 120.2, 115.0, 96.8, 90.0.

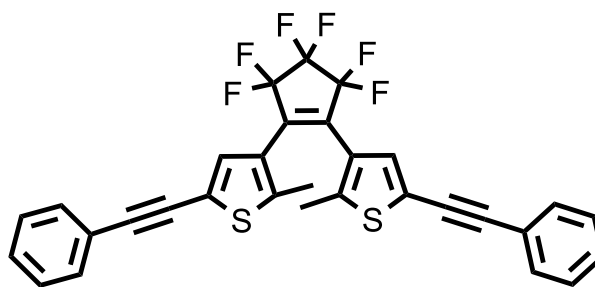
MALDI-TOF-MS: calcd ([C₇₀H₄₀N₄Ir]⁺) m/z = 1129.2882, found m/z = 1129.2900.

3-bromo-2-methyl-5-(4-*tert*-butylphenylacetylene)thiophene

Phenylacetylene (2 g, 0.013 mol), 3,5-dibromo-2-methylthiophene (3.21 g, 0.013 mol), Triphenylphosphine (1 g, 3.81 mmol), Pd(PPh₃)₂Cl₂ (0.099 g, 0.14 mmol) and CuI (0.058 g, 0.3 mmol) were stirred in DMF:NHEt₂ (2:5, 35 mL) and the reaction vessel was placed in a microwave for 35 minutes at 120 °C. 0.5 M HCl (100 mL) was used to quench the reaction. The product was extracted with diethyl ether and washed with water and dried with magnesium sulphate. Excess solvent was reduced under vacuum and the product was recrystallised using ice-cold methanol (3.23 g, 0.0093 mol, 75%).

¹H-NMR: (400 MHz, CDCl₃) δ: 7.32 (d, 2H), 7.44 (d, 2H), 3.50 (s, 3H), 1.45 (s, 9H).

¹³C{¹H} NMR: (151 MHz, CDCl₃) δ: 151.51, 135.58, 133.34, 130.71, 124.96, 120.59, 119.07, 108.44, 93.40, 80.69, 34.40, 30.71, 14.43.

3,3'-(perfluorocyclopent-1-ene-1,2-diyl)bis(2-methyl-5(phenylethynyl)thiophene), MC1

To a cooled solution (-85 °C) of diethyl ether (100 mL) and 3-bromo-2-methyl-5-(phenylethynyl)thiophene (2.01 g, 7.2 mmol), *n*-butyllithium (4.4 mL, 11.0 mmol) was added under an inert atmosphere. The solution was left to stir for 2 hours. Octafluorocyclopentene (1.2 mL, 8.7 mmol) was added directly to the reaction mixture dropwise and the resulting solution was maintained at -78 °C for a further two hours. The reaction was left to continue to completion and monitored with TLC. The solution was slowly allowed to warm to room temperature overnight, and neutralised with HCl (10%), and the product was extracted into methylene dichloride. The organic layers were washed

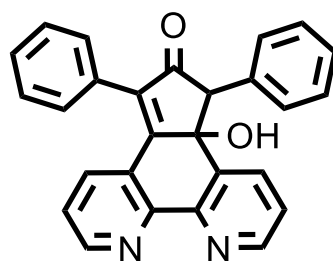
Chapter 6: Experimental

with water and brine and dried with MgSO_4 . The methylene dichloride was reduced *in vacuo* and the products were purified using column chromatography (SiO_2) with hexane as eluent (5) (0.40 g, 0.7 mmol, 19.4%)

$^1\text{H NMR}$ (400 MHz, CDCl_3) δ : 7.58 – 7.46 (m, 4H), 7.43 – 7.32 (m, 6H), 7.28 (s, 3H), 1.97 (s, 6H), 1.60 (d, $J = 21.5$ Hz, 3H).

$^{13}\text{C NMR}$ (151 MHz, CDCl_3) δ 131.46, 128.77, 128.46, 14.54.

11b-hydroxy-1,3-diphenyl-1,11b-dihydro-2H-cyclopenta[*l*]phenanthrene-2-one, 28-OH

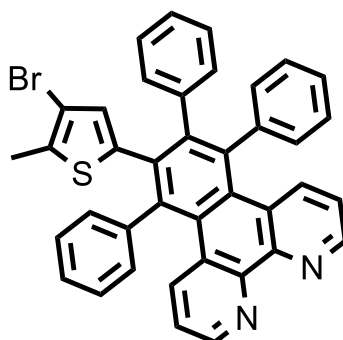


A solution of 1,10-Phenanthroline-5,6-dione (1.0 g, 5.0 mmol) 1,3-diphenylpropan-2-one (1.5 g, 7.0 mmol) and dried methanol (15 mL) was stirred under an inert atmosphere. To the reaction mixture KOH (50 mg, 0.8 mmol) and piperidine (1.25 mL, 2.5 mmol) were added and the solution was stirred for 2 hours and 30 minutes. The product was collected and washed with cold methanol, dissolved in DCM and recrystallised from methanol. (1.65g, 4.1 mm, 82%).

$^1\text{H NMR}$ (600 MHz, CDCl_3): δ 8.79 (d, 1H, $J = 3.7$ Hz), 8.80 (d, 1H, $J = 3.5$ Hz, H_{13}), 8.11 (dd, 1H, $J = 7.8$ Hz), 7.59 (dd, 1H, $J = 8.0$ Hz), 7.54 (d, 2H, $J = 7.2$), 7.51 (t, 2H, $J = 7.6$ Hz), 7.45-7.40 (m, 4H) 7.39-7.36 (m, 3H), 7.15 (dd, 1H, $J = 8.0$ Hz), 4.49 (s, 1H), 2.55 (s, 1H, OH) ppm. ppm.

HRMS (m/z): $[\text{M}+\text{H}]$ ($\text{C}_{27}\text{H}_{19}\text{N}_2\text{O}_2$) Calc.: 403.1447, Found: 403.1447

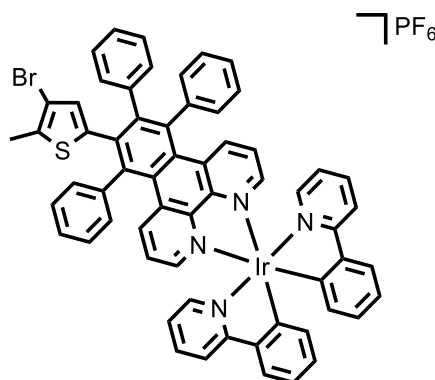
6-(4-bromo-5-methylthiophen-2-yl)-5,7,8-triphenylbenzo[f][1,10]phenanthroline, 29



A mixture of 3-bromo-2-methyl-5-(phenylethynyl)thiophene (0.26 g, 0.94 mmol), 5, 7-diphenyl-6H-cyclopenta[f][1,10]phenanthroline-6-one (0.38g, 0.94 mmol) and benzophenone (0.5 g) was mixed under inert atmosphere for 1 hour. The solution was heated incrementally to 300 °C for a period of 6 hours and the reaction's progress was monitored by TLC. The product was then collected with DCM, which was reduced *in vacuo* and purified on a silica plate using a mixture of solvents; hexane, DCM, acetonitrile to wash the product from the silica (0.3 g, 0.47 mmol, 50%).

$^1\text{H NMR}$ (400 MHz, CDCl_3) δ 8.94 – 8.82 (m, 2H), 7.82 (ddd, $J = 13.2, 8.7, 4.0$ Hz, 2H), 7.75 – 7.62 (m, 2H), 7.29 – 7.20 (m, 3H), 7.20 – 7.06 (m, 5H), 7.06 – 6.92 (m, 8H), 6.87 – 6.77 (m, 2H), 6.08 – 5.92 (m, 2H).

MALDI-TOF (m/z): $[\text{M}]^+$ ($\text{C}_{39}\text{H}_{26}\text{N}_2\text{SBr}$) Calc: 633.1000, Found: 633.1008

Ir-7

6-(4-bromo-5-methylthiophen-2-yl)-5,7,8-triphenylbenzo [f][1,10]phenanthroline, 30, (0.1 g, 0.16 mmol) $[\text{Ir}(\text{Ppy})_2\text{Cl}]_2$ (0.2g, 0.18 mmol) were dissolved in a mixture of DCM (4 mL)

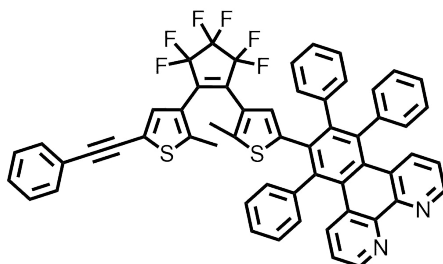
Chapter 6: Experimental

and methanol (1 mL). The reaction was heated to 45^oC for a period of 12 hours. A solution of NH₄PF₆ (0.5g, 3 mmol) in methanol (5 mL) was slowly added slowly. The product was purified on a silica plate using a CH₂Cl₂: MeOH (20:1 v/v) solvent system. The product was then extracted from the silica using a mixture of solvents; DCM, Methanol, Acetonitrile, Hexane (0.11g, 0.095 mmol, 60%)

¹H NMR (600 MHz, CDCl₃) δ 8.29 – 8.19 (m, 3H), 8.17 – 8.06 (m, 2H), 8.02 – 7.87 (m, 4H), 7.82 – 7.73 (m, 2H), 7.56 – 7.28 (m, 5H), 7.27 – 7.21 (m, 2H), 7.20 – 7.13 (m, 1H), 7.00 – 6.90 (m, 2H), 6.87 – 6.77 (m, 1H), 6.51 – 6.35 (m, 2H), 6.25 (d, *J* = 14.2 Hz, 1H), 5.64 (s, 2H), 2.13 (s, 3H).

HRMS (*m/z*): Calc.: 1133.1865, Found: 1133.1846

6-(4-(3,3,4,4,5,5-hexafluoro-2-(2-methyl-5-(phenylethynyl)thiophen-3-yl)cyclopent-1-en-1-yl)-5-methylthiophen-2-yl)-5,7,8-tri-phenylbenzo[f][1,10]phenanthroline, 30



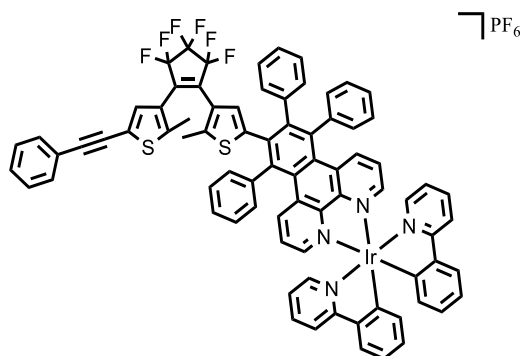
MC1 (0.140 g, 0.24 mmol), **28-OH** (0.160 g, 0.40 mmol) and benzophenone (3 g) were mixed under an inert atmosphere for 1 hour. The solution was heated incrementally to 300 °C for a period of 6 hours and the reaction was monitored by TLC. The product was then extracted into DCM, which was reduced *in vacuo*. The product was purified using column chromatography (SiO₂) with hexane as eluent.

¹H NMR (400 MHz, CDCl₃) δ 8.94 – 8.86 (m, 2H), 7.90 – 7.71 (m, 1H), 7.56 – 7.44 (m, 1H), 7.39 – 7.31 (m, 2H), 7.29 – 7.24 (m, 3H), 7.23 (t, *J* = 2.5 Hz, 1H), 7.20 – 7.07 (m, 3H), 7.06 – 6.97 (m, 4H), 6.89 – 6.80 (m, 1H), 6.35 (d, *J* = 11.0 Hz, 1H).

¹³C NMR (151 MHz, CDCl₃) δ 149.32, 148.97, 143.23, 142.46, 141.54, 139.40, 138.45, 136.68, 134.40, 131.49, 130.59, 130.53, 129.46, 129.02, 128.47, 127.94, 127.35, 126.30,

125.15, 123.51, 122.47, 120.34, 93.79, 81.61, 77.37, 77.16, 76.74, 42.70, 30.93, 29.70, 14.83. **HRMS** (m/z): Calc.: 925.2146, Found: 925.2187.

Ir-8



8 (0.05 g, 0.054 mmol) and [Ir(Ppy)₂Cl]₂ (0.1g, 0.09 mmol) were dissolved in a mixture of DCM (4 mL) and methanol (1 mL). The reaction was heated to 45⁰C for a period of 12 hours. A solution of NH₄PF₆ (0.25g, 1.5 mmol) in methanol (5 mL) was slowly added slowly. Excess solvent was reduced *in vacuo* and the product was purified using column chromatography (SiO₂) with acetonitrile as eluent (0.047g, 0.035 mmol, 64%).

¹H NMR (600 MHz, CDCl₃) δ 8.29 – 8.22 (m, 3H), 8.20 (d, $J = 3.9$ Hz, 1H), 8.16 (s, 1H), 8.08 – 8.03 (m, 1H), 7.92 (dt, $J = 18.1, 10.6$ Hz, 5H), 7.75 (dd, $J = 13.4, 7.6$ Hz, 1H), 7.63 – 7.39 (m, 7H), 7.32 (td, $J = 11.7, 4.5$ Hz, 3H), 7.23 (ddd, $J = 14.2, 11.2, 6.8$ Hz, 4H), 7.14 – 7.06 (m, 1H), 7.06 – 6.99 (m, 3H), 6.93 (dd, $J = 7.3, 3.4$ Hz, 2H), 6.47 (s, 1H), 6.37 (dd, $J = 7.6, 2.1$ Hz, 2H), 6.30 – 6.18 (m, 1H).

¹³C NMR (151 MHz, CDCl₃) δ 167.83, 152.00, 150.52, 149.23, 148.43, 144.13, 138.64, 132.45 – 117.87 (m), 94.80 – 92.60 (m), 82.31 – 80.34 (m), 79.06 – 77.22 (m), 54.07, 28.95.

HRMS (m/z): Calc.: 1425.3011, Found: 1425.3044.

References

1. S. Kobatake, S. Takami, H. Muto, T. Ishikawa & M. Irie, *Nature*, **2007**, *446*, 778
2. K. Matsuda and M. Irie, *Journal of Photochemistry and Photobiology C: Photochemistry Reviews*, **2004**, *5*, 169-182.
3. B. L. Feringa, N. Koumura, R. A. van Delden and M. K. J. ter Wiel, *Applied Physics A: Materials Science & Processing*, **2002**, *75*, 301.
4. C. Yun, J. You, J. Kim, J. Huh and E. Kim, *Journal of Photochemistry and Photobiology C: Photochemistry Reviews*, **2009**, *10*, 111-129.
5. T. J. Huang, A. H. Flood, B. Brough, L. Yi, P. A. Bonvallet, K. Seogshin, C. Chih-Wei, G. Tzung-Fang, L. Weixing, Y. Yang, J. F. Stoddart and H. Chih-Ming, *Automation Science and Engineering*, **2006**, *3*, 254-259.
6. H.-h. Liu, X. Zhang, Z. Gao and Y. Chen, *The Journal of Physical Chemistry A*, **2012**, *116*, 9900-9903.
7. G. Mehta and S. Sen, *Chemical Communications*, **2009**, 5981-5983.
8. E. Zahedi, S. Emamian and A. Shiroudi, *Chinese Journal of Structural Chemistry*, **2012**, *31*, 240-244.
9. B. L. Feringa, *Molecular switches*, Wiley-VCH Verlag GmbH, 2001.
10. N. Sakai and S. Matile, *Beilstein Journal of Organic Chemistry*, **2012**, *8*, 897-904.
11. V. Richards, *Nature chemistry*, **2016**, *8*, 1090-1090.
12. P. L. Anelli, N. Spencer, J. F. Stoddart, "A molecular shuttle", *Journal of the American Chemical Society* **1991**, *113*, 5131-5133.
13. D. L. Jiang, T. Aida, *Nature* **1997**, *388*, 454.
14. F. Würthner, J. Rebek, *Angewandte Chemie International Edition*, **1995**, *34*, 446-448.
15. S. Shinkai, *Pure and Applied Chemistry*, **1987**, *59*, 425.
16. C. Zhang, M. H. Du, H. P. Cheng, X. G. Zhang, A. Roitberg, J. Krause, *Physical review letters* **2004**, *92*, 158301.
17. W. Fu, C. Kosmidis, W. E. Schmid, S. A. Trushin, *Angewandte Chemie International Edition*, **2004**, *43*, 4178-4182.
18. G. Berkovic, V. Krongauz, V. Weiss, *Chemical Reviews*, **2000**, *100*, 1741-1754.
19. Y. Zeng, S. Liao, J. Dai, Z. Fu, *Chemical Communications*, **2012**, *48*, 11641-11643.
20. S. AnithaáNagamani, D. ShankaráRao, S. KrishnaáPrasad, *Journal of Materials Chemistry*, **2001**, *11*, 1818-1822.
21. Y. Yokoyama, *Chemical Reviews*, **2000**, *100*, 1717-1740.
22. B. L. Feringa, W. F. Jager, B. de Lange, *Tetrahedron*, **1993**, *49*, 8267-8310.
23. K. Kirchberg, T. Y. Kim, S. Haasea, U. Alexiev, *Photochemistry & Photobiological Sciences*, **2010**, *9*, 226-233
24. A. S. Lukas, M. R. Wasielewski, *Molecular Switches*, Wiley-VCH Verlag GmbH: **2001**; 1-35.
25. B. L. Feringa, W. F. Jager, B. de Lange, *Tetrahedron*, **1993**, *49*, 8267-8310.
26. M. Irie, *Molecular Switches*, Wiley-VCH Verlag GmbH: **2001**; 37-62.
27. G. Szalóki, J. L. Pozzo, *Chemistry – A European Journal* **2013**, *19*, 11124-11132.

28. H. Tian, S. Yang, *Chemical Society Reviews* **2004**, *33*, 85-97.
29. J. P. Desvergne, H. Bouas-Laurent, *J. Chem. Soc., Chem. Commun.*, **1978**, 403 - 404
30. H. Bouas-Laurent, A. Castellán, J. P. Desvergne, *Pure Applied Chemistry*, **1980**, *52*, 2633
31. I. Tamashita, M. Fujii, T. Kaneda, S. Misumi, T. Otsubo, *Tetrahedron Letters.*, **1980**, *21*, 541-544
32. S. Shinkai, O. Manabe, *Journal of American Chemical Society*, **1980**, *102*, 5860
33. S. Shinkai, O. Manabe, *Journal of American Chemical Society*, **1980**, *103*, 111
34. S. Shinkai, *Pure & Applied Chemistry*, **1987**, *59*, 425
35. J. J. Davis, G. A. Orłowski, H. Rahman and P. D. Beer, *Chemical Communications*, **2010**, *46*, 54-63.
36. F. A. Murphy and S. M. Draper, *The Journal of Organic Chemistry*, **2010**, *75*, 1862-1870.
37. P. L. Anelli, N. Spencer and J. F. Stoddart, *Journal of the American Chemical Society*, **1991**, *113*, 5131-5133.
38. R. A. Bissell, E. Cordova, A. E. Kaifer and J. F. Stoddart, *Nature*, **1994**, *369*, 133-137.
39. J. E. Green, J. Wook Choi, A. Boukai, Y. Bunimovich, E. Johnston-Halperin, E. DeIonno, Y. Luo, B. A. Sheriff, K. Xu, Y. Shik Shin, H.-R. Tseng, J. F. Stoddart and J. R. Heath, *Nature*, **2007**, *445*, 414-417.
40. S. AnithaáNagamani, D. ShankaráRao, S. KrishnaáPrasad, *Journal of Materials Chemistry*, **2001**, *11*, 1818-1822.
41. Y. Yokoyama, *Chemical Reviews*, **2000**, *100*, 1717-1740.
42. B. L. Feringa, W. F. Jager, B. de Lange, *Tetrahedron*, **1993**, *49*, 8267-8310.
43. M. Irie, *Molecular Switches*, Wiley-VCH Verlag GmbH: **2001**; 37-62.
44. G. Szalóki, J. L. Pozzo, *Chemistry: A European Journal*, **2013**, *19*, 11124-11132.
45. H. Tian, S. Yang, *Chemical Society Reviews* **2004**, *33*, 85-97.
46. A. S. Lukas, M. R. Wasielewski, *Molecular Switches*, Wiley-VCH Verlag GmbH: **2001**; 1-35.
47. P. Zacharias, M. C. Gather, A. Köhnen, N. Rehmman, K. Meerholz, *Angewandte Chemie International Edition*, **2009**, *48*, 4038-4041.
48. R. B. Woodward, R. Hoffmann, *Journal of the American Chemical Society*, **1965**, *87*, 395-397.
49. B. Seefeldt, R. Kasper, M. Beining, J. Mattay, J. Arden-Jacob, N. Kemnitzer, K. H. Drexhage, M. Heilemann and M. Sauer, *Photochemistry & Photobiological Sciences*, **2010**, *9*, 213-220.
50. G. Berkovic, V. Krongauz and V. Weiss, *Chemical Reviews*, **2000**, *100*, 1741-1754.
51. H. A. Wegner, *Angewandte Chemie International Edition*, **2012**, *51*, 4787-4788.
52. K. Sonogashira, *Journal of Organic Chemistry*, **2002**, *653*, 46-49.
53. R. Chinchilla and C. Nájera, *Chemical Reviews.*, **2007**, *107*, 874-922.
54. M. Erdélyi and A. Gogoll, *Journal of Organic Chemistry*, **2001**, *66*, 4165-4169.
55. E. Fischer, Y. Hirshberg, Y. *Journal of the Chemical Society*, **1952**, 4522-4524.
56. Bergmann, E. D.; Weizmann, A.; Fischer, E. *Journal of the American Chemical*

References

- Society*, **1950**, 72, 5009-5012.
57. C. F. Koelsch, *Journal of Organic Chemistry*, **1951**, 16, 1362-1370.
58. R. Heiligman-Rim, Y. Hirshberg, E. Fischer, *Journal of the Chemical Society*, **1961**, 156-163.
59. J. Kolc, R. S. Becker, *Journal of Physical Chemistry*, **1967**, 71, 4045-4048.
60. Y. Hirshberg, E. Fischer, *Journal of Chemical Physics*, **1953**, 21, 1619-1620.
61. Y. Hirshberg, E. Fischer, *Journal of the Chemical Society*, **1954**, 297-303.
62. Y. Hirshberg, E. Fischer, *Journal of the Chemical Society*, **1954**, 3129-3137.
63. R. Heiligman-Rim, Y. Hirshberg, E. Fischer, *Journal of Physical Chemistry*, **1962**, 66, 2465-2470.
64. T. Bercovici, R. Heiligman-Rim, E. Fischer, *Molecular Photochemistry*, **1969**, 1, 23-55.
65. H. Takahashi, K. Yoda, H. Isaka, T. Ohzeki, Y. Sakaino, *Chemical Physics Letters*, **1987**, 140, 90-94.
66. G. Cottone, R. Noto, G. La Manna, S. L. Fornili, S. L. *Chemical Physics Letters*, **2000**, 319, 51-59.
67. N. P. Ernsting, T. Arthenengeland, *Journal of Physical Chemistry*, **1991**, 95, 5502-5509.
68. A. K. Holm, M. Rini, E. T. J. Nibbering, H. Fidder, *Chemical Physics Letters*, **2003**, 376, 214-219.
69. C. J. Wohl, D. Kuciauskas, *Journal of Physical Chemistry B*, **2005**, 109, 22186-22191.
70. I. Shimizu, H. Kokado, E. Inoue, *Bulletin Chemical Society of Japan*, **1969**, 42, 1730-1734.
71. J. W. Zhou, Y. T. Li, Y. W. Tang, F. Q. Zhao, X. Q. Song, E. C. J Li, *Photochemistry & Photobiology A: Chemistry*, **1995**, 90, 117-123.
72. W. X. Zou, H. M. Huang, Y. Gao, T. Matsuura, B. Meng, *Journal of Structural Chemistry*, **2004**, 15, 317-321.
73. X. F. Guo, Y. C. Zhou, D. Q. Zhang, Y. Bing, Z. L. Liu, C. M. Liu, Z. L. Lu, Y. H. Huang, D. B. Zhu, *Journal of Organic Chemistry*, **2004**, 69, 8924-8931.
74. N. Katsonis, M. Lubomska, M. M. Pollard, B. L. Feringa and P. Rudolf, *Progr. Surface Science*, **2007**, 82, 407-434.
75. *People's Republic of China Patent*, CN 102641215, **2012**.
76. *People's Republic of China Patent*, CN 102631293, **2012**.
77. *People's Republic of China Patent*, CN 102643567, **2012**.
78. H. Stobbe, *Berichte der Deutschen Chemischen Gesellschaft*, **1904**, 37, 2236-2240.
79. H. Stobbe, *Berichte der Deutschen Chemischen Gesellschaft*, **1905**, 38, 3672-3682.
80. H. Stobbe, *Liebigs Annalen der Chemie*, **1908**, 359, 1-48.
81. H. Stobbe, *Zeitschrift für Elektrochemie*, **1908**, 14, 473-483.
82. A. T. Schönberg, *Faraday Society*, **1936**, 32, 514-521.
83. D. P. Chakraborty, T. Sleigh, R. Stevenson, G. A. Swoboda, B. Weinstein, *Journal of Organic Chemistry*, **1966**, 31, 3342-3345.
84. G. Brunow, H. Tylli, *Acta Chemica Scandinavica*, **1968**, 22, 590-596.

85. H. Stobbe, *Berichte der Deutschen Chemischen Gesellschaft*, **1907**, *40*, 3372-3382.
86. F. G. Baddar, L. S. El-Assal, N. A. Doss, A. H. Shehab, *Journal of the Chemical Society*, **1959**, 1016
87. A. Santiago, R. S. Becker, *Journal of the American Chemical Society*, **1968**, *90*, 3654-3658.
88. R. J. Hart, H. G. Heller, *Journal of the Chemical Society*, **1972**, 1321-1324.
89. M. Kaftory, *Acta Crystallography C.*, **1984**, *40*, 1015-1019.
90. P. J. Darcy, H. G. Heller, S. Patharakorn, R. D. Piggott, J. Whittal, *Journal of the Chemical Society*, **1986**, 315-319.
91. P. J. Darcy, R. J. Hart, H. G. Heller, *Journal of the Chemical Society*, **1978**, 571-576.
92. M. Köse and E. Orhan, *Turkish Journal of Chemistry*, **2009**, *33*, 579-588
93. P. J. Darcy, R. J. Hart, H. G. Heller, *Journal of the Chemical Society*, **1978**, 571-576
94. H. G. Heller, R. M. Megit, *Journal of the Chemical Society*, **1974**, 923-927.
95. F. M. Raymo and M. Tomasulo, *Chemical Society Reviews*, **2005**, *34*, 327-336.
96. M. Irie, *Photochemistry & Photobiological Sciences*, **2010**, *9*, 1535-1542.
97. S. Kawata and Y. Kawata, *Chemical Reviews*, **2000**, *100*, 1777-1788.
98. A. Goldberg, A. Murakami, K. Kanda, T. Kobayashi, S. Nakamura, K. Uchida, H. Sekiya, T. Fukaminato, T. Kawai, S. Kobatake and M. Irie, *Journal of Physical Chemistry A*, **2003**, *107*, 4982-4988.
99. S. Delbaere and G. Vermeersch, *Journal of Photochem. Photobio. C: Photochemistry Reviews*, **2008**, *9*, 61-80.
100. S. Nakamura and M. Irie, *The Journal of Organic Chemistry*, 1988, *53*, 6136-6138.
101. K. Uchida, Y. Nakayama and M. Irie, *Bulletin of the Chemical Society of Japan*, **1990**, *63*, 1311-1315.
102. T. Kawai, N. Fukuda, D. Gröschl, S. Kobatake and M. Irie, *Japanese Journal of Applied Physics*, **1999**, *38*, 1194-1196.
103. K. Matsuda and M. Irie, *Chemistry Letters*, **2000**, *29*, 16-17
104. Y. W. Zhong, N. Vila, J. C. Henderson, S. Flores-Torres, H. D. Abruña, *Inorganic Chemistry*, **2007**, *46*, 10470-10472.
105. R. T. F. Jukes, V. Adamo, F. Hartl, P. Belser, L. De Cola, *Inorganic Chemistry*, **2004**, *43*, 2779-2792
106. J. J. D. de Jong, L. N. Lucas, R. Hania, A. Pugzlys, R. M. Kellogg, B. L. Feringa, K. Duppen, J. H. v. Esch, *European Journal of Organic Chemistry*, **2003**, *2003*, 1887-1893.
107. M. Irie, K. Sakemura, M. Okinaka, K. Uchida, *Journal of Organic Chemistry*, **1995**, *60*, 8305-8309.
108. M. Irie, *Tetrahedron*, **1997**, *53*, 12263-12271.
109. A. T. Bens, D. Frewert, K. Kodatis, C. Krysch, H. D. Martin, H. P. Trommsdorff, *European Journal of Organic Chemistry*, 1998, 2333-2338.
110. T. Koshido, T. Kawai, K. Yoshino, *Journal of Physical Chemistry*, **1995**, *99*, 6110-6114.
111. W. R. Browne, J. J. D. de Jong, T. Kudernac, M. Walko, L. N. Lucas, K. Uchida, J. H. van Esch, B. L. Feringa, *Chemistry: A European Journal*, **2005**, *11*, 6414-6429.

References

112. K. Shibata, K. Muto, S. Kobatake, M. Irie, *Journal of Physical Chemistry A.*, **2002**, *106*, 209-214.
113. M. Irie, *Chemical Reviews*, **2000**, *100*, 1685-1716
114. T. Weil, E. Reuther, K. Mullen, *Angewandte Chemie International Edition*, **1997**, *36*, 631
115. P. Schlichting, B. Duchscherer, G. Seisenberger, T. Basche, K. Mullen, *Chemistry: A European Journal*, **1999**, *5*, 2388
116. A. I. Moore, *Journal of the American Chemical Society*, **2006**, *128*, 1818
117. A. E. Keirstead, J. W. Bridgewater, A. L. Moore, *Journal of the American Chemical Society*, **2010**, *132*, 6588
118. H. Seyler, B. Purushothaman, D. J. Jones, A. B. Holmes and W. W. C. Wong, *Pure Applied Chemistry*, **2012**, *84*, 1047-1067.
119. F. A. Murphy and S. M. Draper, *Journal of Organic Chemistry*, **2010**, *75*, 1862-1870.
120. V. Vij, V. Bhalla and M. Kumar, *Chemical Reviews*, **2016**, *116*, 9565-9627.
121. B. T. King, J. Kroulik, P. Rempala, *Journal of the American Chemical Society*, **2004**, *126*, 15002-15003
122. S. M. Draper, D. Gregg, R. Madathil, *Journal of the American Chemical Society*, **2002**, *124*, 3486 - 3487
123. D. F. Perepichka, *Chemistry Materials*, **2008**, *20*, 2484
124. K. Yoshida, I. Morimoto, K. Mitsudo, H. Tanaka, *Tetrahedron Letters*, **2008**, *49*, 2363-2365
125. K. Yoshida, I. Morimoto, K. Mitsudo, H. Tanaka, *Tetrahedron*, **2008**, *64*, 5800-5807.
126. Y. Geng, A. Fechtenkötter and K. Müllen, *Journal of Materials Chemistry*, **2001**, *11*, 163
127. R. Göstl, A. Senf and S. Hecht, *Chemical Society Reviews*, **2014**, *42*, 1982-1996.
128. R. S. Stoll and S. Hecht, *Angewandte Chemie International Edition*, **2010**, *49*, 5054-5075.
129. F. M. Raymo, *Physical Chemistry & Chemical Physics*, **2013**, *15*, 14840-14850.
130. T. Fukaminato, *Journal of Photochemistry and Photobiology C: Photochemistry Reviews*, **2011**, *12*, 177-208.
131. X. Zhang, H. Li, G. Liu and S. Pu, *Journal of Photochemistry and Photobiology A: Chemistry*, **2016**, *330*, 22-29.
132. Y. Fu, Y. Tu, C. Fan, C. Zheng, G. Liu and S. Pu, *New Journal of Chemistry*, **2016**, *40*, 8579-8586.
133. Zacharias, P.; Gather, M. C.; Köhnen, A.; Rehmann, N.; Meerholz, K., *Angewandte Chemie International Edition*, **2009**, *48*, 4038-4041
134. M. Irie, T. Lifka, K. Uchida, S. Kobatake, Y. Shindo, *Chemical Communications*. **1999**, *8*, 747-750.
135. G. Pariani, M. Quintavalla, L. Colella, L. Oggioni, R. Castagna, F. Ortica, C. Bertarelli, A. Bianco, *The Journal of Physical Chemistry C.*, **2017**, *121*, 23592-23598.
136. P. G. Sammes and G. Yahiolu, *Chemical Society Reviews*, **1994**, *23*, 327-334.
137. A. Bencini and V. Lippolis, *Coordination Chemistry Reviews*, **2010**, *254*, 2096-2180.

References

138. H. S. Joshi, R. Jamshidi and Y. Tor, *Angewandte Chemie International Edition*, **1999**, *38*, 2721-2725.
139. B. N. Bandyopadhyay and A. Harriman, *Journal of the Chemical Society, Faraday Transactions 1: Physical Chemistry in Condensed Phases*, **1977**, *73*, 663-674.
140. G. Accorsi, A. Listorti, K. Yoosaf and N. Armaroli, *Chemical Society Reviews*, **2009**, *38*, 1690-1700.
141. R. Ziesel and C. Stroh, *Tetrahedron Letters*, **2004**, *45*, 4051-4055.
142. S. Ji, W. Wu, W. Wu, P. Song, K. Han, Z. Wang, S. Liu, H. Guo, J. Zhao, *Journal of Materials Chemistry*, **2010**, *20*, 1953-1963.
143. Y. Lu, J. Wang, N. McGoldrick, X. Cui, J. Zhao, C. Caverly, B. Twamley, G. M. Ó Máille, B. Irwin, R. Conway-Kenny, S. M. Draper, *Angewandte Chemie International Edition*, **2016**, *128*, 14908-14912.
144. M. Knorn, T. Rawner, R. Czerwieniec and O. Reiser, *ACS Catalysis*, **2015**, *5*, 5186-5193.
145. A. N. Boynton, L. Marcélis, A. J. McConnell and J. K. Barton, *Inorganic Chemistry*, **2017**, *56*, 8381-8389.
146. A. A. Schilt, *Analytical Applications of 1,10-phenanthroline and Related Compounds*, Elsevier Ltd, **1969**.
147. P. Alreja and N. Kaur, *RSC Advance*, **2016**, *6*, 23169-23217.
148. L. Ma, H. Guo, Q. Li, S. Guo, J. Zhao, *Dalton Transactions*, **2012**, *41*, 10680-10689.
149. D. Výprachtický, D. Kaňková, V. Pokorná, I. Kmínek, V. Dzhabarov, V. Cimrová, *Australian Journal of Chemistry*, **2014**, *67*, 915-921.
150. D. Tzalis, Y. Tor, F. Salvatorre and S. Jay Siegel, *Tetrahedron Letters*, **1995**, *36*, 3489-3490.
151. Q. Zhao, S. Liu, M. Shi, F. Li, H. Jing, T. Yi, C. Huang, *Organometallics*, **2007**, *26*, 5922-5930.
152. Y. Saitoh, T. A. Koizumi, K. Osakada, T. Yamamoto, *Canadian Journal of Chemistry*, **1997**, *75*, 1336-1339.
153. M. C. DeRosa and R. J. Crutchley, *Coordination Chemistry Review*, **2002**, *233*, 351-371.
154. A. Ferrer-Ugalde, E. J. Juárez-Pérez, F. Teixidor, C. Viñas, R. Núñez, *Chemistry: A European Journal*, **2013**, *19*, 17021-17030.
155. J. Ponce, J. Aragón, I. Vayá, J. G. Magenti, S. Tatay, E. Ortí, E. Coronado, *European Journal of Inorganic Chemistry*, **2016**, *2016*, 1851-1859.
156. Y. Lu, R. Conway-Kenny, B. Twamley, N. McGoldrick, J. Zhao, S. M. Draper, *ChemPhotoChem*, **2017**, DOI: 10.1002/cptc.201700158
157. Y. Halpin, M. T. Pryce, S. Rau, D. Dini, J. G. Vos, *Dalton Transactions*, **2013**, *42*, 16243-16254.
158. P. Dreyse, I. Gonzalez, D. Cortes-Arriagada, O. Ramirez, I. Salas, A. Gonzalez, A. Toro-Labbe, B. Loeb, *New Journal of Chemistry*, **2016**, *40*, 6253-6263.
159. R. D. Costa, E. Ortí, H. J. Bolink, F. Monti, G. Accorsi, N. Armaroli, *Angewandte Chemie International Edition*, **2012**, *51*, 8178-8211.
160. T. Togano, N. Nagao, M. Tsuchida, H. Kumakura, K. Hisamatsu, F. S. Howell, M.

References

- Mukaida, *Inorganica Chimica Acta*, **1992**, *195*, 221-225.
161. Z. Ji, S. D. Huang and A. R. Guadalupe, *Inorganica Chimica Acta*, **2000**, *305*, 127-134.
162. Y. Lu, J. Wang, N. McGoldrick, X. Cui, J. Zhao, C. Caverly, B. Twamley, G. M. Ó Máille, B. Irwin, R. Conway-Kenny and S. M. Draper, *Angewandte Chemie International Edition*, **2016**, *55*, 14688-14692.
163. C. Dragonetti, L. Falciola, P. Mussini, S. Righetto, D. Roberto, R. Ugo, A. Valore, F. De Angelis, S. Fantacci, A. Sgamellotti, M. Ramon and M. Muccini, *Inorganic Chemistry*, **2007**, *46*, 8533-8547.
164. A. Akihiro K. Noritaka, T. Sachio, *Macromolecules*, **1991**, *24*, 6238.
165. C. K. M. Chan, C. H. Tao, H. L. Tam, N. Zhu, V. W. W. Yam, K. W. Cheah, *Inorganic Chemistry*, **2009**, *48*, 2855.
166. J. P. Clancy, N. Chen, C. Y. Kim, W. F. Chen, K. W. Plumb, B. C. Jeon, T. W. Noh, Y. J. Kim, *Physics Reviews B.*, 2012, *86*, 195131.
167. W. Wu, S. Ji, H. Guo, P. Song, K. Han, L. Chi, J. Shao, J. Zhao, *Journal of Materials Chemistry*, **2010**, *20*, 9775-9786.
168. S. Nagarajan, C. Barthes, A. Gourdon, *Tetrahedron.*, **2009**, *65*, 3767-3772
169. G. O'Maille and S.M. Draper, *Thesis (unpublished results)*, **2013**.
170. R. Gedye, F. Smith, K. Westaway, H. Ali, L. Baldisera, L. Laberge, J. Rousell, *Tetrahedron Letters*, **1986**, *27*, 279-282.
171. R. J. Giguere, T. L. Bray, S. M. Duncan, G. Majetich, *Tetrahedron Letters*, **1986**, *27*, 4945-4948.
172. C. O. Kappe, *Angewandte Chemie International Edition.*, **2004**, *43*, 6250-6284.
173. B. L. Hayes, *Microwave Synthesis - Chemistry at the Speed of Light*; CEM Publishing.
174. J. P. T. P. Lidstrom, *Microwave Assisted Organic Synthesis*; Blackwell Publishing Ltd., **2005**.
175. H. M. Kingston, *Introduction to Microwave Sample Preparation Theory and Practice*; ACS, **1988**.
176. A. Loupy, *Pure & Applied Chemistry*, **2001**, *73*, 161-166.
177. D. M. P. Mingos, D. R. Baghurst, *Chemical Society Reviews.*, **1991**, *20*, 1-47.
178. D. Villemin, F. Caillot, *Tetrahedron Letters.*, **2001**, *42*, 639-642.
179. J. X. Wang, B. Wei, Y. Hu, Z. Liu, Y. Yang, *Synthetic Communications.*, **2001**, *31*, 3885-3890.
180. L. Ohberg, J. Westman, *Synthetic Letters*, **2001**, *2001*, 1893,1896.
181. K. S. A. Vallin, P. Emilsson, M. Larhed, A. Hallberg, *The Journal of Organic Chemistry.*, **2002**, *67*, 6243-6246.
182. M. Kim, S. J. Garibay, S. M. Cohen, S. M. *Inorganic Chemistry*, *50*, 729-731.
183. E. Petricci, M. Radi, F. Corelli, M. Botta, *Tetrahedron Letters*, **2003**, *44*, 9181-9184.
184. S. Nagarajan, C. Barthes, A. Gourdon, *Tetrahedron*, **2009**, *65*, 3767-3772.
185. I. H. Chen, J. N. Young, S. J. Yu, *Tetrahedron*, **2004**, *60*, 11903-11909.
186. M. Sridhar, K. L. Krishna, K. Srinivas, J. M. Rao, *Tetrahedron Letters* **1998**, *39*, 6529-6532.

187. U. S. Sørensen, E. Pombo-Villar, *Tetrahedron* **2005**, *61*, 2697-2703.
188. B. X. Tang, F. Wang, J. H. Li, Y. X. Xie, M. B. Zhang, *The Journal of Organic Chemistry*, **2007**, *72*, 6294-6297.
189. S. M. Draper, D. J. Gregg, R. Madathil, *Journal of the American Chemical Society*, **2002**, *124*, 3486-3487.
190. Y. Goldberg and H. Alper, *Journal of Organic Chemistry*, **1993**, *58*, 3072-3075
191. K. Sonogashira, *Journal of Organic Chemistry*, **2002**, *653*, 46-49.
192. R. Chinchilla and C. Nájera, *Chemical Reviews*, **2007**, *107*, 874-922.
193. M. Erdélyi and A. Gogoll, *Journal of Organic Chemistry*, **2001**, *66*, 4165-4169.
194. N. Miyaura and A. Suzuki, *Chemical Reviews*, **1995**, *95*, 2457-2483.
195. N. Niamnont, N. Kimpitak, K. Wongravee, P. Rashatasakhon, K. K. Baldrige, J. S. Siegel, M. Sukwattanasinitt., *Chemical Communications*, **2013**, *49*, 780-782
196. M. G. Uddin and A.T.M. Zafrul Azam, *American Journal of Biochemistry and Molecular Biology*, *3.*, **2013**, 175181
197. H. Sotome, T. Nagasaka, K. Une, S. Morikawa, T. Katayama, S. Kobatake, M. Irie, M. Miyasaka, *Journal of American Chemical Society*, **2017**, *139*, 17159-17167
198. J. Ma, X. Cui, F. Wang, X. Wu, J. Zhao, X. Li, *Journal of Organic Chemistry*, **2014**, *79*, 10855
199. C. Li, H. Yan, L. X. Zhao, G. F. Zhang, Z. Hu, Z. L. Huang, M. Q. Zhu, *Nature Communications*, **2014**, *5*.
200. T. Fukaminato, T. Doi, N. Tamaoki, K. Okuno, Y. Ishibashi, H. Miyasaka, M. Irie, *Journal of American Chemical Society*, **2011**, *133*, 4984-4990
201. T. Kawai, T. Sasaki, M. Irie, *Chemical Communications*, **2001**, 711-712.
202. D. Williams and I. Fleming, *Spectroscopic Methods in Organic Chemistry*, McGraw-Hill Education, Maidenhead, 6th edn., **2008**.
203. A. H. S. Taniguchi, T. Okazaki, F. Matsui, M. Irie, *Nippon Kagaku Kaishi*, **1990**, *10*, 1138.
204. M. Irie, T. Fukaminato, K. Matsuda, S. Kobatake, *Chemical Reviews*, **2014**, *114*, 12174-12277.
205. Y. He, Y. Yamamoto, W. Jin, T. Fukushima, A. Saeki, S. Seki, N. Ishii, T. Aida, *Advanced Materials*, **2010**, *22*, 829-832
206. D. J. Gregg, E. Bothe, P. Hoefler, P. Passaniti, S. M. Draper, *Inorganic Chemistry*, **2005**, *44*, 5654-5660.
207. G. Tanguy, B. Weinberger, H. des Abbayes, *Tetrahedron Letters*, **1984**, *25*, 5529-5532
208. U. T. Muellerwesterhoff, M. Zhou, *Journal of Organic Chemistry*, **1994**, *59*, 4988-4992
209. K. Tamao, S. Yamaguchi and Y. Ito, *Journal of the Chemical Society, Chemical Communications*, **1994**, 229
210. X. Yang, X. Dou, K. Mullen, *Chemical Asian Journal*, **2008**, *3*, 759 - 766
211. J. F. Durand, C. S. Marvel, F. D. Hager, D. D. Coffman, *Journal of American Chemical Society*, **1927**, *49*, 2323.
212. W. Diltthey, G. Hurtig, *Chemische Berichte*, **1934**, *67*, 2004.

References

213. T. A. Geissman, R. C. Mallatt, *Journal of American Chemical Society*, **1939**, *61*, 1788.
214. K. Harada, H. Hart, Chi-Jen Frank Du, *Journal of Organic Chemistry*, **1985**, *50*, 5524-5528
215. D. Liu, S. De Feyter, M. Cotlet, A. Stefan, U. Wiesler, A. Herrmann, D. Grebel-Koehler, J. Qu, K. Müllen, F. C. De Schryver, *Macromolecules*, **2003**, *36*, 5918
216. G. Hilt, T. Vogler, W. Hess, F. Galbiati., *Chemical Communications*, **2005**, 1474
217. G. Hilt, W. Hess, T. Vogler, C. Hengst, *Journal of Organometallic Chemistry*, **2005**, *690*, 5170
218. G. Hilt, C. Hengst, W. Hess, *European Journal Organic Chemistry*, **2008**, *2008*, 2293
219. R. Rathore, A. S. Kumar, S. V. Lindeman, J. K. Kochi, *Journal of Organic Chemistry*, **1998**, *63*, 5847–5856.
220. D. Tzalis, Y. Tor, *Chemical Communications*, **1996**, 1043-1044.
221. D. Tzalis, Y. Tor, *Jornal of American Chemical Society*, **1997**, *119*, 852-853.
222. P. J. Connors, D. Tzalis, A. L. Dunnick, Y. Tor, *Inorganic Chemistry*, **1998**, *37*, 1121-1123.
223. Y. Saitoh, T.-a. Koizumi, K. Osakada, T. Yamamoto, *Canadian Journal of Chemistry*, **1997**, *75*, 1336-1339.
224. M. Hissler, W. B. Connick, D. K. Geiger, J. E. McGarrah, D. Lipa, R. J. Lachicotte, R. Eisenberg, *Inorganic Chemistry*, **2000**, *39*, 447-457.
225. R. V. Kiran, C. F. Hogan, B. D. James, D. J. D. Wilson, *European Journal of Inorganic Chemistry*, **2011**, *2011*, 4816-4825.
226. B.S. Lankage, *Rajaratne University Journal*, **2015**, *3*, 44
227. K. P. S. Zaroni, B. K. Kariyazaki, A. Ito, M. K. Brennaman, T. J. Meyer, N. Y. Murakami Iha, *Inorganic Chemistry*, **2014**, *53*, 4089-4099.
228. (a) EHMO: C. P. Rao, J. R. Dorfman, R. H. Holm, *Inorganic Chemistry*, **1986**, *25*, 428. (b) R. F. Fenske, *Pure Applied Chemistry*, **1988**, *60*, 1153. (c) INDO: J. E. Ridley, M. C. Zemer, *Theoretical Chimica Acta*, **1973**, *32*, 111; **1976**, *42*, 223. (d) SINDO: D. N. Nanda, K. Jug, *Theoretical Chimica Acta*, **1980**, *57*, 95; 107. (e) MNDO: M. J. S. Dewar, W. Thiel, *Journal of the American Chemical Society*, **1977**, *99*, 4899 (f) J. J. P. Stewart, *Journal of Computational Chemistry*, **1989**, *10*, 209. (g) AM1: M. J. S. Dewar, E. G. Zoebisch, E. F. Healy, J. J. P. Stewart, *Journal of the American Chemical Society*, **1985**, *107*, 3902. (h) A. Broo, P. Lincoln, *Inorganic Chemistry*, **1997**, *36*, 2544.
229. J. B. Foresman, E. Frisch, Exploring Chemistry with Electronic Structure Methods, 2nd ed.; *Gaussian Inc.: Pittsburgh, PA*, **1996**;
230. M. J. Frisch, G. W. Trucks, H. B. Schlegel, P. M. W. Gill, B. G. Johnson, M. A. Robb, J. R. Cheeseman, T. Keith, G. A. Petersson, J. A. Montgomery, K. Raghavachari, M. A. Al-Laham, V. G. Zakrzewski, J. V. Ortiz, J. B. Foresman, J. Cioslowski, B. B. Stefanov, A. Nanayakkara, M. Challacombe, C. Y. Peng, P. Y. Ayala, W. Chen, M. W. Wong, J. L. Andres, E. S. Replogle, R. Gomperts, R. L. Martin, D. J. Fox, J. S. Binkley, D. J. Defrees, J. Baker, J. P. Stewart, M. Head-Gordon, C. Gonzalez, J. A. Pople, *Gaussian 94*; Gaussian, Inc.:Pittsburgh, PA, **1995**

References

231. M. J. Frisch, G. W. Trucks, H. B. Schlegel, G. E. Scuseria, M. A. Robb, J. R. Cheeseman, V. G. Zakrzewski, J. A. Montgomery, J. Stratmann *Gaussian 98*; Gaussian, Inc.: Pittsburgh, PA, **1998**.
232. M. J. Frisch, *Gaussian 98*, User's Reference, 2nd. ed.; Gaussian, Inc.: Pittsburgh, PA, **1999**.
233. (a) W. R. Wadt, P. J. Hay, *Journal of Chemical Physics*, **1985**, *82*, 284. (b) P. J. Hay, W. R. Wadt, *Journal of Chemical Physics*, **1985**, *82*, 270, 299.
234. (a) N. H. Damrauer, B. T. Weldon, J. K. McCusker, *Journal of Physical Chemistry A*, **1998**, *102*, 3382. (b) P. Brandt, T. Norrby, B. Akermark, B. *Inorganic Chemistry*, **1998**, *37*, 4120. (c) A. Karlsson, A. Broo, P. Ahlberg, *Canadian Journal of Chemistry*, **1999**, *77*, 628. (d) K. C. Zheng, D. B. Kuang, J. P. Wang, Y. Shen, *Acta Physico-Chimica Sinica*, **2000**, *16*, 608; in Chinese. (e) K. C. Zheng, D. Kuang, J. P. Wang, Y. Shen, *Chinese Journal of Chemical Physics*, **2000**, *13*, 551
235. Y. Lu, N. M., F. Murphy, B. Twamley, X. Cui, C. Delaney, G. M. Maille, J. Wang, J. Zhao, S. M. Draper *Chemistry: A European Journal*, **2016**, *22*, 11349–11356.
236. C. S. Liang, W. H. Bu, C. L. Li, *Dalton Transactions*, **2015**, *44*, 11352
237. E. Alvarez, M. L. Fernandez-Marcos, C. Monterroso, M. J. Fernandez-Sanjurjo, *Forest Ecology and Management*, **2005**, *211*, 227.
238. J. Barcelo, C. Poschenrieder, *Environmental and Experimental Botany*, **2002**, *48*, 75
239. S. Das, M. Dutta, D. Das, *Analytical Methods*, **2013**, *5*, 6262
240. K. H. Falchuk, Springer US. **1998**, *41*
241. A. Krezel, W. J. Maret, *Journal of Biological Inorganic Chemistry*, **2006**, *11*, 1049
242. Y. N. Li, Q. Li, *Organic Letters*, **2012**, *14*, 4362
243. S. J. Xia, G. Liu, S. Z. Pu, *Journal of Materials Chemistry C.*, **2015**, *3*, 4023
244. J. Li, P. I. Djurovich, B. D. Alleyne, *Inorganic Chemistry*, **2005**, *44*, 1713–1727.
245. H. Lv, T. Purnima A. Ruberu, V. E. Fleischauer, W. W. Brennessel, M. L. Neidig, R. Eisenberg, *Journal of the American Chemical Society*, **2016**, *138*, 11654–11663
246. J. Liu, Y. Liu, Q. Liu, C. Li, L. Sun, F. Li, *Journal of the American Chemical Society* **2011**, *133*, 15276–15279.
247. R. S. Khnayzer, J. Blumhoff, J. A. Harrington, A. Haefele, F. Deng, F. N. Castellano, *Chemical Communications*, **2012**, *48*, 209–211.
248. J. Zhao, *Journal of Physical Chemistry A*, **2015**, *119*, 468–481
249. R. T. F. Jukes, V. Adamo, F. Hartl, P. Belser, and L. De Cola, *Inorganic Chemistry*, **2004**, *43*, 2779–2792.

Annex

Crystal data and structure refinement for Compound 3

Identification code	tcd933a	
Empirical formula	C ₃₁ H ₁₈ F ₆ S ₂	
Formula weight	568.57	
Temperature	100(2) K	
Wavelength	0.71073 Å	
Crystal system	Triclinic	
Space group	P $\bar{1}$	
Unit cell dimensions	a = 10.7438(4) Å	α = 100.4101(13)°.
	b = 14.0625(5) Å	β = 101.1821(13)°.
	c = 18.3688(7) Å	γ = 101.4820(14)°.
Volume	2597.73(17) Å ³	
Z	4	
Density (calculated)	1.454 Mg/m ³	
Absorption coefficient	0.268 mm ⁻¹	
F(000)	1160	
Crystal size	0.32 x 0.08 x 0.06 mm ³	
Theta range for data collection	2.680 to 26.464°.	
Index ranges	-13 ≤ h ≤ 13, -17 ≤ k ≤ 17, -22 ≤ l ≤ 23	
Reflections collected	34402	
Independent reflections	10668 [R(int) = 0.0332]	
Completeness to theta = 25.242°	99.8 %	
Absorption correction	Semi-empirical from equivalents	
Max. and min. transmission	0.7454 and 0.6971	
Refinement method	Full-matrix least-squares on F ²	
Data / restraints / parameters	10668 / 6 / 765	
Goodness-of-fit on F ²	1.029	
Final R indices [I > 2σ(I)]	R1 = 0.0378, wR2 = 0.0807	
R indices (all data)	R1 = 0.0563, wR2 = 0.0890	
Largest diff. peak and hole	0.326 and -0.383 e.Å ⁻³	

Crystal data and structure refinement for Compound **Ir-1**

Identification code	Ir-1	
Empirical formula	C ₃₄ H ₂₃ BrF ₆ IrN ₄ P	
Formula weight	904.04	
Temperature	105(2) K	
Wavelength	0.71073 Å	
Crystal system	Monoclinic	
Space group	P $\bar{1}$	
Unit cell dimensions	a = 10.9346(5)Å	$\alpha = 90^\circ$.
	b = 23.7348(10)Å	$\beta = 98.893(2)^\circ$.
	c = 13.4894(6)Å	$\gamma = 90^\circ$.
Volume	3458.8(3)Å ³	
Z	4	
Density (calculated)	1.737Mg/m ³	
Absorption coefficient	5.123 mm ⁻¹	
F(000)	1744	
Crystal size	0.19 x 0.08 x 0.05 mm ³	
Theta range for data collection	2.990 to 26.090°.	
Index ranges	-13 ≤ h ≤ 13, -29 ≤ k ≤ 29, -16 ≤ l ≤ 16	
Reflections collected	109104	
Independent reflections	9792 [R(int) = 0.0297]	
Completeness to theta = 25.242°	99.9 %	
Absorption correction	Semi-empirical from equivalents	
Max. and min. transmission		
Refinement method	Full-matrix least-squares on F ²	
Data / restraints / parameters	9792 / 198 / 424	
Goodness-of-fit on F ²	1.252	
Final R indices [I > 2σ(I)]	R1 = 0.0951, wR2 = 0.2384	
R indices (all data)	R1 = 0.1073, wR2 = 0.2453	
Largest diff. peak and hole	12.520 and -7.043e.Å ⁻³	